

GEOLOGICAL COMPARISON OF THE SOUTH HOPEDALE
AND WEST ORPHAN BASINS, NORTHWEST
ATLANTIC MARGIN

JORDAN E. STEAD



Geological Comparison of the South Hopedale
and West Orphan Basins, Northwest Atlantic Margin

by

©Jordan E. Stead

A thesis submitted to the
School of Graduate Studies
in partial fulfillment of the
requirements for the degree of
Master of Science

Department of Earth Sciences/Faculty of Science

Memorial University

March, 2007

St. John's

Newfoundland and Labrador



Library and Archives
Canada

Published Heritage
Branch

395 Wellington Street
Ottawa ON K1A 0N4
Canada

Bibliothèque et
Archives Canada

Direction du
Patrimoine de l'édition

395, rue Wellington
Ottawa ON K1A 0N4
Canada

Your file *Votre référence*
ISBN: 978-0-494-57492-8
Our file *Notre référence*
ISBN: 978-0-494-57492-8

NOTICE:

The author has granted a non-exclusive license allowing Library and Archives Canada to reproduce, publish, archive, preserve, conserve, communicate to the public by telecommunication or on the Internet, loan, distribute and sell theses worldwide, for commercial or non-commercial purposes, in microform, paper, electronic and/or any other formats.

The author retains copyright ownership and moral rights in this thesis. Neither the thesis nor substantial extracts from it may be printed or otherwise reproduced without the author's permission.

AVIS:

L'auteur a accordé une licence non exclusive permettant à la Bibliothèque et Archives Canada de reproduire, publier, archiver, sauvegarder, conserver, transmettre au public par télécommunication ou par l'Internet, prêter, distribuer et vendre des thèses partout dans le monde, à des fins commerciales ou autres, sur support microforme, papier, électronique et/ou autres formats.

L'auteur conserve la propriété du droit d'auteur et des droits moraux qui protègent cette thèse. Ni la thèse ni des extraits substantiels de celle-ci ne doivent être imprimés ou autrement reproduits sans son autorisation.

In compliance with the Canadian Privacy Act some supporting forms may have been removed from this thesis.

While these forms may be included in the document page count, their removal does not represent any loss of content from the thesis.

Conformément à la loi canadienne sur la protection de la vie privée, quelques formulaires secondaires ont été enlevés de cette thèse.

Bien que ces formulaires aient inclus dans la pagination, il n'y aura aucun contenu manquant.


Canada

Abstract

The South Hopedale and West Orphan Basin developed concurrently during the Late Jurassic to Early Cretaceous rifting stage on the northwest Atlantic margin. These basins, and the intervening Paleozoic Cartwright Arch and St. Anthony Basin, were interpreted using 2D reflection seismic, borehole and potential fields data to compare stratigraphic and structural features along the margin, analyze the extension and basin evolution, and examine the petroleum prospectivity of the region.

Mapping indicates that the Labrador synrift sequence thins seawards but extends past the slope break, and that the West Orphan synrift sequence becomes thicker and more structurally complex towards the east and south of the basin. A thick postrift sequence is evident along the entire Labrador margin and West Orphan Basin. In the South Hopedale Basin, a complex extensional postrift fault system is observed along the shelf break, and complimentary compressional features are observed downslope. This structural system was not evident in the West Orphan Basin, where the postrift sequence thins significantly seawards. Comparisons of the postrift seismic markers and sequences in both basins show many similarities. Areally extensive, polygonally faulted sequences are present along the entire margin.

Comparisons of the mapped extensional fault systems to analogue models of orthogonal, oblique and multi-phase rift systems indicate that the Hopedale Basin is characteristic of an orthogonal rift while the West Orphan Basin is typical of an oblique rift. Analysis of the extension along the margin suggests that higher stretching values occur in the West Orphan Basin, where there is significant variation of the postrift-to-

synrift ratio across the seismic profiles. The extension values are lower in the South Hopedale Basin, where the postrift-to-synrift ratio is consistently high.

The petroleum prospectivity of both regions is significant. The established source and reservoir bearing sequences in the Hopedale Basin were mapped onto the outer shelf and slope, where maturation is predicted to increase. The West Orphan Basin has no proven hydrocarbon accumulations, but the similarity of the stratigraphy to that of the Labrador Shelf in the northwest, and that of the producing Jeanne d'Arc Basin in the southeast suggest that the area has considerable potential. Numerous structural and stratigraphic traps were mapped throughout both these regions.

Acknowledgements

First and foremost, I'd like to thank my supervisor, Dr. Jeremy Hall, for all his effort and for providing such excellent guidance throughout this project. I also wish to thank Dr. Michael Enachescu for all his suggestions, help and encouragement. Funding for this project was provided by the Pan-Atlantic Petroleum Consortium (PPSC), the School of Graduate Studies, and the Department of Earth Sciences. Geophysical Service Incorporated (GSI) donated the seismic reflection data, and Landmark (Halliburton) provided the software necessary for the seismic interpretation. I also thank IHS Energy for donating digital well data, and Canstrat for donating lithostratigraphic logs to help with the analysis.

Many thanks go to Dan Vasiliu, Clyde Clements, Tony Kokurko and Peter Bruce for all their technical expertise and assistance. I would like to thank Trevor Bennett, Lewis Manual, Lisa Clarke and Sheila Duff at the Canada-Newfoundland and Labrador Offshore Petroleum Board for providing maps and access to data, as well as Bob Ratliff at Geo Logic Systems for all his help and assistance.

I also thank all my friends in the Earth Sciences Department for making this project so enjoyable, especially my office mate, Julie Smith. Much appreciation also goes to my family and friends for their continued support, for which I am very grateful. Last, but not least, I thank Aron for all his love, support and encouragement.

Table of Contents

Abstract	ii
Acknowledgements.....	iv
Table of Contents.....	v
List of Tables	vii
List of Figures	viii
Chapter 1: Introduction and Regional Overview	1
1.1 Introduction.....	1
1.1.1 Hopedale Basin	4
1.1.2 Cartwright Arch and Hawke Basin	5
1.1.3 St. Anthony Basin	5
1.1.4 Orphan Basin	6
1.2 Tectonic Framework	9
1.2.1 Overview	9
1.2.2 Precambrian and Paleozoic Tectonics	10
1.2.3 Mesozoic Tectonics	18
1.3. Objectives	27
Chapter 2: Data, Methods, Stratigraphic and Seismic Sequences	30
2.1 Introduction:.....	30
2.2 Overview of the Data:.....	30
2.3 Methods.....	34
2.4 Labrador Shelf: Tectonic Stages, Stratigraphic and Seismic Sequences	38
2.4.1 Prerift Sequence	42
2.4.2 Synrift Sequence	46
2.4.3 Predrift Sequence:.....	50
2.4.4 Syndrift Sequence	52
2.4.5 Postdrift Sequence	56
2.5 West Orphan Basin: Tectonic Stages, Stratigraphic and Seismic Sequences.....	58
2.5.1 Prerift Sequence	59
2.5.2 Synrift Sequence	59
2.5.3 Transition to drift sequences:.....	60
2.5.4 Postrift Sequence	63
2.6 St Anthony Basin: Tectonic Stages and Stratigraphic Sequences	64
Chapter 3: Regional Architecture	66
3.1. Objective	66
3.2 Seabed Morphology	66
3.3 Introduction to the Sedimentary Fill	67
3.3.1. Basement Structure	67
3.3.2 Synrift Sedimentary Fill.....	71
3.3.3 Postrift Sedimentary Fill	76

3.4. Structural History.....	82
3.4.1. Prerift Structure.....	82
3.4.2. Synrift Structure.....	85
3.4.3. Postrift Structure.....	87
3.5. Regional Gravity Anomalies.....	90
3.6 Summary of Observations.....	91
Chapter 4: Rift Systems.....	94
4.1 Rift System Structure.....	94
4.2 Classification of Rift Systems.....	95
4.2.1 South Hopedale Basin.....	98
4.2.2 Orphan Basin.....	101
4.3. Summary.....	106
Chapter 5: Analysis of Extension.....	108
5.1. Lithospheric Stretching.....	108
5.2. Methods.....	110
5.2.1 Time interpretation.....	110
5.2.2. Depth conversion.....	111
5.3 Restoration Techniques.....	123
5.4 Section balancing.....	124
5.5 Backstripping.....	127
5.6 Results.....	132
5.6.1 Hopedale Basin.....	145
5.6.2 Orphan Basin.....	147
5.7 Considerations.....	148
Chapter 6: Petroleum Prospectivity.....	153
6.1 Petroleum Overview.....	153
6.2. South Hopedale Petroleum System.....	154
6.2.1 Reservoir Potential.....	156
6.2.2 Source Potential.....	159
6.2.3 Petroleum Entrapment.....	161
6.2.4 Maturation and Thermal Evolution.....	163
6.2.5. Prospectivity.....	165
6.3 West Orphan Basin Petroleum System.....	170
6.3.1 Reservoir Potential.....	171
6.3.2. Source Potential and Maturation.....	173
6.3.3. Petroleum Entrapment.....	177
6.3.4 Prospectivity.....	179
6.4 Summary.....	184
7.0 Conclusions.....	185
References.....	190

List of Tables

Chapter 2

Table 2.1. Location, status, total depth (TD), spud and velocity data for the Labrador Shelf and Western Orphan Basin wells in the study area.

Chapter 5

Table 5.1. This table indicates the extended and unextended lengths, the actual and percentage extension, as well as the extended to unextended ratio (β factor) for each profile. These values were obtained from backstripped vertical slip restorations, fault heave measurement, as well as vertical slip kinematic restorations without application of decompaction and isostatic corrections.

Table 5.2. This table indicates the total basement length, the measured fault heaves across the top basement, the calculated unextended profile length and the measured extended profile length. The β factor is calculated from the extended to unextended profile length ratio. A more detailed explanation of this process is contained in the text. A similar procedure was carried out for each profile, with the results summarized in Table 5.1.

List of Figures

Chapter 1

Figure 1.1. Basins and structural features located offshore northeast Newfoundland and Labrador. Mesozoic basins are shown in yellow, Late Paleozoic (Carboniferous) in orange and Early Paleozoic in pink. The dashed line indicates the study area. (Modified from Enachescu, 2006 c).

Figure 1.2. Appalachian Tectono-stratigraphic zones within the island of Newfoundland in relation to Paleozoic Basins. Light grey=tectonic zones; Grey= Upper Paleozoic basins; Dark grey= Lower Paleozoic basins.

Figure 1.3. Regional framework for the Orphan Basin in relation to the Jeanne d'Arc and Flemish Pass basins, the Flemish Cap, and Orphan Knoll (Enachescu et al., 2005).

CGFZ=Charlie Gibbs Fracture Zone; CBFZ=Cumberland Belt Fault zone. Bathymetry and ODP sites from Tucholke et al., 2004.

Figure 1.4. Precambrian Tectonic Provinces in northeastern Canada. (Modified from Funck et al., 2001).

Figure 1.5. Lithotectonic zones of the Newfoundland Appalachians. BBL Baie Verte-Brompton line. From Valverde-Vaquero and van Staal (2001).

Figure 1.6. Magnetic Anomaly map for the Labrador Sea. Thick red lines are magnetic anomalies, dashed black line represents the extinct spreading ridge, thick black lines are fracture zones, and thin black lines are bathymetry. Modified from Roest and Srivastava (1989).

Figure 1.7. Crustal reconstruction of the Greenland-Labrador conjugate margin at the point of break-up, corrected for the effects of sediment and water loading. The rift appears to be asymmetric, with a thinned continental crust on the Labrador side on the margin. Red and yellow sections are interpreted to result from serpentinization of mantle. From Chian et al. 1995 *a, b*; Loudon, 2002.

Chapter 2

Figure 2.1. Reflection seismic lines used in the study. Lines shown in blue are older vintage (pre 1985), while those shown in red were acquired during recent surveys in 2003, 2004 and 2005 by Geophysical Services Incorporated (GSI).

Figure 2.2. Lithostratigraphic ties for the Gudrid H-55 borehole. This well is located on a basement horst and did not intersect the synrift sequence. However, synrift Bjarni Formation sediments are interpreted to exist in lows adjacent to the high.

Figure 2.3. Lithostratigraphic ties for the Roberval K-92 and C-02 wells. The Roberval C-02 well was located at the crest of a basement high and did not intersect any synrift sediments. Roberval K-92 was located on the flank of the high and intersected a thin synrift sequence.

Figure 2.4 Lithostratigraphic ties for the Cartier D-70 borehole. The synrift sequence is absent at this location.

Figure 2.5. Lithostratigraphic ties for the North Leif I-05 well. This borehole intersected a full synrift sequence, including Alexis Formation volcanics.

Figure 2.6. Lithostratigraphic ties for the Leif M-48 borehole. A time-depth conversion was obtained by plotting the velocity functions from nearby wells onto a single graph and taking a curve of best fit as no direct velocity information is available for the well. The obtained curve tied the upper postrift markers to the seismic satisfactorily, but misties occur deeper within the borehole.

Figure 2.7. Lithostratigraphic ties for the Indian Harbour M-52 well. The velocity curve for this location is derived from a sonic log, which may account for the misties in the borehole.

Figure 2.8. Lithostratigraphic ties for the Freydis B-87 well. Prerift basement is composed of Ordovician limestones and siltstones at this location.

Figures 2.9a and 2.9b. Lithostratigraphic ties for the Hare Bay E-21 well following both Labrador (left) and Jeanne d'Arc(right) stratigraphic nomenclature. The Labrador lithostratigraphic picks are from Moir (1989) and the Jeanne d'Arc picks are from the C-NLOPB. Jeanne d' Arc stratigraphy is currently in use for the Orphan Basin, as this area likely contains sequences similar to the Jeanne d'Arc Basin. The western portion of the Orphan Basin, however, likely contains stratigraphy similiar to that encountered on the Labrador Shelf. Both sets of picks were tied to the seismic markers to help relate the stratigraphy between the Orphan and Hopedale basins. Additionally, postrift unconformities (red and gold horizons) that were mapped throughout the western Orphan Basin are identified in Figure 2.9b.

Figure 2.10. Lithostratigraphic picks for the Baie Verte J-57 borehole. Two postrift unconformities (red and gold horizons) and a top synrift unconformity (green horizon) mapped from regional seismic markers are also shown. The Kenamu Formation marker was mapped from the Hare Bay E-21 well.

2.11. Lithostratigraphic picks for the Blue H-28 well. The synrift sequences was not encountered in the borehole but is interpreted in the half graben adjacent to the basement

high. Postrift unconformities (red and gold horizons) interpreted from regional seismic markers are also shown.

Figure 2.12. Lithostratigraphic picks for the Bonavista C-99 borehole. This location encountered a thick postrift succession but a very thin synrift sequence. Postrift unconformities (red and gold horizons) interpreted from regional seismic markers are also shown.

Figure 2.13. Lithostratigraphic ties for the Cumberland B-55 and Sheridan J-87 wells. Postrift (red and gold horizons) and synrift (green horizon) unconformities are also shown. The time depth data for the Sheridan J-87 well is derived from sonic logs, which may account for the Base Tertiary unconformity and basement misties.

Figure 2.14. Lithostratigraphic ties for the Linnet E-63 borehole. Postrift unconformities (red and gold horizons) and top synrift unconformity (green horizon) interpreted from regional seismic markers are also shown.

Figure 2.15. Lithostratigraphy, geodynamic stages, structural styles and seismic markers for the Labrador Shelf. Modified from Enachescu et al., 2007.

Figure 2.16. Synrift seismic sequence at the North Leif I-05 well. Top synrift unconformity (Avalon Unconformity) coincides with the top of the Bjarni Formation (green horizon).

Figure 2.17. Postrift seismic sequence, including Gudrid Member sands (yellow interval) at the Gudrid H-55 borehole location.

Figure 2.18. Seismic sequences at the Freydis B-87 well. At this location, prerift basement is composed of Ordovician siltstones and limestones. The Freydis, Gudrid and Leif Members (highlighted in yellow) are identified within the postrift sediments.

Figure 2.19. Lithostratigraphy and associated tectonic stages for the Hopedale, St. Anthony and West Orphan basins.

Figure 2.20. Seismic sequences within the Orphan Basin. Highly faulted synrift sediments are overlain by predominantly horizontal postrift layers. In places, the Paleogene and Neogene postrift sequences are deformed due to movement of underlying synrift and basement structures.

Chapter 3

Figure 3.1. Depth to water bottom in metres. Regional seismic grid is indicated by thin black lines.

Figure 3.2. Representative profile for the South Hopedale Basin extending past the continental slope and into deep water. The pre-, syn- and postrift tectonic sequences are indicated on the inner part of the shelf. Typical horst and graben structures are evident and an extensional fault system exists within the postrift sequence below the outer shelf and slope. A compensation feature is interpreted downslope from the fault system. Further seaward, a tentative interpretation of exhumed continental mantle, based on refraction studies north of the area of interest, is indicated (Chian et al., 1995 *a*; Chian et al., 1995 *b*).

Figure 3.3. Profile extending across the Paleozoic St. Anthony Basin, Cartwright Arch and deepwater areas north of the West Orphan Basin. A Paleozoic sequence is evident in the area of the St. Anthony Basin, and several strike slip faults are interpreted in the basin and through the Cartwright Arch. Further seaward, the arch is disrupted by extensional faults and overlapped a thin, Mesozoic synrift sequence. A basement high feature that resulted in uplift of the Base Tertiary and Baffin Bay and Postrift 1 unconformities is located to the east of the profile. Comparisons of this structure to the Mauzy peridotite ridge show similarity.

Figure 3.4. Representative profile across the West Orphan Basin and the Central Orphan High. The western side of the profile is characterized by a thick postrift sequence and a thinner synrift sequence. Towards the east, the postrift sequence thins while the synrift

sequence is thicker and more extensively faulted. The listric faults bounding the half graben structures also have more kinks towards the east and recent movement and reactivation is evident as one of the faults breaches the waterbottom marker. Additionally, uplift of the top synrift and Base Tertiary unconformities in places suggests that reactivation of basement structures occurred during postrift time.

Figure 3.5. Representative profile across the West Orphan Basin and the eastern East Orphan Basin. The western side of the profile is characterized by a thick postrift sequence and a thinner synrift sequence. Towards the east, the postrift sequence thins while the synrift sequence is substantially thicker and more extensively faulted. A reverse fault (shown in orange) in the synrift rollover anticline structure towards the east side of the profile indicates transtensional movement that was likely caused by the rotation of the extension vector associated with each rifting episode. Pink areas within the prerift basement are interpreted to be Late Paleozoic sedimentary sequences.

Figure 3.6. Schematic model of principal seismic characteristics of contourite drifts. Modified from Stow et al, 2002.

Figure 3.7. Time-depth map to the top of prerift basement, showing major basin border faults and intrarift fault systems. Dashed white boxes indicate areas interpreted as accommodation zones. CGFZ=Charlie Gibbs Fracture Zone.

Figure 3.8. Synrift isopach map of the South Hopedale Basin. The sequence is thickest within half graben structures on the inner shelf. Stratigraphic growth is suggested by the thickening of the sequence towards the bounding faults. The sequence thins seawards, but localized areas of thicker sedimentation occur on the outer shelf and slope break.

Figure 3.9. Synrift isopach map for the West Orphan Basin. The sequence is thickest along the western margin (Bonavista Fault zone) and within half graben structures in the central and eastern areas. Thickening of the sequence towards marginal faults is evident in these locations. The sequence thins over intrabasin ridges in the central part of the basin, and also in the southwest and northeast areas.

Figure 3.10. Postrift isopach map for the South Hopedale Basin. The sequence thickens seawards, which suggests that the shoreline prograded eastwards. The sequence thins substantially towards Cartwright Arch in the southwest.

Figure 3.11. Post rift isopach map for the West Orphan Basin. The sequence is thickest along the western margin and thinner towards the east.

Figure 3.12. Free_Air gravity (2000m grid spacing), showing basin bounding faults and regional tectonic framework interpreted from the top prerift time structure map.

Chapter 4

Figure 4.1. Displacement transfer by vertical or near vertical transfer faults in a three-dimensional extensional fault system (hard linked model). Modified from McClay and White (1995).

Figure 4.2. Displacement transfer by an accommodation zone in a three dimensional extensional fault system (soft linked model). Modified from McClay and White, 1995).

Figure 4.3. Mapped Labrador Extensional fault system. Extensional directions associated with each rifting phase are indicated by red arrows. Adapted from McClay et al. (2002).

Figure 4.4. Analogue model of a low-extension orthogonal rift system. Rift border and intra-rift faults are more linear than those associated with an oblique system. Subbasins within the rift zone are isolated. Modified from McClay et al. (2002).

Figure 4.5. Interpreted hard-linked transfer zone within the southern Labrador Shelf. Transfer Fault is shown in orange, and interpreted profiles are highlighted on location map in blue.

Figure 4.6. Mapped extensional fault system in the West and Central Orphan Basin. Extension directions associated with each rifting episode are indicated by red arrows. Dashed red boxes signify interpreted accommodation zones. CGFZ-Charlie Gibbs Fracture Zone, CBTZ= Cumberland Belt Transfer Zone.

Figure 4.7. Analogue model of a highly extended oblique rift system. Faults have a sigmoidal shape and form an en-echelon pattern. Rift border faults are segmented and linked by relay systems. Modified from McClay et al, 2002.

Figure 4.8. Dip line profiles from the West and central Orphan Basin indicating a change in polarity of extensional faults and half graben structures. Profile A shows a westward dipping half graben structure and westward dipping extensional faults. Profile B shows elevated prerift basement and a smaller half graben structure. Profile C depicts the development of eastward dipping half graben and extensional faults, which suggests that an accommodation zone exists between the two profiles. A corresponding strike profile (above) shows a zone with an elevated prerift basement and highly deformed synrift sediments, further implying that an accommodation zone is present.

Chapter 5

Figure 5.1. Location map showing profiles used in the backstripping and balanced section reconstructions.

Figure 5.2. Time interpretations for the Hopedale and West Orphan basins. Colors correspond to specific tectonic sequences, as indicated on the time scale chart.

Figure 5.3. Above: Interval velocities obtained from borehole data, with colors referring to corresponding tectonic sequences: Dark Yellow=Postdrift, Purple=Synrift, Brown=Predrift, Green=Synrift. Below: Velocity profile from wide angle seismic refraction data acquired on the Labrador Shelf, north of the area of interest. Colours (yellow, green, orange and red) approximate velocity contours (Chian et al, 1995a; Chian et al., 1995b).

Figure 5.4. Plot of interval velocities vs. two-way travel time for the Labrador Shelf boreholes. The velocities obtained for the postrift sequence are consistent but greater variation occurs within the synrift sequence. Freydis B-87 was the only borehole with velocity data for the prerift sequence, which are identified by the sharp velocity increase at approximately 1.8s.

Figure 5.5 Graphical representation of the prerift interval velocity variation within the Freydis B-87 borehole. The red arrow and dashed line indicate the chosen velocity value, which is higher than the velocities obtained from the borehole data. The chosen value is largely based on refraction data, as only a few boreholes intersected the prerift sequence and velocity information was limited to the Freydis B-87 well.

Figure 5.6. Graphical representation of the synrift and predrift interval velocities from borehole data. The red arrows and dashed lines indicate the estimated velocities used in the depth conversion, which were derived from a combination of borehole and refraction seismic data.

Figure 5.7. Graphical representation of the syn- and postdrift interval velocities from borehole data. The red arrow and dashed line indicate the estimated velocities used in the depth conversion, which were derived from a combination of the borehole and refraction seismic data.

Figure 5.8. Interval velocities for the West Orphan Basin derived from borehole data and reflection seismic processing. Colors represent the interpreted tectonic sequences: Blue-green= Postrift Tertiary sequence, Yellow= Cretaceous postrift and synrift sequences, pink=prerift sequence.

Figure 5.9. Graphical representation of the borehole and seismic processing interval velocities vs. two-way travel time. Hare Bay E-21 has lower velocities which may be attributed to shallower water depths and location outside the main part of the basin. The remaining boreholes have more consistent time-velocity curves with the highest velocities occurring in the Bonavista C-99 borehole. The interval velocities derived from reflection seismic processing are from a range of water depths.

Figure 5.10. Graphical representation of borehole and seismic processing interval velocities for the prerift, synrift and Cretaceous postrift sequences. The velocities applied for depth conversion are indicated by the red arrows and dashed lines.

Figure 5.11. Graphical representation of the tertiary postrift interval velocities from both borehole data and seismic processing velocities. The estimated velocity used for the depth conversion is indicated by the red arrow and dashed line.

Figure 5.12. Estimated velocities used to convert the time sections to depth. The values are obtained from a combination of borehole data and velocities applied during processing of a reflection seismic line north of the West Orphan Basin.

Figure 5.13. Schematic diagram depicting the mantle depression associated with water loading.

Figure 5.14. Area balance for extension. l_0 is the original length of section which is compared with the length in the deformed state and area, d is the depth to detachment (Modified from Gibbs, 1983).

Figure 5.15. Comparison of vertical and oblique slip kinematic models. These types of models are typically applied in extensional environments, and are based on area

preservation between deformed and restored states. The vertical slip model maintains horizontal bedlength distances.

Figure 5.16. The principles of Airy backstripping. Modified from Watts, 2001.

Figure 5.17. The principles of flexural backstripping. The shaded region shows a wedge of sediments. The dashed line shows where the sediment wedge would be in the absence of sediment loading. Modified from Watts, 2001.

Figure 5.18. Restored and balanced Labrador Shelf profiles. Each color represents a tectonic sequence, as indicated on the timescale chart. The top profile represents the present day margin stratigraphy and structure. on the margin. Each subsequent profile is backstripped and isostatically adjusted to represent the structure and stratigraphic configuration of the margin during each tectonic stage.

Figure 5.19. Restored and balanced West Orphan Basin profiles. Each tectonic sequence is represented by a color, as indicated on the timescale chart. The top profile represents the present day stratigraphy and structure on the margin. Each subsequent profile is backstripped and isostatically adjusted to represent the structure and stratigraphic configuration of the margin during each tectonic stage.

Figure 5.20. Areal distribution of calculated extension values in the West Orphan and South Hopedale basins. β values estimated from profile restorations are shown in red, and β values calculated from fault heave measurement are shown in black.

Figure 5.21. Example of a fault heave measurement.

Figure 5.22. Comparisons of vertical slip reconstruction with and without isostatic and decompaction corrections applied (left and right sides, respectively). The unextended length is less on the uncorrected profile, which implies that the isostatic and decompaction corrections affect the vertical slip restorations.

Figure 5.23. Typical “Steer’s head” geometry showing onlap of postrift sediments onto prerift basement at the basin margin.

Figure 5.24. The faulted synrift sequence in the South Hopedale Basin is truncated by the Avalon unconformity (green horizon), which implies that this sequence is partially eroded.

Figure 5.25. The faulted synrift sequence in the West Orphan Basin is truncated by the Avalon unconformity (green horizon), which implies that this sequence is partially eroded.

Figure 5.26. Schematic diagram showing the mass water depth, sediment and basement thickness, and mantle upwarp (X) along a typical West Orphan Basin profile. Depth of compensation used in the mass balance is 25 km.

Chapter 6

Figure 6.1. Discovered resources on the Labrador Shelf. Modified from Department of Mines and Energy, Government of Newfoundland and Labrador, 1993.

Figure 6.2. Labrador lithostratigraphy, with proven and potential reservoir and source rocks indicated on applicable formations. Modified from McWhae et al., 1980 and Enachescu, 2006a.

Figure 6.3. Map of the synrift Bjarni Formation, which contains proven source and reservoir units.

Figure 6.4. Map of the postrift Cartwright Formation. The Gudrid Member sands are present along the inner shelf. In this region, however, the thickest sequences are adjacent to immature or marginally mature source intervals, so the reservoir prospectivity is limited.

Figure 6.5. Map of the postrift Markland Formation. The extension of this sequence onto the outer shelf and slope indicates significant source potential, as progressively younger sequences are predicted to become mature seawards (Beaumont and Issler, 1987).

Figure 6.6. Petroleum traps targeted on the Labrador Shelf, which include: drape of Bjarni sandstones over basement horsts (top left), pinchout of Bjarni sandstones against tilted fault blocks (bottom right), drape of lower Tertiary marine sandstones above basement horsts forming anticlinal closure traps (top right and bottom left), listric faults and associated roll over-anticlines in the outer shelf (top right), and preserved Paleozoic reservoirs on rotated basement blocks (bottom right).

Figure 6.7. Comparison of mapped Cartwright, Markland and Bjarni formations on the Labrador, with thick, potential source and reservoir units indicated by dashed white circles.

Figure 6.8. Deepwater petroleum prospect located northwest of the Gudrid and Roberval wells. Numerous extensional faults within the postrift sequence and drape of Bjarni and Markland sequences over elevated prerift basement are potential trapping mechanisms. Bjarni, Markland and Early Tertiary shales are potential source intervals, while Bjarni Formation and Leif Member sandstones are prospective reservoirs.

Figure 6.9. Petroleum prospect on the outer shelf southeast of the Indian Harbour well. Drape of the Bjarni Formation over a basement high forms a potential structural trap. Bjarni, Markland and Early Tertiary shales are potential source intervals, while Bjarni Formation and Leif Member sandstones are prospective reservoirs.

Figure 6.10. Petroleum prospect on the outer shelf northeast of the North Leif I-05 well. Drape and pinchout of the Bjarni Formation over rotated basement blocks are potential structural traps. The Bjarni, Markland and Early Tertiary shales are potential source intervals, while Bjarni Formation and Leif Member sandstones are prospective reservoirs. Paleozoic carbonate reservoirs within the prerift basement are also targets in this area. The Bjarni shales, which are marginally mature in the North Leif I-05 well, may be mature enough for significant hydrocarbon generation at this location.

Figure 6.10. Lithostratigraphy for the West Orphan Basin, with potential source and reservoir units indicated. Modified from C-NLOPB, 2007.

Figure 6.11. Map of the West Orphan Basin synrift sequence, which likely contains reservoir and source intervals equivalent to the Bjarni Formation sandstones and shales. The thickest, and most prospective, sequences are located adjacent to the Bonavista platform and in half graben structures towards the central and eastern part of the basin.

Figure 6.12. Map of the West Orphan Basin Late Cretaceous postrift sequence, which likely contains sandstone intervals sourced from the Bonavista Platform or intrabasin ridges. The thicker sequences in the central areas are prospective as they appear to have structural closure.

Figure 6.13. Map of the West Orphan Basin Early Tertiary postrift sequence, which contains organic rich Tertiary marine shales. These shales are thickest in the West Orphan Basin, and comparisons to Figure 6.14 indicate that the thickest sequences correspond with thick sequences of mid-to-Late Tertiary sediments, suggesting that the shales are buried at sufficient depths for maturation.

Figure 6.14. Map of the mid- to Late Tertiary postrift sequence, which is thickest in the West Orphan Basin. Comparisons to Figure 6.13 indicate that the thickest sequences correspond with thick sequences of Early Tertiary sediments, suggesting that the Early Tertiary shales are buried at sufficient depths for maturation.

Figure 6.15. Petroleum traps targeted in the West Orphan Basin, which include: drape of synrift Cretaceous sandstones over basement horsts (top and bottom left), pinchout of synrift Cretaceous sandstones against tilted fault blocks (bottom right), drape of lower Tertiary sandstones above basement horsts and Tertiary prograding sedimentary wedges (top right and bottom left), and preserved Paleozoic reservoirs on rotated basement blocks (bottom right).

Figure 6.16. Comparison of the mapped intervals in the West Orphan Basin. The synrift and Early postrift sediments (bottom right and upper left, respectively) are prospective reservoir bearing intervals, with potential targets are indicated by the dashed white circles. Maps of the Early Tertiary and overlying sedimentary cover (bottom right and upper right, respectively) suggest that the western area of the basin contains thick sequences of Early Tertiary marine organic rich shales that may be buried at sufficient depths for maturation.

Figure 6.17. Prospective area in the central West Orphan Basin. Major targets include synrift Early Cretaceous sandstones and older Mesozoic or prerift Paleozoic sandstones or carbonates, an early postrift Late Cretaceous fan, as well as drape of Tertiary postrift sandstones over rotated basement blocks. Potential source intervals include Early Cretaceous Bjarni equivalent shales, Late Cretaceous Markland equivalent shales or early Tertiary marine shales.

Figure 6.18. Prospective area in the northwest West Orphan Basin. Major targets include drape of synrift Early Cretaceous sandstones over prerift basement, and Tertiary prograding wedges over a prerift basement high. Potential source intervals include Early Cretaceous Bjarni equivalent shales, Late Cretaceous Markland equivalent shales or early Tertiary marine shales.

Figure 6.19. Roll-over anticline in the central West Orphan Basin. The rollover structure is interpreted to contain Early Cretaceous and possible Jurassic sandstone reservoirs sourced by Early Cretaceous Bjarni Equivalent or possible Kimmeridgian Jurassic shales. Secondary targets include drape of Tertiary sandstones over the structure, which could be sourced by Late Cretaceous Markland equivalent shales.

Chapter 1: Introduction and Regional Overview

1.1 Introduction

The area offshore northeastern Newfoundland and southern Labrador encompasses the western Orphan Basin, Cartwright Arch, St. Anthony Basin, Hawke Basin and southern Hopedale Basin, as shown in Figure 1.1. The rock record here includes evidence of Precambrian, Paleozoic and Mesozoic-Cenozoic geological events, making the area an ideal location to investigate the relationship between contemporary rift-related structures and features associated with earlier tectonic cycles. The Labrador Shelf was explored for petroleum during the 1970s and early 1980s and several large gas deposits were discovered. As the exploration focus was for oil at that time, these fields were not developed. Their presence, however, proves the existence of a rich petroleum system (Enachescu, 2006 *a*). When compared to more southern Grand Banks basins, the Orphan Basin is relatively unexplored due to its northerly location and deep water setting. Recently, the basin has experienced renewed interest and exploration, as the eastern portion of the basin likely contains Jurassic sedimentary rocks similar to those sourcing the hydrocarbons in the producing Jeanne d'Arc Basin (Enachescu et al., 2005). In addition, the western side of the basin is thought to contain a petroleum system comparable to that encountered on the Labrador Margin.

The thesis objectives are to compare the tectonic evolution, structural framework and seismic stratigraphy of the Hopedale, West Orphan, and St. Anthony basins. Additionally, the petroleum potential of the region will be investigated. These objectives are achieved through correlation of borehole data and 2D reflection seismic profiles, mapping of the major tectonic sequences and balanced section restoration. A more detailed description of the objectives is contained in section 1.3

1.1.1 Labrador Shelf

The Labrador Shelf is an Atlantic-type extensional margin within the southern zone of extended cratonic and oceanic crust connecting the Arctic and Atlantic Ocean basins (Balkwill, 1987; Balkwill et al., 1990; Enachescu, 2006 *a*). Initially part of a Mesozoic intracontinental basin network formed between North America and North Africa and Europe, the region has first order attributes for classification as an Atlantic type margin (Balkwill, 1987; Balkwill et al., 1990; Bell, 1989; Enachescu, 2006 *a*). These attributes include:

- 1) Merging of a flat continental shelf and a more steeply inclined continental slope, with the outer shelf and slope comprising a thick prism of seaward dipping Late Cretaceous and younger clastic sediments;
- 2) Position of landward sections of the shelf prism over extended continental crust. These sections locally contain large, fault bounded Early Cretaceous and early Late Cretaceous synrift clastics. The outer part of the shelf prism lies on and is intercalated with thick basalts, possible gabbros and peridotites associated with transitional and oceanic crust domains;

3)

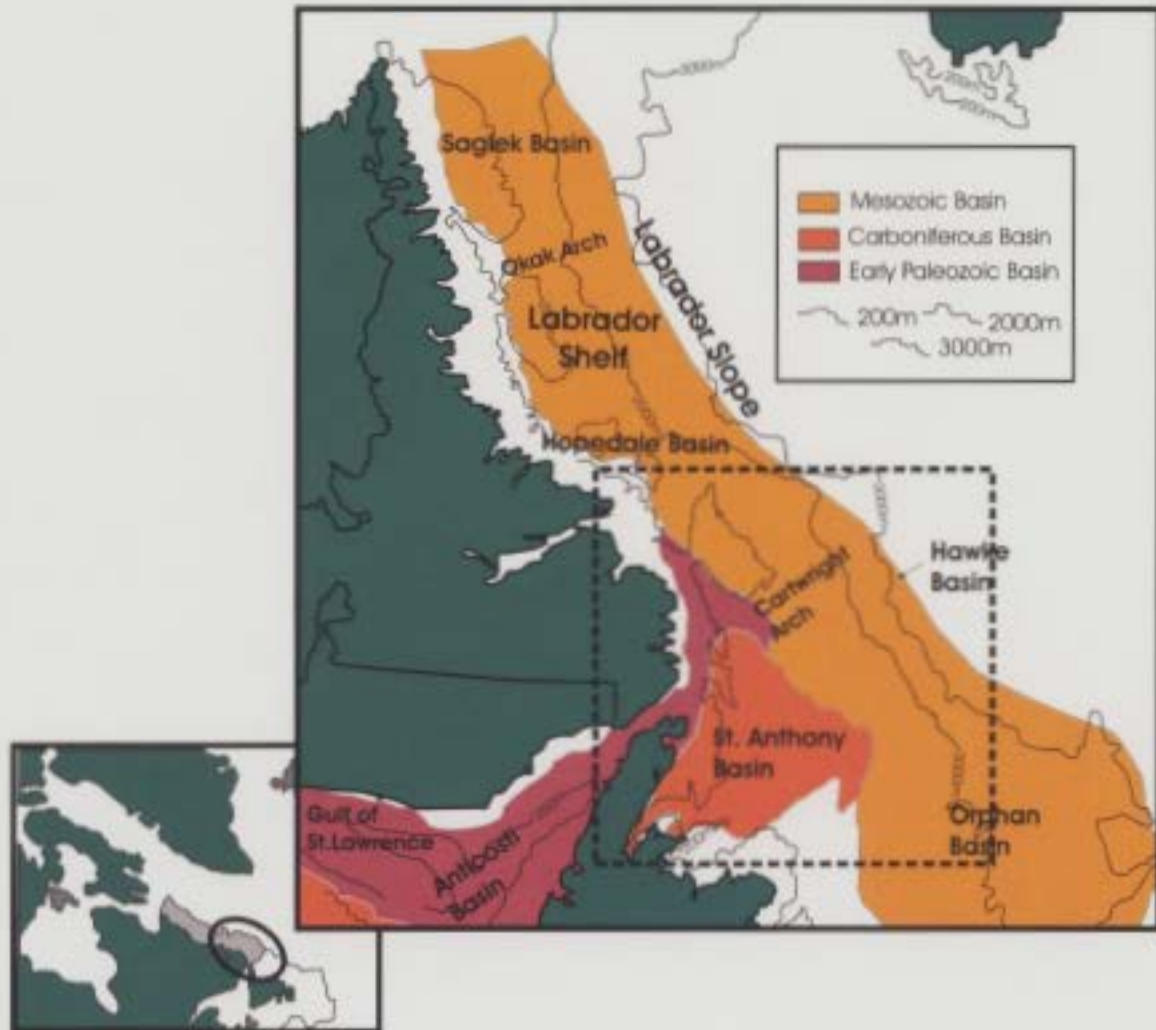


Figure 1.1. Basins and structural features located offshore northeast Newfoundland and Labrador. Mesozoic basins are shown in yellow, Late Paleozoic (Carboniferous) in orange and Early Paleozoic in pink. The dashed line indicates the study area. (Modified from Enachescu, 2006 c)

- 3) Indication that all late Phanerozoic structures are products of crustal or supra-crustal extension with no evidence of significant lateral compression.

The Labrador margin contains approximately four million cubic kilometres of Cretaceous, Tertiary and Quaternary terrigenous clastic sediments derived from

widespread erosion of central Canada and local erosion of coastal uplands and intrabasinal ridges during Phanerozoic separation of Greenland and North America. Approximately half of this material comprises terrace prisms along the Labrador and Greenland cratonic margins, with the remainder forming a thick blanket on the basin floor (Balkwill, 1987; Bell, 1989; Balkwill et al., 1990).

1.1.2. Hopedale Basin

The Hopedale Basin lies within the southern part of the Labrador Shelf and is positioned north of the St Anthony Basin and Cartwright Arch, as indicated in Figure 1.1. The basin is approximately 500 kilometres long and up to 200 kilometres wide, and is situated in water depths ranging from 100 to 3000 metres (Balkwill, 1987; Enachescu, 2006). On the western flank of the basin, cratonic basement is disrupted by a complex system of Cretaceous rift faults (Bell, 1989; Structure III). This faulted area ranges in width from 40 km in the north to 120 km in the south (Balkwill, 1987; Bell, 1989). Recent glaciation is evident and several banks, plateaus and troughs are apparent along the shelf section. The slope is relatively gentle with fewer canyons than the Scotian Shelf or Southern Grand Banks margins (Enachescu, 2006 *a*). The Hopedale Basin is bounded in the west by onlap of Mesozoic beds onto either a prerift basin hinge zone or, in certain places, a basin bounding fault. In the south, the Cartwright Transfer Fault zone separates the basin from the Cartwright Arch, while in the north an implied transfer zone partitions it from the Okak Arch and Saglek Basin (Figure 1.1) (Enachescu, 2006 *a*).

1.1.3 Cartwright Arch and Hawke Basin

The Cartwright Arch is a broad, northeast plunging prerift basement high comprised of shelf and upper slope areas that lie seaward of the Grenville Tectonic Province outcrop and south of the Hopedale Basin (Balkwill, 1987; Enachescu, 2006 *b*). In this area, the seabed is underlain by Paleogene and Neogene sequences that overlie a strongly reflective prerift basement. Towards the inner northwest part of the arch, a half graben containing Barremian-Coniacian sediments opens and plunges northwards towards the Hopedale basin (Balkwill, 1987). This complex half graben contains a large, westward dipping, basin bounding fault (Balkwill, 1987). The upper slope section, located approximately 120 km offshore, is identified with a zone of east dipping faults that separate rotated basement blocks (Enachescu, 2006 *b*).

The Mesozoic Hawke Basin lies east of the Cartwright Arch (Enachescu, 2006 *b*). This basin, which is structurally connected to the Hopedale Basin, has not been extensively studied because of its location in deeper water. The Hopedale and Hawke basins are separated by the Cartwright Transfer Fault Zone (CTFZ), which is marked by abrupt changes in the direction of structural lineaments (Enachescu, 2006 *b*).

1.1.4 St. Anthony Basin

The Paleozoic St. Anthony Basin is bordered by the Orphan Basin in the southeast, the southern Anticosti Basin in the northwest and the Cartwright Arch in the northeast, as shown in Figure 1.1. The basin is filled with Carboniferous sediments that extend across the southern part of the Labrador Shelf, and is relatively unexplored in

comparison with the Mesozoic continental margin (Bell and Howie, 1990). It is assumed to be a continuation of the Carboniferous sedimentary formations that outcrop in the Bay St. George and Deer Lake sub-basins in Western Newfoundland and the Gulf of St. Lawrence, as shown in Figure 1.2 (Keen et al., 1990). The Bay St. George sub-basin is an extension of the regionally extensive Maritimes Basin, which contains numerous narrow and deep sub-basins filled with Late Devonian to Early Carboniferous, mainly fluvial-lacustrine sediments (Williams, 1974; Bradley, 1982; Hall et al., 1992). These sub-basins formed close to major faults predominantly trending northeastwards parallel to the Appalachian Orogen (Bradley, 1982; Hall et al., 1992). The depth, proximity to major faults, and stratigraphic changes within these sub-basins suggest their development was related to strike-slip fault movements (Bradley, 1982; Hall et al., 1992).

1.1.5. Orphan Basin

Orphan Basin is situated northeast of Newfoundland on the continental margin and covers an approximate area of 160 000 km² (Enachescu et al., 2005). In comparison with more southerly basins on the eastern Canadian continental margin, the Orphan Basin has not been subjected to extensive research or exploratory drilling due to its northerly location and deep water setting (Enachescu et al., 2005). The basin is bounded by the Cumberland Belt Transfer Zone (CBTZ) to the south; the Charlie Gibbs Transform Zone (CGTZ) to the north; the Bonavista Platform to the east and the continental-ocean boundary to the west (Figure 1.3).

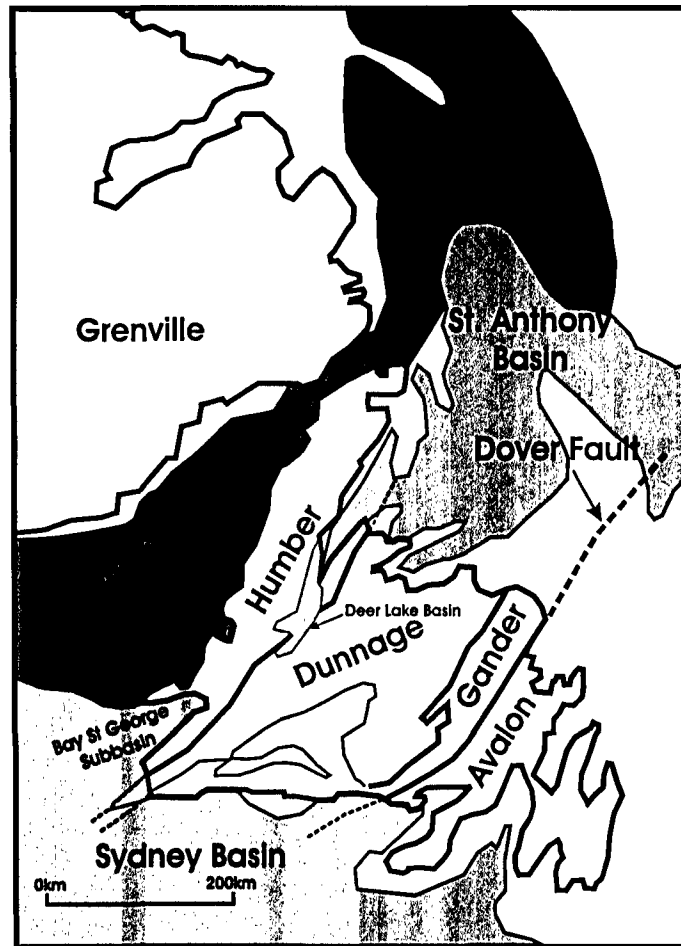


Figure 1.2. Appalachian Tectono-stratigraphic zones within the island of Newfoundland in relation to Paleozoic Basins. Light grey=tectonic zones; Grey= Upper Paleozoic basins; Dark grey= Lower Paleozoic basins

Orphan Basin formed during Mesozoic intra-continental extension and continental break-up associated with the opening of the Atlantic Ocean, and can be subdivided into two parts associated with different rifting episodes. The older, eastern section is situated in water depths ranging from 1500-3000m and developed during a Late Triassic to Early Jurassic rifting episode. In contrast, the younger western section is located in shallower water (1000-1500m) and developed during the latest Jurassic to Early Cretaceous

(Enachescu et al., 2005). The western basin section is of primary focus for this study as it lies adjacent to the St Anthony Basin and south of the Cartwright Arch (Figure 1.1).

The western basinal area is bounded by the Bonavista Fault and its associated imbricates, as shown in Figure 1.3. This crustal detaching fault zone is a continuation of the Murre-Mercury Fault system, which is located in Jeanne d'Arc Basin to the south (Enachescu et al., 2005). The Bonavista platform, a peneplained remnant of the

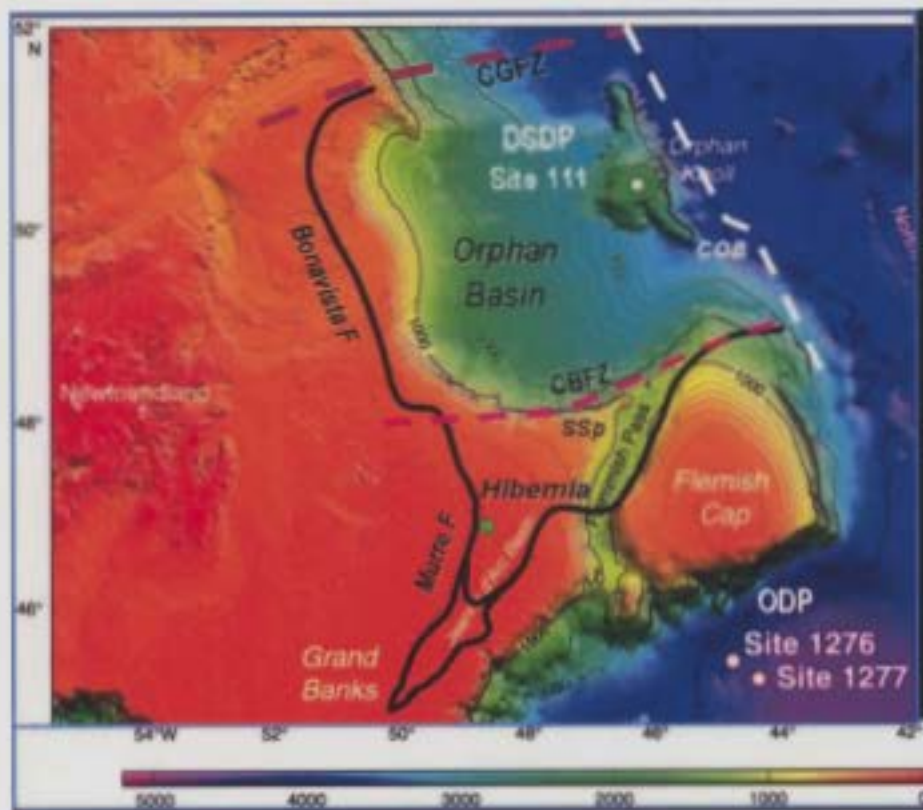


Figure 1.3. Regional framework for the Orphan Basin in relation to the Jeanne d'Arc and Flemish Pass basins, the Flemish Cap, and Orphan Knoll (Enachescu et al., 2005). CGFZ=Charlie Gibbs Fracture Zone; CBFZ=Cumberland Belt Fault zone. Bathymetry and ODP sites from Tucholke et al., 2004.

Appalachian Orogeny, forms the footwall of the fault zone (Enachescu et al., 2005). The northern edge of the basin is considered to be a transfer zone marking the continuation of

the Charlie-Gibbs oceanic fracture zone. This transfer region coincides with a bend in the Bonavista fault (Enachescu et al., 2005). Within the continental crust the fracture zone appears to connect with the Dover fault, a prerift feature separating the Precambrian Avalon platform from the central Appalachian mobile belt. Offshore, the Charlie-Gibbs fracture zone is aligned with the projection of this fault zone, suggesting that the major offset in the Atlantic Ocean crust coincides with the Gander/Avalon collisional zone boundary (Williams et al., 1999; Enachescu et al., 2005). Consequently, the prerift geology may have controlled the position of the Charlie Gibbs fracture zone as well as the different geological styles to the north and south of the margin (Enachescu et al., 2005).

1.2 Tectonic Framework

1.2.1 Overview

The tectonic evolution of offshore eastern Canada can be described within the context of the Wilson Cycle of ocean opening and closing. Structural features between the northwest Orphan and southern Hopedale basins are a result of both Paleozoic and younger Wilson cycles. The Paleozoic cycle involved the opening and closure of the Atlantic Ocean predecessor, the Iapetus Ocean, which closed during the Silurian. During the early stages of the Iapetus cycle, passive margin sediments were deposited on the continental shelf (Williams and Stevens, 1974; Keen et al., 1990). This included an Early Paleozoic limestone platform in the area of the present-day Labrador Shelf (Rodgers, 1968; Keen et al, 1990; Enachescu, 2006 *a*). The closing stage of the Iapetus Ocean

destroyed its western passive margin and resulted in subduction and several accretionary events (Williams, 1979; Keen et al, 1990). Atypical plate interactions associated with this closing also led to the development of several Late Paleozoic basins along the present day Gulf of St. Lawrence and southern Labrador Shelf (Keen et al., 1990; Enachescu, 2006 *a*; Enachescu, 2006 *b*). These basins and the other Paleozoic structures were later modified by Mesozoic rifting and seafloor spreading, resulting in the passive margins that exist along the eastern offshore region today (Keen et al., 1990).

The West Orphan Basin formed during the Late Jurassic to Early Cretaceous and experienced rifting episodes into the Late Cretaceous (Louden, 2002; Enachescu et al., 2005). Development of sedimentary basins between Labrador and Greenland began in the Early Cretaceous due to rifting between North America and Greenland (Balkwill, 1987). By Late Albian time, Greenland separated from Labrador and the Orphan Basin separated from the basins on the Irish conjugate margin (Enachescu et al., 2005). The subsequent onset of sea-floor spreading resulted in the continued opening of the Atlantic, and formation of the Labrador Sea, Baffin Bay and Davis Strait (Balkwill, 1987; Keen et al., 1990; Enachescu et al., 2005).

1.2.2 Precambrian and Paleozoic Tectonics

Prerift basement along the southern Labrador Shelf consists of Precambrian metamorphic and magmatic rocks as well as Paleozoic clastics and carbonates (Balkwill, 1987; Enachescu, 2006 *a*). The Precambrian rocks of Labrador connect the Canadian Shield with similar age rocks of Greenland and North Europe. A series of Proterozoic

accretionary events build out from the Archean cores, which are welded by collisional events. On the Labrador margin, this includes the Nain Province, which was assembled with the North Atlantic Greenland craton and northwest Europe between 1.9 and 1.8 Ga.

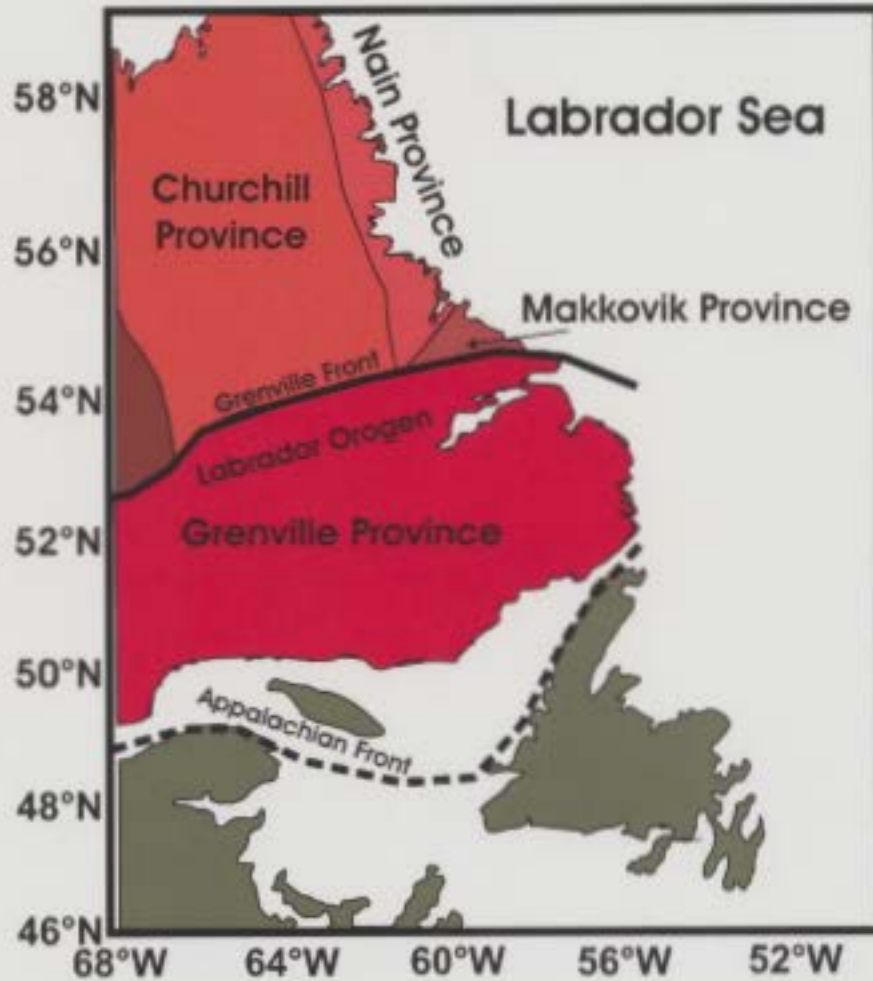


Figure 1.4. Precambrian Tectonic Provinces in northeastern Canada. (Modified from Funck et al., 2001)

Further south, the Labrador margin developed through three main accretionary phases: the first which resulted in the Makkovik-Ketilidian Orogen (1.9-1.7 Ga), a second that created most of the northern Grenville province (1.7-1.6), and a third that led to the

terminal continent-continent collision (Grenville Orogeny: 1.6-1.0Ga) (Wardle and Hall, 2002). Archean rocks are regionally metamorphosed to granulite and amphibolite facies, and later Proterozoic units include amphibolites and lower grade meta-sedimentary terranes with anorthosite and granite plutons. In general, these Precambrian rocks form topographically high, incised and glaciated rims within the shelf, and also form the coastal margins of Labrador, southern Baffin Island and West Greenland (Balkwill et al, 1990).

The island of Newfoundland is situated on the northeast extremity of the Appalachian Mountains, which developed during the formation, evolution and eventual closure of the Iapetus Ocean (e.g. Williams 1979; Chian et al., 1998; D'Lemos and Holdsworth, 1995). Newfoundland terrane can be divided into a series of tectono-stratigraphic zones that were accreted to the Laurentian continent during several orogenic events (e.g. Williams, 1979; van der Velden et al., 2004; Cawood et al., 1995; Langdon and Hall, 1994). From west to east, these are the Humber, Dunnage, Gander and Avalon zones, as shown in Figure 1.5 (Williams and Hatcher, 1982; Williams and Hatcher, 1983; Keen et al., 1990). The geology of these zones preserve remnants of both Laurentian and Gondwanan margins of Iapetus, as well as Iapetus crust itself (Williams, 1979; Chian et al, 1998).

The Humber Zone represents the Laurentian continent and preserves a record of continental margin initiation and destruction associated with the opening and closing phases of the Iapetus Ocean (e.g. Williams, 1979; van der Velden et al., 2004; Cawood et al, 2001; Cawood et al., 1995; Keen et al., 1990; Chian et al., 1998). Structural data

from the Humber zone suggests that Iapetus originated by initial lithospheric stretching, followed by lithospheric dyking, volcanism and accumulation of thick clastic sequences (Williams and Stevens, 1974; Keppie, 1992; Keen et al., 1990). In western Newfoundland the zone contains two tectonic assemblages: an allochthonous upper assemblage including oceanic and continental margin rocks structurally superposed on the shelf during the Taconic Orogeny, and a lower autochthonous sequence comprised of a Cambrian-Ordovician clastic to carbonate shelf succession underlain by Grenvillian basement rocks (Williams and Stevens, 1974; Keen et al., 1987; Hall et al., 1992; van der Velden et al., 2004).

The Dunnage terrane represents vestiges of Iapetus crust thrust against its borderlands during ocean closure (Williams, 1979). Throughout much of the region, early Paleozoic volcanics and associated sediments overlie an ophiolitic substrate (Colman-Sadd and Swinden, 1984; Keen et al., 1986; Keen et al., 1990; Chian et al., 1998). Interaction of the Dunnage zone with both the Humber and Gander zones began during the Ordovician (Arenig) with the emplacement of ophiolites onto the opposing margins of Iapetus (Williams and Stevens, 1974; Piasecki, 1995). The Dunnage zone is thought to be allochthonous over the Gander Zone, as the boundary between the ophiolitic Exploits subzone and granitic Gander zone is tectonic in nature (Kennedy and McGonigal, 1972; Colman-Sadd and Swinden, 1984; Piasecki, 1995).

The Dunnage zone is subdivided into the Dashwoods, Notre Dame and Exploits subzones, which contain rocks with both Laurentian and Gondwanan affinities (Williams et al., 1988; Williams and Piasecki, 1990; Piasecki, 1995; van der Velden et al., 2004).

Both the Dashwoods and Notre Dame subzones have Laurentian attributes, while the Exploits subzone is characteristic of Gondwana (Waldron et al., 1998; Williams 1979; Williams, 1995; van der Velden et al., 2004). The Notre Dame and Exploits regions are separated by the Red Indian line, which is interpreted as an Ordovician suture due to the contrasting stratigraphy, faunal assemblages and tectonics between the two terranes (Williams et al., 1993; Piasecki, 1995).

The Gander zone is a meta-sedimentary unit characterized by thick terrigenous clastic Ordovician and earlier sequences that pass eastward into migmatites (D'Lemos and Holdsworth, 1995; Keen et al., 1986; Keen et al., 1990). The provenance of the meta-sedimentary sequence, the nature and affinities of the underlying basement and the causes and source of granite magmatism in the zone are not well understood (D'Lemos and Holdsworth, 1995). Generally, the terrane is interpreted to represent the distal clastic portion of the passive margin that developed on the Gondwana margin (Williams 1964; Colman-Sadd and Swinden, 1984; Keen et al., 1990; Stockmal et al., 1990; van der Velden et al., 2004). Sediments of the Gander group were deposited from the Middle to Late Cambrian to the Tremadocian, a timespan of approximately 30 Ma (O'Neill, 1991; Colman-Sadd et al., 1992; McNicoll et al., 2001; van der Velden et al., 2004). Locally, Gander group sediments are overlain by allochthonous sheets of Late Cambrian ophiolites associated with the Exploits subzone of the Dunnage terrane (Colman-Sadd and Swinden, 1994; van der Velden et al., 2004).

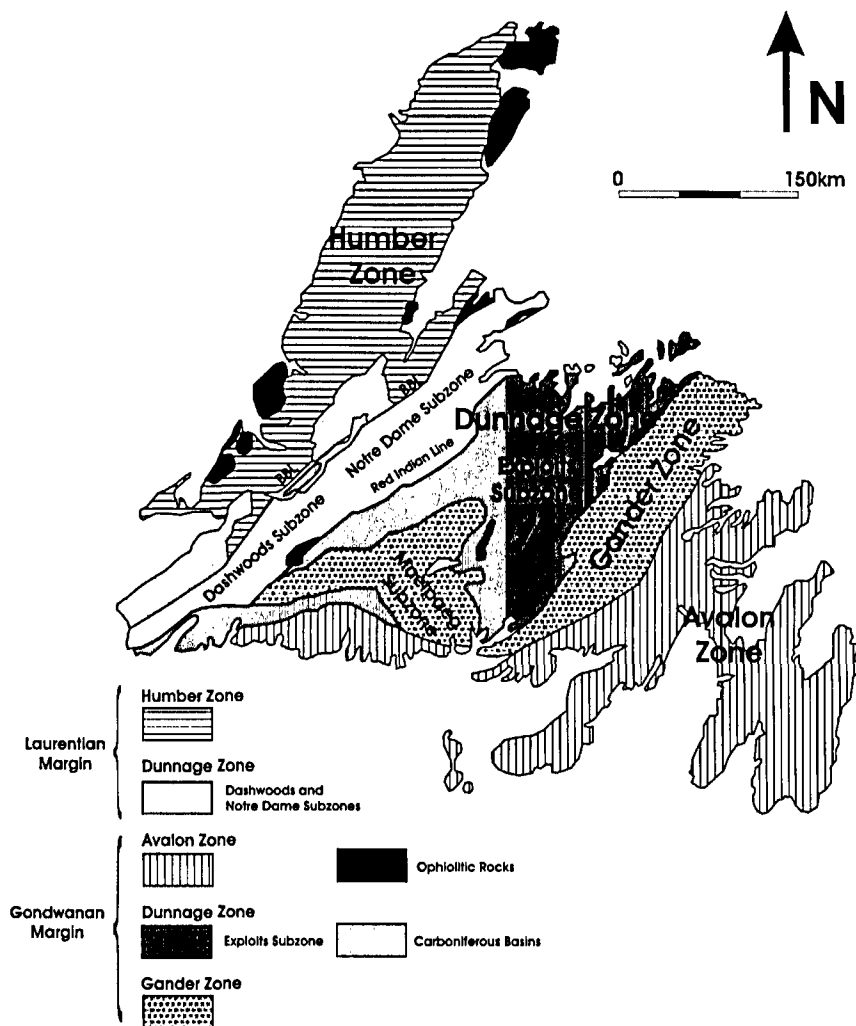


Figure 1.5. Lithotectonic zones of the Newfoundland Appalachians. BBL Baie Verte-Brompton line. From Valverde-Vaquero and van Staal (2001).

The Avalon zone, in contrast to zones to the west, was a stable platform during the early Paleozoic and is characterized by thick upper Precambrian sedimentary and volcanic sequences and overlying Cambrian shales (O'Brien et al., 1983; O'Brien et al., 1986; Keen et al., 1990; Stockmal et al., 1990). This zone is interpreted as an archipelago

of volcanic islands related to subduction and a Pan-African orogenic cycle predating the opening of Iapetus, as detrital provenance studies and paleomagnetic data suggest the region was peripheral to northeastern Amazonia or northwestern Africa (Van der Voo, 1988; Nance and Murphy, 1994; Nance and Murphy 1996; Keen et al., 1990; van der Velden et al., 2004). On land, the Gander-Avalon zone boundary is marked by major subvertical strike-slip faults, known as the Dover and Hermitage Bay faults in Newfoundland (Keen et al., 1986; Stockmal et al, 1990; van der Velden et al., 2004). In contrast to the Gander-Dunnage boundary, the steep ductile shears and brittle strike-slip faults suggest transcurrent movements, rather than collisional motion (Keen et al., 1990).

Appalachian orogenesis in Newfoundland commenced with the Taconic Orogeny, which occurred in two major pulses during the Cambrian-Early Ordovician (Cawood et al., 1995). The first phase relates attempted subduction of the Laurentian margin beneath one or more island arc terranes, and resulted in ophiolite obduction, assembly and emplacement of Taconian allochthons. The second pulse involved short-lived (490-460 Ma) west dipping subduction and consumption of oceanic lithosphere outboard of the accreted Notre Dame subzone (Cawood et al., 1995). By the early Late Ordovician, Laurentian and Gondwanan terranes were juxtaposed along the Red Indian Line and faunal differences between both sides of the orogen had diminished (Williams et al, 1988; van Staal et al., 1998; van der Velden et al., 2004). The Taconian Orogeny was previously thought to involve large-scale subduction, deformation and metamorphism of the Laurentian margin. However, geochronological data from the Humber zone indicate the main metamorphic and deformational events to be Silurian in age (Cawood et al,

1995). Orogenesis occurred throughout the Silurian and into the Early Devonian as a result of closure of the Exploits marginal basin and convergence between Gander and Avalonia (Williams et al., 1993; van Staal et al., 1998; van der Velden et al., 2004). These events led to the Silurian Salinic and Early Devonian Acadian orogenies which are evident from the intense folding, faulting, metamorphism and collision-related plutonism concentrated in the Notre Dame, Dashwoods, Exploits and Gander terranes (Dunning et al., 1990; van der Velden et al., 2004). In the southeastern United States, the Appalachian Orogeny terminated in the Carboniferous with the Alleghanian continent-continent collision. However, in Newfoundland Carboniferous deformation is restricted to strike-slip faulting along the Baie Verte line-Cabot Fault system and associated sediment deposition in pull-apart basins (e.g, Deer Lake sub-basin) (Hall et al.; 1998; van der Velden et al., 2004).

Paleozoic rocks associated with the development and destruction of the Iapetus Ocean are distributed on the seafloor and beneath Mesozoic and Cenozoic sediments throughout the eastern Canadian continental margins (Bell and Howie, 1990). On the southern Labrador Shelf, an unmetamorphosed Lower Paleozoic carbonate platform sequence underlies the Mesozoic sediments. This carbonate sequence is dated as Ordovician and is folded into a northwest trending anticlinorium. The anticlinorium may have existed prior to Mesozoic rifting or resulted from tilting during the early stages of rifting within the Labrador Sea (Bell and Howie, 1990). Lower Paleozoic sediments are also present on the northeastern Newfoundland shelf and are overlain locally by upper Paleozoic units. These units outcrop on the Notre Dame Bay seafloor and extend

northeastwards beneath overlapping Mesozoic rocks, forming the St. Anthony Basin (Bell and Howie, 1990).

The depositional gap existing for the majority of the Permian suggests a period of uplift occurred prior to the opening of the present day Atlantic (Keen et al., 1990). Paleozoic deposition was followed by several crustal stretching episodes affecting both the Precambrian shield and the Paleozoic platform. These episodes are associated with the formation of the Mesozoic intracontinental network of basins and the emplacement of transitional and oceanic crusts (Enachescu, 2006 *a*). Uplift and erosion associated with these events likely resulted in the removal of 1-3 km of Carboniferous sediments (Ryan and Zentilli, 1993; Langdon and Hall, 1994).

1.2.3 Mesozoic Tectonics

The passive margin offshore of eastern Newfoundland and Labrador evolved during multiple rifting episodes occurring as the supercontinent Pangea split apart. The rifting affected the east coast of Canada between Late Triassic and Early Cretaceous time, occurring in several phases as North America separated successively from Africa, Europe and Greenland (Enachescu, 1987; Loudon, 2002). These extensional episodes caused thinning and heating of the continental crust and lithosphere; followed by subsidence and development of a complex marginal basin chain (Enachescu, 1987; Loudon, 2002). During the Late Triassic to Early Jurassic, the intra-continental rift zone and basin chain extended from the future Gulf of Mexico to Northern Europe (Enachescu et al., 2005). At this stage, the Western Orphan Basin was still an elevated part of the supercontinent, and

rifting along the Labrador margin had not commenced (Balkwill et al, 1990; Keen et al.1990; Enachescu et al., 2005).

By the mid Jurassic, Nova Scotia separated from Morocco and the early Atlantic Ocean started to form (Enachescu et al., 2005). This was followed in the Kimmeridgian by development of a shallow sea extending from Nova Scotia into Northern Europe and resulted in the deposition of organic rich shales. There is some evidence suggesting that arms of this sea may have extended northwest into the proto Labrador Sea rift, as Oxfordian–Kimmeridgian dinoflagellates have been encountered on the Greenland side of the margin. As well, geochemistry of oil seeps suggests the existence of several pre-Upper Cretaceous marine sources in that region (Bojesen-Koefoed et al., 2004). However, to date these rocks have not been documented on the Labrador Shelf.

The separation between Nova Scotia and Morocco was followed by the North American-Iberia-Northern Europe rift and separation at the end of the Jurassic to Early Cretaceous. During this phase, the extension direction rotated from NW-SE to NE-SW causing oblique slip and transpression on earlier faults (Enachescu, 1987; Loudon, 2002). This episode was followed by the Labrador rift and opening in the Early Cretaceous and by further postrift subsidence on the banks and extension in the Orphan Basin during Late Cretaceous time (Enachescu, 1987; Loudon, 2002).

As discussed in section 1.1, the Orphan Basin can be subdivided into two sections that formed during different rifting phases. Gravity highs associated with the shelf edge indicate the presence of mantle material and suggest the presence of a failed rift abandoned when continental break-up shifted further to the northeast (Loudon, 2002). As

a consequence, the eastern part of the basin likely contains sedimentary sequences associated with Late Triassic-Early Jurassic rifting. The western portion, however; formed during the Latest Jurassic-Early Cretaceous and experienced rifting episodes continuing into the Late Cretaceous (Louden, 2002; Enachescu et al., 2005). By the end of the Albian, the basin began to separate from the Irish conjugate margin (Enachescu et al., 2005).

With the progression of extensional episodes, the western rift shoulder of the Orphan Basin migrated to the west. This migration eventually caused the Bonavista Platform to become entrained in rifting (Enachescu et al., 2005). In addition, successive Early Cretaceous troughs developed and dissected the underlying Paleozoic platform. These troughs deepened due to thermal subsidence and were filled by mainly siliclastic sediments. A very thick sequence of Tertiary sediment, particularly in the western regions of the basin, suggests that post-rift subsidence was predominant (Louden, 2002).

Dating of coast parallel dyke swarms in southwest Greenland implies that rift related Mesozoic extension in the Labrador Sea may have begun as early as ~160 Ma. However, borehole data indicates that rifting and break-up in the region began in the Early Cretaceous and ended in Late Cretaceous time (Keen et al., 1994; Chian et al., 1995a; Louden, 2002). Onset of the Early Cretaceous rifting along the margin resulted in the development of normal faults within Precambrian and Paleozoic basement (Balkwill et al., 1990; Keen et al., 1990). As well, the rifting reactivated structural highs and caused transtensional strain on sedimentary sequences in the East Orphan Basin (Enachescu et al., 2005). Progression of this extensional stage resulted in the separation of Greenland

and Labrador, and the formation of the Hopedale and Saglek basins along the Canadian side of the margin (Enachescu et al., 2005). The rifting occurred with little volcanic activity along the Labrador margin, as less than 800m of synrift basalts were extruded (Chian et al., 1995*a*; Balkwill 1987). Volcanism associated with the rifting occurred in the Berriasian to Hauterivian, with minor activity continuing into Aptian time. The distribution of these volcanics, however; is not particularly well known (Keen et al., 1990).

During the synrift and postrift periods, oval shaped sedimentary basins separated by crustal arches formed along the Labrador shelf. Hauterivian to lower Cenomanian nonmarine synrift sediments overlie the Early Cretaceous volcanic sequence, and are generally confined to regions between basement highs (Keen et al, 1990). Deposition of these coarse grained synrift successions was followed by a short period of sediment starvation (Louden, 2002). However, a large clastic sediment influx during the Late Cretaceous and Paleogene resulted in a seaward progradation of sediment over rift-age grabens and ridges (Louden, 2002). A mid-Cretaceous erosional unconformity, equivalent to the Avalon unconformity, separates the predominantly nonmarine rift stage sediments from the marine Cenozoic postrift sediments (Keen et al., 1990, Enachescu, 2006 *a*). Postrift subsidence and sedimentation along the margin did not commence until the early Paleocene due to uplift occurring prior to the onset of seafloor spreading. Once initiated, the postrift subsidence resulted in deposition of successive Paleogene and Neogene sedimentary sequences that downlap and thicken seaward (Louden, 2002; Keen et al., 1990).

There is considerable debate concerning the onset of seafloor spreading, extent of oceanic crust and placement of the ocean-continent boundary in the Labrador Sea. Roest and Srivastava (1989) identified sea-floor spreading magnetic lineations 25 (59 Ma) and older in the Labrador Sea (Figure 1.6). These lineations suggest seafloor spreading began in the Late Cretaceous and propagated northward to end in the late Eocene. Between chrons 34 and 35 (84-59 Ma), the direction of motion between Greenland and North America was east-northeast and a triple junction with branches to the south (Grand Banks-Iberia), east (Bay of Biscay) and northwest (Flemish Cap-Labrador) was active northeast of the Flemish Cap area (Enachescu et al., 2005; Roest and Srivastava, 1989). However, between chrons 25 and 24 (57-54 Ma), rifting began separating Greenland from Europe and the direction of sea-floor spreading changed (Roest and Srivastava, 1989; Loudon, 2002). As a result of the shift, sea-floor spreading in the Labrador Sea became oblique and ceased there between chrons 20 to 13 (45-36 Ma) (Roest and Srivastava, 1989). The oldest magnetic anomalies, chrons 28-33, are relatively continuous and linear, but are weak and variable in character (Roest and Srivastava, 1989). These small amplitude anomalies resemble equivalent lineations to the south and display symmetry across the extinct ridge (Srivastava and Roest, 1995). In this regard, they appear compatible with geomagnetic reversals associated with seafloor spreading (Srivastava and Roest, 1995). The presence and origin of these older anomalies, however, has been disputed.

Studies of reprocessed regional reflection seismic data in the Labrador Sea by Chalmers (1991) and Chalmers and Laursen (1995) argues against the existence of chrons

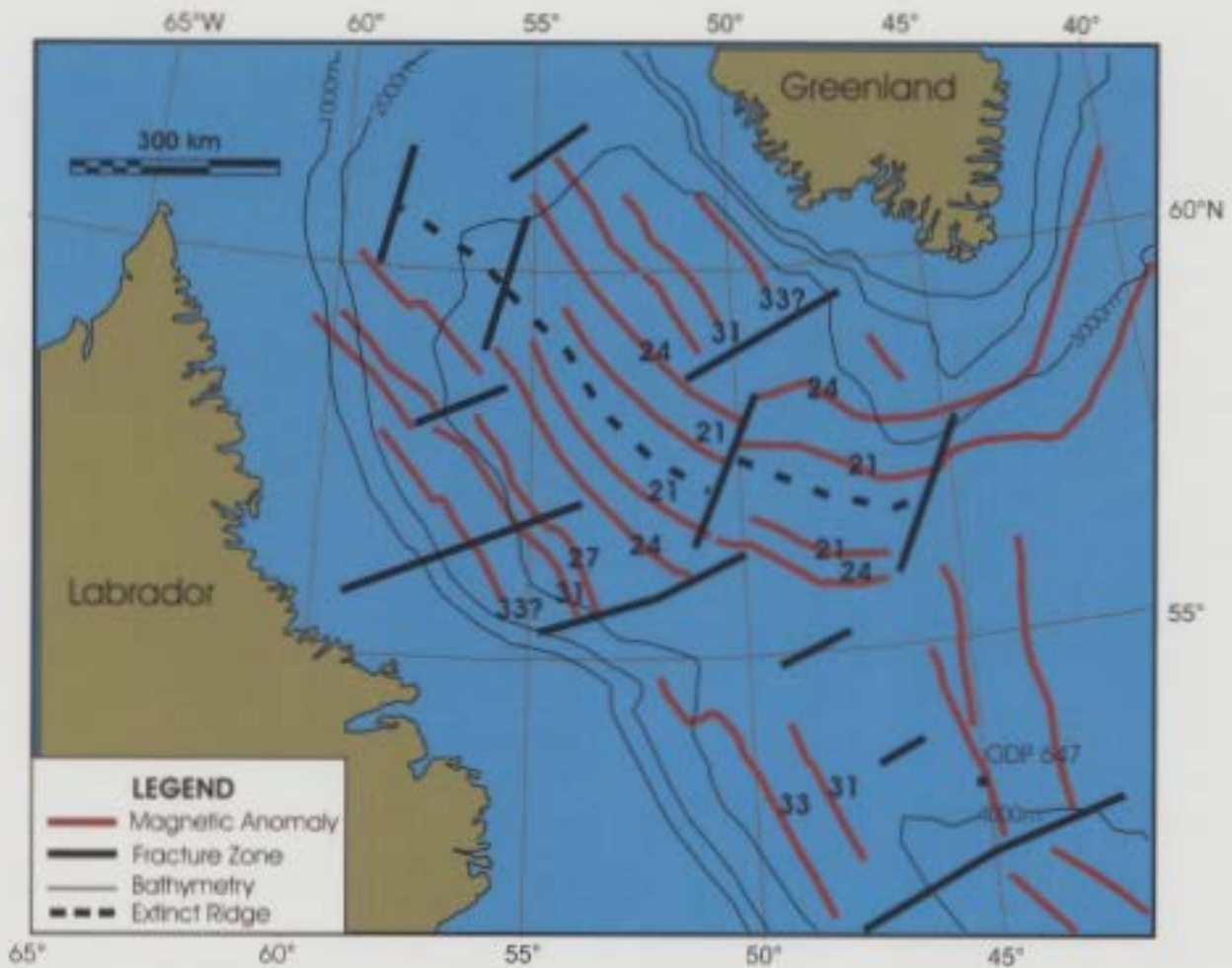


Figure 1.6. Magnetic Anomaly map for the Labrador Sea. Thick red lines are magnetic anomalies, dashed black line represents the extinct spreading ridge, thick black lines are fracture zones, and thin black lines are bathymetry. Modified from Roest and Srivastava (1989)

28-33 due to difficulties in satisfactorily constraining the magnetic anomalies and seismic data using the average spreading model of Roest and Srivastava (1989). Chalmers (1991) and Chalmers and Laursen (1995) also identify rotated basement blocks and possible synrift sediments in close proximity to chron 33 on the Greenland margin. The presence

of these rotated blocks in this region suggests that the crust could be continental in origin. The author(s) propose that the area landward of chron 27 arises from thinned continental crust extensively overlain by reversely magnetized volcanic material, and that seafloor spreading began in Paleocene rather than the Campanian or Maastrichtian time (Chalmers and Laursen, 1995; Chalmers, 1991). The chron 27 -33 anomalies are explained by intrusion of igneous material along cracks and fissures in the extended continental crust (Chalmers, 1991).

However, a subsequent study of the Labrador margin suggests that there is little generation of volcanic material at slow rates of lithospheric rifting, which likely occurred in the Labrador Sea (Chian et al., 1995 *b*). Additionally, rotated basement blocks similar to those observed on the Greenland margin are present in the central area of the Labrador Sea, which was unequivocally formed by seafloor spreading (Srivastava and Keen, 1995). The presence of these features in undisputed oceanic crust suggests that similar features in the area of anomalies 33-27 could have formed at slow spreading rates and that the thinned crust may instead be oceanic in origin (Roest and Srivastava, 1999).

Seismic reflection and refraction data acquired across the southwest Greenland margin indicates the existence of uncharacteristically thin crust (Chian et al., 1995 *a,b*; Keen et al., 1994). The detailed refraction and reflection surveys suggest a thin low velocity layer overlies a higher velocity layer in an 80-100 km long zone. The upper crust is interpreted as thinned continental crust, similar to the Chalmers model, but refraction data suggests that it overlies serpentinite mantle rather than volcanic material, as shown in Figure 1.7 (Chian et al. 1995 *a, b*; Louden, 2002). Thinning of the continental crust

from 30 km below Greenland to 3 km across the continental slope is also evident from the refraction data, and basement highs further seaward are interpreted as serpentized mantle. A simple shear mechanism is proposed for the formation of the margin, with the thin continental crust off Greenland forming the upper plate and the similar crust observed off Labrador forming the lower plate (Chian et al. 1995 *a, b*).

Deep seismic reflection data recorded in the same region as the Chian et al. (1995 *a b*) studies also indicate a thinned crust. The reflection seismic data suggests that the crust may be continental in origin due to disturbance and faulting in the acoustic basement and deeper sediments (Keen et al., 1994). Deformed sedimentary sequences in this region lie between basement blocks beneath the continental rise and are separated from undeformed sedimentary sequences by a prominent reflector. The reflector can be traced back to the break-up unconformity on the shelf. However, the continuity of this reflector changes seaward, making it uncertain as to whether it has the same tectonic implication as the break-up unconformity (Keen et al., 1994). If the reflector is a result of another tectonic process, the underlying crust could be oceanic or transitional in nature (Keen et al., 1994). The interpretation of the thinned crust as continental in nature has several problems: (1) continental crust is predicted to rupture completely before being stretched to a high β value to form a thin crust 80-100 km long, and (2) this model does not account for the observed symmetric magnetic anomalies across the extinct spreading axis (Srivastava and Roest, 1999; Srivastava and Roest, 1995). Development of magnetic anomalies 28-33 by injection of volcanics through continental crust cannot be ruled out due to their small amplitudes and variable shape.

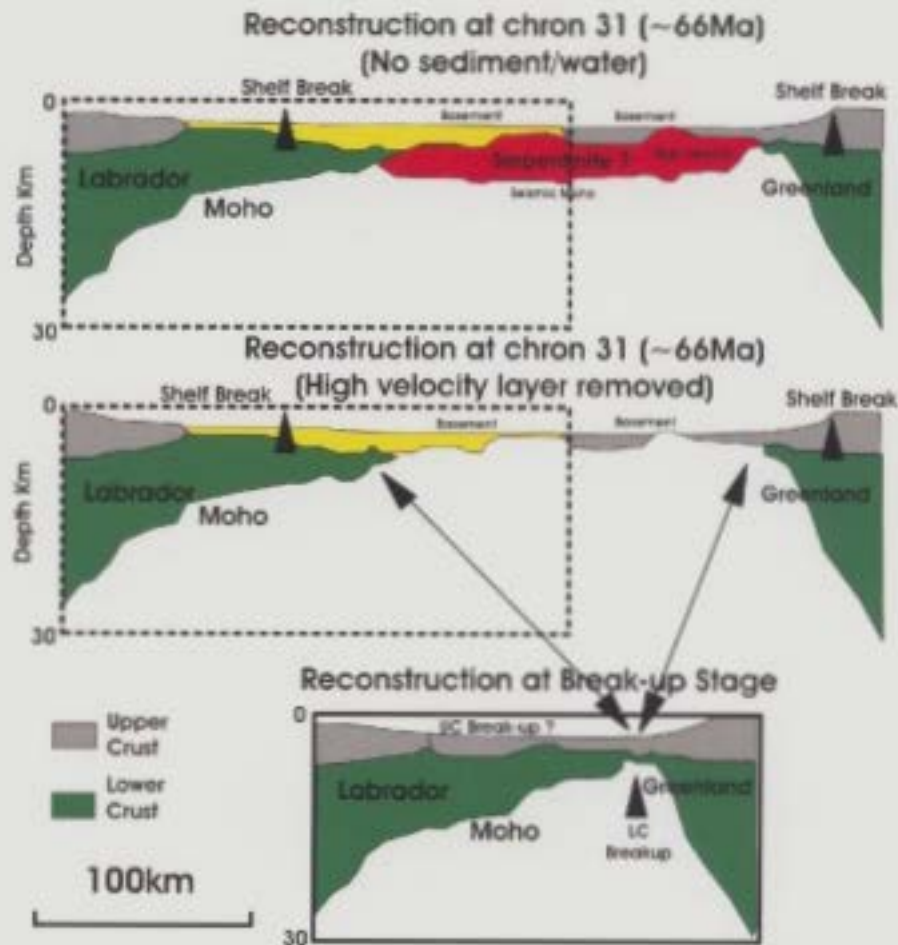


Figure 1.7. Crustal reconstruction of the Greenland-Labrador conjugate margin at the point of break-up, corrected for the effects of sediment and water loading. The rift appears to be asymmetric, with a thinned continental crust on the Labrador side on the margin. Red and yellow sections are interpreted to result from serpentinization of mantle. From Chian et al. 1995 *a, b*; Loudon, 2002.

However, the variable shapes of the magnetic anomalies may be caused by the basement topography identified in the seismic data (Srivastava and Roest, 1995). Additionally, the small amplitude anomalies could be the result of a very slow rate of seafloor spreading (approximately 6mm/year), which is consistent with plate kinematic

motions derived from North American and Eurasian Plates. At slower spreading rates crustal accretion becomes episodic, resulting in fragmentation and a rougher basement surface resembling topography observed across foundered continental crust (Srivastava and Roest, 1999; Srivastava and Roest, 1995; Srivastava and Keen, 1995). For example, the crust in the Labrador Sea between chrons 21 and 25 formed at a moderate spreading rate of 10 mm/yr and exhibits a smooth basement surface with minor normal faults. However, the crust in the younger central region, which is an extinct spreading centre, formed at a slower spreading rate of 3 mm/year and displays evidence of intense normal faulting (Srivastava and Keen, 1995). This suggests that at exceedingly slow spreading rates, tectonism plays a major role in thinning the crust and giving rise to rough basement topography similar to that observed across foundered continental crust (Srivastava and Roest, 1999). A slower rate would also cause inhomogeneities in magmatic source rocks, reduce the intensity of magnetization, and give rise to smaller magnetic anomalies (Srivastava and Roest, 1995).

1.3. Objectives

The main objectives of this thesis are to:

- 1) define the regional structural and tectonic framework throughout the study area, including the deep water areas adjacent to the slope break;
- 2) compare the stratigraphy of the West Orphan and Hopedale basins and outline the stratigraphic relationships common to the two areas;

- 3) examine the rift system structure within the West Orphan and South Hopedale basins by comparisons to analogue models of oblique, orthogonal and multiphase rift systems;
- 4) map the synrift and postrift sediment thicknesses and explain their relative variations throughout the study region;
- 5) determine and discuss the magnitude of extension on the margin through balanced section restoration and backstripping techniques;
- 6) investigate the petroleum potential of the region and identify the most prospective areas for hydrocarbon accumulation

These objectives have been accomplished by identifying major seismic and sedimentary sequences using exploration borehole results, 2D reflection seismic data and available public domain potential field data. Software from Halliburton (Landmark[®] Graphics) was used to interpret the seismic grid and tie the seismic markers to geological units using wellbore velocity checkshot surveys and sonic logs. These markers were then mapped throughout the seismic grid. Major structural features, including the predominant fault systems, were also traced throughout the study area. The potential fields data was used to help constrain the seismic interpretations.

A suite of maps was compiled from the seismic interpretation to help explain the regional tectonic and stratigraphic framework. This suite includes a prerift subcrop basement map identifying the major fault systems and structural features. The synrift and postrift sequences were also defined throughout the study area. On the Labrador Shelf and in the West Orphan Basin, there is a significant variation between the thickness of the

postrift and synrift units. This thickness variation was investigated by (1) producing isopach maps; and (2) carrying out backstripping and restoration techniques on several representative profiles to analyze the subsidence history of the region and estimate the crustal stretching factors.

Regions with petroleum potential were identified within the study area by mapping the synrift stratigraphic sequences to indicate places likely to contain significant thickness of reservoir quality sandstones. Additionally, mapping of source bearing intervals combined with an investigation of the thermal history of the region allowed potentially mature sequences to be recognized.

Chapter 2: Data, Methods, Stratigraphic and Seismic Sequences

2.1 Introduction:

To attain the objectives outlined in Chapter 1, a database consisting of exploration borehole data, reflection seismic data, and potential field data was assembled. Previous work on the tectonic evolution, lithostratigraphy and seismic stratigraphy of the area, discussed in sections 2.4 and 2.5, was compiled to help guide the seismic interpretation. The seismic figures in the following sections depict the interpretation produced in the study, which is based on the stratigraphic nomenclature established in previous work. The lithostratigraphic picks were tied to the seismic data at each borehole using available velocity data, as discussed in section 2.3. The seismic markers identified at the boreholes were then mapped throughout the dataset.

2.2 Overview of the Data:

To meet the research objectives outlined in Chapter 1, a database consisting of exploration borehole data, seismic reflection data, potential field data, and core data was compiled. These datasets are described below:

1) Borehole data:

Twenty one exploration wells have been drilled in the Hopedale Basin, with only 16 reaching their planned exploration target. On the southern Labrador margin, the Leif E- 38 and Pining E-16 wells were abandoned in upper Tertiary sediments, and the Verrazzano L-77 well was abandoned after spudding into and drilling only several hundred metres of Paleozoic strata (Balkwill et al., 1990). Consequently, these

shallow wells were not tied into the seismic database. In the West Orphan Basin seven exploration wells were drilled. Two of these reached Carboniferous sediment basement, while the remainder reached granitic or metasedimentary basement rocks. All of the wells in this area encountered an Upper Cretaceous-Neogene sedimentary sequence and are integrated into the seismic interpretation. The wells used in the seismic interpretation are depicted in Figure 2.1, and listed in Table 2.1. Velocity information used to tie the wells to corresponding reflection seismic profiles is also identified in Table 2.1.

2) 2D Reflection Seismic

i) Hard copy

An extensive 1970's to mid 1980's seismic database exists over the southern Labrador margin, but the majority of data was collected only over the shelf and upper slope. The bulk of seismic data over the St Anthony Basin was acquired during the 1970s through to the mid 1980s, with no recent or older digital data available. Consequently, several vintages of older 2D multichannel reflection seismic data were used to interpret this region. Many of these early seismic profiles are not migrated, and imaging of the subsurface suffers because of contamination by multiples wherever a hard water bottom is present. The data quality generally ranges from poor to good.

ii) Reprocessed GSI data (digital format)

Several datasets acquired by Geophysical Services Incorporated (GSI)

Table 2.1

Well	Location (NAD 83)	Status	TD (m)	Spud Date	Velocity Data
Gudrid H-55	54° 54' 30.19" N; 55° 52' 28.47" W	Abandoned Gas Well	2 838	7/14/1974	Seismic Velocity (Checkshot) Survey
Roberval C-02	54° 51' 08.06" N; 55° 46' 00.76" W	Abandoned	2 823	7/7/1980	Seismic Velocity (Checkshot) Survey
Roberval K-92	54° 51' 35.69" N; 55° 44' 32.01" W	Abandoned	1 680	10/2/1978	Seismic Velocity (Checkshot) Survey
Leif M-48	54° 17' 46.03" N; 55° 07' 16.27" W	Abandoned	1 879.1	8/1/1973	N/A
North Leif I-05	54° 24' 39.07" N; 55° 15' 06.69" W	Abandoned Oil Show	423	9/14/1980	Seismic Velocity (Checkshot) Survey
Indian Harbour M-52	54° 21' 51.42" N; 54° 23' 47.81" W	Abandoned	2 363.1	8/21/1975	Synthetic Seismogram
Cartier D-70	54° 39' 02.55" N; 55° 40' 26.16" W	Abandoned	1 927.0	9/27/1975	Seismic Velocity (Checkshot) Survey
Freydis B-87	53° 56' 13.48" N; 54° 42' 35.86" W	Abandoned	2 314.1	7/2/1975	Seismic Velocity (Checkshot) Survey
Blue H-28	49° 37' 26.49" N; 49° 17' 58.18" W	Abandoned	6103.1	4/28/1979	Synthetic Seismogram
Hare Bay E-21	51° 10' 21.80" N; 51° 04' 23.32" W	Abandoned	4874	6/14/1979	Synthetic Seismogram
Sheridan J-87	48° 26' 39.56" N; 49° 57' 35.30" W	Abandoned	5486.4	6/15/1981	Synthetic Seismogram
Bonavista C-99	49° 08' 06.16" N; 51° 14' 24.21" W	Abandoned	3685.1	6/26/1974	Synthetic Seismogram
Linnet E-63	48° 12' 29.27" N; 50° 25' 22.28" W	Abandoned	4520.2	7/18/1982	Synthetic Seismogram
Baie Verte J-57	50° 16' 43.58" N; 51° 07' 49.77" W	Abandoned	4911	7/15/1985	N/A
Cumberland B-55	48° 24' 12.21" N; 50° 07' 54.49" W	Abandoned	4136.5	8/9/1975	Synthetic Seismogram

Location, status, total depth (TD), spud and velocity data for the Labrador Shelf and Western Orphan Basin wells within the study area.

over the St. Anthony Basin, Cartwright Arch and West Orphan Basin in the early 1980's were reprocessed and converted to digital SEG Y data. This reprocessed data set was donated to Memorial University. Approximately 5378 km of this dataset, shown in red in Figure 2.1, were used in the interpretation. The data quality ranges from poor to very good, with imaging of the subsurface suffering wherever a hard water bottom is present.

iii) Digital

Multichannel 2D seismic reflection data acquired by Geophysical Services Incorporated (GSI) during 2003, 2004 and 2005 were donated to Memorial University of Newfoundland and all lines covering the southern portion of the Labrador Shelf and West Orphan Basin were used in the interpretation. Acquisition parameters include a 6 to 8 km long streamer and a minimum recording time of 12 seconds. The modern processing sequence, which includes Kirchoff prestack time migration, results in fair to excellent quality data (Enachescu, 2006 *a*; Enachescu, 2006 *b*). On the Labrador shelf, the data quality suffers over the shelf break and upper slope region whenever a rough and/or hard water bottom is present. In general, the regional dip lines have 5 km spacing and are tied by long strike lines approximately 20 km apart. The total seismic line length used from this data set is approximately 11137 km: 6602 km in the Hopedale Basin and 4535 km in the Orphan Basin.

3) Potential Fields

Gravity and Aeromagnetic data acquired through the Canadian *Geodetic Information System (2007)* and *Canadian Aeromagnetic Data Base (2007)* were used to help interpret the 2D seismic reflection data. The datasets include:

- 1) Free Air Gravity Anomaly, gridded 2000 m resolution
- 2) 1st Vertical Derivative of Free Air Gravity Anomaly, gridded 2000 m resolution
- 3) Isostatic Residual Gravity Anomaly, gridded 2000 m resolution
- 4) Residual Total Magnetic Field, gridded, 1000 m resolution

2.3 Methods

The first step of the interpretation process included selecting the higher-quality older-vintage reflection seismic lines acquired over the St. Anthony Basin and Cartwright Arch to incorporate into the more recent digital datasets of the Labrador Shelf and West Orphan Basin. This selection was based on the recording length, effective multiple removal and migration and the source bandwidth used in the collection. In total, 15 lines representing approximately 2648 km were chosen. Once the older vintage data were selected, the lines were scanned to black and white tiff files. These files were converted into SEG Y data using a UNIX based conversion program, and imported into a Halliburton Graphics (Landmark[®] Seisworks 2D) interpretation package. The 2003, 2004, 2005 GSI digital data for the southern Labrador Shelf and West Orphan Basin were also loaded into the project database, as were older reprocessed GSI lines acquired in the

St. Anthony and West Orphan Basin regions. A location map showing the seismic data used in the interpretation is shown in Figure 2.1

The borehole data were tied into the seismic grid using available velocity data and lithostratigraphic picks for each well. Each of the well-ties is shown in Figures 2.2 to 2.14. The velocity data used includes wellbore check shot surveys and synthetic seismograms, as indicated in Table 2.1. Sufficient velocity information is available for the Gudrid H-55, Roberval C-02, Roberval K-92, Freydis B-87, Cartier D-70, North Leif I-05, Indian Harbour M-52, Hare Bay E-21, Blue H-28, Bonavista C-99, Cumberland B-55, Sheridan J-87 and Linnet E-63 wells. However, for the Baie Verte J-57 and Leif M-48 wells, time depth conversions are estimated by using the velocity functions from nearby wells. This is accomplished by plotting the velocity functions onto a single graph and taking the curve of best fit through all the functions to obtain an average regional time-depth curve. This curve was then used to tie the Leif M-48 and Baie-Verte J-57 stratigraphic picks to the seismic. The ties made with this estimated curve were adjusted slightly to match the ties identified in wells with checkshot surveys.

The Hare Bay E-21 borehole has stratigraphic picks with both Labrador and Jeanne d'Arc nomenclature. Each set of picks was tied to the seismic data to help facilitate a comparison of the stratigraphy in the Hopedale and Orphan basins. The only stratigraphic marker that was traced with confidence into Orphan Basin was the top Kenamu Formation (Baffin Bay unconformity), which is noted as the Kenamu equivalent in the Figures 2.10 and 2.11. However, this marker is present only in the northern and

western West Orphan Basin, as it downlaps onto the Base Tertiary unconformity to the east and south. Additional regional postrift seismic markers were identified in the

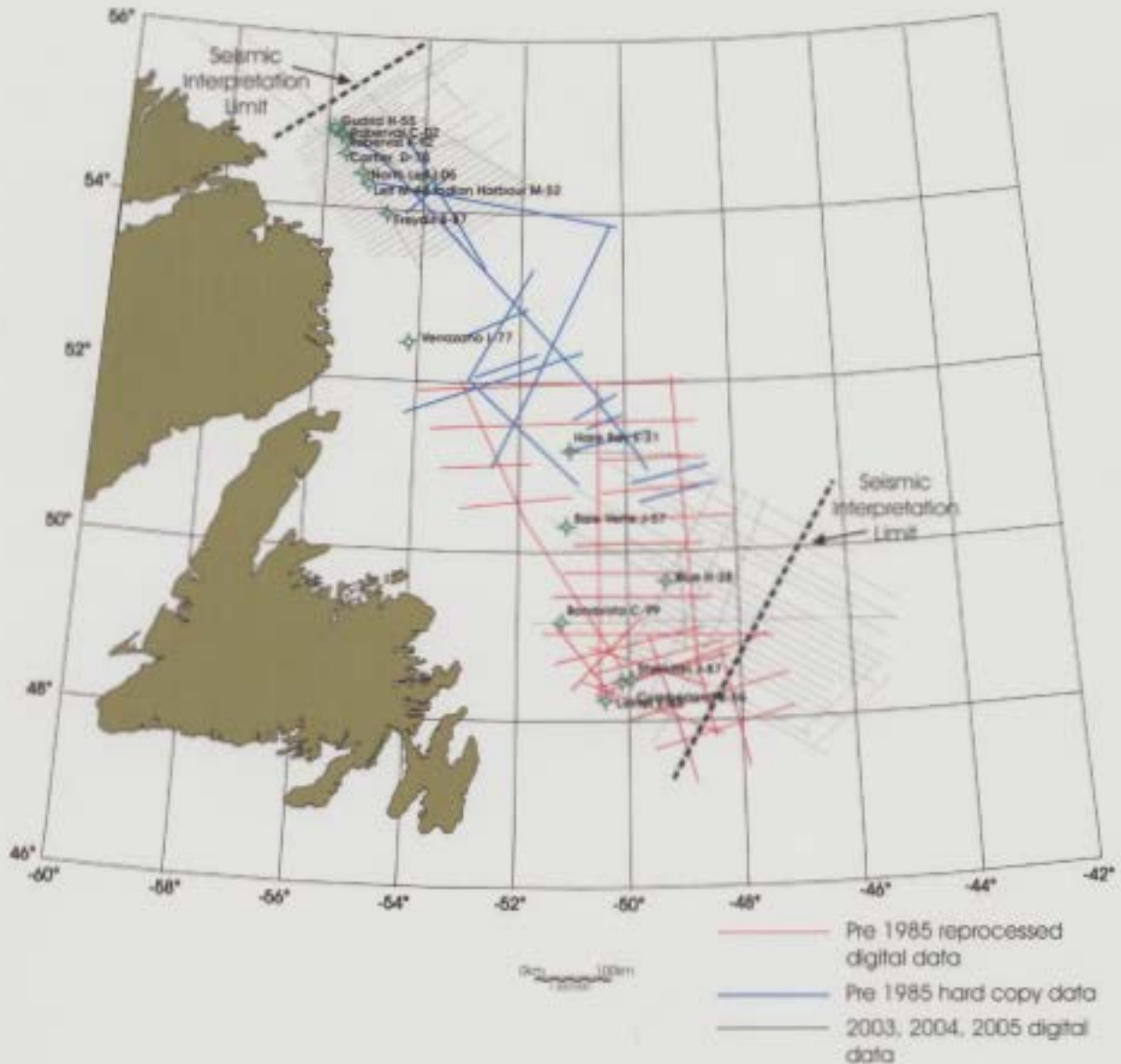


Figure 2.1. Reflection seismic lines used in the study. Lines shown in blue are older vintage (pre 1985), while those shown in red were acquired during recent surveys in 2003, 2004 and 2005 by Geophysical Services Incorporated (GSI).

Orphan Basin, as shown in Figures 2.9b-2.14. Similar markers are also evident in the deepwater Labrador Shelf, although no direct correlation could be made as the only tie lines cross the Cartwright Arch where these markers are not present. Comparisons of these sequences are discussed further in Chapter 3.

Because the seismic data used in the interpretation are from different sources, misties occur when trying to compile the data into a single grid. The misties range from 35 to 75 ms, with the older vintage lines having the largest misties. The magnitude of the misties between various seismic lines can be attributed to acquisition or processing parameters, the type of migration, incorrect positioning and use of different datums. The GSI 2003, 2004, 2005 seismic lines over the West Orphan Basin and the southern Labrador Shelf tied together without any problems as they were acquired with similar in water lay out, processed with same parameters and correctly positioned using a Digital Global Positioning System (DGPS). Consequently, these sets were used as a datum when correcting for larger misties associated with the older vintage lines. To correct for the discrepancies, the waterbottom reflection was traced throughout the dataset and a constant shift for this horizon was calculated for each line. These shifts were then applied and the seismic was re-examined. The constant shift calculations corrected for the waterbottom misties, as well as misties for horizons deeper in the section. This suggests that different processing parameters used for each survey are responsible for most of the inconsistencies between data sets.

The integration of seismic and well data permitted the main seismic sequences to be identified and mapped. Major structural features and fault systems were also identified

on each line and mapped throughout the region. As the southern Labrador Shelf has the densest and most recent seismic coverage, that area was mapped first and the interpretations were extended southwards into the St. Anthony and Western Orphan basins.

In the interpretation that follows, the term basement refers to the acoustic basement, which herein describes prerift sequences that vary in age, composition and structure throughout the study region.

2.4 Labrador Shelf: Tectonic Stages, Stratigraphic and Seismic Sequences

The following section discusses the previous work on the stratigraphy and tectonic evolution of the Labrador Shelf, which provided the basis for the seismic interpretation depicted in the figures.

Stratigraphic sequences on the Labrador Shelf developed during several geodynamic evolutionary stages, as shown in Figure 2.15. These phases include conventional prerift, synrift and postrift periods. However, in the Labrador Sea, the postrift period is further broken down into predrift, syndrift and postdrift stages (Enachescu, 2006 *a*).

Stratigraphic nomenclature for the Labrador Shelf has undergone several revisions, including that by Umpleby (1979) and by McWhae et al. (1980). The study by Umpleby (1979) was based largely on well data, while McWhae et al. (1980) included seismic data and introduced seismic-stratigraphic sequences (Balkwill et al., 1990). Subsequent wells and improved seismic definition have allowed the stratigraphy to be

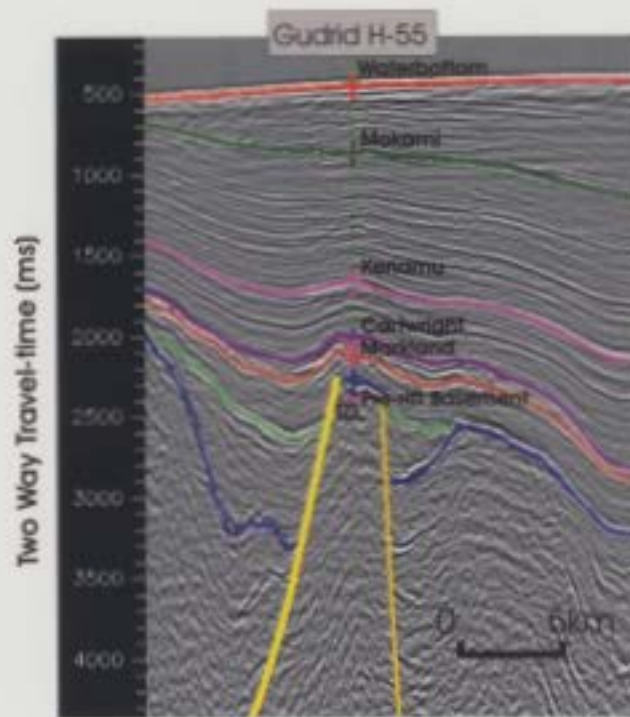


Figure 2.2. Lithostratigraphic ties for the Gudrid H-55 borehole. This well is located on a basement horst and did not intersect the synrift sequence. However, synrift Bjarni Formation sediments are interpreted to exist in lows adjacent to the high.

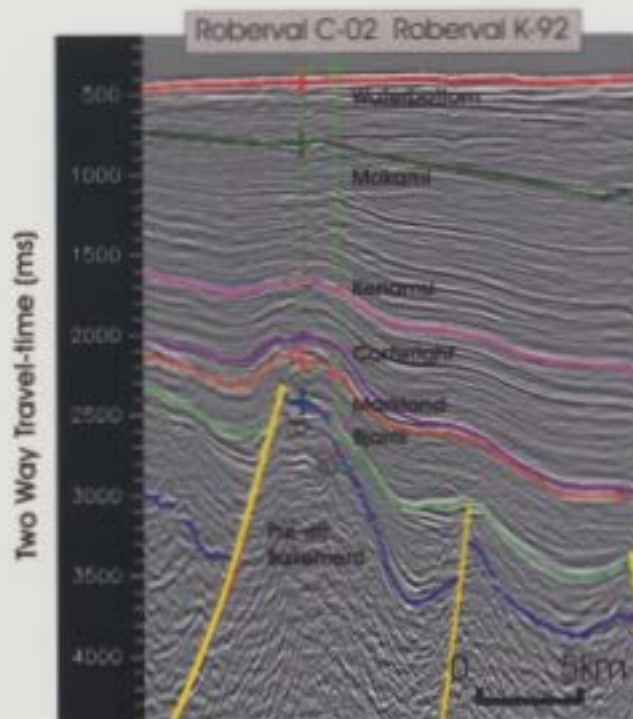


Figure 2.3. Lithostratigraphic ties for the Roberval K-92 and C-02 wells. The Roberval C-02 well was located at the crest of a basement high and did not intersect any synrift sediments. Roberval K-92 was located on the flank of the high and intersected a thin synrift sequence.

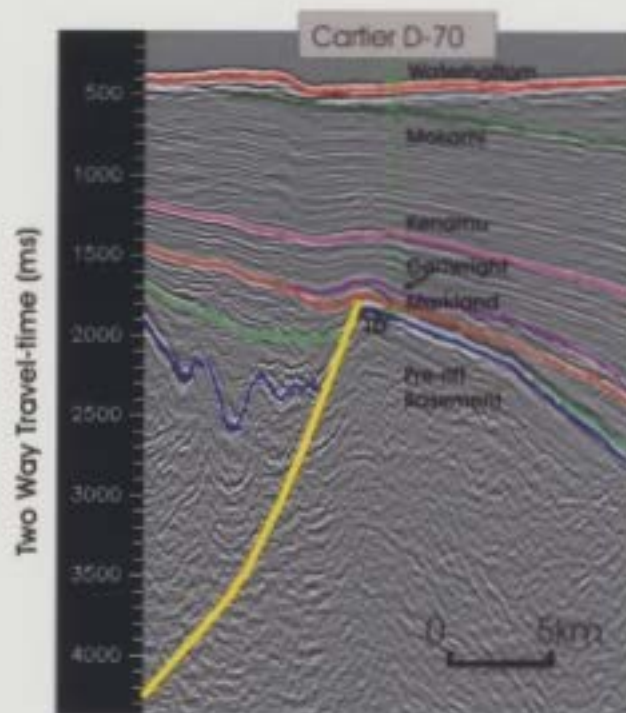


Figure 2.4 Lithostratigraphic ties for the Cartier D-70 borehole. The synrift sequence is absent at this location.

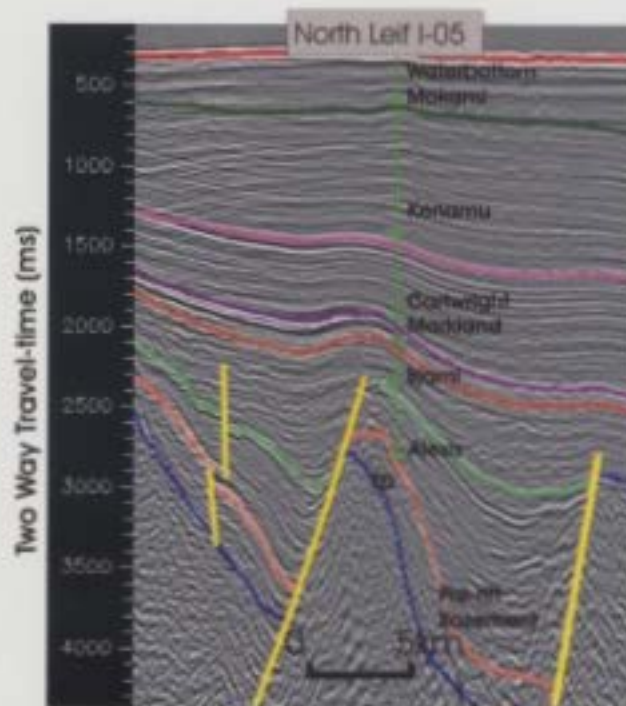


Figure 2.5. Lithostratigraphic ties for the North Leif I-05 well. This borehole intersected a full synrift sequence, including Alexis Formation volcanics.

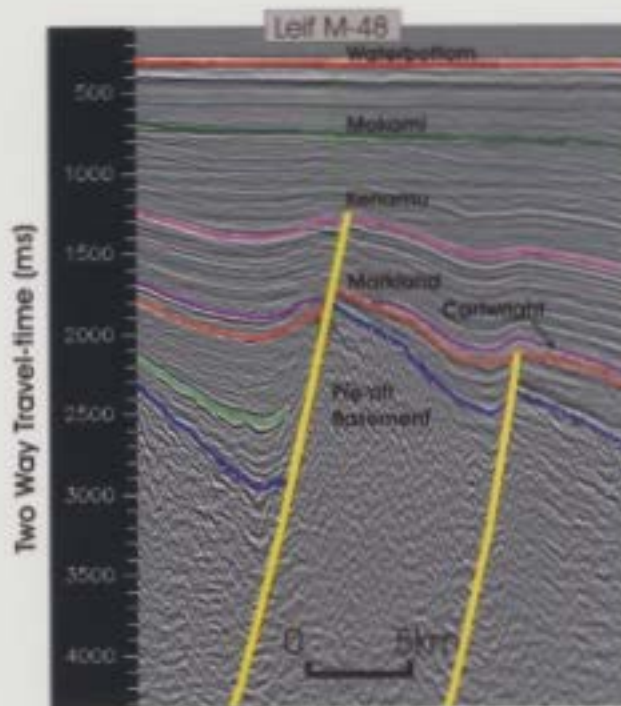


Figure 2.6. Lithostratigraphic ties for the Leif M-48 borehole. A time-depth conversion was obtained by plotting the velocity functions from nearby wells onto a single graph and taking a curve of best fit as no direct velocity information is available for the well. The obtained curve tied the upper post-rift markers to the seismic satisfactorily, but misties occur deeper within the borehole.

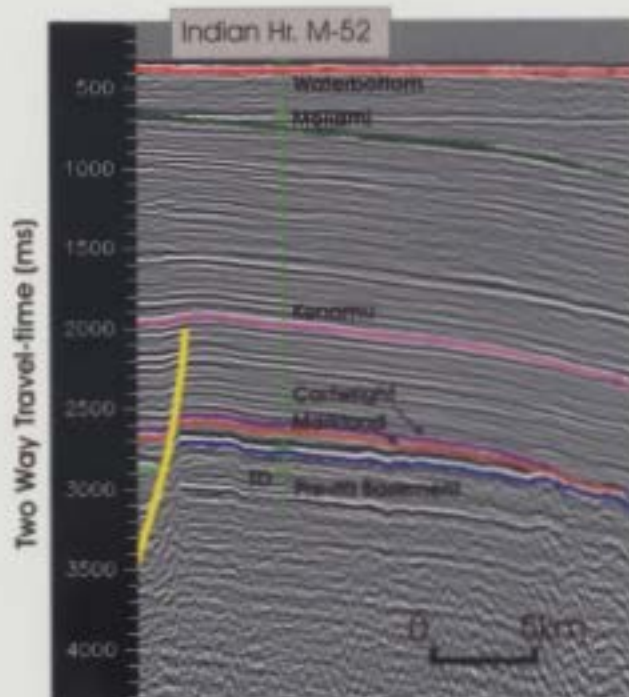


Figure 2.7. Lithostratigraphic ties for the Indian Harbour M-52 well. The velocity curve for this location is derived from a sonic log, which may account for the misties in the borehole.

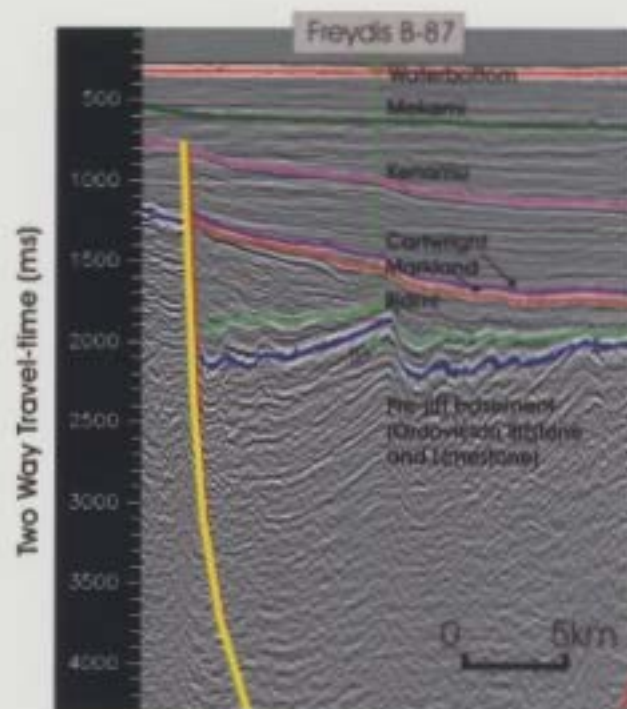


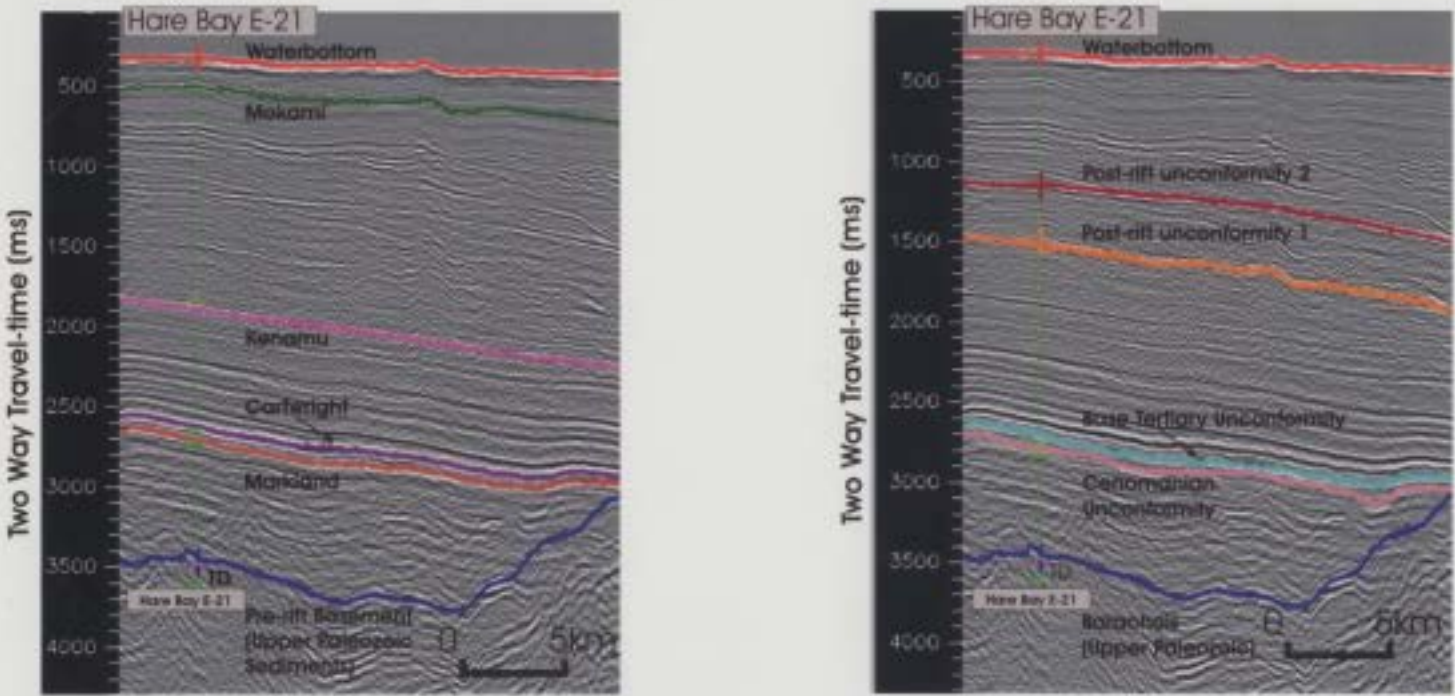
Figure 2.8. Lithostratigraphic ties for the Freydis B-87 well. Prerift basement is composed of Ordovician limestones and siltstones at this location.

further refined (Balkwill et al, 1990; Enachescu, 2006 *a*; Enachescu, 2006 *b*). The sequences on the Labrador Shelf can be divided into six formations commencing with Early Cretaceous rift phase sediments (McWhae et al., 1980).

2.4.1 Prerift Sequence

The term “prerift” refers to all metamorphic, igneous and sedimentary formations that were present prior to the onset of intracontinental extension. As discussed in section 1.2, these units include Precambrian gneisses and metasediments as well as Paleozoic formations (McWhae et al, 1980; Balkwill et al., 1990; Balkwill, 1987). These rocks were

partially peneplained during the Late Paleozoic to Early Cretaceous, and form the basement in the Hopedale, St. Anthony and West Orphan basins (Enachescu, 2006 a).



Figures 2.9a and 2.9b. Lithostratigraphic ties for the Hare Bay E-21 well following both Labrador (left) and Jeanne d'Arc(right) stratigraphic nomenclature. The Labrador lithostratigraphic picks are from Moir (1989) and the Jeanne d'Arc picks are from the C-NLOPB. Jeanne d'Arc stratigraphy is currently in use for the Orphan Basin, as this area likely contains sequences similar to the Jeanne d'Arc Basin. The western portion of the Orphan Basin, however, likely contains stratigraphy similar to that encountered on the Labrador Shelf. Both sets of picks were tied to the seismic markers to help relate the stratigraphy between the Orphan and Hopedale basins. Additionally, postrift unconformities (red and gold horizons) that were mapped throughout the western Orphan Basin are identified in Figure 2.9b.

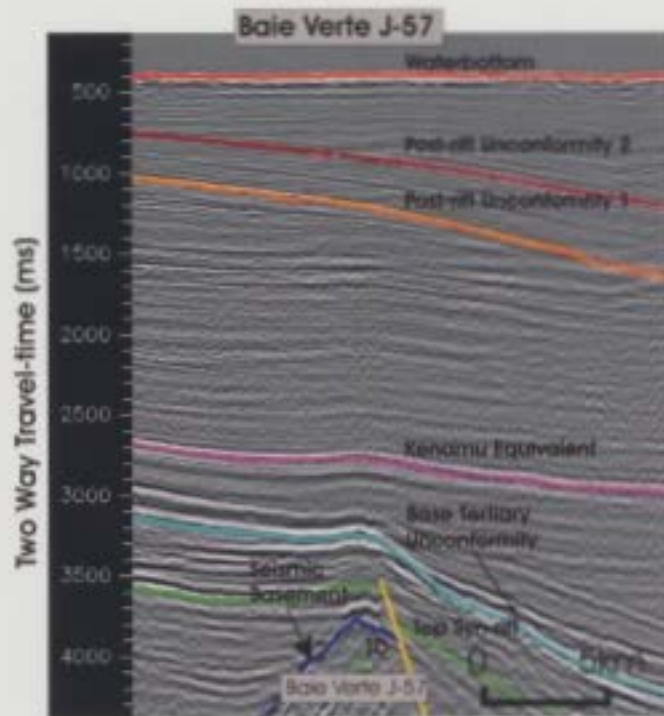
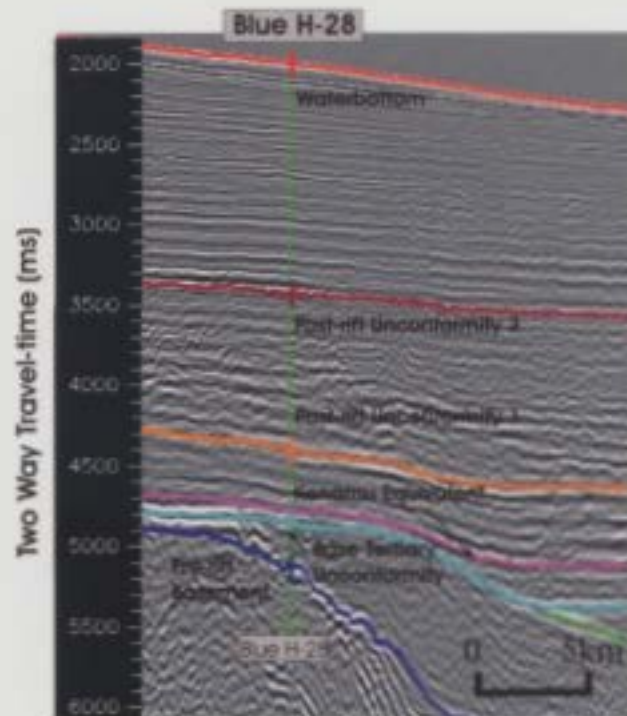


Figure 2.10. Lithostratigraphic picks for the Baie Verte J-57 borehole. Two postrift unconformities (red and gold horizons) and a top synrift unconformity (green horizon) mapped from regional seismic markers are also shown. The Kenamu Formation marker was mapped from the Hare Bay E-21 well.



2.11. Lithostratigraphic picks for the Blue H-28 well. The synrift sequences was not encountered in the borehole but is interpreted in the half graben adjacent to the basement high. Postrift unconformities (red and gold horizons) interpreted from regional seismic markers are also shown.

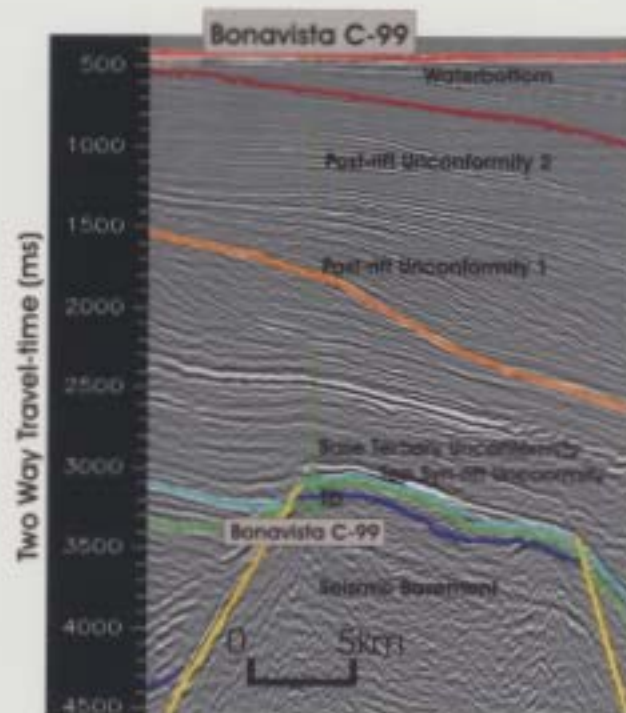


Figure 2.12. Lithostratigraphic picks for the Bonavista C-99 borehole. This location encountered a thick postrift succession but a very thin synrift sequence. Postrift unconformities (red and gold horizons) interpreted from regional seismic markers are also shown.

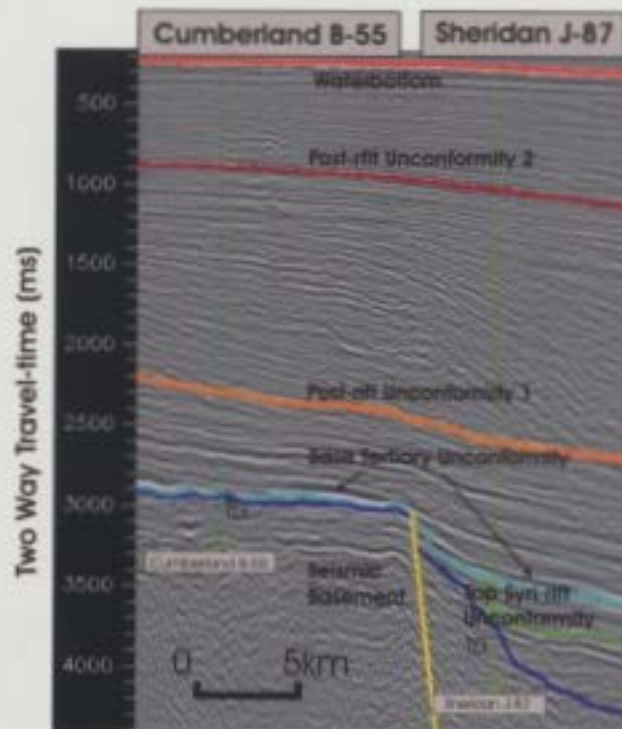


Figure 2.13. Lithostratigraphic ties for the Cumberland B-55 and Sheridan J-87 wells. Postrift (red and gold horizons) and synrift (green horizon) unconformities are also shown. The time depth data for the Sheridan J-87 well is derived from sonic logs, which may account for the Base Tertiary unconformity and basement misties.

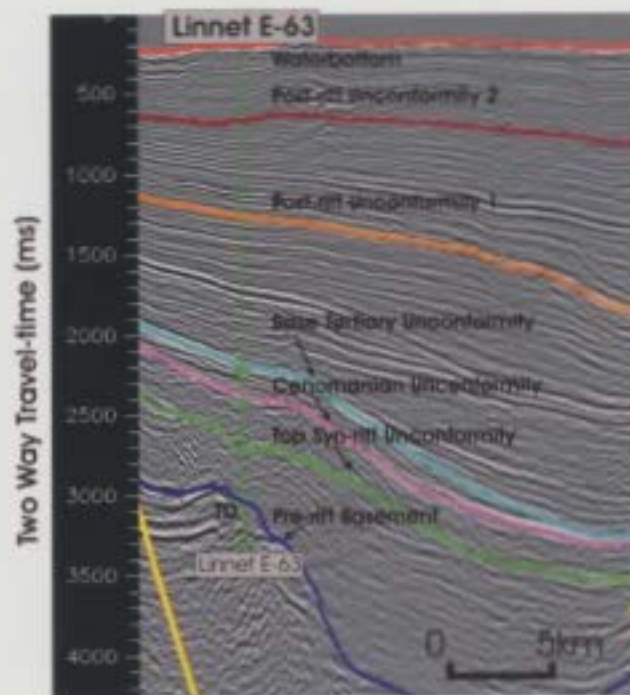


Figure 2.14. Lithostratigraphic ties for the Linnet E-63 borehole. Postrift unconformities (red and gold horizons) and top synrift unconformity (green horizon) interpreted from regional seismic markers are also shown.

2.4.2 Synrift Sequence

Sedimentary sequences deposited during intracontinental extension are referred to as “synrift” stage sediments. During this phase, the Earth’s crust and lithosphere are being pulled apart but there is no production of oceanic crust (Enachescu, 2006). Volcanic rocks of the Alexis Formation are associated with the crustal thinning and continental extension that occurred during this phase (McWhae et al., 1980). With increased continental stretching and rift shoulder uplift, elongated rift valleys and intervening ridges within the Labrador-Greenland region received a major pulse of coarse clastics, resulting in the development of the Bjarni Formation (Enachescu, 2006 b)

Alexis Formation

This Berriasian to Barremian formation is typically composed of volcanic rocks, including basic lavas and dikes, partly lateritic soils, lapilli and subordinate epiclastic sediments (McWhae et al., 1980). In general, the sequence is altered by weathering and hydrothermal activity and varies in colour from grey to purplish and greenish grey (McWhae et al., 1980). The lavas rest unconformably on Paleozoic sediments and Precambrian basement and have a conformable to disconformable relationship with overlying Bjarni Sandstones, and an angular unconformable relationship when overlain by Markland formation shales (McWhae et al., 1980). A strong high amplitude seismic reflection usually occurs at the top of the formation (McWhae et al., 1980). However, the marker at the base of the unit is often weak or absent, making it difficult to distinguish the unit from the top of the prerift basement. A typical example of the seismic character of the Alexis Formation is shown in Figure 2.16.

Bjarni Formation

This unit is Barremian to Albian in age and contains coarse arkosic sandstone, and shales (Umpleby, 1979; McWhae et al., 1980). The Bjarni Formation was deposited as a series of delta plain sands during a period of mild tectonism, and likely originated from western sources. Some coarse clastics may originate from local sources such as intrabasinal ridges (Enachescu, 2006b). During early Barremian times the deposition was

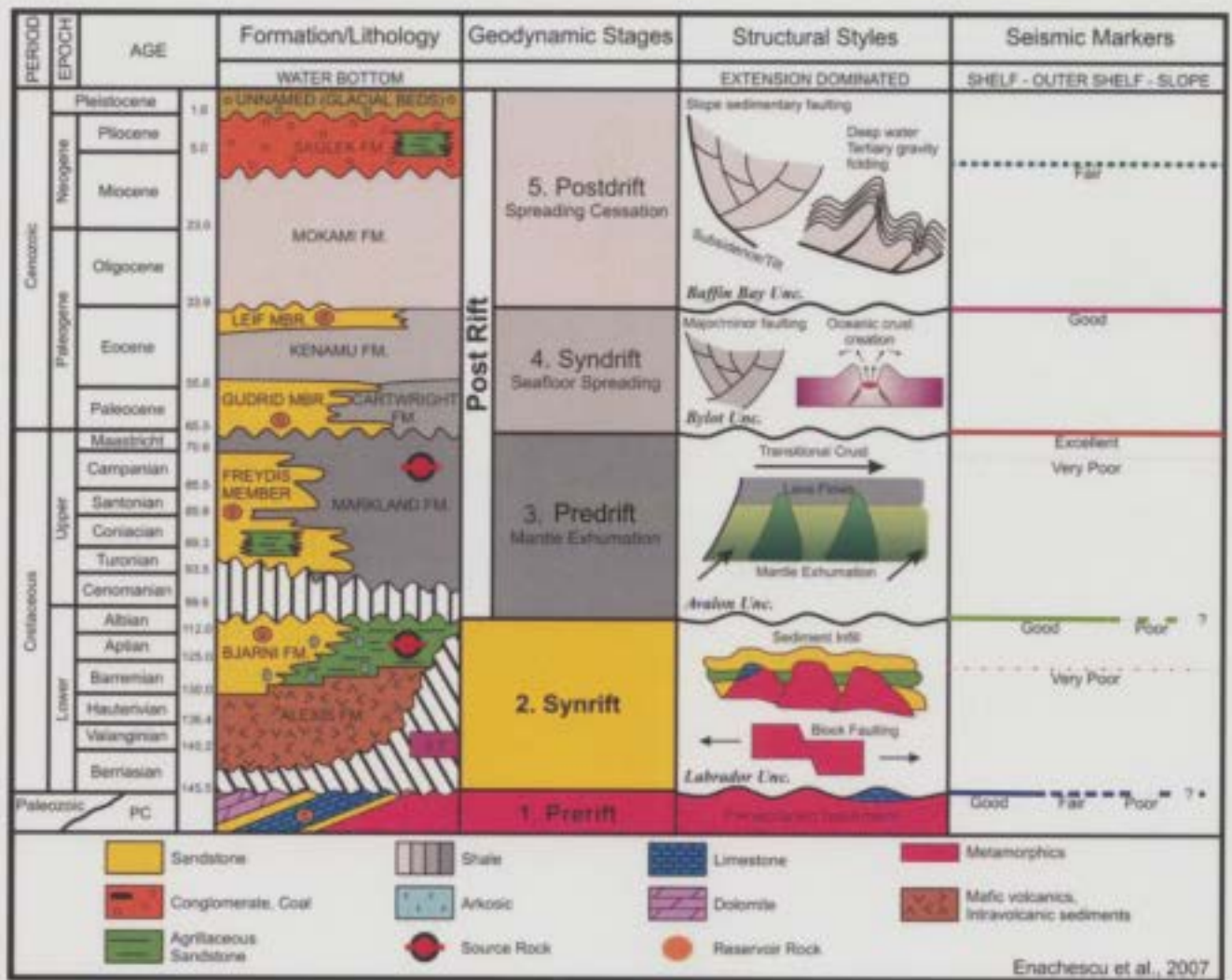


Figure 2.15. Lithostratigraphy, geodynamic stages, structural styles and seismic markers for the Labrador Shelf. Modified from Enachescu et al., 2007.

shale dominated, and relief within the basin was low. By Aptian and Albian times, sand deposition commenced and stronger movements occurred between faulted blocks and adjacent basin areas (Umpleby, 1979).

A regional unconformity, known as the Labrador unconformity, separates the base of the Bjarni Formation from Precambrian crystalline or Paleozoic rocks and gives rise to

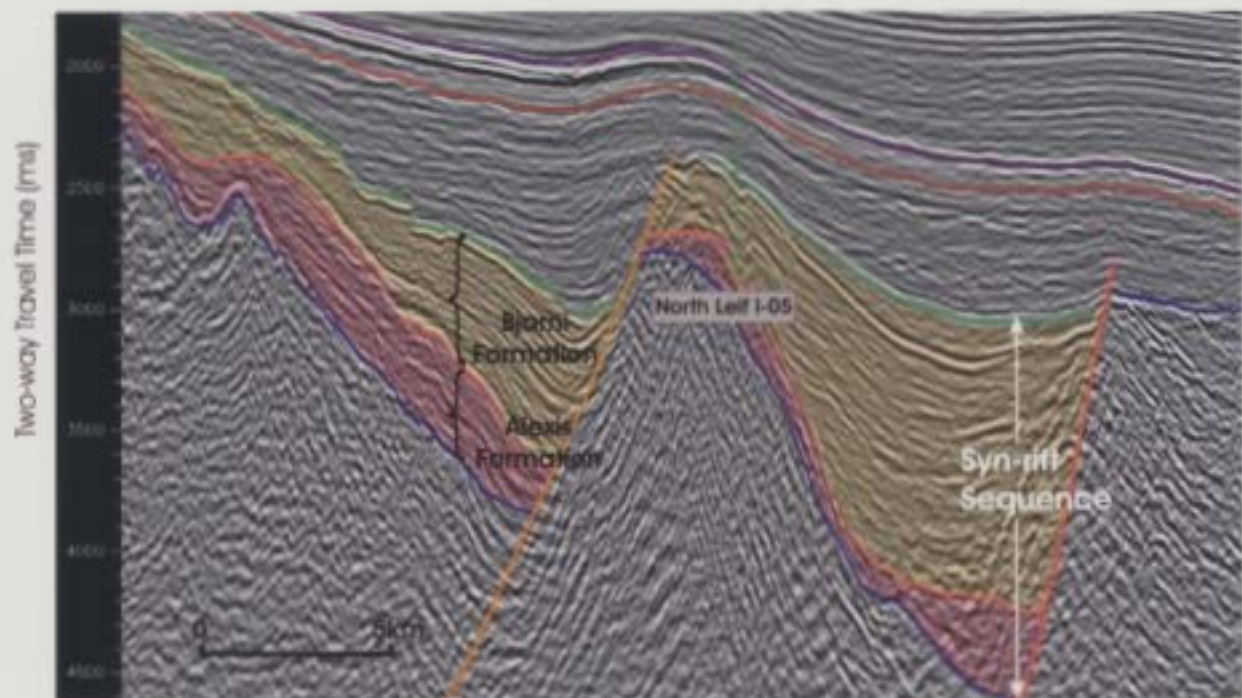


Figure 2.16. Synrift seismic sequence at the North Leif I-05 well. Top synrift unconformity (Avalon Unconformity) coincides with the top of the Bjarni Formation (green horizon).

a strong reflection on seismic profiles (McWhae et al., 1980). In some areas Bjarni clastic rocks have a disconformable relationship to underlying Alexis volcanics, suggesting that the upper part of the Alexis formation and the lower part of the Bjarni Formation may be coeval (McWhae et al., 1980). The top of the Bjarni formation lies unconformably below the Markland formation. A strong seismic reflection usually occurs at the top of the unit and is associated with an angular unconformity, known as the Avalon unconformity (Figures 2.15 and 2.16). The angular relationship of the unconformity tends to disappear as the unit approaches the paleoshoreline (McWhae et al., 1980). The formation has variable internal reflectivity and shows stratigraphic growth towards marginal faults associated with half graben structures.

2.4.3 Predrift Sequence:

In the Labrador Sea, the sediments deposited after initial continental extension but prior to the onset of seafloor spreading are referred to as “predrift” sediments. This tectonic stage occurred during Cenomanian to Maastrichian time and is thought to be synchronous with mantle exhumation and formation of serpentinite ridges, which are interpreted from seismic data but not yet proven by scientific drilling (Chian and Loudon, 1994; Loudon 2002; Enachescu, 2006). However, similar features on the Iberian Abyssal plain were drilled during legs 159 and 173 of the Ocean Drilling Program (ODP) and determined to be exhumed mantle peridotite. The findings from the ODP drilling indicate that the tectonic interval following the break-up of Iberian and North America and preceding onset of seafloor spreading was characterized by mantle exhumation (Skelton and Valley, 2000). Based on these findings, a similar sequence of events could have occurred in the Labrador Sea. Sediments associated with this tectonic stage compose the Markland Formation.

Markland Formation

The Cenomanian-Turonian to Early Paleocene Markland formation consists of dark green to dark gray shale, silty shale, minor siltstone and sandstone and thin brown dolomitic limestone beds (McWhae et al., 1980). Generally, it is fine to very fine bedded and lacks the brown colouring of the overlying Paleogene-Neogene sequence. The lower boundary at the Avalon unconformity is marked by an abrupt lithological change into Bjarni Formation sandstones or older rocks. The contact with the overlying Cartwright

Formation ranges from unconformable to disconformable and is known as the Bylot unconformity. Lithological changes are most noticeable wherever the sandy Gudrid Formation is developed over Markland shales (McWhae et al., 1980). Both the top and base of the unit have generally strong seismic markers associated with these regional unconformities (McWhae et al., 1980). A typical example of the seismic character of the unit is shown in Figure 2.17. Here the formation has a strong reflection at the top and bottom but a weak internal reflectivity.

a. Freydis Member

The Freydis Member of the Markland Formation is composed of nearshore, shallow water fans that developed during the Upper Cretaceous. The lithology is typically light grey, fine to coarse quartzose sandstone and poorly sorted arkosic sandstone with an argillaceous matrix (McWhae et al., 1980). The unit has two contrasting stratigraphic styles: thick narrow, half-graben confined wedges proximal to the contact between the Mesozoic terrace wedge and Precambrian basement, and narrow seaward facing prisms that locally overstep older beds both landward and seaward (Balkwill et al., 1990). In the south Hopedale Basin, thin wedges of Freydis sandstone are present and consist of light grey, fine-to coarse-grained quartzose and arkosic sandstone (Balkwill et al., 1990).

Figure 2.18 shows the seismic sequence associated with this stratigraphic style. A seismic reflection can sometimes be distinguished at the top of the Freydis Member but weakens and dissipates basinward, probably indicating a facies change to silts and basinal shales. The internal seismic character is variable: stronger internal reflections are associated with thicker nearshore sequences, while weak internal reflectivity occurs wherever the

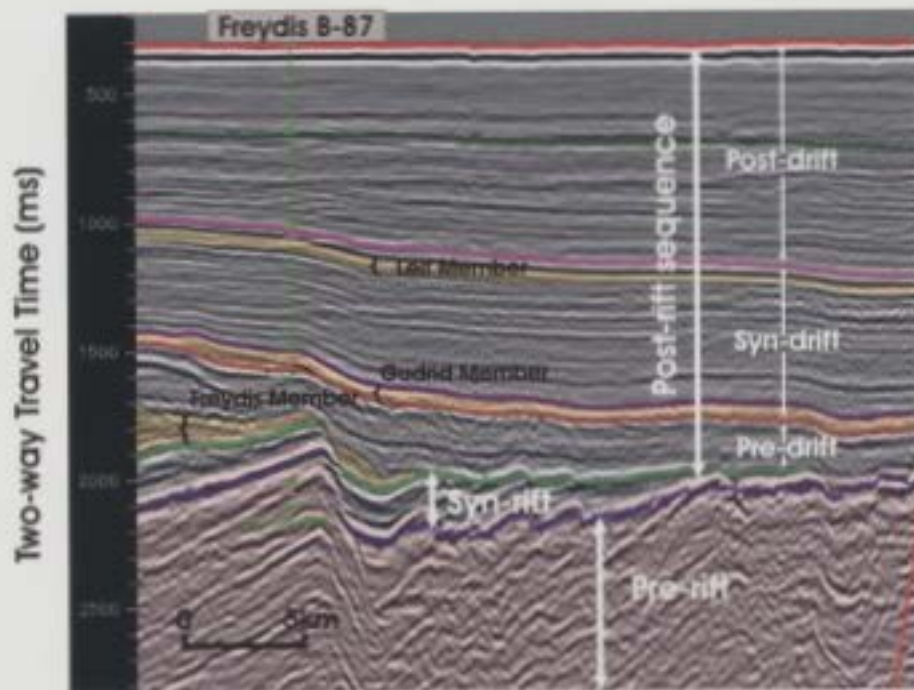


Figure 2.17. Postrift seismic sequence, including Gudrid Member sands (yellow interval) at the Gudrid H-55 borehole location.

sequence thins. Generally, a seismic marker cannot be identified at the base of the member unless it is developed immediately over the Bjarni Formation (McWhae et al, 1980).

2.4.4 Syndrift Sequence

The term “syndrift” refers to the period of time in which oceanic crust was being produced in the Labrador Sea. In the southern part of the margin, this occurred during the Paleocene to earliest Oligocene, transforming the area from an intracontinental setting into a plate margin basin (Enachescu, 2006 *a*). Sea floor spreading subsequently ceased

during the earliest Oligocene due to extinction of the oceanic ridge. Sediments deposited during this tectonic stage are grouped into the Cartwright and Kenamu formations.

Cartwright Formation

The Paleocene to early Eocene Cartwright Formation consists of brown-grey claystone, silty claystone, siltstone, thin distal turbidite partings of buff fine sandstone and thin brown carbonate beds. The formation also contains a sandstone succession, known as the Gudrid member (Balkwill et al., 1990). The shale units are considered an

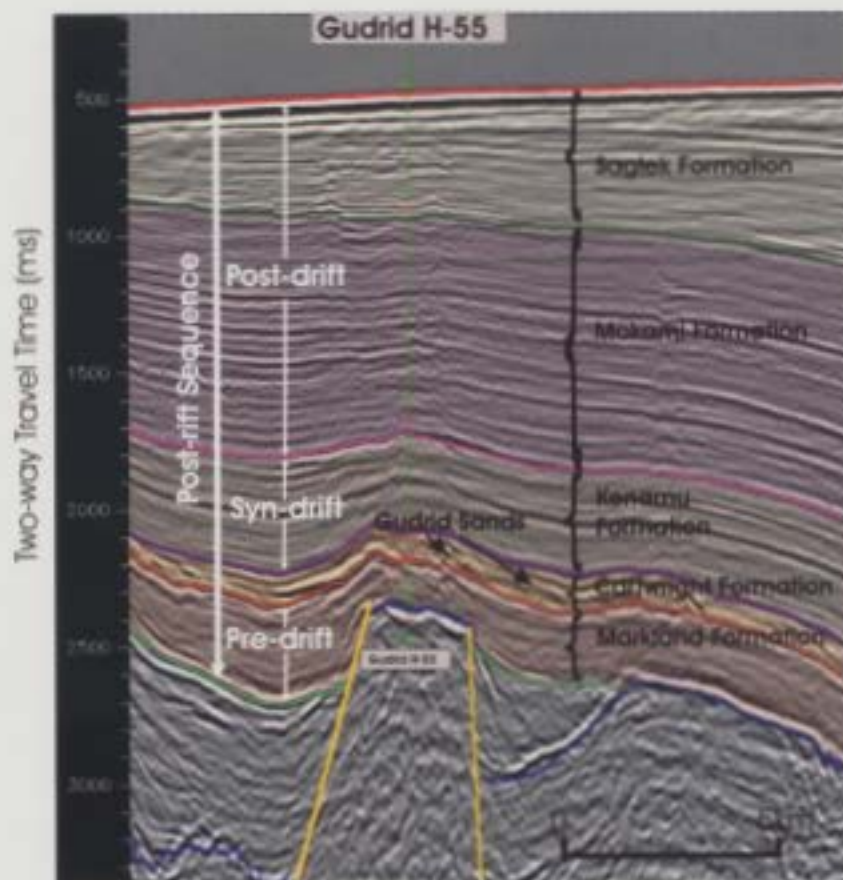


Figure 2.18. Seismic sequences at the Freydis B-87 well. At this location, prerift basement is composed of Ordovician siltstones and limestones. The Freydis, Gudrid and Leif Members (highlighted in yellow) are identified within the postrift sediments.

outer shelf and slope sequence, while the sandstone facies are coastal sand deposits and associated downdip fans (McWhae et al., 1980; Balkwill et al., 1990). The base of the formation is defined by an unconformity, known as the Bylot unconformity, below which lie the shales of the Markland Formation (McWhae et al., 1980). Because the general colour, texture, and fabric of the Cartwright shales are similar to the Markland Formation, they were originally considered as part of that succession (Balkwill et al., 1990). However, the Cartwright Formation is bounded by unconformities and recognizable as a separate entity. In most wells, the unit is easily distinguishable and can be delineated seismically (Balkwill et al., 1990). The Cartwright Formation extends parallel to the Labrador Shelf, forming an elongate prism that thins landward by depositional onlap onto older rocks. The prism also thins seaward by downlap or intercalation with Paleocene sedimentary and volcanic rocks (Balkwill et al., 1990). In the Hopedale Basin, the formation is relatively thin, with the thickest section measured as 495 m (Balkwill et al., 1990). Typical examples of the seismic sequence containing this stratigraphic unit are shown in Figures 2.17 and 2.18. The top of the Cartwright Formation is denoted by a persistent seismic reflection, while the bottom is marked by an even stronger reflection associated with the Bylot unconformity (McWhae et al., 1980). The internal character of the sequence is variable as strong, discontinuous reflections are evident in nearshore areas where the Gudrid Member sands are well developed, but weaker internal reflections occur seaward.

a. Gudrid Member

The Gudrid member contains sandstone sequences that are the landward equivalent of the Cartwright Formation shales. This sandstone unit is regarded as a turbiditic, deep sea fan with feeder channels deposited mainly on the slope and rise of the outer continental shelf (McWhae et al., 1980). The Gudrid sands and Cartwright shales become interdigitated in several wells, causing the development of upper and lower sandstones with a middle shale unit (McWhae et al., 1980). Examples of the seismic character associated with this unit are depicted in Figures 2.17 and 2.18. The internal Gudrid member is characterized by strong, discontinuous reflections that downlap in places onto the Bylot unconformity. Strong reflections are also associated with both the top and bottom of the formation (McWhae et al., 1980).

Kenamu Formation

This Eocene aged, shale-dominated succession consists of marine silty shale, shale, siltstone and fine grained sandstone with thin, dolomitic limestone beds (Balkwill et al., 1990). Marine shelf and slope deposition conditions are interpreted for the unit, and planktonic foraminiferal studies suggest that the water was tropical at the time (McWhae et al., 1980). A regional unconformity, likely partly subaerial, forms the upper surface of the formation while the base rests conformably on the top of the Cartwright unit (McWhae et al., 1980). The Kenamu Formation is thickest in the depocentre of the Saglek Basin and thins to the south. This thinning is evident as the thickest sequence encountered in the Hopedale basin is approximately 1000m, while in the Saglek Basin the

sequence reaches a thickness of approximately 2200m (Balkwill et al., 1990). Distinctive seismic markers are found at both the top and base of this formation, as shown in Figures 2.17 and 2.18. Internally, the sequence is characterized by continuous moderate to strong reflections.

b. Leif Member

The Leif Member is a fine grained quartzose white to light grey-brown sandstone unit with varying amounts of siltstone and mudstone, and is best developed in the Hopedale Basin (McWhae et al., 1980; Balkwill et al., 1990). Foraminiferal studies indicate the age of the unit to be Late Eocene to earliest Oligocene (McWhae et al., 1980). The unit was likely deposited in a neritic environment close to the time at which seafloor spreading ceased in the Labrador Sea (McWhae et al., 1980). Seismic markers are not generally associated with the Leif Member, but it can be distinguished in places when a strong reflection occurs at the top of the unit (Figure 2.18).

2.4.5 Postdrift Sequence

In the Labrador Sea, “Postdrift” refers to the period of time after the cessation of seafloor spreading due to ridge extinction (Enachescu, 2006). Sediments deposited during this tectonic stage are grouped into the Mokami and Saglek formations. The seismic sequences associated with the stratigraphy are shown in Figures 2.17 and 2.18.

Mokami Formation

The Eocene to Miocene Mokami formation is composed of partly consolidated brown claystones and soft shales (Balkwill et al., 1990; McWhae et al., 1980). The shales are interbedded with thin layers of siltstone, sandstone, calcareous sandstone and limestone (McWhae et al., 1980). The unconformable upper contact of the sequence is overlain by sandstones and conglomerates of the Saglek Formation. A seismic marker occurs at the top of the formation but is difficult to map as it is often obscured by seabed multiples or by harsh processing to remove them. The base of the formation is a strong, regionally persistent seismic marker, which is associated with a weak transgressive event closer to shore. This unconformable surface is known as the Baffin Bay unconformity, which likely represents a minor sea-level fall that occurred during earliest Oligocene time (McWhae et al., 1980). This unit is characterized internally by moderate to strong continuous reflections.

Saglek Formation

This mid-Late Miocene to Pliocene sequence contains very porous, white, brown to grey unconsolidated feldspathic and cherty sandstones with subordinate siltstone and claystone beds. Quaternary boulder beds overlie the top of the formation, which is marked by an erosional unconformity. This unconformity is not clearly defined within conventional seismic surveys (McWhae et al., 1980). The base of the formation is usually unconformable with a sharp lithologic break into the soft brown claystones of the Mokami Formation (McWhae et al., 1980). The base of the unit is defined by a strong

reflection in nearshore areas that becomes weaker seaward. Internally, the sequence is characterized by moderate to weak reflectivity.

The Saglek Formation represents the proximal coarse-grained facies of two thick, widespread progradational wedges. Maximum thickness of the sequence occurs beneath the present outer shelf. The formation can be subdivided into an upper and lower unit separated by a regional unconformity with high erosional relief. This unconformity likely marks a significant tectonic event associated with renewed uplift of coastal regions (Balkwill et al., 1990).

2.5 West Orphan Basin: Tectonic Stages, Stratigraphic and Seismic Sequences

The stratigraphy of the Orphan Basin is generally thought to be similar to that encountered in the neighbouring Jeanne d'Arc Basin. All exploration boreholes in the Orphan Basin are located over prerift basement highs in the shallow-water western portion of the basin and encountered only a Late Cretaceous-Neogene section. Consequently, the remaining sedimentary section in the deep basin is unknown. As discussed in Chapter 1, the basin can be divided into two sections: an eastern portion which likely contains a thick Cretaceous and Jurassic stratigraphic sequence, and western part that developed during the latest Jurassic to Early Cretaceous and actively subsided throughout the Cretaceous. The descriptions of sedimentary sequences in the following sections assume that the sedimentary sequences of the West Orphan Basin are similar to contemporaneous sequences in the Jeanne d'Arc Basin. However, because this portion of the Orphan Basin mainly developed concomitantly with the onset of Early Cretaceous

Labrador rifting, some of the stratigraphic sequences may be similar to those encountered on the Labrador margin. Figure 2.19 shows the lithostratigraphy and tectonic stages for the Orphan Basin in relation to the Labrador Shelf as well as the adjacent St. Anthony Basin. Figure 2.20 indicates the seismic sequences for the basin.

2.5.1 Prerift Sequence

The structural style of Orphan Basin involves a complex array of Paleozoic fault blocks (Bell and Campbell, 1990). These Paleozoic blocks form the prerift basement in the Orphan Basin, and include Carboniferous sediments encountered in the Hare Bay E-21 and Blue H-28 wells. As well, some of the prerift basement may also include older Paleozoic and Precambrian rocks (Enachescu et al., 2005).

2.5.2 Synrift Sequence

During the period between the Late Jurassic and Neocomian, major vertical uplift occurred on the Newfoundland continental margin. This uplift, called the Avalon uplift, is associated with a major Late Jurassic unconformity of Middle Kimmeridgian age and to the renewal of rifting between North America and Europe. Subsidence associated with the rifting appears to be influenced by the northwest trending Atlantic Labrador rift system, as major faults in the region with a northwest trend parallel to the Mesozoic basins on the Labrador Shelf show growth coinciding with the initiation of rifting and volcanic activity on the Labrador Shelf (Grant and McAlpine, 1990). In the Jeanne d' Arc Basin, sequences deposited at this time include fluvial fan and fan deltas of the Jeanne

d'Arc Formation; coastal plain delta top and delta front-prodelta sediments of the Hibernia Formation; shallow marine shoreface facies of the Catalina Formation and estuarine to tidal flat siltstones and sandstones of the Eastern Shoals Formation (Grant and McAlpine, 1990). The source area for these sediments was the Bonavista Platform, located to the west of the rifted area (Grant and McAlpine, 1990). The sandstone units are vertically isolated by shale units deposited during times when the source areas were low or when high sea levels and associated marine transgressions occurred (Grant and McAlpine, 1990). Figure 2.20 indicates the seismic sequences associated with this tectonic phase. The synrift sediments are generally confined to half graben or graben structures and are extensively faulted. The top and base of this sequence are denoted by strong reflections associated with regional unconformities (Figure 2.20). In the west, the internal character of the sequence is weak, but stronger internal reflections occur towards the central part of the basin. The sequence is also affected by extensional faulting and stratigraphic growth is evident towards the fault-bounded margin of half graben structures.

2.5.3 Transition to drift sequences:

During the Barremian to Cenomanian a transition from rifting to continental separation and formation of oceanic crust occurred between the Grand Banks and Iberia.

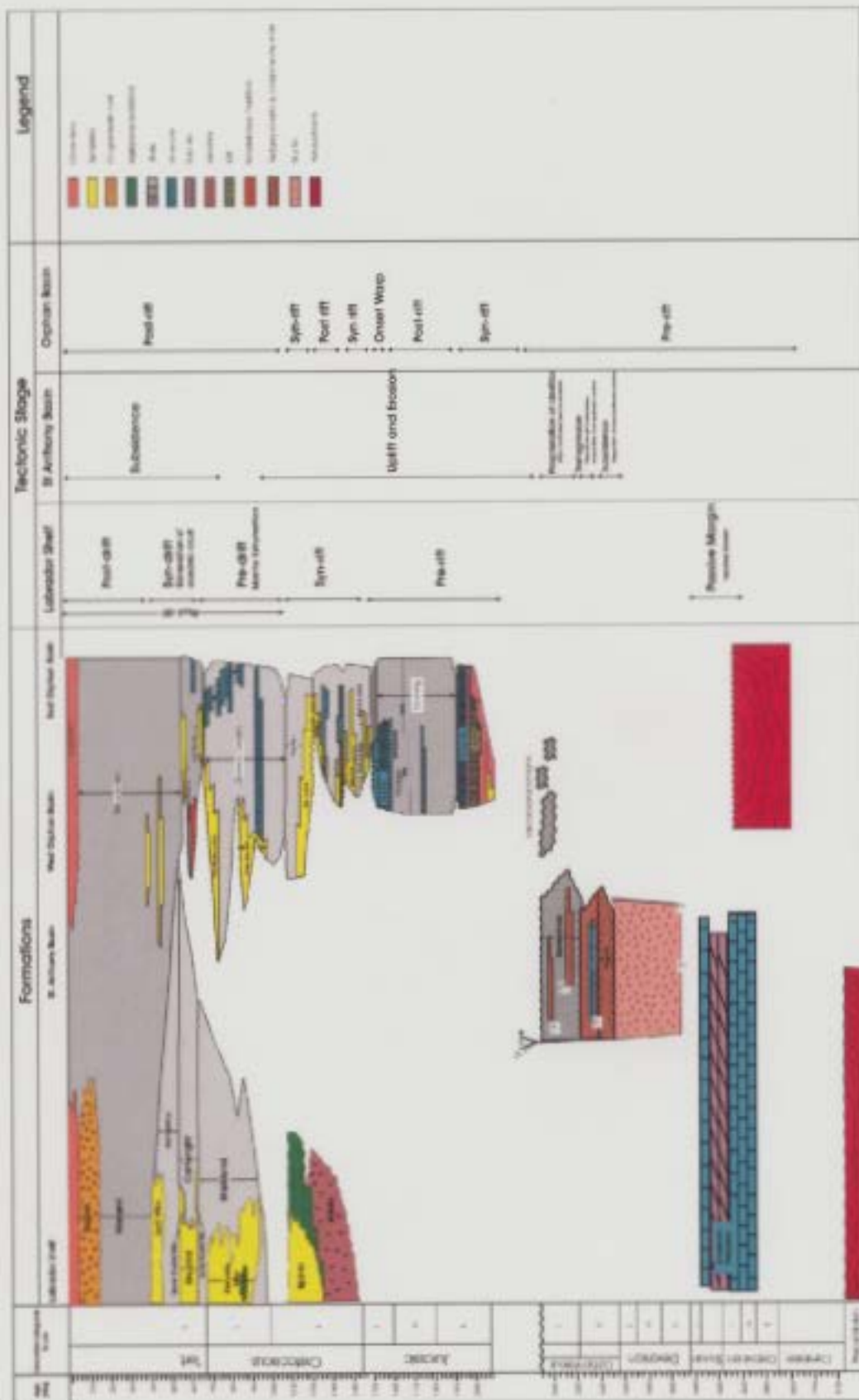


Figure 2.19. Lithostratigraphy and associated tectonic stages for the Hopeedale, St. Anthony and West Orphan basins. Modified from McWhae et al., 1980; C-NLLOPB, 2004; Enachescu, 2006 *a*; Enachescu 2006 *b*.

Incipient spreading may have also occurred between the Grand Banks and Northern Europe (Grant and McAlpine, 1990). The Lower Cretaceous sequence deposited at this time likely contained fine grained sandstones and lagoonal and tidal flat shales, as well as the shallow estuarine channel and tidal flat sands. The sands could have been sourced from high standing fault blocks (Grant and McAlpine, 1990).

During Late Cretaceous to Paleocene time, the continental margin of Newfoundland underwent a transition phase into a passive margin setting. Complete separation of Grand Banks and Northern Europe occurred during this period, and intermittent sediment supplies produced overlapping deltaic sequences with turbidites. During times when subsidence outstripped sediment supply, deepwater chalky limestones were deposited. The Dawson Canyon Formation, a transgressive Cenomanian-Turonian marine sedimentary unit composed of shales with minor siltstones and sandstones, was deposited in a neritic environment at this time. Towards the end of the period the chalky Petrel member was deposited in an outer neritic environment (Grant and McAlpine, 1990). By Coniacian-Maastrichtian time, sediment influx from the west formed an overlapping clastic wedge and chalky outer neritic limestones continued to be deposited (Grant and McAlpine, 1990). At the top of the Late Cretaceous is an unconformity exhibiting prominent channeling into the underlying Dawson Canyon Formation. The

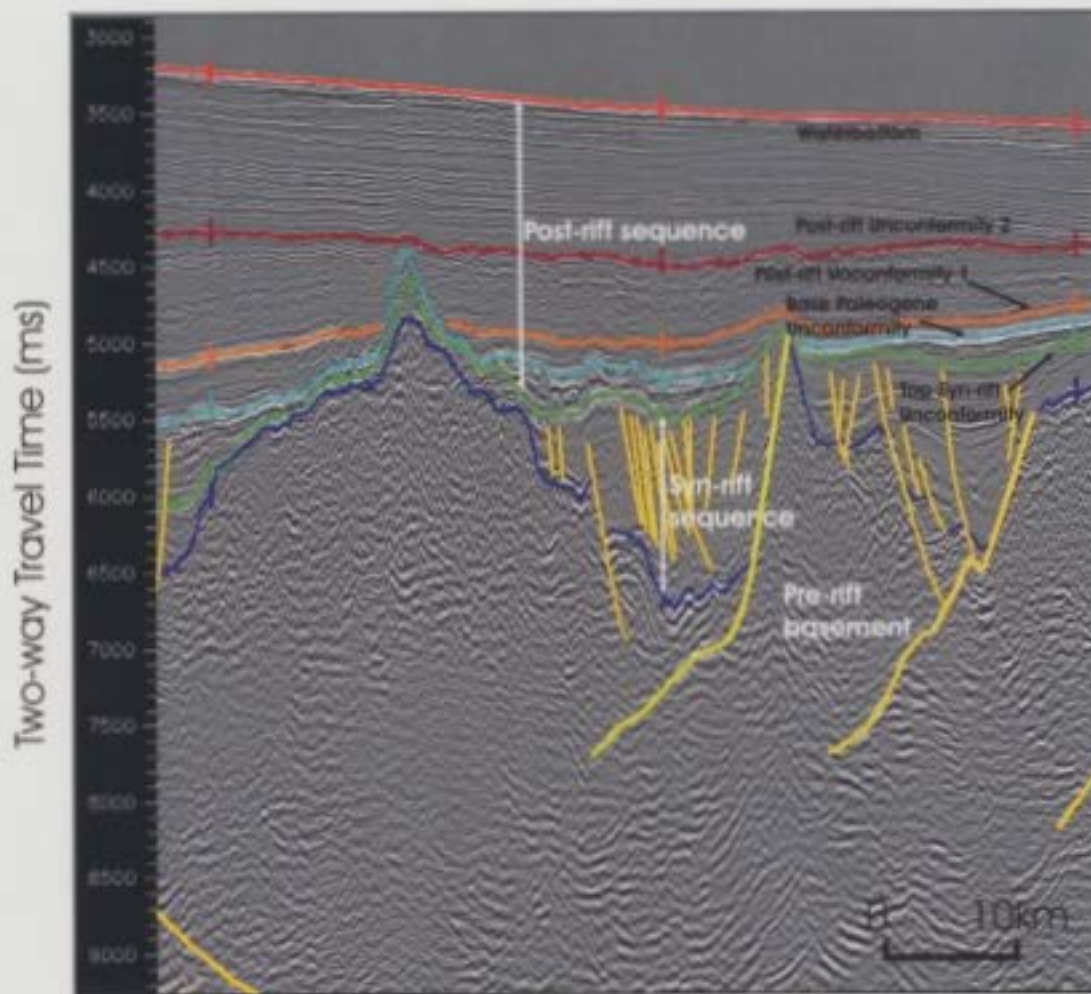


Figure 2.20. Seismic sequences within the Orphan Basin. Highly faulted synrift sediments are overlain by predominantly horizontal postrift layers. In places, the Paleogene and Neogene postrift sequences are deformed due to movement of underlying synrift and basement structures.

overlying Paleocene unit consists of delta front sands and prodelta turbidites (Grant and McAlpine, 1990).

2.5.4 Postrift Sequence

By Eocene time the Grand Banks were surrounded by oceanic crust, and thermal subsidence and seaward tilting of the margin led to deposition of the deep neritic

Banquereau Formation shales (Grant and McAlpine, 1990). Paleoenvironmental data from Paleogene sequences suggest that a change from deep neritic and bathyal depositional conditions to shallow neritic environments occurred during Oligocene time. In Middle to Late Miocene time, sea level dropped again and much of the Grand Banks may have been subaerially exposed. The thickest drift section occurs within the Orphan Basin where it locally exceeds 4 km, as observed in the Sheridan J-87 well (Grant and McAlpine, 1990). The seismic sequences associated with this tectonic phase are shown in Figure 2.20. A strong regional unconformity, the top synrift unconformity, marks the base of this sequence. Within the sequence, the Base Tertiary unconformity and two strong regional markers (red and gold horizons, Figure 2.20) were mapped throughout the study area. Internally, the postrift sequence has moderate to strong reflectivity, with the strongest reflections occurring between the top synrift and Base Tertiary unconformities. Discontinuous, moderate to strong reflections occur between the red and gold horizons, and the uppermost post-rift sequence is characterized by more continuous, horizontal reflections.

2.6 St Anthony Basin: Tectonic Stages and Stratigraphic Sequences

As mentioned in Chapter 1, the St. Anthony Basin is considered to be an offshore extension of the Bay St. George and Deer Lake subbasins, which are part of the regionally widespread Maritimes Basin. In general, the stratigraphy of the Maritimes Basin can be divided into three gross intervals (Langdon and Hall, 1994). The first occurred during the Late Devonian-Tournaisian and involved the deposition of alluvial

and fluvial clastics of the Anguille Group in fault bounded, rapidly subsiding intermontane basins. The second phase occurred during a Visean marine transgression resulting in the deposition of carbonates, evaporates and fine grained clastics of the Codroy Group. The third stage occurred between the Namurian and Early Permian, during which the basin was gradually filled by thick clastic successions, collectively known as the Barachois Group, that prograded out from fault-controlled source terranes along the basin margins (Langdon and Hall, 1994).

In the St. Anthony Basin, drill core samples indicate a stratigraphic sequence similar to that of the Maritimes Basin. This stratigraphy is depicted in relation to the bordering Mesozoic sedimentary basins in Figure 2.19. The cores from the St. Anthony Basin show granite of possible Devonian age underlying a Mississippian unit equivalent to the Anguille Group. Sandstones encountered within this interval are lithologically similar to the Cape Rouge Formation. The Anguille unit is overlain by a Mississippian unit equivalent to the Codroy and Windsor Groups. This correlation was determined from three limestone sequences encountered within the unit. Above the limestone bearing interval lies a Mississippian-Pennsylvanian sequence composed of grey, red and brown sandstone, shale and conglomerate (Haworth et al., 1976 a,b; Bell and Howie, 1990) . This unit is equivalent to the Barachois Formation and was also encountered in the Verrazano L-77 and Hare Bay E-21 exploration wells (Bell and Howie, 1990).

Chapter 3: Regional Architecture

3.1. Objective

This chapter identifies similarities and differences in the structural framework and seismic stratigraphy between the West Orphan, South Hopedale and St. Anthony basins. This objective was accomplished by mapping the major seismic markers and structural features throughout the reflection seismic dataset.

3.2 Seabed Morphology

The South Labrador continental shelf consists of a near-shore variably incised pediment surface carved in Precambrian crystalline rocks, and an offshore, smoother surface underlain by Mesozoic and Cenozoic clastic sediments (Balkwill, 1987). The seabed morphology for the study region was mapped by picking the continuous, high amplitude water bottom reflector. A seabed map was constructed by dividing the picked values by 2000 to obtain a one way travel time in seconds and then multiplying this time horizon by a water velocity value of 1460 m/s. This particular value was chosen to account for the low temperature and salinity of the Labrador Sea.

The seabed map (Figure 3.1) indicates a water depth range of 0 to 3800 metres. The Cartwright Arch is identified as a large, shallow feature stretching from the southern part of Labrador to the northeast of Newfoundland. This feature is characterized by a smooth, unbroken inner basement surface that slopes gently seaward. The outer part of the arch is highly faulted and abruptly plunges to an approximate depth of 3.6 km, as

indicated in Figure 3.1. Further south, a similar shallow prerift feature is identified as the Bonavista Platform.

3.3 Introduction to the Sedimentary Fill

To gain insight into the similarities and differences of the structural and stratigraphic features within the study region, interpreted representative profiles for the South Hopedale Basin, St. Anthony Basin, Cartwright Arch and the West Orphan Basin are compared. The following sections describe the sedimentary fill and features of each region in terms of the pre-, syn- and post-rift tectonic stages.

3.3.1. Basement Structure

Composition, age and structure of the acoustic basement vary throughout the study region. On the southern Labrador shelf, prerift basement includes Early Paleozoic limestones and Precambrian Grenville rocks. The prerift St. Anthony Basin contains Late Paleozoic sedimentary sequences deposited between the Late Devonian and Early Permian (Haworth et al., 1976 *b*; Bell and Howie, 1990). Basement in the Orphan Basin is composed of Late Paleozoic rocks, including a Carboniferous sedimentary sequence, and possibly older Paleozoic and Precambrian rocks (Bell and Howie, 1990; Enachescu et al., 2005). Additionally, in the deepwater areas of the Labrador margin, the prerift basement may be juxtaposed against exhumed continental mantle associated with rifting and the onset of seafloor spreading (Chian et al., 1995*a*; Chian et al., 1995*b*).

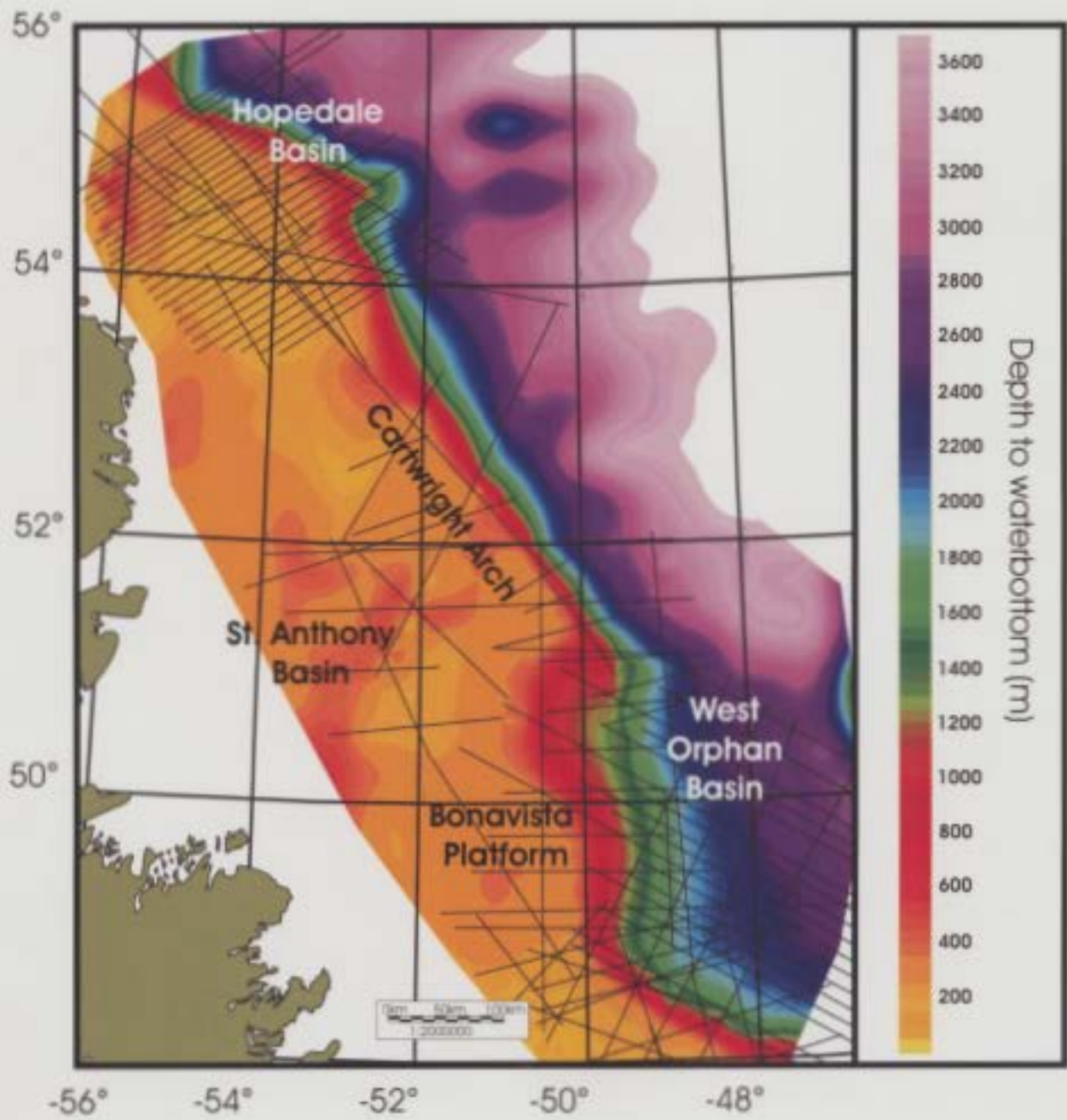


Figure 3.1. Depth to water bottom in metres. Regional seismic grid is indicated by thin black lines.

South Hopedale Basin

Figure 3.2 is a profile across the south Hopedale Basin showing onlap of Mesozoic and Cenozoic sediments onto prerift basement towards the shore. On the inner shelf, the prerift sequence lacks internal reflections, which suggests a low impedance contrast within the sequence or a lack of seismic penetration into it. Prerift rocks in this area are interpreted to be part of Precambrian Grenville province. In the mid to outer shelf area, there are a few places where the prerift basement has some internal reflection and structure (Figure 3.2). The reflections are highly deformed and are interpreted to be Early Paleozoic sediments, as the Gudrid H-55, Freydis B-87, and Indian Harbour M-52 boreholes intersect an Early Paleozoic carbonate platform.

Past the shelf break, a tentative interpretation of exhumed continental mantle is indicated on the seismic profile, as this area is within the ocean-continent transitional region interpreted to be exhumed mantle peridotite from seismic refraction data (Chian et al., 1995a; Chian et al., 1995b). Further south, on the Newfoundland margin, drilling and seismic refraction data results confirm the presence of intensely serpentinized mantle and basaltic lava flows (Tucholke and Sibuet, 2007; Robertson, 2007). The basalt flows are interpreted to have been erupted during ultra slow sea-floor spreading, or following the completion of mantle exhumation (Robertson, 2007). Figure 3.2 also indicates numerous oceanward dipping detachment faults proximal to the interpreted transitional region. Examination of a fossil passive margin (Jurassic-Tethyan margin) in the eastern Alps suggests that ocean-continent transition zones are characterized by oceanward dipping

detachment faults that lead to exhumation of subcontinental mantle rocks (Schaltegger et al., 2002).

Cartwright Arch and St. Anthony Basin

Figure 3.3 is a profile extending over the Paleozoic St. Anthony Basin and Cartwright Arch. It indicates a smooth, seaward dipping prerift basement surface that is onlapped by a thin postrift succession. A deformed prerift sequence, interpreted as Late Paleozoic, is evident in the St. Anthony Basin. This folded sequence is interrupted by zones of poor seismic imaging, which implies that strike slip faults, or other prerift structural features are likely present in this area. Further seaward, the prerift continental arch has fewer internal reflections, which suggests a lower acoustic impedance contrast within the sequence at this location. The continental arch is cut by extensional faults and onlapped by a thin Mesozoic synrift sequence at the shelf break.

A structural high, bordered by steep normal faults, is located at the seaward end of the profile. The uplift of this feature post-dates the deposition of the lower postrift sequence, as the Base Tertiary, Baffin Bay and Postrift 1 unconformities have been deformed due to movement of the structure. Comparisons of this structure to the Mauzy Peridotite Ridge, located further south on the Newfoundland Continental margin, show similarity. This peridotite ridge is imaged seismically and confirmed by scientific drilling (Scientific Results, Leg 210). Reflection seismic profiles indicate that deep seismic reflections lap against the ridge, suggesting that it likely formed during or shortly after the final stages of break-up (Robertson, 2007). The Mauzy ridge appears to have

undergone uplift, and two main explanations are put forward: (i) it formed within the ocean-continent transition zone during exhumation of the mantle. Bending stresses associated with large-scale deformation and detachment faulting are thought to have broken the footwall and uplifted seafloor ridges hundreds of meters high on the Mid-Atlantic Ridge, and (ii) the ridge was uplifted by normal faulting during a later phase of extension well after the mantle was first exhumed (Robertson, 2007). The second possibility is currently the most favoured (Robertson, 2007). The similarities between this ridge and the one imaged in Figure 3.3 suggest that the feature could be a peridotite ridge.

West Orphan Basin

Figures 3.4 and 3.5 are profiles across the West Orphan Basin that extend into the Central Orphan Basin High and East Orphan Basin. Poor seismic imaging on the western side of each line prevents description of the internal characteristics of the prerift sequence. However, towards the central part of the profile there are some deformed, high amplitude reflections. A folded, high amplitude sequence is also located adjacent to the Blue H-28 borehole. This prerift succession is interpreted to be Upper Paleozoic in age as Carboniferous sediments were encountered in the Blue H-28 borehole.

3.3.2 Synrift Sedimentary Fill

On the Labrador Shelf, the synrift sequence is composed of Alexis Formation volcanic rocks and siliciclastic Bjarni Formation sands and shales. The top-syn rift horizon corresponds to the unconformity marking the top Bjarni formation (Avalon

Unconformity). Both the Cartwright Arch and St. Anthony Basin are devoid of synrift sediments, but a thin synrift sequence is interpreted adjacent to the faulted seaward edge of the arch. In the Orphan Basin, the top synrift seismic horizon cannot be correlated to a specific stratigraphic marker due to the lack of well control for the deeper part of the stratigraphic section. However, an angular unconformity truncating the deformed, faulted sediments interpreted as synrift age was traced throughout the dataset. Because of the similarities in seismic character and proximity to the Jeanne d'Arc Basin, the top synrift marker is interpreted to be equivalent to the Avalon unconformity.

South Hopedale Basin

Figure 3.2 indicates that synrift sediments are confined to half graben structures on the inner shelf. The upper part of the synrift sequence contains high amplitude, stratified horizons that show stratigraphic growth towards faults bounding half graben structures on the inner shelf. Beneath the shelf break the seismic quality is poor and distinguishing the internal characteristics of the sequence is difficult. However, further seaward the imaging improves and the synrift sequence appears to thin and downlap onto the acoustic basement.

St. Anthony Basin

The Mesozoic synrift sequence located seaward of the Cartwright Arch is thin and poorly imaged, which makes it difficult to define its internal seismic character. In places,

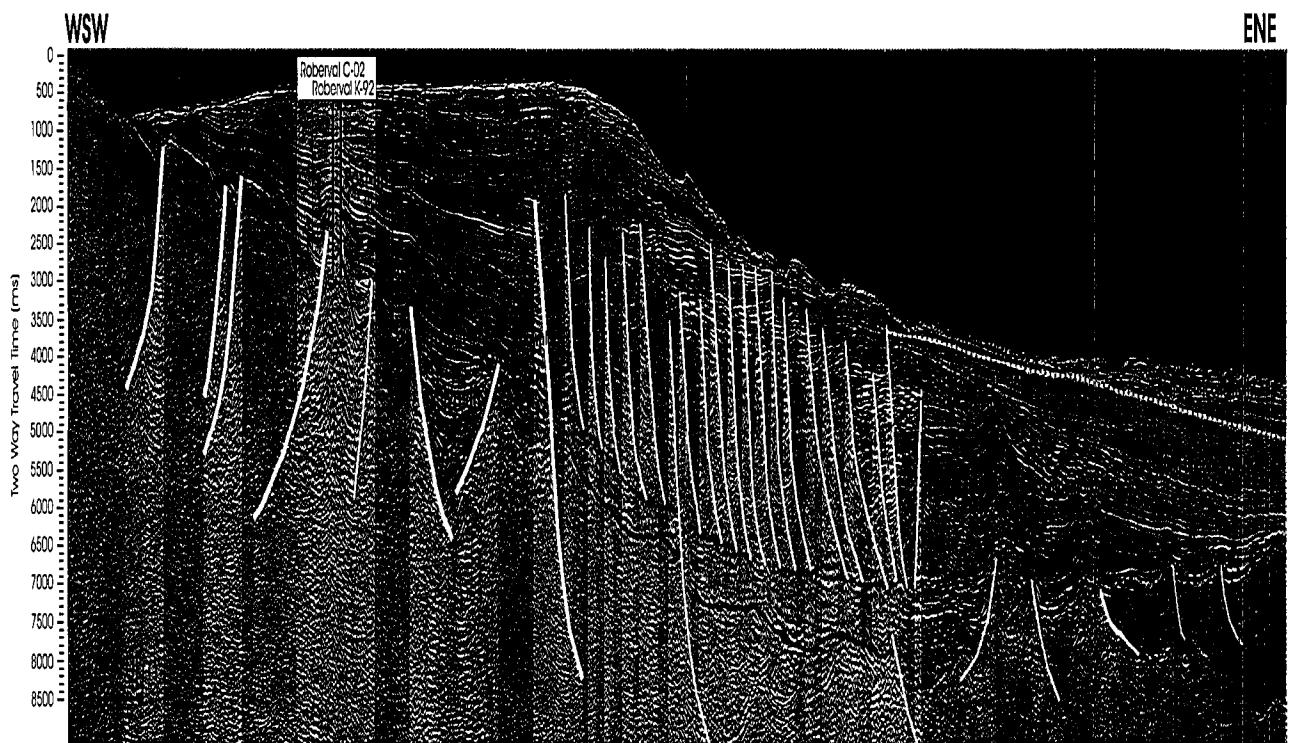


Figure 3.2. Representative profile for the South Hopedale Basin extending past the continental slope and into deep water. The pre-, syn- and post-rift tectonic sequences are indicated on the inner part of the shelf. Typical horst and graben structures are evident and an extensional fault system exists within the postrift sequence below the outer shelf and slope. A compensation feature is interpreted downslope from the fault system. Further seaward, a tentative interpretation of exhumed continental mantle, based on refraction studies north of the area of interest, is indicated (Chian et al., 1995 a; Chian et al., 1995 b).

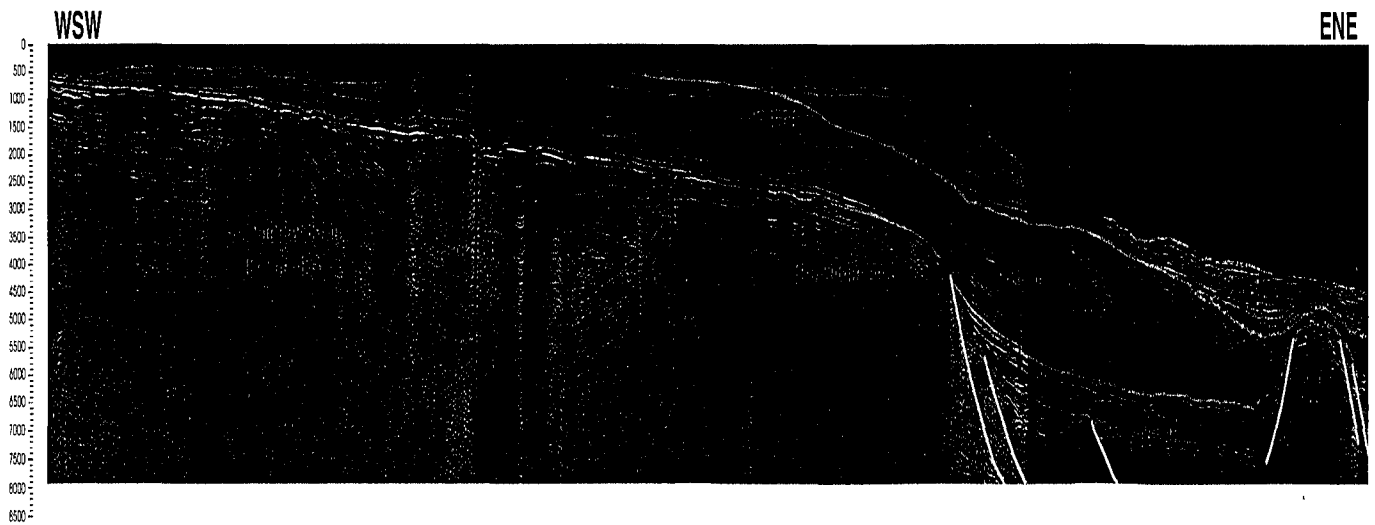


Figure 3.3. Profile extending across the Paleozoic St. Anthony Basin, Cartwright Arch and deepwater areas north of the West Orphan Basin. A Paleozoic sequence is evident in the area of the St. Anthony Basin, and several strike slip faults are interpreted in the basin and through the Cartwright Arch. Further seaward, the arch is disrupted by extensional faults and overlapped a thin, Mesozoic synrift sequence. A basement high feature that resulted in uplift of the Base Tertiary and Baffin Bay and Postrift 1 unconformities is located to the east of the profile. Comparisons of this structure to the Mauzy peridotite ridge show similarity.

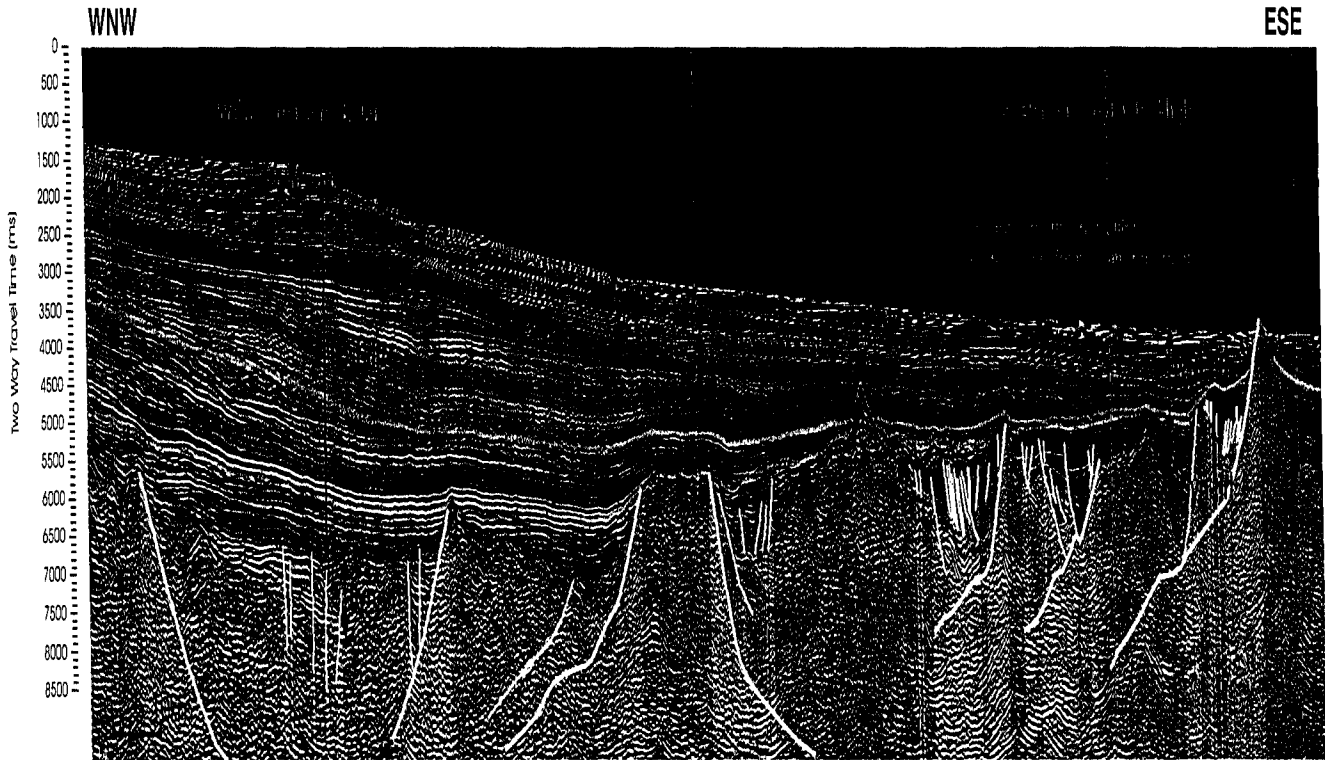


Figure 3.4. Representative profile across the West Orphan Basin and the Central Orphan High. The western side of the profile is characterized by a thick postrift sequence and a thinner synrift sequence. Towards the east, the postrift sequence thins while the synrift sequence is thicker and more extensively faulted. The listric faults bounding the half graben structures also have more kinks towards the east and recent movement and reactivation is evident as one of the faults breaches the waterbottom marker. Additionally, uplift of the top synrift and Base Tertiary unconformities in places suggests that reactivation of basement structures occurred during postrift time.

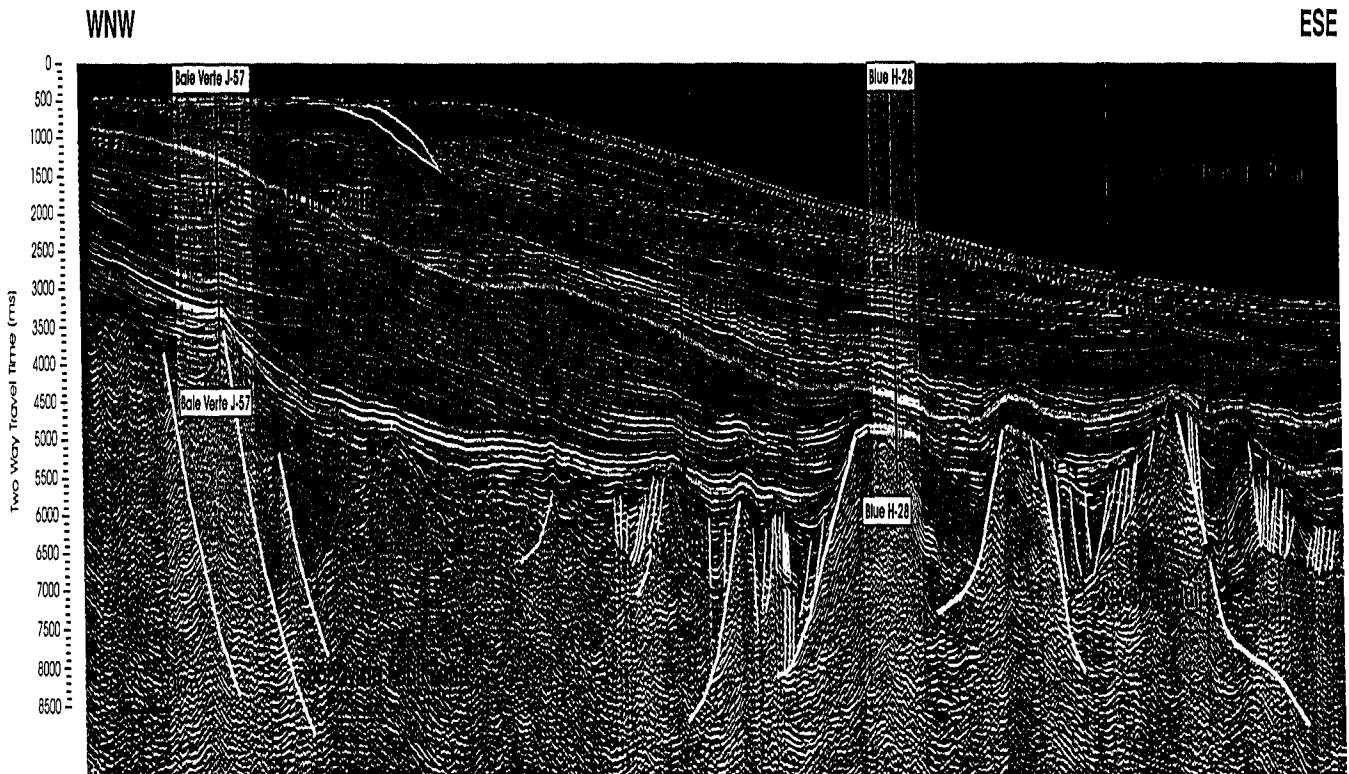


Figure 3.5. Representative profile across the West Orphan Basin and the eastern East Orphan Basin. The western side of the profile is characterized by a thick postrift sequence and a thinner synrift sequence. Towards the east, the postrift sequence thins while the synrift sequence is substantially thicker and more extensively faulted. A reverse fault (shown in orange) in the synrift rollover anticline structure towards the east side of the profile indicates transensional movement that was likely caused by the rotation of the extension vector associated with each rifting episode. Pink areas within the prerift basement are interpreted to be Late Paleozoic sedimentary sequences.

the sequence appears to have low angled, dipping layers that are affected by the extensional faulting. The faults extend midway through the sequence and there is much less stratigraphic growth towards them, which implies that less extensional movement occurred in this area.

Orphan Basin

Figure 3.4 depicts a relatively thin, layered, and extensionally faulted synrift sequence with high amplitude markers on the west side of the profile. This sequence is interpreted as Early Cretaceous and is co-eval with the Bjarni Formation on the Labrador Shelf. Poor imaging on the west side of Figure 3.5 prevents detailed descriptions of the internal character of the sequence, but it appears to thicken towards the east dipping Bonavista Fault Zone. Towards the center of both profiles, the synrift sediments are contained within half graben structures that dip primarily westwards in the south (Figure 3.5), and eastwards further north (3.4). The faults extend to the top of the synrift sequence in the west and central areas of the profiles, and stratigraphic growth towards them suggests that they were active during Early to Late Cretaceous time. Further eastwards, the synrift sequence is substantially thicker and is contained within half graben structures bounded by folded and kinked extensional faults dipping westwards in the north and eastwards to the south (Figures 3.4 and 3.5). Figure 3.5 shows a synrift rollover anticline with a highly faulted sequence containing numerous high amplitude horizons at the eastern end of the profile. The thicker synrift sequence and kinked extensional faults suggest that this area was formed during the earlier Late Triassic-Early

Jurassic rift phase, and later reactivated during subsequent periods of rifting. Thickening of the synrift sequences towards the faults indicates that they were active at this time. Additionally, Figure 3.4 depicts an extensional listric fault that breaches the waterbottom horizon, which implies that this area has undergone recent reactivation. Presence of a reverse fault within the synrift roll over anticline structure (Figure 3.5) suggests that transpression likely occurred in this area. This transpressional stress likely resulted from the rotation of the extension vector with each extensional episode occurring in the Orphan Basin.

3.3.3 Postrift Sedimentary Fill

The thickness of the postrift sequence varies substantially throughout the area of interest. The thickest sequences are present in the West Orphan and Hopedale basins, as well as seaward of the Cartwright Arch. The thinnest postrift sequences occur towards the East Orphan Basin and over the prerift Cartwright Arch and St. Anthony Basin.

Hopedale Basin

Figure 3.2 indicates onlapping of a thin postrift sequence onto the prerift basement in the nearshore part of the Labrador Shelf. This sequence thickens substantially seawards. The upper part of the succession, the postdrift tectonic stage, is characterized by stratified layers with several high amplitude markers. Progradation of the paleoshoreline is evident within this sequence (Figure 3.2). The sediments deposited during the syndrift stage are stratified with several internal high amplitude markers in the

nearshore area of the shelf. Further seaward, these layers progressively downlap onto the Bylot unconformity, as shown in Figure 3.2. The top-most downlapping marker (dashed black horizon in Figure 3.2) is overlapped by horizontal reflectors, which are also included in the syndrift sequence. The downlapping and overlapping stratum suggest a deposition hiatus occurred during this time (Boggs, 2001). The earliest postrift sediments, deposited during the predrift phase, are layered with low to moderate amplitude reflections on the nearshore part of the shelf. The internal reflectivity is higher towards the middle part of the shelf.

Below the shelf break poor seismic imaging masks the internal characteristics of the postrift sequence; however, several extensional faults are interpreted in this area. The listric fault system is more widespread past the shelf break, where the seismic imaging improves, and the faults appear to detach within the lower Kenamu/ upper Markland Formation shales. A compressional anticlinal feature is evident in the region downslope from the fault system. This structure appears to compensate for the extension created by the fault system, as the same sedimentary sequences affected by the extensional faulting form the folded anticlinal structure.

Further seaward, a tentative correlation of the postrift unconformities interpreted in the West Orphan Basin are indicated by the red and gold dashed horizons. Direct correlation of these sequences between the Orphan and Hopedale basins is difficult as the majority of lines linking the Labrador Shelf and Orphan Basin cross the Cartwright Arch in areas where the sequences are not present, or where the seismic quality is insufficient to trace the horizons. However, comparison of the seismic character of the outer Labrador

Shelf stratigraphic sequences with the deep water postrift sequences in the Orphan Basin show striking similarity. In both locations, the sequence between the two upper post rift unconformities has an internal structure characterized by discontinuous, high amplitude reflections. The discontinuity of the reflections suggests that the sequence could be affected by polygonal faulting. Polygonal fault systems are generally located on passive margins, and form onlap fill units comprised of very fine grained sediments (Dewhurst et al., 1999). These systems usually extend over areas of several thousand square kilometres and primarily affect continental slopes and basin axes (Hansen et al., 2004). Polygonal faults are closely spaced, normal faults with throws of less than 100m, and lengths of 500-1000m that are organized into polygonal networks in planview (Hansen et al, 2004). On seismic sections, these systems are characterized by sequences of discontinuous reflections that are often bound by more stratified units. These characteristics are evident in both the Hopedale and Orphan basins (Hansen, et al., 2004; Dewhurst et al., 1999).

Cartwright Arch and St. Anthony Basin

Within the postrift sequence, the Base Tertiary and upper postrift unconformities (red and gold horizons) were traced from the Orphan Basin dataset into this area. Additionally, the Baffin Bay unconformity (Top Kenamu marker) was traced from both the Hare Bay E-21 well and from the boreholes in the South Hopedale Basin. The sequence between the unconformities appears to have similar, moderate to strong discontinuous reflectors that are also encountered in the Orphan Basin and on the Labrador Shelf. However, the internal character of this sequence is less clear in this area

due to the poor resolution in the deepwater areas, and from the uplift of the basement feature described in 3.2.1

The postrift sequence is thin over the St. Anthony Basin and the Cartwright Arch, but thickens seaward to form a convex, lenticular, downlapping sequence that is truncated by the postrift unconformity 1 (gold horizon). The morphology of this feature is typical of contourite structures, which are sediments deposited or substantially reworked in deepwater by the action of slope-parallel bottom currents (Rebesco and Stow, 2002). A schematic model identifying principal characteristics of contourite deposits is shown in Figure 3.4. Mounded, elongated contourite deposits typically have a high relief, and are broadly lenticular, upward convex seismic units (Rebesco and Stow, 2002). These characteristics are evident in the structure identified in Figure 3.3. Contourite deposits can occur anywhere from the outer shelf/upper slope, to the abyssal plains (Stow et al., 2002). Seismic facies associated with contourite deposits include: (i) semi-transparent, reflector-free intervals; (ii) continuous, sub-parallel, moderate- to low-amplitude reflectors; (iii) regular, migrating-wave, moderate-to-low amplitude reflectors; (iv) irregular, wavy to discontinuous moderate amplitude reflectors; and (v) irregular, continuous high-amplitude reflectors (Stow et al., 2002). The structure interpreted in Figure 3.3 has a moderate amplitude, continuous reflector seismic facies, which may reflect a greater proportion of silt/sand content, more hiatuses and condensed sedimentation due to increased bottom current intensity (Stow et al., 2002). In contrast, more transparent seismic facies likely have less silt/sand, reflecting decreased bottom intensity (Stow et al., 2002). Downlapping and progradational reflector patterns are also

common contourite features (Rebesco and Stow, 2002). These patterns are evident on the seismic profile which further suggests that this sequence could be a contourite deposit.

However, interpretation of contourites on the evidence of seismic data alone is rarely possible and margins of uncertainty exist (Rebesco and Stow, 2002). For instance, another explanation for the postrift sequence could be a deltaic deposit, as deltas occur in marginal marine environments and typically form wedge or lens shape bodies in cross section (Boggs, 2002). Additionally, sediments deposited on the slope of delta front commonly have seaward dipping beds with a steep initial dip, which is evident on the profile (Boggs, 2004). With additional data (eg. biostratigraphic, paleoceanographic, sedimentological), this uncertainty could be resolved.

Orphan Basin

Figures 3.4 and 3.5 indicate a thick postrift succession in the West Orphan Basin that thins eastwards. Several markers were interpreted throughout the postrift sequence. These include two upper post rift unconformities (red and yellow horizons), the Baffin Bay unconformity (top Kenamu marker), and the Base Tertiary unconformity. The Baffin Bay unconformity was traced from the Hare Bay E-21 well into the West Orphan Basin. This marker is present throughout the northern part of the basin but downlaps onto the Base Tertiary unconformity to the east and south.

The seismic imaging is poor to fair on the western side of the basin, so description of the internal character of the postrift sequence is difficult in places. However, Figure

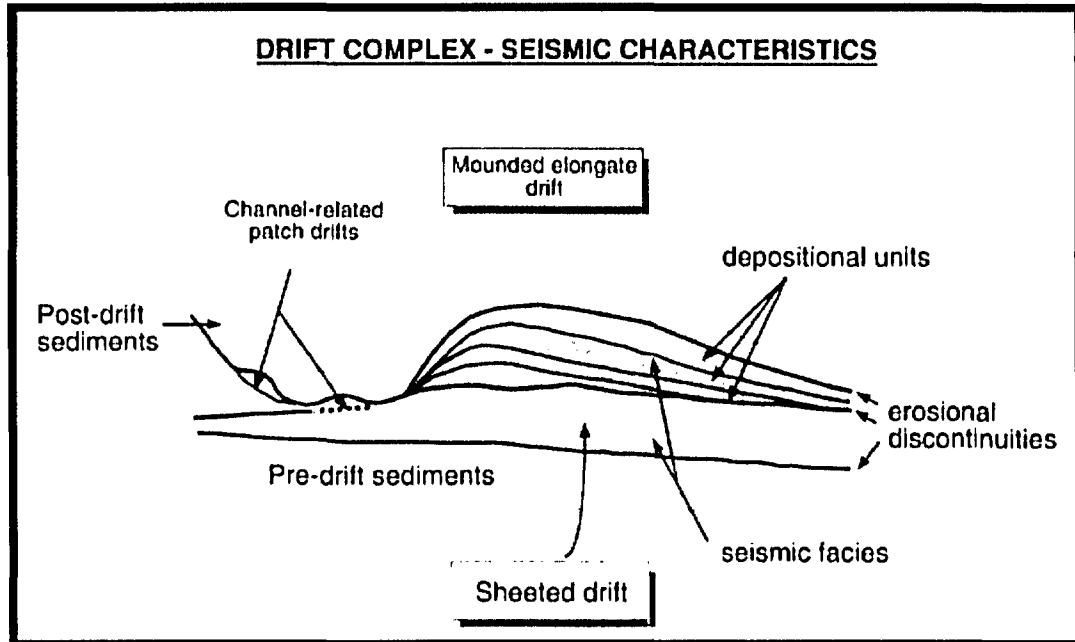


Figure 3.6. Schematic model of principal seismic characteristics of contourite drifts. Modified from Stow et al, 2002.

3.5 indicates that the upper postrift sequence is horizontally layered with moderate to high amplitude reflectors. This profile also contains a downlapping sequence interpreted as a paleoshelf-break, which suggests that shelf prograded eastwards during the later part of the postrift tectonic phase.

The sequence between Postrift unconformities 1 and 2 is characterized by moderately reflective horizons that become increasingly discontinuous towards the central part of the basin, particularly along profile 3.4. The thickness of this sequence is more variable in Figure 3.5. The discontinuity of the reflections towards the basin axis

suggests that this sequence may be a polygonal normal fault system. As discussed in 3.2.3, a similar sequence is also evident in the deep water areas of the Labrador Shelf. As polygonal fault systems extend over areas of several thousand square kilometres and affect both continental slopes and basin axes (Hansen et al., 2004), the sequences evident on the Labrador Shelf, seaward of the Cartwright Arch and in the West Orphan Basin may be part of the same regional system.

The sequence between the Upper Postrift 1 unconformity (gold horizon) and the Base Tertiary unconformity has weak to moderate reflectivity, with the stronger reflections occurring near the Base Tertiary unconformity. This sequence thins to the east on both profiles and is thickest in the southwest, as indicated on Figure 3.5. The early postrift sequence between the Top Synrift and Base Tertiary unconformities has moderate reflectivity, with the strongest reflections also occurring close to the Base Tertiary unconformity. This sequence thins to the east on both profiles, but is thicker towards the west side of Figure 3.4.

3.4. Structural History

3.4.1. Prerift Structure

Figure 3.7 is a time-depth structure map of the top of prerift basement showing the major faults and structural elements within the area of study. Listric faults detaching within the prerift basement dip both landward and seaward on the inner Labrador shelf, but become predominantly seaward dipping past the shelf break. The changes in fault polarity may be a function of prerift basement composition or reactivation of prerift

features. In many rifts, prerift structural fabrics can weaken the basement, reduce its strength and become reactivated during later tectonic deformation (Younes and McClay, 2002). This weakening may have controlled the orientation of the extensional faults, as re-activation of favorably oriented pre-existing fractures is naturally more efficient than forming new ones, particularly during the early stages of rifting (Younes and McClay, 2002). However, other rift induced normal faults cross preexisting sutures and major fault zones, suggesting that rift structures are not all formed by reactivation (Enachescu, 1992; Enachescu et al, 2005).

Border faults and basement ridges within the western and central Orphan Basin are north-northeast to east-northeast trending, while extensional faults on the Labrador Shelf trend north-northwest to northwest. The extensional faults within the Orphan Basin are highly segmented in places, cover a more widespread area, and have larger throws than those mapped on the southern Labrador Shelf. In several locations, the extensional faults and half graben structures change polarity along strike. The differences in fault trend between the Labrador Shelf and Orphan Basin regions can be attributed to the differences in original direction of rifting, and also locally to pre-existing structural fabrics, such as foliations, fractures, faults and dykes. These fabrics can reduce the strength of the basement and become reactivated, particularly if planes of extension are oriented normal or oblique to the extensional direction (Younes and McClay, 2002). This theory is supported as Appalachian structures, which form the prerift basement in the Orphan Basin, trend east-northeast offshore Newfoundland. The east-northeast trends are a result of right-lateral flexure suggested by a swing in northeast-trending magnetic

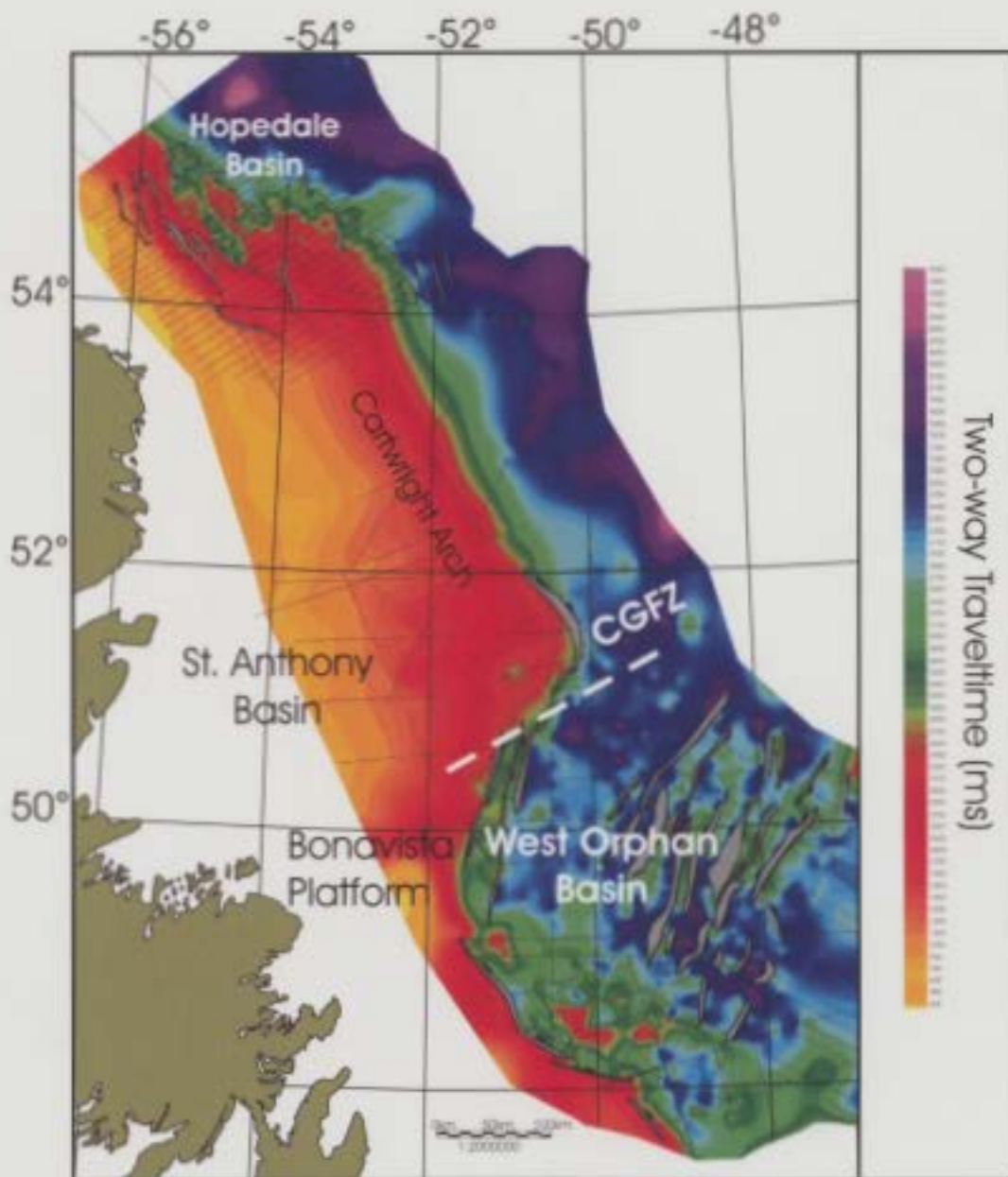


Figure 3.7. Time structure map to the top of prerift basement, showing major basin border faults and intrarift fault systems. Dashed white boxes indicate areas interpreted as accommodation zones. CGFZ=Charlie Gibbs Fracture Zone.

anomalies (Bell and Howie, 1990). This right-lateral flexure explains the east-northeast trend of the Charlie Gibbs Fracture Zone, which is believed to be a continuation of the northeast trending Dover Fault (Enachescu et al., 2005). These pre-existing trends within

the prerift sequence may have controlled the orientation of east-northeast trending faults evident in Figure 3.7. However, the Bonavista Fault Zone and major faults within the Orphan Basin are oblique to the east-northeast trend, implying that not all features result from reactivation of pre-existing structures (Enachescu, 2002; Enachescu et al, 2005).

3.4.2. Synrift Structure

Isopach maps of the synrift sequence were constructed for the West Orphan and Hopedale basins (Figures 3.8 and 3.9). A two-way time thickness map of the rift stage sediments was first obtained by subtracting the seismic basement horizon from the top Bjarni Formation marker (Hopedale Basin) and the top synrift marker in the Orphan Basin (Avalon Unconformity equivalent). This time interval was then divided by 2000 to get a one way time thickness value in seconds, and then multiplied by a velocity of 3900 m/s in the Hopedale Basin and 3800m/s in the Orphan Basin to get a rough estimate of the thickness in metres. These particular velocity values were obtained by comparing borehole velocity data, velocity data from seismic refraction surveys, and processing velocities available for reflection seismic lines within the area of interest. A more detailed explanation of these velocity estimates is discussed in Chapter 5.

The isopach maps for both the South Hopedale and the West Orphan basins indicate increasing thickness of sedimentary fill towards listric bounding faults of half graben structures. On the inner Labrador Shelf, thicker synrift sequences are confined to the half graben structures, while thinner sequences with localized areas of thickening are

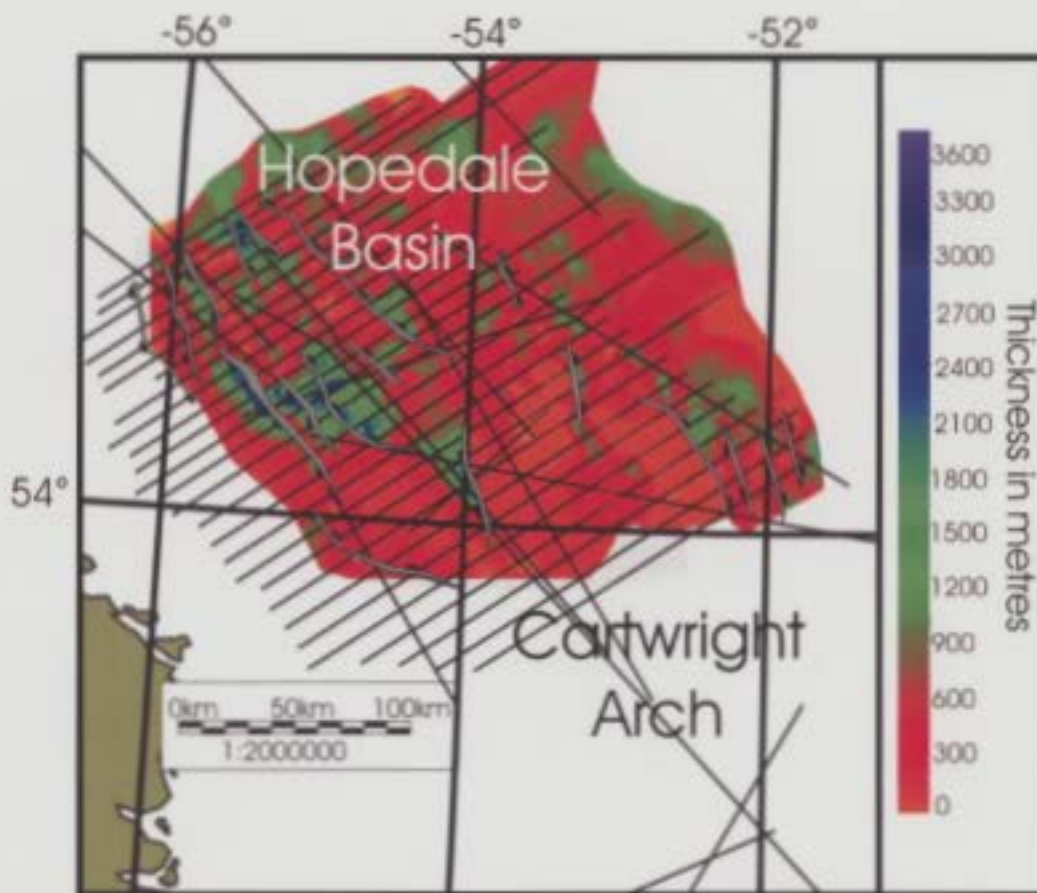


Figure 3.8. Synrift isopach map of the South Hopedale Basin. The sequence is thickest within half graben structures on the inner shelf. Stratigraphic growth is suggested by the thickening of the sequence towards the bounding faults. The sequence thins seawards, but localized areas of thicker sedimentation occur on the outer shelf and slope break.

evident on the outer shelf. In the West Orphan Basin, the thickness of synrift sediments is greatest in the areas adjacent to the Bonavista Fault, and within fault bounded structures towards the central and eastern areas. A continuous thin sequence, similar to that encountered on the outer Labrador Shelf, is present throughout most of the basin. The synrift sequence in the West Orphan Basin was deposited during the Late Jurassic to Early Cretaceous rifting stage, which is the second stage rifting fill for the Orphan Basin.

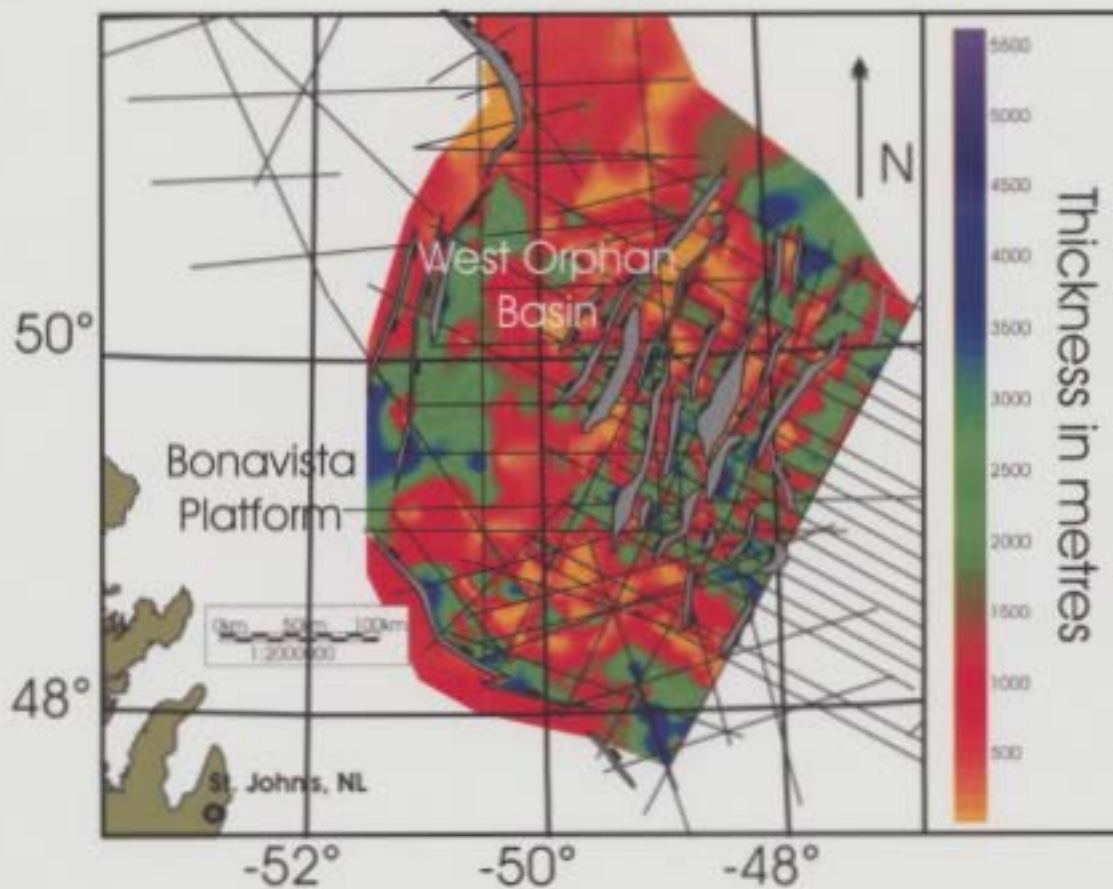


Figure 3.9. Synrift isopach map for the West Orphan Basin. The sequence is thickest along the western margin (Bonavista Fault zone) and within half graben structures in the central and eastern areas. Thickening of the sequence towards marginal faults is evident in these locations. The sequence thins over intrabasin ridges in the central part of the basin, and also in the southwest and northeast areas.

The first stage rifting fill includes late Triassic- Early Jurassic rocks that were deposited primarily in the East Orphan Basin. As the East Orphan Basin is outside the region of interest, this interval was not mapped. Accordingly, these maps compare synrift sequences deposited during the later Atlantic and Labrador rifting stages.

3.4.3. Postrift Structure

Postrift isopach maps were constructed by subtracting the base postrift marker

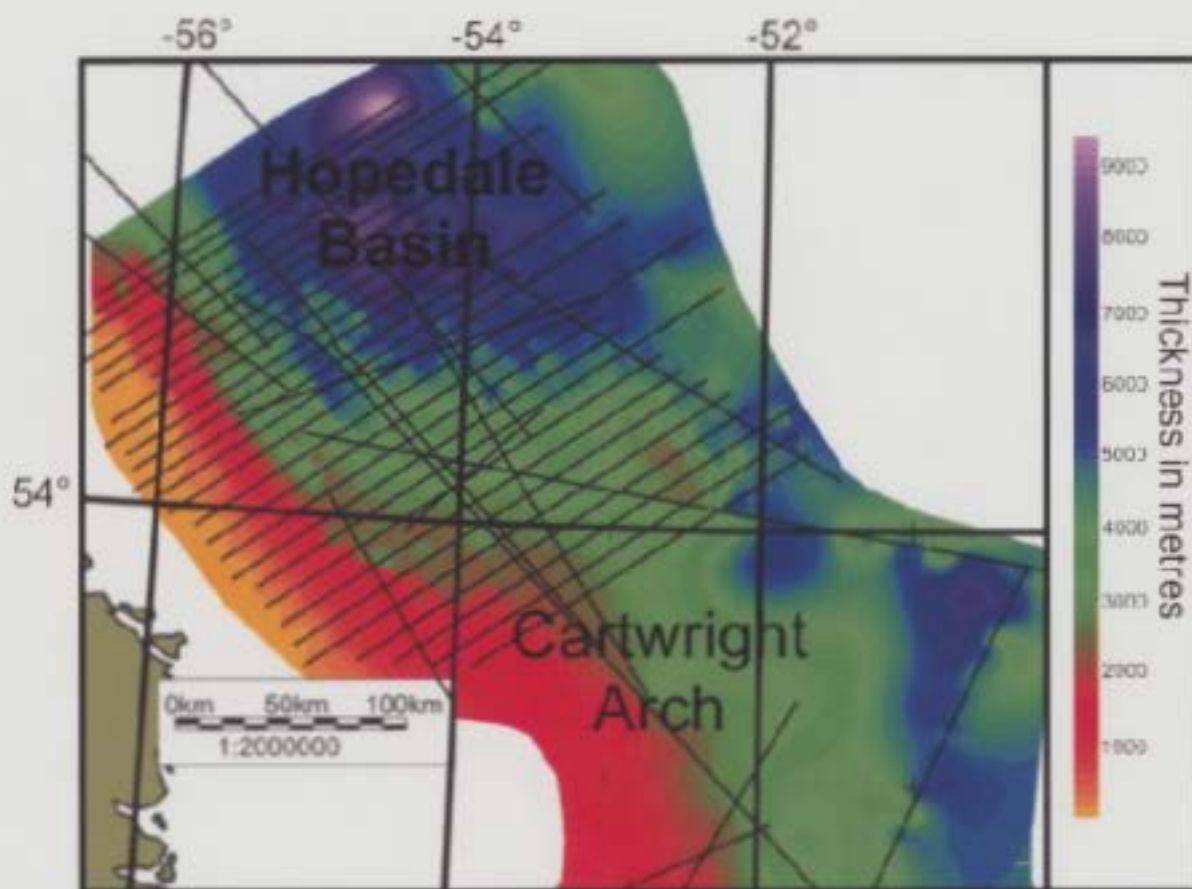


Figure 3.10. Postrift isopach map for the South Hopedale Basin. The sequence thickens seawards, which suggests that the shoreline prograded eastwards. The sequence thins substantially towards Cartwright Arch in the southwest.

from the water bottom horizon (Figures 3.10 and 3.11). Over the Cartwright Arch and areas without synrift sequences, the base postrift marker is the seismic basement horizon. In areas with synrift sequences, the base postrift marker is the Avalon unconformity. The obtained isochron was divided by 2000 to obtain a one way time thickness interval in seconds, and multiplied by an average velocity value of 3200 m/s to convert to depth.

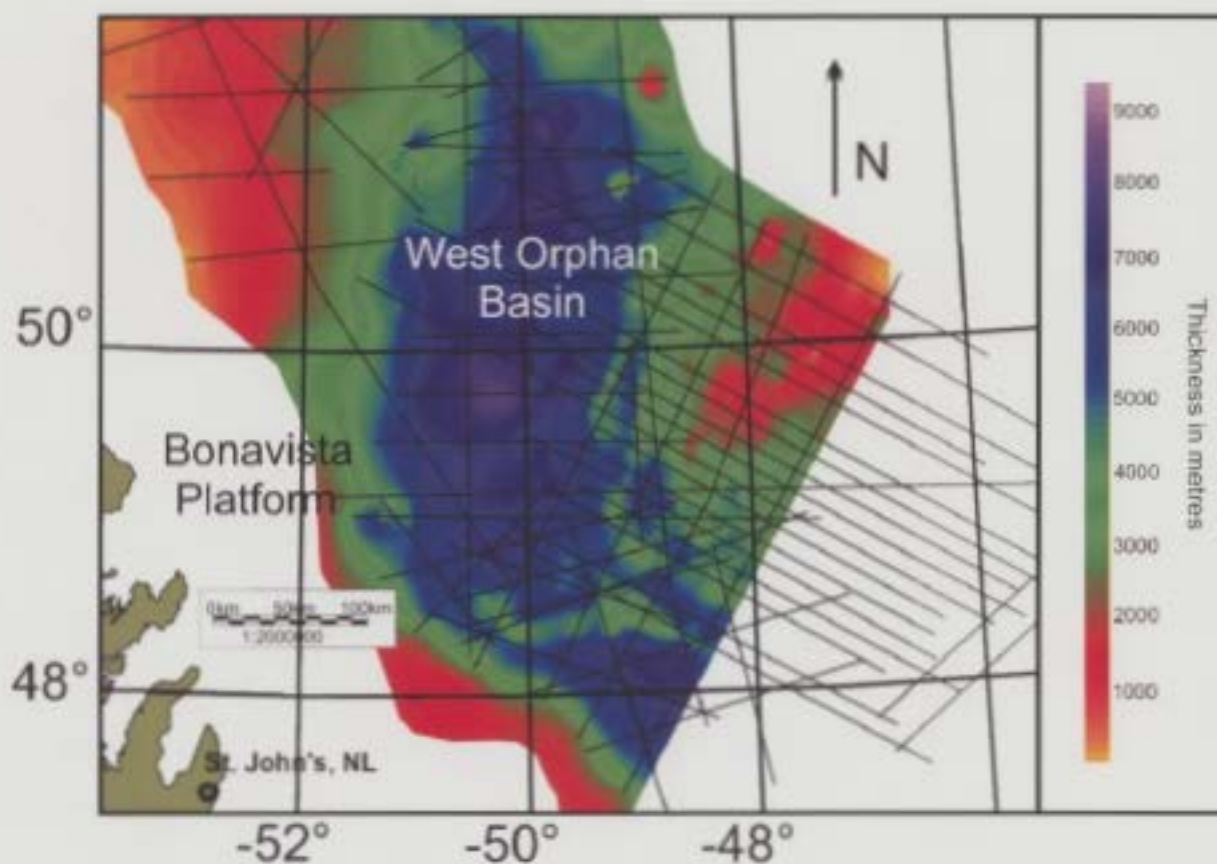


Figure 3.11. Post rift isopach map for the West Orphan Basin. The sequence is thickest along the western margin and thinner towards the east.

This particular velocity value was estimated from comparison of postrift interval velocities from borehole, seismic refraction and reflection seismic processing and is discussed in more detail in Chapter 5.

The postrift isopach maps indicate two areas of significant post rift accumulation: the first along the slope of the South Hopedale Basin, and the second in the West Orphan Basin. In general, these areas correspond to regions with thin, laterally extensive synrift sequences. The postrift isopach maps also indicate an eastward progradation of the shelf edge. Significant thinning of the sequence is evident in the nearshore margin of the Hopedale Basin, and towards the eastern edge of the West Orphan Basin.

3.5. Regional Gravity Anomalies

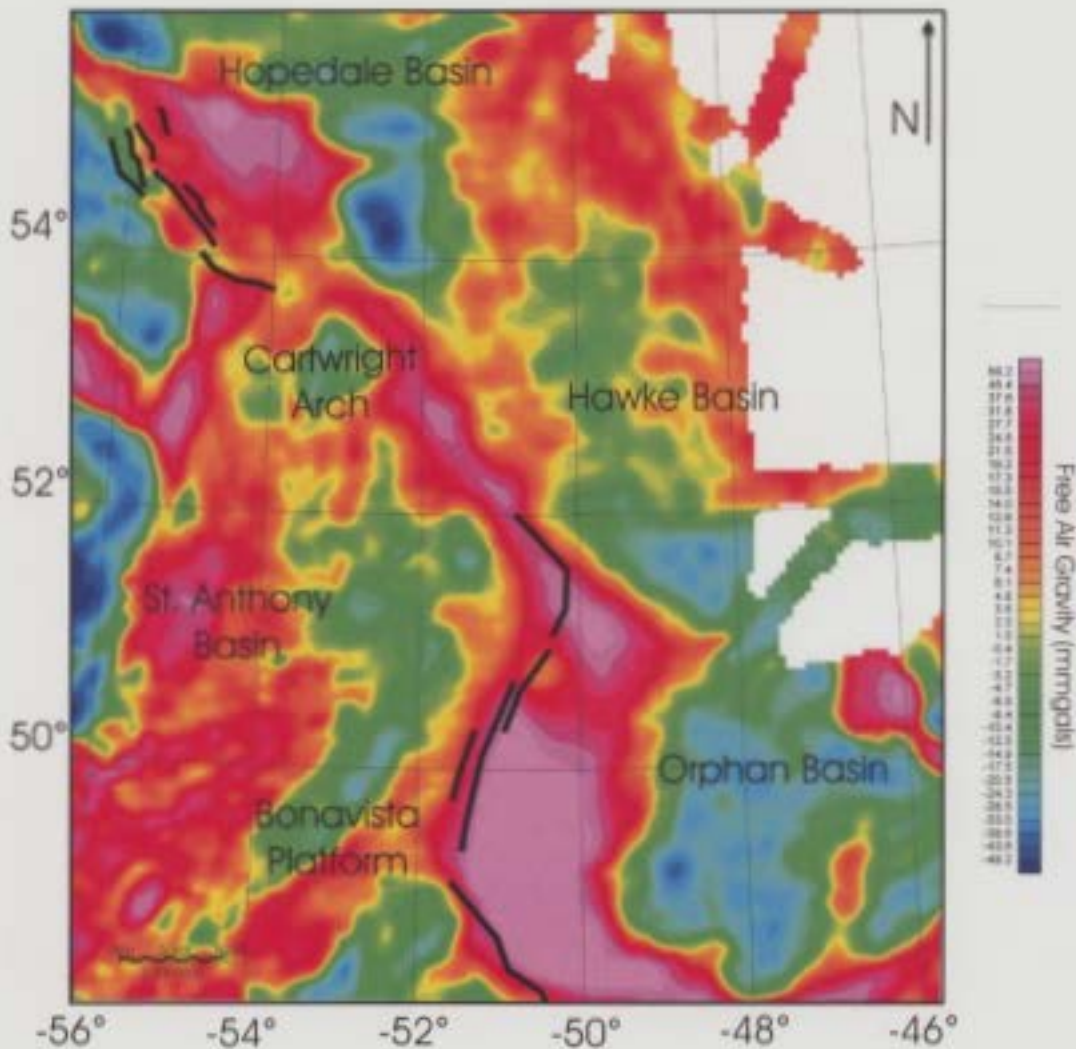


Figure 3.12. Free Air gravity (2000m grid spacing), showing basin bounding faults and regional tectonic framework interpreted from the top prerift time structure map. Gravity data obtained from the Geological Survey of Canada (GSC) Data Repository.

A Free Air gravity map was constructed using gridded data from the Geological Survey of Canada (Figure 3.12). Basin border faults and prerift features interpreted from the seismic are indicated on the map. High gravity anomalies denote the shelf break, and gravity lows characterize the Mesozoic Hopedale, Hawke and Orphan basins. Prerift features (St. Anthony Basin, Cartwright Arch, and Bonavista Platform) are associated

with both high and low anomalies, which may be a function of basement/prerift sediment composition or thickness of overlying Cenozoic postdrift sediments.

The high free-air gravity anomaly in the East Orphan Basin is interpreted to be a result of mantle upwelling (Enachescu et al., 2005). Modeling of potential fields data suggests that this upwelling remains in the lower crust with no large quantities of volcanic material intruding into the sedimentary fill. This gravity high is located east of the seismic interpretation limit for this project. However, a certain degree of mantle upwarp likely occurs in deepwater areas within the area of interest, which is discussed in Chapter 5.

3.6 Summary of Observations

In comparing the sedimentary fill and structural features throughout the study region, numerous similarities and differences are apparent. Examination of the reflection seismic data indicates that the structure and composition of prerift, synrift and postrift sequences vary spatially along the continental shelf, slope and in deepwater.

The seismic character of the acoustic basement ranges from non-reflective Precambrian and Paleozoic sequences to high amplitude, highly deformed Paleozoic sequences along the continental shelf. Exhumed continental mantle is interpreted past the shelf break within the continent-ocean transitional zone adjacent to the South Hopedale Basin. A ridge with similar seismic character to a peridotite ridge further south on the Newfoundland continental margin is evident seawards of the Cartwright Arch (Figure 1.1).

Both the South Hopedale and West Orphan basins have a high postrift-to-synrift sediment ratio and contain similar seismic markers within the postrift sequence. In the South Hopedale Basin, the synrift seismic sequence thins and downlaps onto prerift basement while the postrift sequence thickens substantially past the slope break. The thick postrift sequence is affected by significant extensional faulting over the slope, which is complemented further seawards by the development of a slump system. In contrast, the West Orphan Basin contains a thinner postrift cover and thicker, more deformed synrift sequence in deep water areas. These thicker synrift sequences are interpreted, in places, to be affected by reverse faulting, which suggests rotation of the extension vector with each rifting episode. The thickness variations of these sequences are investigated further in Chapter 5 through palinspastic reconstruction of profiles along margin.

The Mesozoic synrift sequence is not evident in the Paleozoic St Anthony Basin or intervening Cartwright Arch, but a thin synrift sequence and a thick, lenticular shaped postrift seismic sequence is interpreted seaward of the Cartwright Arch. In the deepwater region of the entire margin, a discontinuous, high amplitude reflection seismic sequence is interpreted as a regionally extensive polygonal fault system.

Orientation of the extensional rift fault systems varies throughout the region. Differences in the orientation of the faults are attributed to both pre-existing structural fabrics and rotation of the extension vector with each rifting episode. The fault structure and trend for each area are examined in the following chapter to identify correlations

between the different extensional regimes and the structural features evident throughout the study region. While the Hopedale and West Orphan Basins appear to contain similar stratigraphy, there are major differences in the orientation and areal coverage of the extensional faults in each area. For example, the fault structure within the pre-and-synrift sequences is much more complicated in the easternmost West Orphan Basin. These differences are analyzed by comparing both the South Hopedale and West Orphan rift systems to analogue models of orthogonal, oblique and multi-phase rifts.

Chapter 4: Rift Systems

4.1 Rift System Structure

The Hopedale and Orphan basins are examples of intracontinental rifts, which are typically formed by a system of narrow half grabens bounded by rift-border faults (Gawthorpe and Hurst, 1993). Rift systems often display along-strike changes in extensional fault polarities and in offset grabens and depocentres along the rift axis (e.g. Gibbs 1984; Gawthorpe and Hurst, 1993; McClay and White, 1995; McClay et al., 2002; Younes and McClay, 2002). Individual half grabens can be linked along strike by a variety of combinations of overlapping border fault systems, which leads to development of complex patterns of structurally controlled syn-rift stratigraphy within individual rift basins (Younes and McClay, 2002).

Transfer zones, also known as accommodation zones or relay zones, are important elements in extensional sedimentary basins as they accommodate extension between fault and basin segments along the length of the deformational zone (Gawthorpe and Hurst, 1993). Two end member models are proposed to account for the changes in fault polarities and offset depocentres: (i) compartmentalization by discrete strike-slip or oblique-slip transfer faults (hard-linked model), and (ii) displacement transfer by development of accommodation zones between faults and arrays of faults (soft-linked model) (McClay et al., 2002; McClay and White, 1995). With a hard-linked model, along strike changes in polarity of extension are accommodated by vertical or near vertical transfer faults with significant strike-slip displacement. In contrast, a soft-linked model accounts for along strike changes in extensional polarity via accommodation zones where

extensional faults are segmented and displacement transfer between individual segments is accomplished by relay systems (McClay et al., 2002; McClay and White, 1995;)

Figures 4.1 and 4.2 depict simplified examples of each end member.

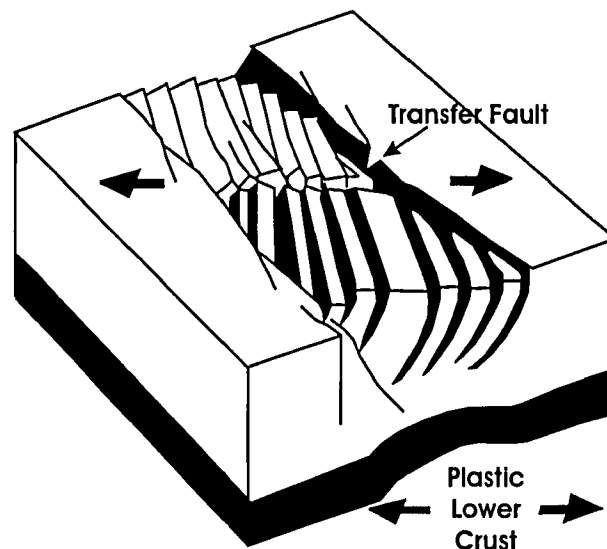


Figure 4.1. Displacement transfer by vertical or near vertical transfer faults in a three-dimensional extensional fault system (hard linked model). Modified from McClay and White (1995).

4.2 Classification of Rift Systems

Scaled, physical, analogue rift basin models and observation of natural rift systems suggests that rift zones can be classified as orthogonal, oblique or multi-phase (McClay et al., 2002; Younes and McClay, 2002; McClay and White, 1995; Keep and

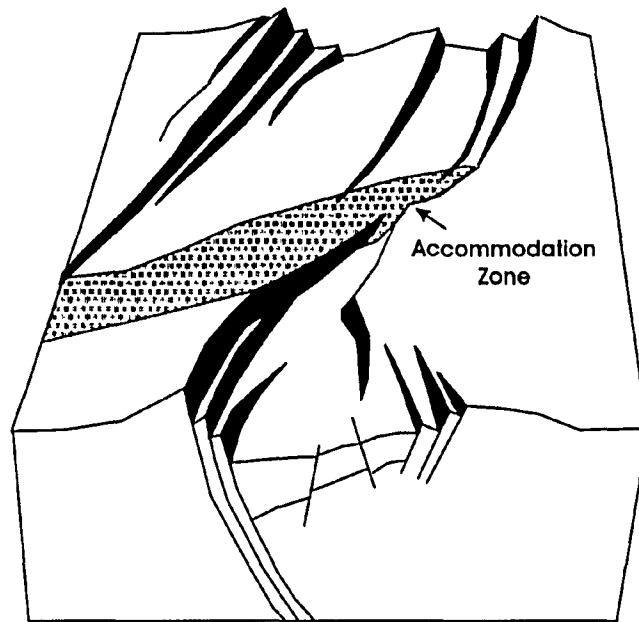


Figure 4.2. Displacement transfer by an accommodation zone in a three dimensional extensional fault system (soft linked model). Modified from McClay and White, 1995).

McClay, 1997). Rift basins produced by orthogonal and oblique rifting are defined by segmented border fault systems parallel to the rift axis and by intrarift systems that are sub perpendicular to the extension direction (McClay et al., 2002; McClay and White; 1995). In an orthogonal rift system, the underlying zone of basement stretching and the extension direction are oriented at 90° to one another. In oblique rift systems, however, the angle between the axis of rifting and the extensional direction is less than 90° (McClay et al., 2002; McClay and White; 1995). With increasing obliquity of the rift axis, segmentation of the rift margin increases and causes an increase of displacement on intrarift fault systems (McClay et al, 2002; McClay and White, 1995). Multiphase rift systems have undergone one or more phases of extension, either with different extension vectors, or where the extension vector rotated with time (Keep and McClay, 1997).

Analogue models suggest that two differently-oriented phases of extension produce complex extensional fault patterns that reflect the first phase of extension and may control or influence later fault geometries (Keep and McClay, 1997).

As discussed in section 1.2.3, the Hopedale and Orphan rift basins developed during several phases of Mesozoic intracontinental extension (e.g. Enachescu, 1987; Enachescu et al., 2005; Loudon, 2002). During these rifting phases, the extension direction around the continental margin of Newfoundland and Labrador changed. In the Late Triassic to Early Jurassic, the extension direction was NW-SE, but rotated to E-W during the Late Jurassic to Early Cretaceous. By the Late Cretaceous, the extension direction again changed to ENE-WSW (eg. Enachescu, 1987; Enachescu et al., 2005; Loudon 2002). Finally, during the Labrador Sea rifting phase, the extension direction rotated from ENE-WSW to NNE-SSW in the Eocene (~55Ma) due to separation of Europe and Greenland (Roest and Srivastava, 1989; Loudon 2002).

As discussed in Chapter 3, the border faults and basement ridges in the West and Central Orphan Basin are northeast trending, while extensional faults on the Labrador Shelf trend north-northwest to northwest. The extensional faults in the Orphan Basin are highly segmented in places, cover a more extensive area, and have larger throws than those mapped on the southern Labrador Shelf. The differences between these two areas are examined by comparisons of the rift systems to oblique, analogue and multiphase rifting models.

4.2.1 South Hopedale Basin

The South Hopedale Basin is characterized by relatively linear extensional faults, along with isolated subbasin and half graben structures. Analogue models predict that early stages of deformation in orthogonal rift systems are characterized by long, linear extensional faults forming as a result of along-strike linkage of initially smaller linear fault segments. Figures 4.3 and 4.4 depict modeled fault systems associated with a low extension orthogonal rift and the fault system mapped within the southern part of the Hopedale Basin. Comparison of these two systems show similarity, which is expected as the initial ENE extension in the Labrador Sea was orthogonal to the northwest trending rift axis. However, the southern Hopedale basin also experienced oblique NNE extension in Eocene time. This may explain the rotated tips, kinking and minor sigmoidal shape evident on several of the faults, as indicated in Figure 4.4.

Changes in fault polarity along strike occur on the southern part of the inner shelf, as shown in Figure 4.4. Examination of strike lines in this region suggest that a hard-linked intrabasin transfer fault zone may be present (Figure 4.5). Intrabasin transfer faults link two or more normal faults, have a strike-slip deformation component, and are generally associated with minor changes in structural relief (Gawthorpe and Hurst, 1993). The 2D seismic reflection strike profiles through the interpreted transfer zone indicate near vertical faults with minor amounts of dip slip. Differences in structure and seismic character on either side of the faults suggest that a considerable strike-slip component may be present. Minor structural relief is indicated in profiles A and C, while profile B

Labrador Rift System

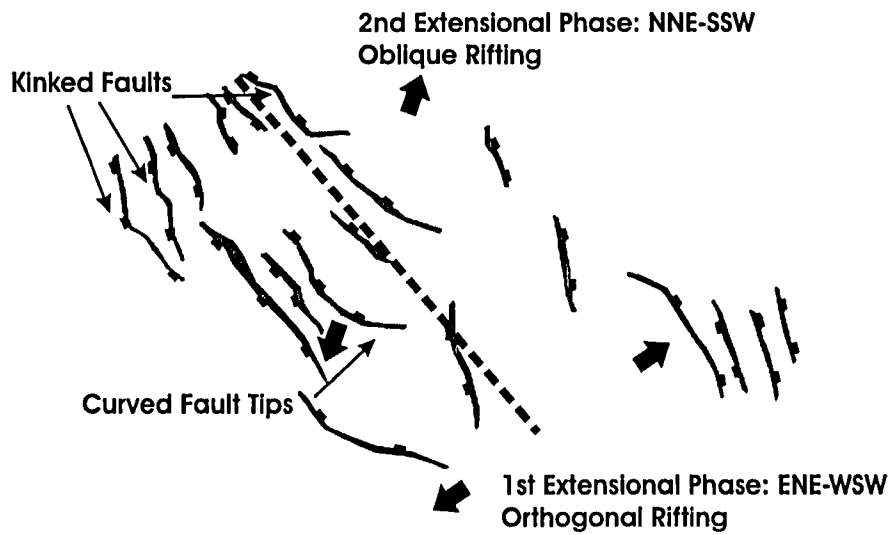


Figure 4.3. Mapped Labrador Extensional fault system. Extensional directions associated with each rifting phase are indicated by red arrows. Adapted from McClay et al. (2002).

Modelled Orthogonal Rift System

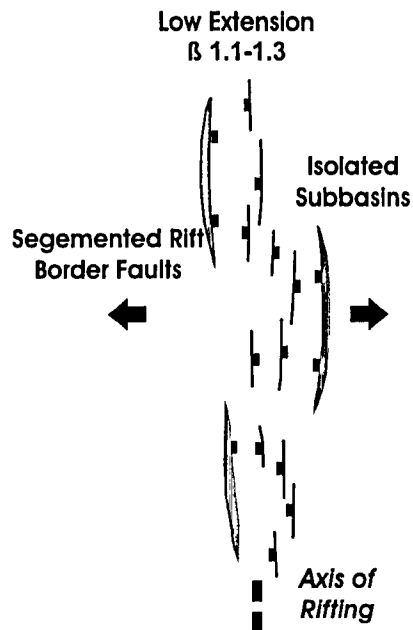


Figure 4.4. Analogue model of a low-extension orthogonal rift system. Rift border and intra-rift faults are more linear than those associated with an oblique system. Subbasins within the rift zone are isolated. Modified from McClay et al. (2002).

shows a slightly more elevated basement structure and a more significant vertical displacement associated with the interpreted transfer fault. Additionally, the syn-rift sequence is thin to non-existent in this area, and typical folding and deformation associated with a soft-linked accommodation zone is not present. These characteristic attributes suggest that this feature is a transfer fault. However, the difficulties associated

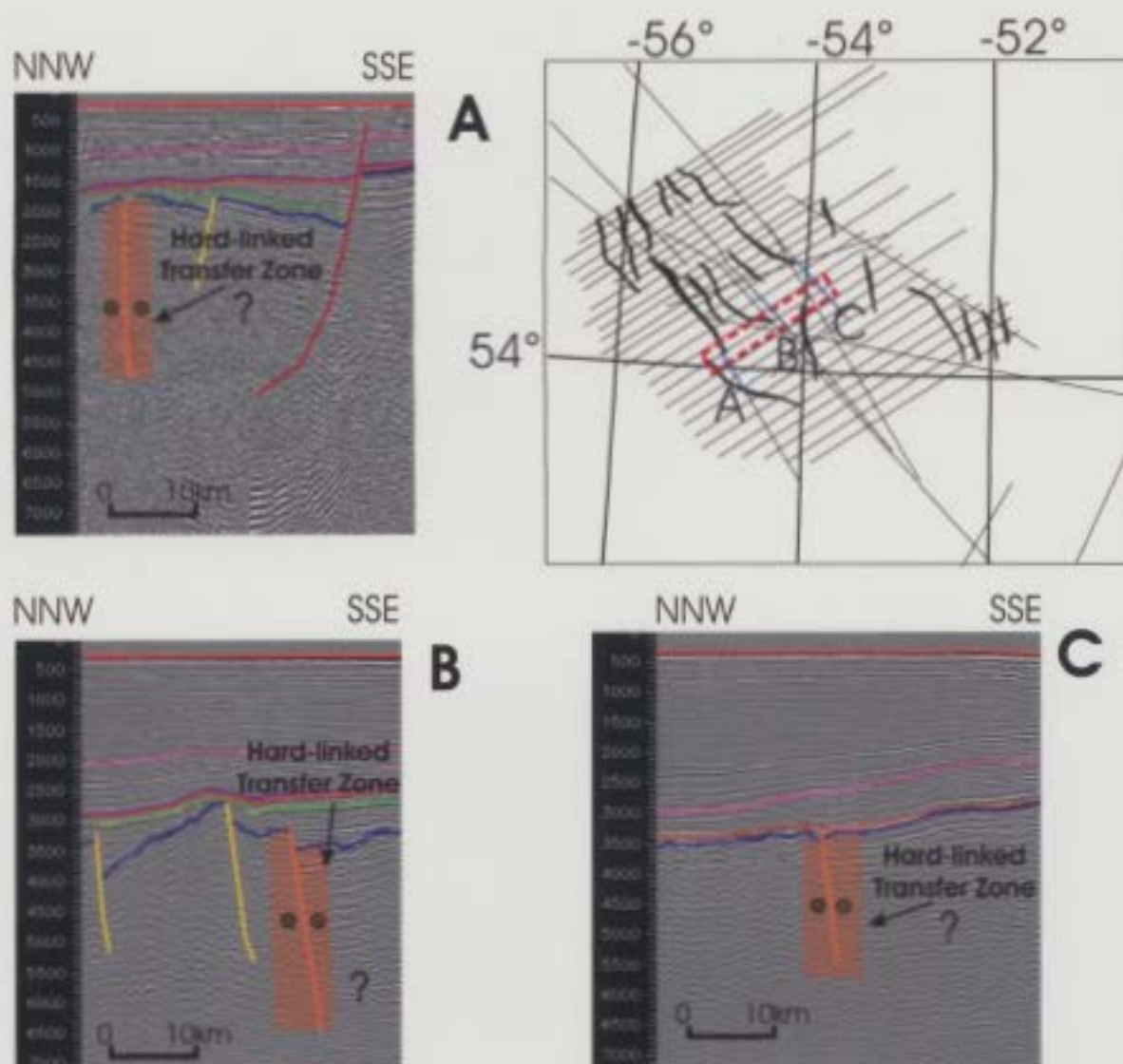


Figure 4.5. Interpreted hard-linked transfer zone within the southern Labrador Shelf. Transfer Fault is shown in orange, and interpreted profiles are highlighted on location map in blue.

with mapping transfer zones in the subsurface should be considered. For instance, definition of transfer zones is dependent on the grid spacing and line orientation of 2D seismic reflection data. Additionally, most surveys are acquired perpendicular to strike and are subparallel to the main transfer elements (Gibbs, 1989; Gawthorpe and Hurst, 1993). In cases where grid spacing is not close enough, many transfer features are not identified, and there is a tendency to link faults on separate lines as one continuous fault zone (Grawthorpe and Hurst, 1993). Consequently, the interpreted transfer fault could actually be separate, linked segmented faults more characteristic of a soft-linked system (Gawthorpe and Hurst, 1993). In addition, physical analogue models of orthogonal rift systems do not indicate development of any distinct hard linked transfer faults (McClay and White, 1995; McClay et al., 2002). However, this may be explained by the lack of pre-existing basement features in the analogue model that, when reactivated during extension, would form a discrete transfer system (McClay and White, 1995).

4.2.2 Orphan Basin

The mapped fault systems in the West Orphan Basin were compared to fault systems developed in orthogonal, oblique and multi-phase analogue rift models. In the West Orphan Basin, the rifting phase during the Late Jurassic-Early Cretaceous affected the easternmost side while the Early to Late Cretaceous phase was dominant (Enachescu et al., 2005). The eastern portion of the basin was also affected by initial Late Triassic-Early Jurassic rifting, but this extensional phase likely had minimal effects in the West Orphan Basin (Enachescu et al., 2005). With the changes in extension direction

associated with each rifting episode, the rift system likely became increasingly oblique (Figure 4.6).

Comparisons of the fault patterns in the West Orphan Basin with fault patterns from a highly extended oblique rift system analogue model show similarity (Figures 4.6 and 4.7). In physical models, oblique rifts are characterized by strongly segmented fault systems and offset basin depocentres (McClay et al., 2002; McClay and White, 1995). Border faults closely parallel the rift axis, and intrarift fault domains are oriented at a high angle to the extension direction (McClay et al., 2002; McClay and White, 1995). The West Orphan Basin faults are highly segmented in places and several have significant throws, suggesting that the area is highly extended. The faults also have sigmoidal shapes similar to the analogue model. However, the en-echelon fault pattern is less apparent, which could be because of the orthogonal (less oblique) rifting in the first and second extensional episodes. These initial rifting phases likely produced long, linear extensional faults that were highly segmented by later oblique extension (McClay et al., 2002; McClay and White, 1995; Keep and McClay, 1997). This notion is supported by the presence of highly segmented faults in the easternmost West Orphan Basin, which was likely the most affected by the early rifting phases. Another consideration is the resolution limitations associated with the 2D seismic reflection grid, as the grid spacing does not permit accurate mapping of smaller features (Gawthorpe and Hurst, 1993). A tendency to link faults picked on separate profiles as a continuous curvilinear structure may also occur, resulting in fault aliasing (Gawthorpe and Hurst, 1993). Consequently,

the interpreted fault patterns may not honor the true nature of the fault system, particularly in areas with less coverage. Additionally, the rifting history of the Orphan Basin is much more multifaceted than that what can be produced with a simple

West Orphan Basin Fault Structure

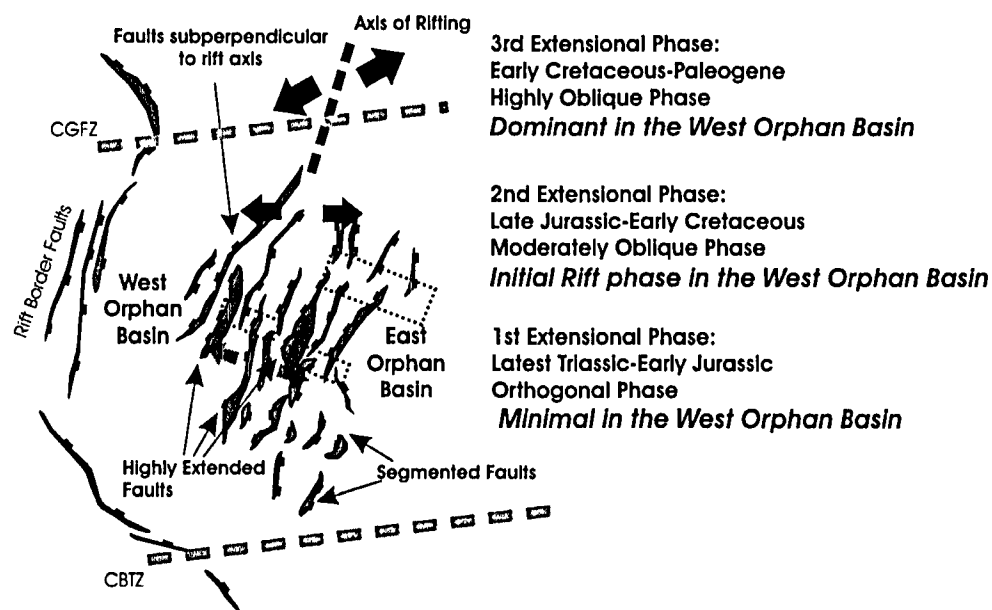


Figure 4.6. Mapped extensional fault system in the West and Central Orphan Basin. Extension directions associated with each rifting episode are indicated by red arrows. Dashed red boxes signify interpreted accommodation zones. CGFZ=Charlie Gibbs Fracture Zone, CBTZ= Cumberland Belt Transfer Zone.

analogue model. This area likely experienced many secondary extensional vectors due to movement of neighbouring plates, and the basement composition and structure is much more complex than in the analogue model simulations (Enachescu, pers. comm., 2007).

Significant structural variations occur along the length of the rift zone in analogue oblique rift models. These variations include fault polarity switching, which results in the

generation of intrarift subbasins (McClay et al., 2002). Different fault polarity domains are separated by accommodation zones that are both parallel and oblique to the extension

Modelled Oblique Rift System

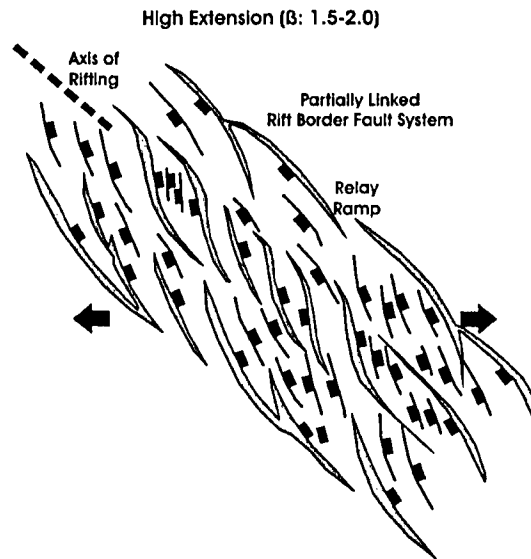


Figure 4.7. Analogue model of a highly extended oblique rift system. Faults have a sigmoidal shape and form an en-echelon pattern. Rift border faults are segmented and linked by relay systems. Modified from McClay et al, 2002.

direction. These accommodation zones are characterized by interlocking fault arrays of opposite dip polarities that define areas of relatively high relief in highly oblique rifts, and areas of lower relief in less oblique rifts (McClay et al., 2002). The West Orphan Basin contains sets of extensional faults that switch from seaward dipping to landward dipping. The regions between oppositely dipping faults are interpreted as accommodation zones (Figure 4.5). In rift systems, accommodation zones are typically 15-30 km wide, higher in elevation than surrounding sections of the rift, and cut by numerous steeply

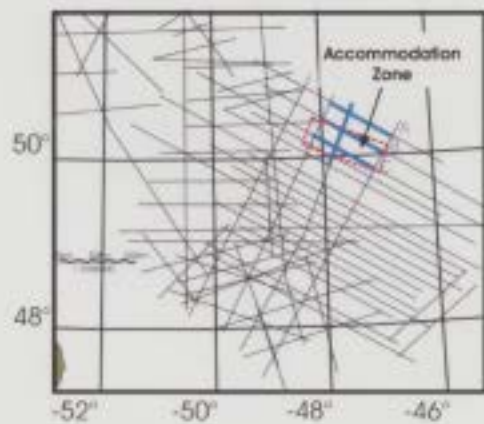
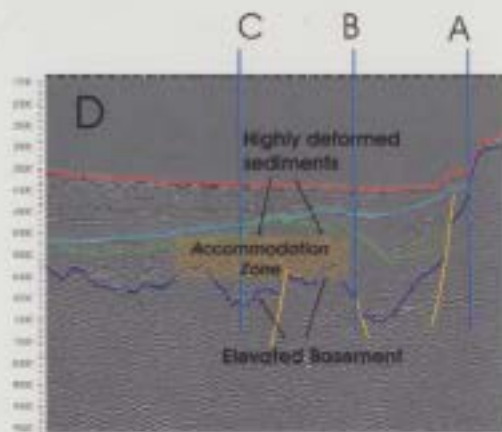
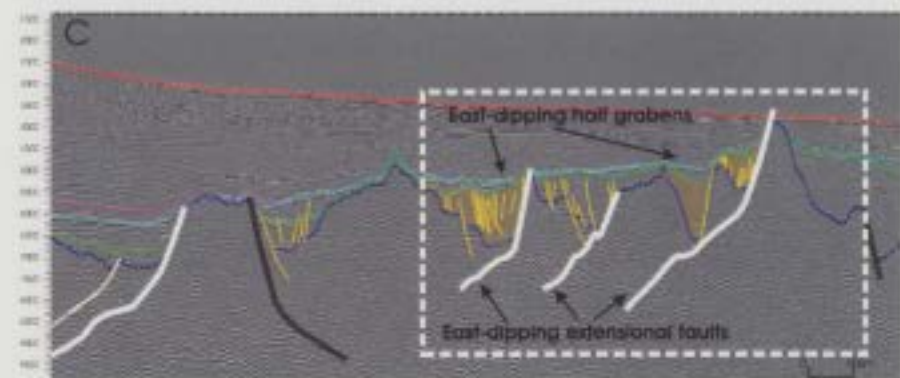
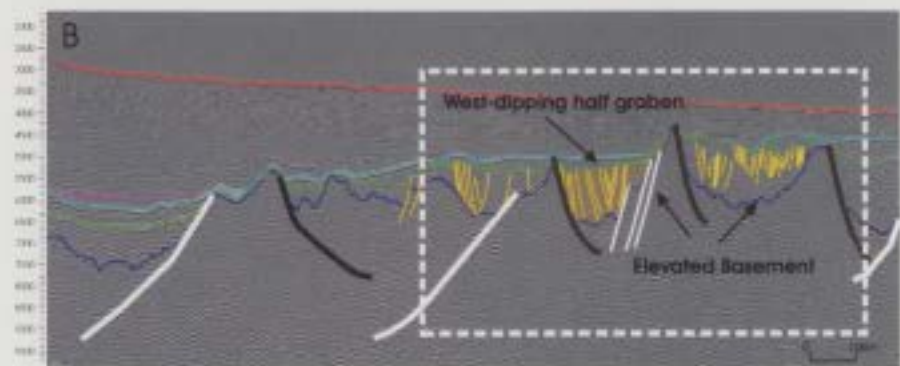
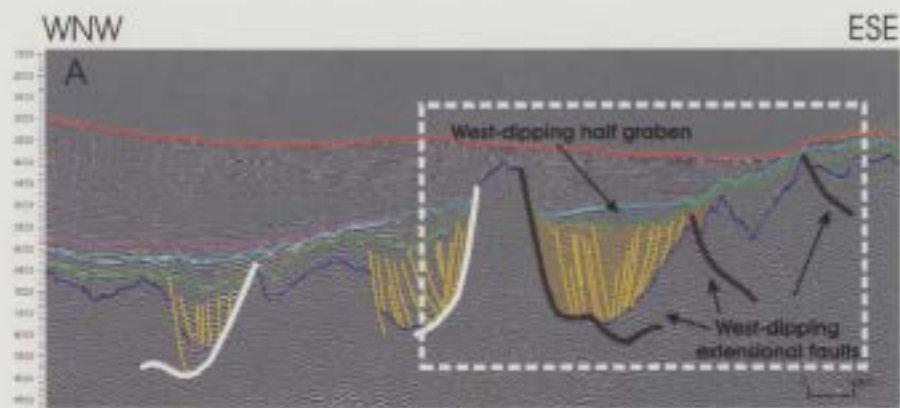


Figure 4.8. Dip line profiles from the West and Central Oephan Basin indicating a change in polarity of extensional faults and half graben structures. Profile A shows a westward dipping half graben structure and extensional faults. Profile B shows elevated pre-rift basement and a smaller half graben structure. Profile C depicts the development of eastward dipping half grabens and extensional faults, which suggests that an accommodation zone exists between the two profiles. A corresponding strike profile (above) shows a zone with an elevated pre-rift basement and highly deformed syn-rift sediments, which further implies that an accommodation zone is present.



dipping antithetic and synthetic faults (Younes and McClay, 2002). Often, accommodation zones do not exhibit strike-slip faulting but folded sequences resulting from sediment draping over normal fault terminations are evident (Coffield and Schamel, 1989; Younes and McClay, 2002)

Figure 4.8 shows three dip profiles and the corresponding strike profile over an area in the northeast West Orphan Basin identified as an accommodation zone. Profile A indicates southwest dipping faults and a large half graben structure. Moving south, (profile B), the half graben structure is thinner and located over elevated prerift basement. The next profile (C) shows a reversal of both fault and half graben polarity along with highly elevated prerift basement. Intense tectonism is indicated by late movement of extensional faults and subsequent breaching of the uppermost postrift sediments and waterbottom. The synrift sequences are cut by numerous antithetic and synthetic faults in each of these locations. The corresponding strike section (D), shows a region of highly deformed, folded sediments. The folded sediments and absence of a discrete transfer fault system are typical of a soft-linked accommodation zone. These features, coupled with characteristics identified on the dip profiles, suggest that this area is an accommodation zone.

4.3. Summary

Comparisons of the South Hopedale and West Orphan basins to analogue models of orthogonal and oblique rifting indicate that the Hopedale rift system is predominantly an orthogonal rift, while the Orphan rift system is more characteristic of an oblique rift.

Differences between the natural rift systems and those of analogue models can be attributed to pre-rift structural complexity, which likely influences the development of rift features. Natural systems are also influenced by numerous secondary extension vectors related to the complicated motion of the Earth's plates, which is not accounted for in the analogue models. Additionally, the spacing and orientation of the seismic data can limit the interpretation of structural features and result in fault aliasing, which may affect the interpretation of transfer systems.

Chapter 5: Analysis of Extension

5.1. Lithospheric Stretching

Subsidence history and crustal structure of rifted margins can be compared by modeling lithospheric stretching (Keen and Dehler, 1993). The basic principle is that stretching and thinning of the lithosphere occur during rifting and perturb the isostatic and thermal equilibrium in a predictable manner (Keen and Dehler, 1993). Lithospheric stretching can be estimated if the amount of crustal thinning or subsidence is known (Keen and Dehler, 1993). On rifted continental margins, the end member stretching models are the simple shear and pure shear models (Wernicke, 1985; McKenzie, 1978). Pure shear models imply that stretching is uniform vertically through the lithosphere, while simple shear stretching is localized along faults and shear zones (Keen and Dehler, 1993). A variety of pure and simple shear geometrical configurations can be accounted for using models, such as those that divide the lithosphere into two layers that stretch and thin independently (Keen and Dehler, 1993).

In pure shear models, the lithosphere deforms as a single layer and the amount of stretching and thinning at each point is specified by the parameter β (Keen and Dehler, 1993; McKenzie, 1978). However, this type of stretching model does not adequately explain the variation between syn and postrift sequences commonly observed on passive margins, as different layers within the crust have variable rheologies that are expected to react non-uniformly to extension (Dehler and Keen, 1997; Meredith and Egan, 2002). Comparisons of the West Orphan Basin and the South Hopedale Basin indicate

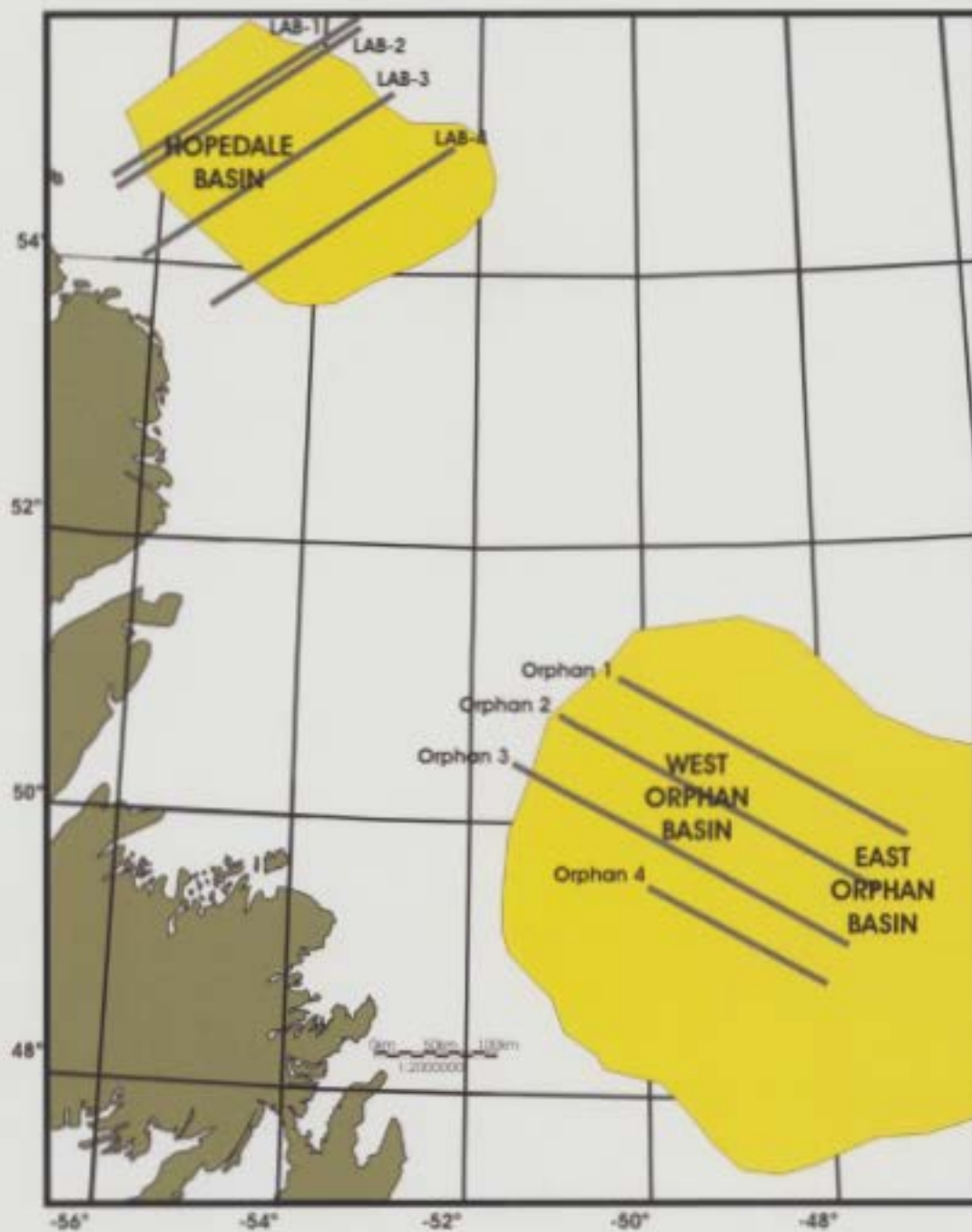


Figure 5.1. Location map showing profiles used in the backstripping and balanced section reconstructions.

substantial variations in syn- and post-rift sedimentary thickness. To investigate this disparity, the amount of extension was estimated through section balancing and palinspastic reconstruction. The methods also allow examination of the margin's tectonic evolution. LithoTect software (Geo-Logic Systems, 2005) was used to reconstruct eight profiles across the South Hopedale and West Orphan basins. The profiles were selected on the basis of their length and orientation (Figure 5.1). In the south West Orphan Basin, a shorter profile was also chosen as longer profiles were not available in that area.

5.2. Methods

5.2.1 Time interpretation

As discussed in Chapters 2 and 3, a 2D reflection seismic dataset covering the South Labrador Shelf and West Orphan Basin was interpreted to identify major structural and stratigraphic features in the area of interest. Four representative profiles from each basin were converted into digital image files and imported into LithoTect. The selected profiles, shown in Figure 5.1, were calibrated and converted to depth, as discussed in the following sections. Time interpretations of each profile are based on the tectonic sequences discussed in Chapter 2, which are the pre-, syn-, and post-rift phases. For the Hopedale Basin profiles, the postrift phase is further subdivided into the pre-, syn- and post-drift sequences. The postrift sequence is also subdivided on the Orphan Basin profiles: one sequence extends from the water bottom to the Base Tertiary unconformity

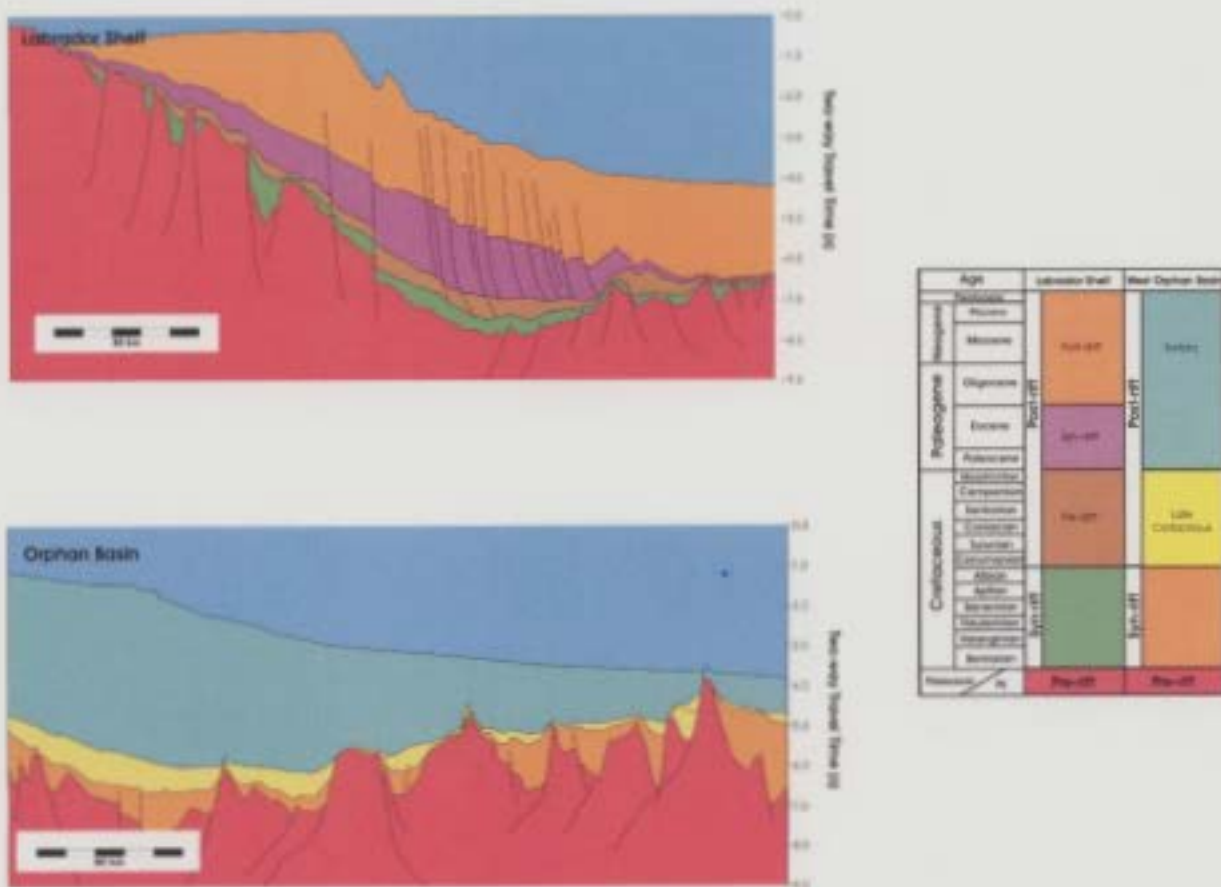


Figure 5.2. Time interpretations for the Hopedale and West Orphan basins. Colors correspond to specific tectonic sequences, as indicated on the time scale chart.

and the second extends from the Base Tertiary unconformity to the top synrift marker.

Examples of the time interpretations are shown in Figure 5.2.

5.2.2. Depth conversion

The selected seismic profiles were converted to depth prior to the section balancing and palinspastic reconstruction. Depth conversion was accomplished by assigning an interval velocity to each layer defined in the time interpretation. Interval velocities from a combination of checkshot data and seismic processing velocities were

used to estimate the depth of the base of each layer. The depth, d_n to the base of the n th

layer is defined by:

$$d_n = \sum \frac{t_1 v_1}{2} + \frac{t_2 v_2}{2} + \dots + \frac{t_n v_n}{2}$$

Where t_i is the reflection travel time through the i^{th} layer and v_i is the interval velocity.

In ideal situations, the velocity model is constrained by a combination of borehole and seismic processing velocities. However, processing velocities were not available for any of the recent GSI profiles, and well control in the area is sparse and limited to shallow water depths. Consequently, the resulting depth conversion is considered a rough estimate to provide reasonable depth values (Solvason, 2006).

The interval velocities applied to the Hopedale Basin profiles are derived from a combination of borehole and wide-angle seismic data. Most of the boreholes are located on structural highs along the inner shelf, which is an inadequate representation of the velocity structure in deeper sediments, on the slope and in deep-water areas. To compensate for this deficiency, velocity values derived from wide angle seismic studies conducted on the Labrador margin north of the area of interest were also considered (Chian et al., 1995 *a*; Chian et al., 1995 *b*). Figures 5.3 to 5.7 show the borehole interval velocities in table and plot form, the velocity model obtained from the wide angle seismic



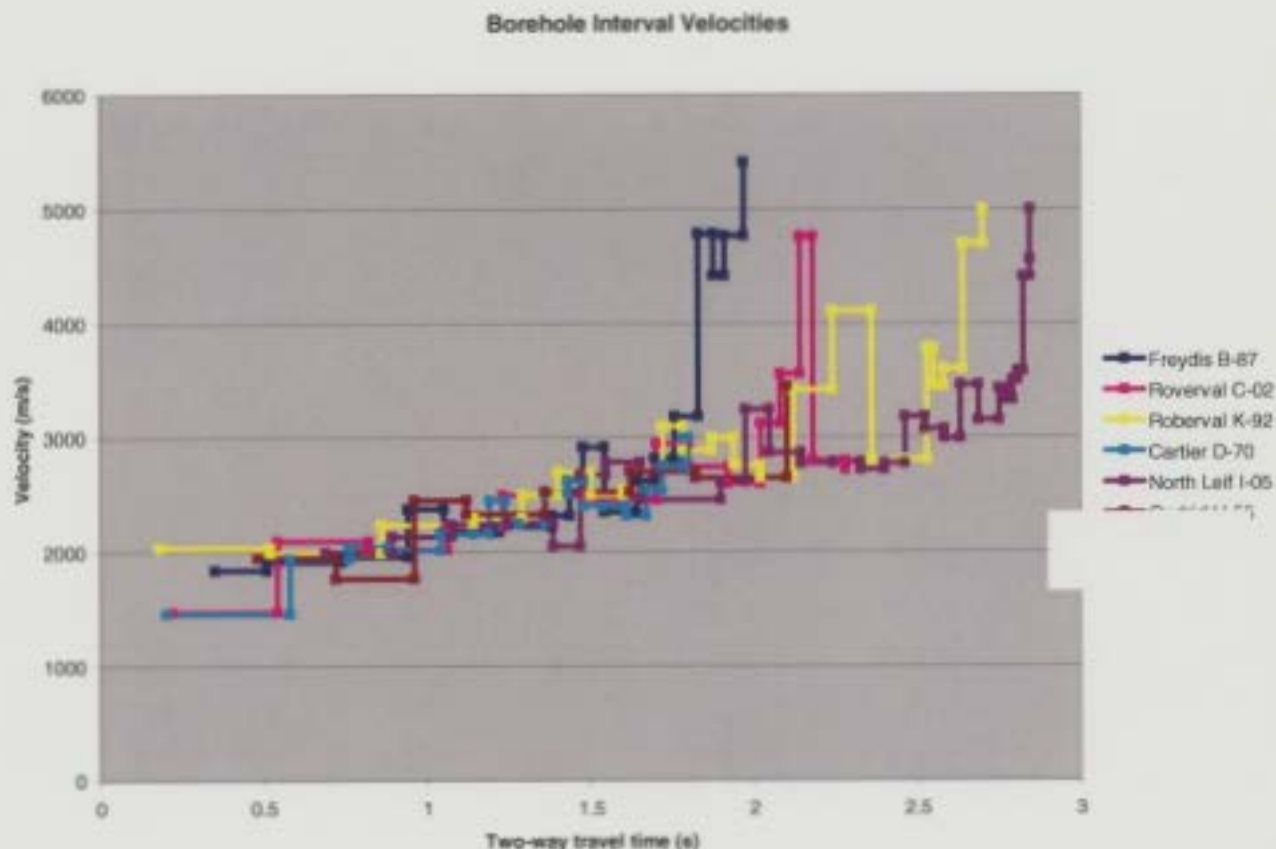


Figure 5.4. Plot of interval velocities vs. two-way travel time for the Labrador Shelf boreholes. The velocities obtained for the postrift sequence are consistent but greater variation occurs within the synrift sequence. Freydis B-87 was the only borehole with velocity data for the prerift sequence, which are identified by the sharp velocity increase at approximately 1.8s

data (Chian et al., 1995 *a*; Chian et al., 1995 *b*), plots of the interval velocities for each tectonic sequence, and the estimated velocities applied to each sequence.

The borehole interval velocities are plotted against two-way travel time to identify variation with increasing time-depth. Figure 5.4 indicates a linear increase with two-way travel time for the postrift sediments but a greater variation within the synrift and prerift sequences. Similar plots were constructed for each tectonic sequence, with the estimated

values used in the conversion indicated by red arrows and dashed lines. It should be noted that the linear velocity increase for the postrift sequence reflects only the inner shelf and does not account for the deep water and slope areas, and that the estimated values applied to each sequence are generally higher than the average values from the borehole data

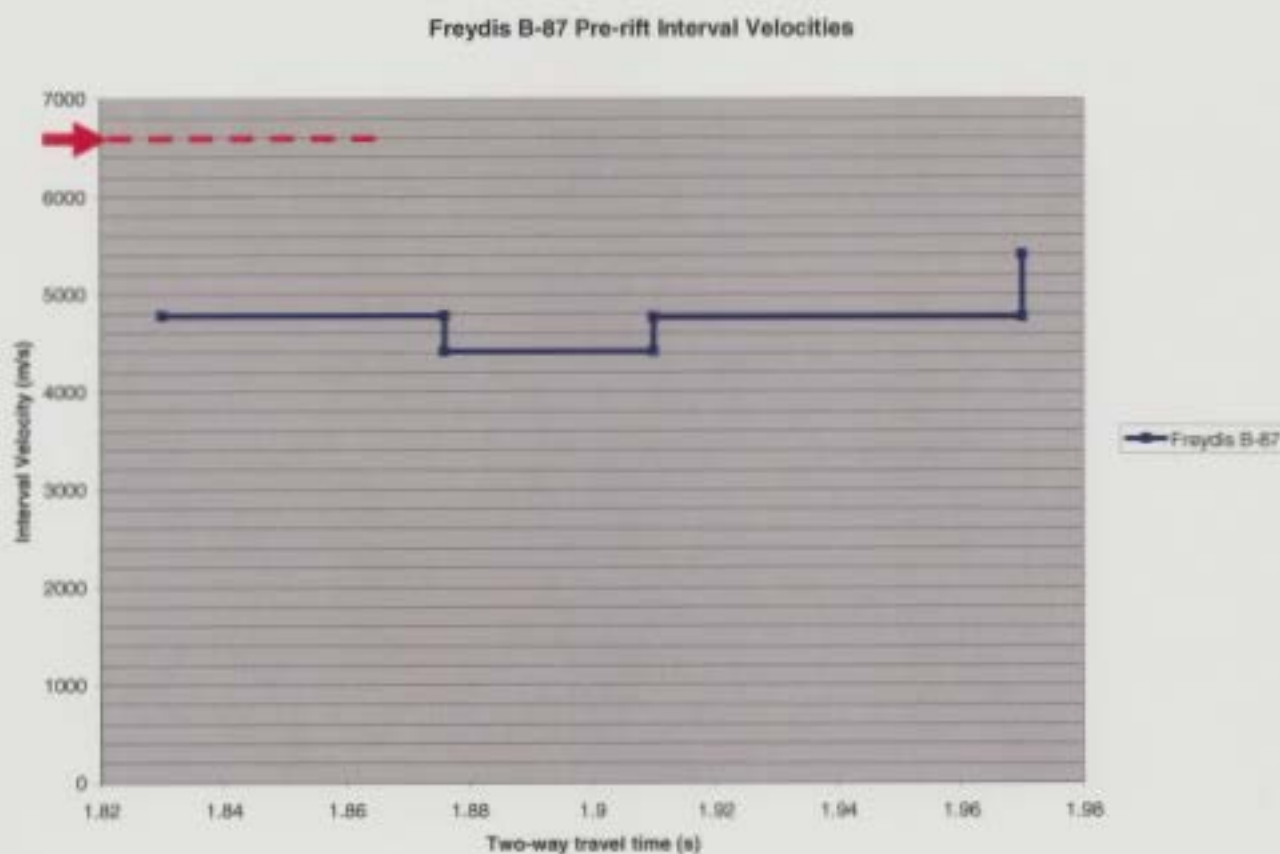


Figure 5.5 Graphical representation of the prerift interval velocity variation within the Freydis B-87 borehole. The red arrow and dashed line indicate the chosen velocity value, which is higher than the velocities obtained from the borehole data. The chosen value is largely based on refraction data, as only a few boreholes intersected the prerift sequence and velocity information was limited to the Freydis B-87 well.

alone. This reflects the use of velocities obtained from seismic refraction profiles to account for the deeper pre and synrift sedimentary sequences and sequences on slope and in deep water. These areas have higher velocities, which are reflected in the estimates used for depth conversion.

Depth conversion for the West Orphan Basin is more challenging as well data is limited and all boreholes are located on structural highs where thinner sedimentary sequences occur. In addition, most of the borehole velocity information is derived from sonic logs. To compensate for the limited borehole data, available velocities applied during processing of a reflection seismic line in the north of the basin were used to estimate velocities for deeper sediments. This particular line was chosen as the processing velocities were available and it extends into deep water. However, the synrift sequence is thin along this profile. Both the borehole and processing interval velocities were plotted against two-way travel time to examine variation associated with increasing water depth and within each tectonic sequence. However, the Late Cretaceous postrift and Early Cretaceous synrift sequences were combined into one plot due to limited velocity data within these sequences. The processing velocities are higher in shallow water regions, which is likely a function of a thin Mesozoic-Cenozoic sedimentary sequence over Paleozoic prerift basement. In deeper water, the velocities are lower, which is likely a result of increasing post and synrift sediment thickness and greater depth to the top prerift basement. Figures 5.8 to 5.12 identify borehole interval velocities and reflection seismic processing interval velocities in both table and plot form, and the estimated velocities applied to each sequence.

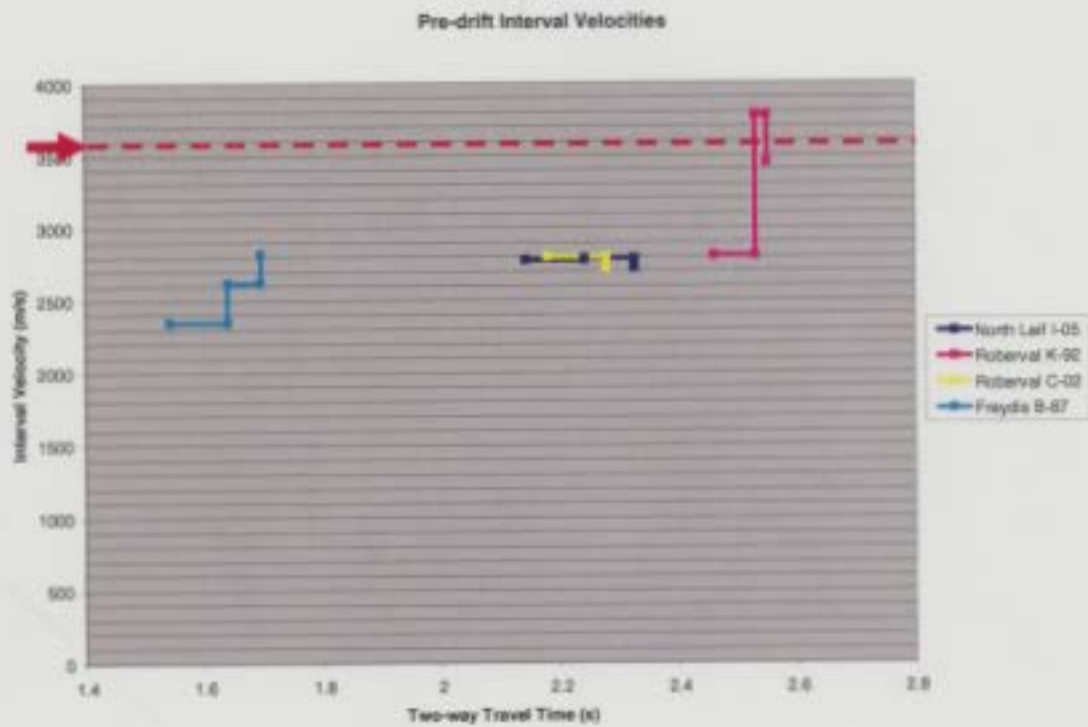
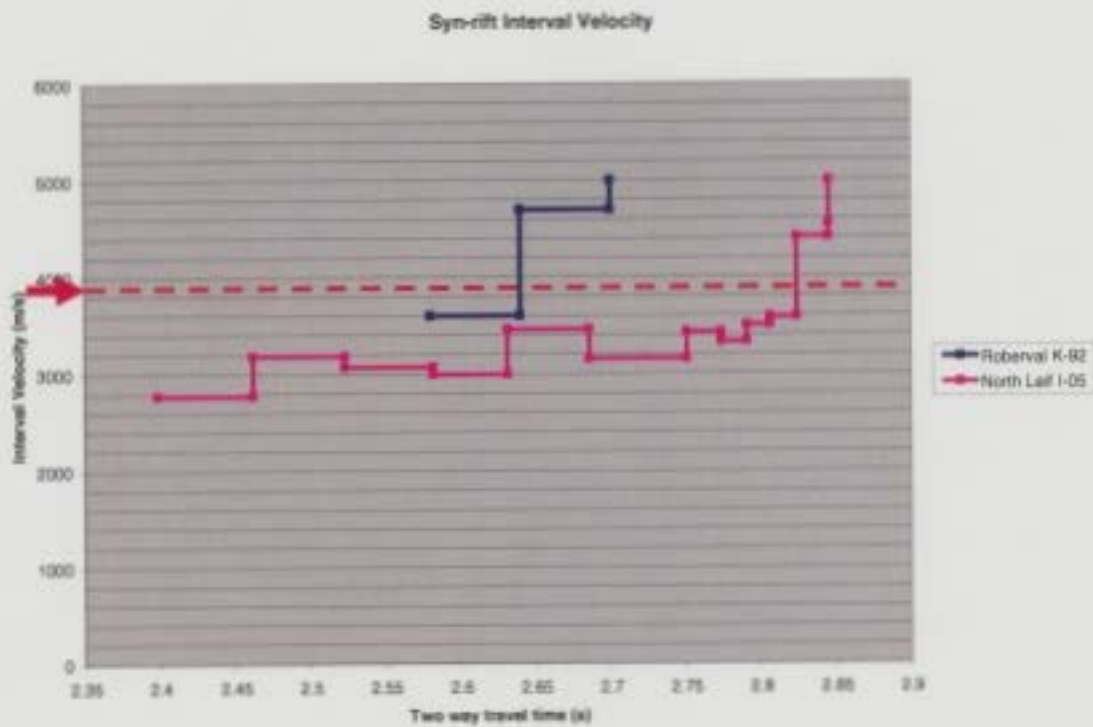


Figure 5.6. Graphical representation of the synrift and predrift interval velocities from borehole data. The red arrows and dashed lines indicate the estimated velocities used in the depth conversion, which were derived from a combination of borehole and refraction seismic data.

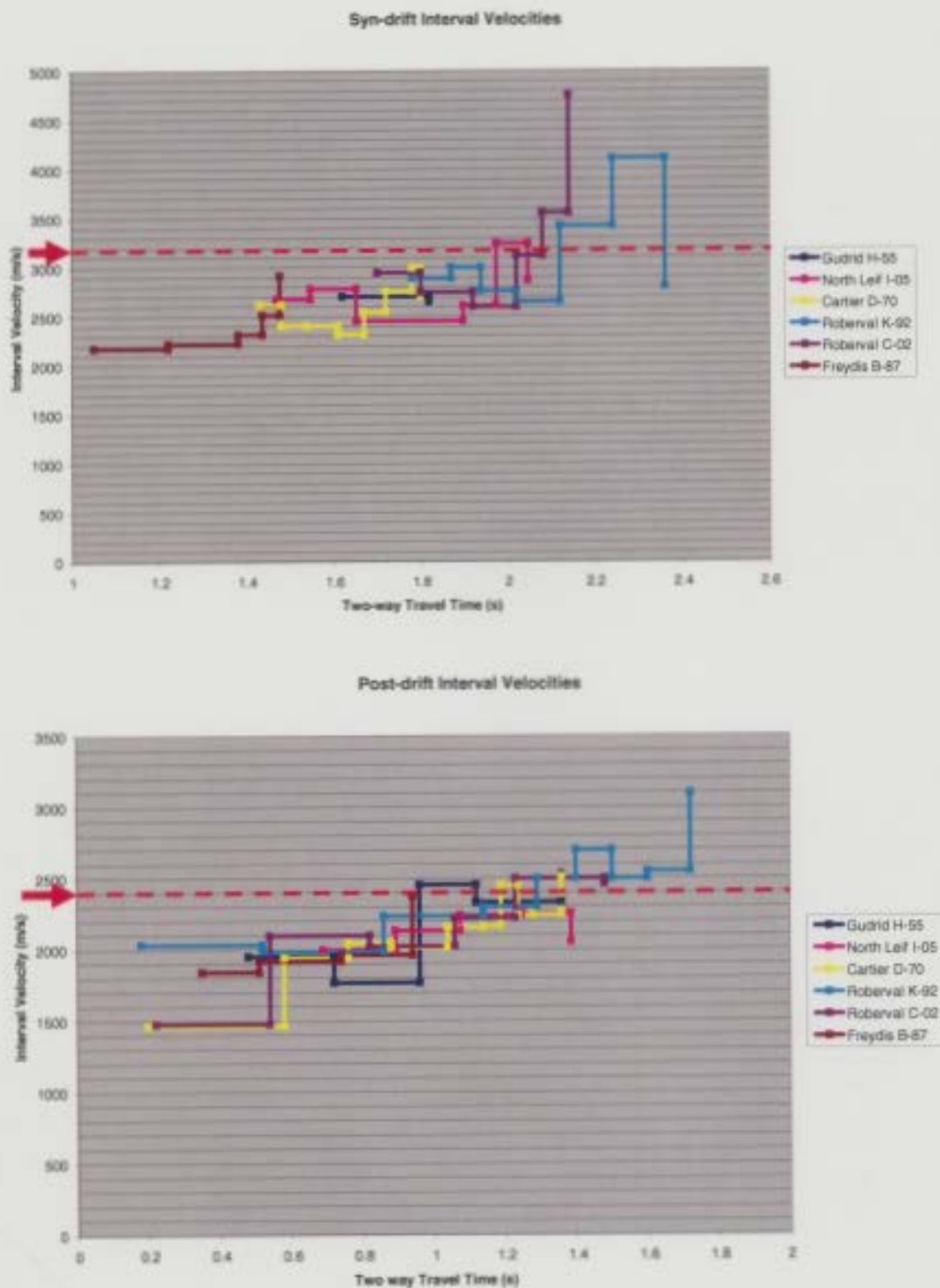


Figure 5.7. Graphical representation of the syn- and postdrift interval velocities from borehole data. The red arrow and dashed line indicate the estimated velocities used in the depth conversion, which were derived from a combination of the borehole and refraction seismic data.

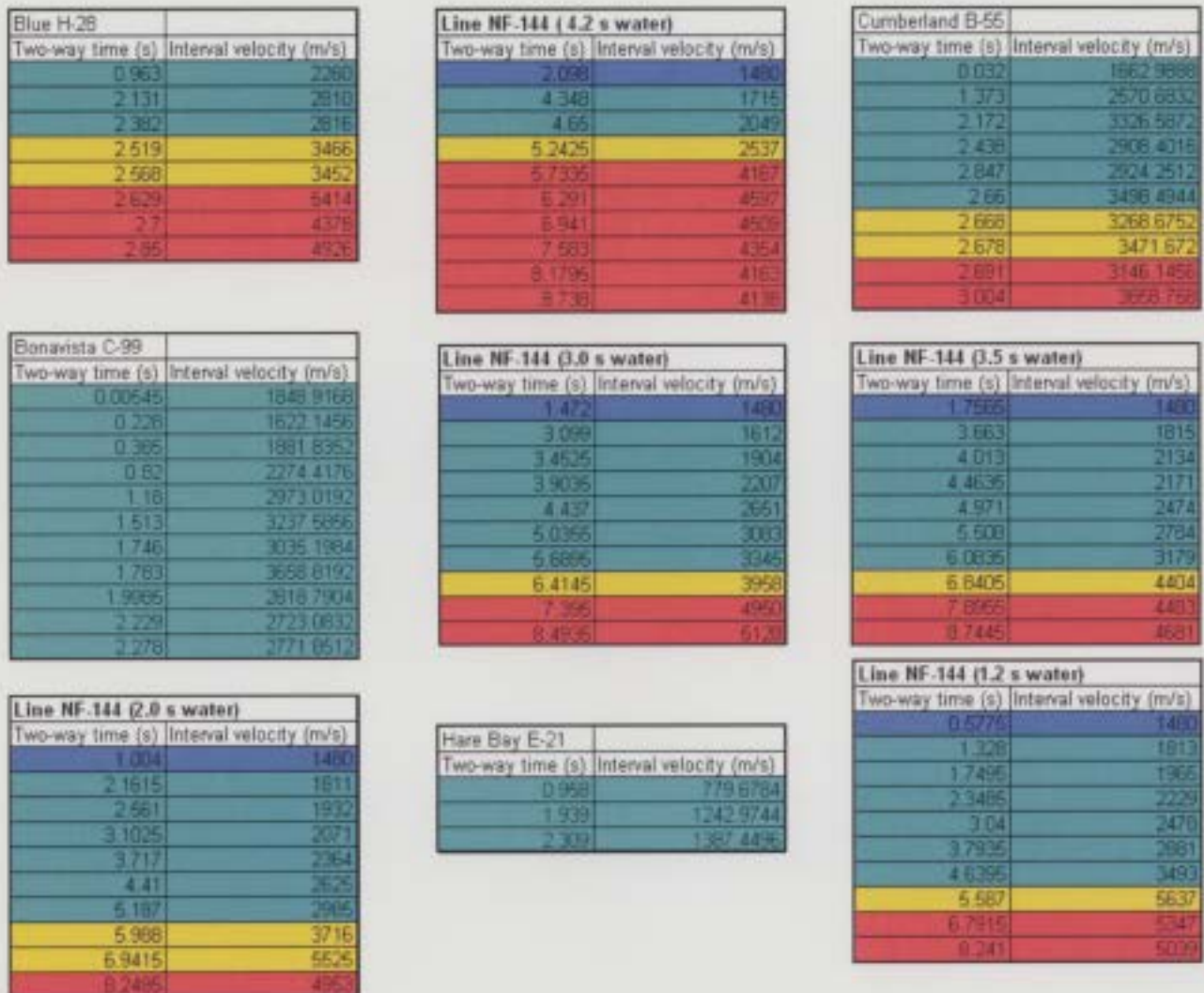


Figure 5.8. Interval velocities for the West Orphan Basin derived from borehole data and reflection seismic processing. Colors represent the interpreted tectonic sequences: Blue-green= Postrift Tertiary sequence, Yellow= Cretaceous postrift and synrift sequences, pink=prerift sequence.

The spread of the velocity data make assigning a single average velocity for each sequence appropriate for depth conversion within the area of interest. Once the profiles were depth converted, an arbitrary layer was added below the basement layer to

accommodate fault displacement. When the LithoTect program restored the basement, it assumed that this extra layer acted as a ductile layer in which the brittle fault

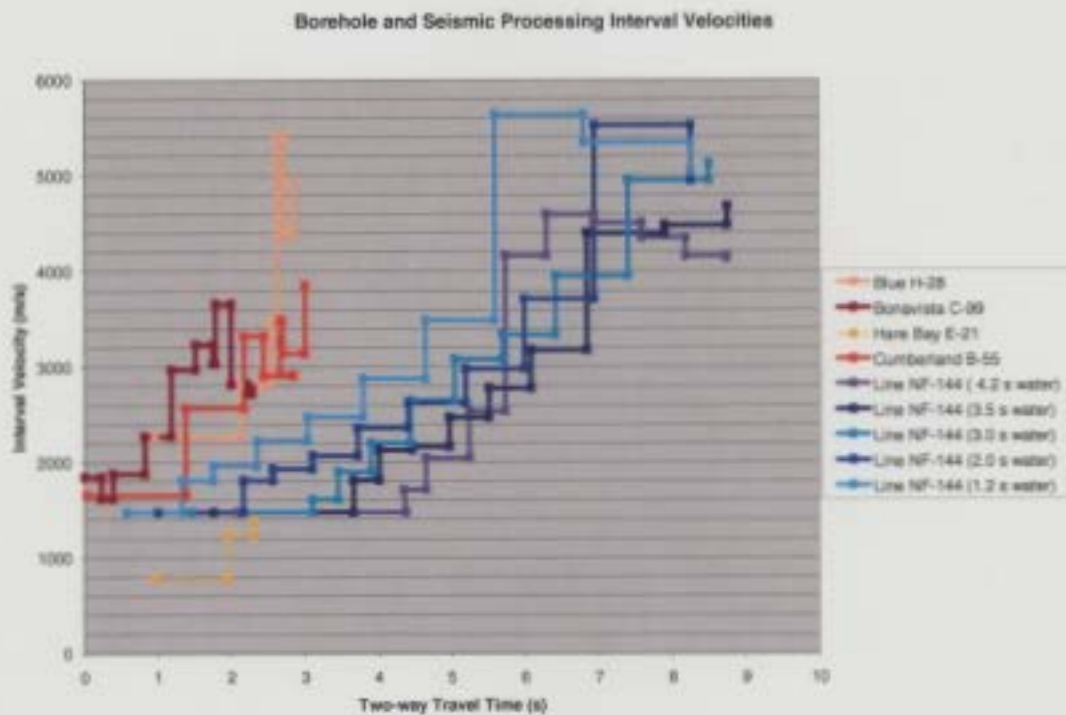


Figure 5.9. Graphical representation of the borehole and seismic processing interval velocities vs. two-way travel time. Hare Bay E-21 has lower velocities which may be attributed to shallower water depths and location outside the main part of the basin. The remaining boreholes have more consistent time-velocity curves with the highest velocities occurring in the Bonavista C-99 borehole. The interval velocities derived from reflection seismic processing are from a range of water depths.

displacement soles (Solvason, 2006; GeoLogic Systems, 2005). The base of this layer is only used as a construction artifact: it has no geologic significance and is excluded from the figures.

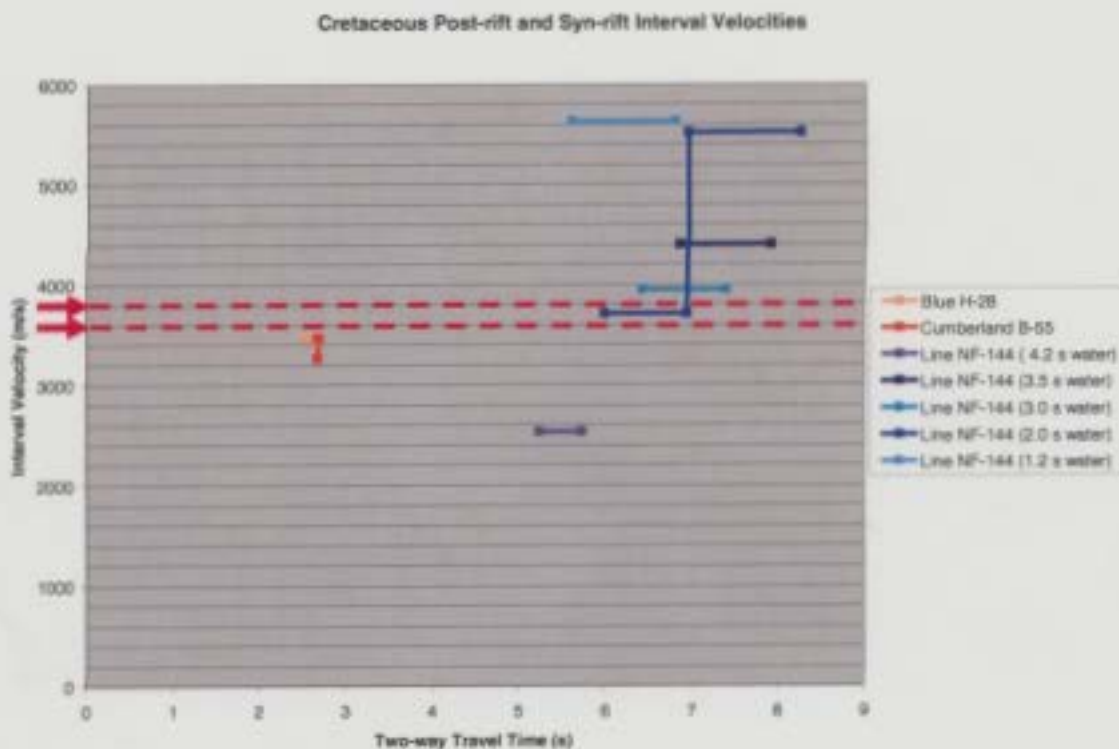
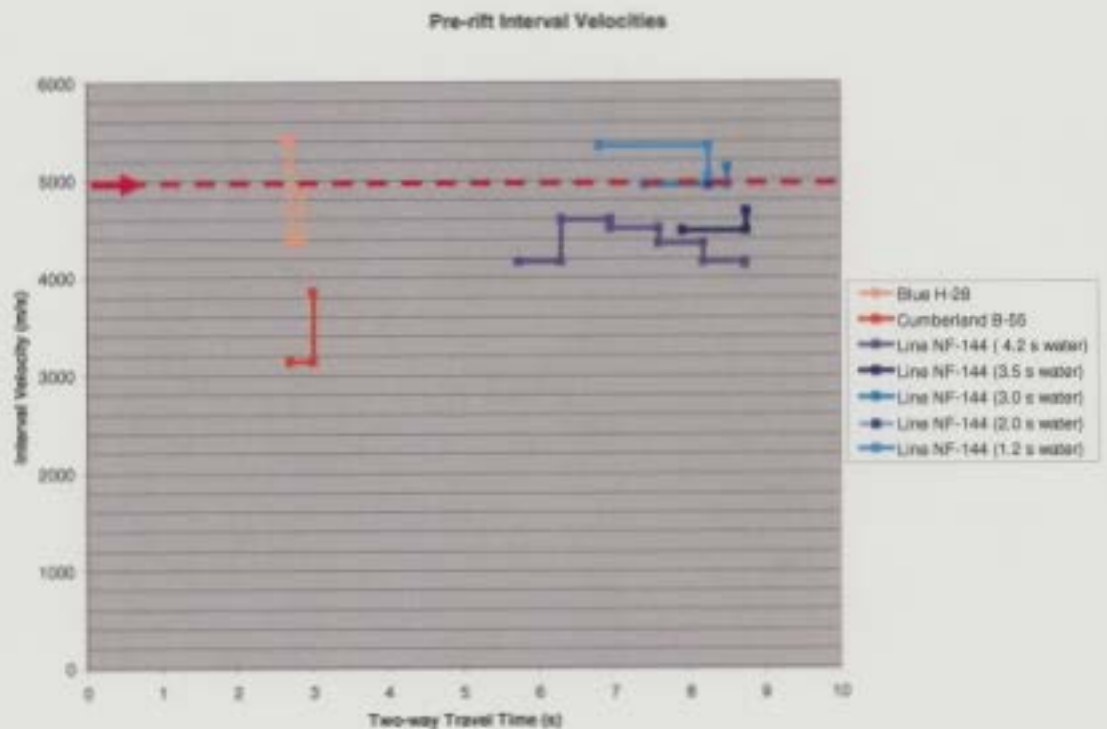


Figure 5.10. Above: Graphical representation of borehole and seismic processing interval velocities for the prerift sequence. The applied velocity is indicated by the red arrow and dashed line. Below: Graphical representation of borehole and seismic processing interval velocities for the synrift and Cretaceous postrift sequences. The velocities applied for depth conversion are indicated by the red arrows and dashed lines (3600= Cretaceous postrift; 3800 m/s=synrift).

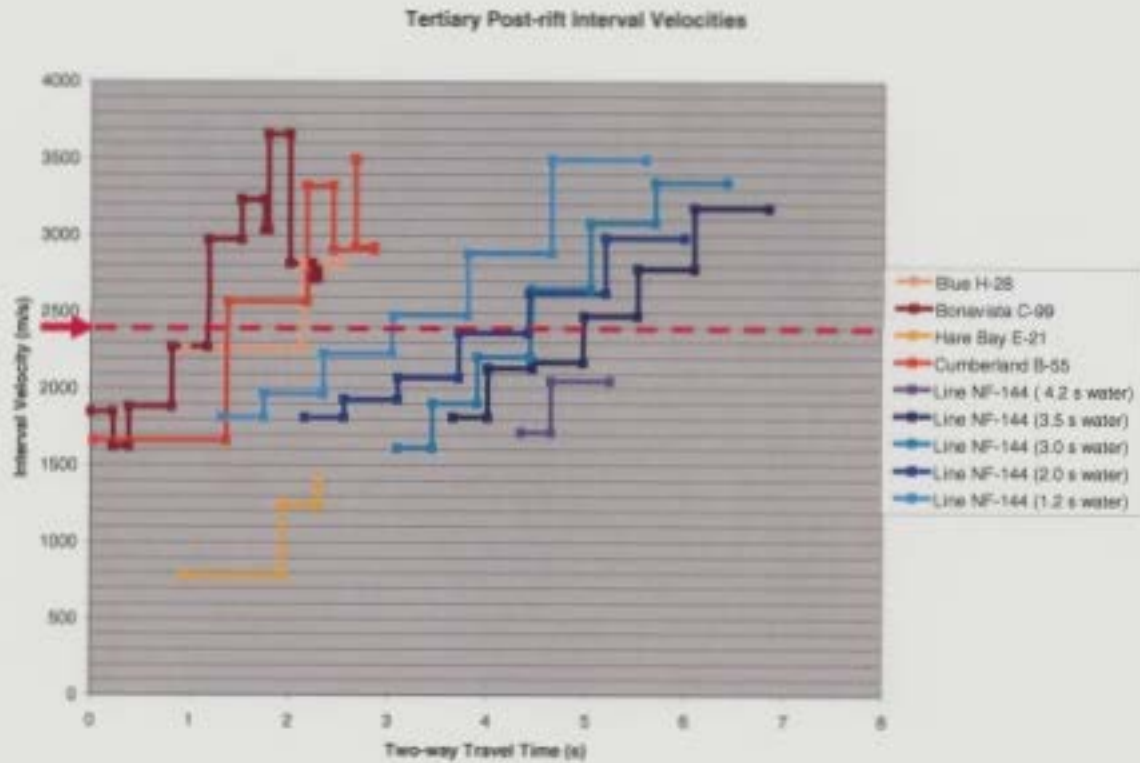


Figure 5.11. Graphical representation of the Tertiary post-rift interval velocities from both borehole data and seismic processing velocities. The estimated velocity used for the depth conversion is indicated by the red arrow and dashed line.

	Layer	Velocity (m/s)
Post-rift	Water	1480
	Tertiary	2300
	Late Cretaceous	3600
	Syn-rift	3800
	Pre-rift	5000

Figure 5.12. Estimated velocities used to convert the time sections to depth. The values are obtained from a combination of borehole data and velocities applied during processing of a reflection seismic line north of the West Orphan Basin.

5.3 Restoration Techniques

The depth converted profiles were restored to prerift configuration through a combination of backstripping and section balancing techniques. The theory behind these techniques is discussed in the following sections. This “backstripping approach” involved removing the water layer and systematically stripping away, decompacting and restoring each tectonic sequence. An isostatic adjustment was also applied during each stage.

The restoration procedure follows a series of steps, which include:

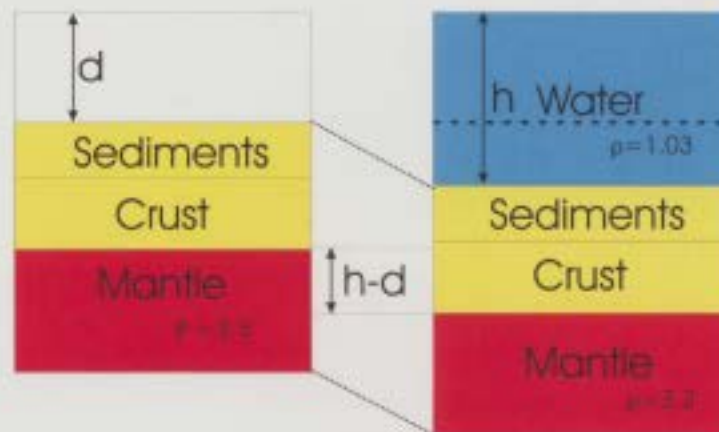


Figure 5.13. Schematic diagram depicting the mantle depression associated with water loading.

- 1) Removal of the water layer and computation of the associated isostatic response. The uppermost stratigraphic unit is then restored to sea level and the calculated isostatic response to the water layer removal is applied. The water load causes subsidence which can be examined by comparing a depression filled with air to one filled with an equivalent amount of water and then isostatically compensated. Figure 5.13 indicates that the initial depth to the sediments, d , increases to h when

the basin is filled with water. This results in a mantle depression which can be calculated by a simple mass balance:

$$h\rho_w = (h - d)\rho_m \quad (5.1)$$

Where $\rho_w=1.03$ and $\rho_m=3.3$ are the densities of the sea water and mantle, respectively. Solving the equation for h gives:

$$h = 1.45d \quad (5.2)$$

This implies that a water depth of 1000 m results in subsidence ($h-d$) of 450m. As this is less than the thermal and tectonic subsidences, which are on the order of kilometres in magnitude, the effect of the water was ignored in this study.

- 2) The uppermost layer is then removed and the remaining sedimentary units are decompacted and an isostatic response to the removal is calculated. The top most remaining layer is then restored to sea-level and the calculated isostatic adjustment is applied.
- 3) The layer restored in (2) is stripped away and the steps described in (2) are repeated. This procedure continues until the prerift configuration is reached.

5.4 Section balancing

Section balancing assumes plane strain, or conservation of cross-sectional area (Geo-Logic Systems, 2005; Gibbs, 1983). Figure 5.14 indicates an area balance for extension, where the original length of the section (l_o) is compared with length in deformed state and area (Gibbs, 1983). The equation expressing the relationship between

the undeformed and deformed length of the section and the depth to decollement, d , is given by:

$$l_o = l_1 + \frac{A}{d} \quad (5.3)$$

where A is the cross-sectional area. This equation can also be expressed in terms of the average stratigraphic thickness, d , above a decollement surface, where:

$$l_o = l_1 \frac{d_1}{d_o} \quad (5.4)$$

Additionally, the equation can be stated in terms of the extension, e measured as conventional engineering strain:

$$e = \left(\frac{l_1 - l_o}{l_o} \right) \quad (5.5)$$

Which gives:

$$d_1 = \frac{A}{e} \quad (5.6)$$

The stretching or extension factor, β , may be substituted for unit length l_o (Gibbs, 1983):

$$\beta = (1 + e); \beta = \frac{l_1}{l_o} \quad (5.7)$$

LithoTect allows the user to perform reconstructions using either flexural, vertical/oblique or complex slip kinematic models. A vertical slip kinematic model was used in the restoration process. This model assumes that the hanging wall deformation can be approximated by a horizontal displacement (heave) combined with a displacement parallel to a slip vector (vertical or oblique) which should replicate the internal

deformation mechanisms undergone by the rocks (Bulnes, McClay, 1999). In a vertical slip model, each region is filled with vertical narrow columns, as shown in Figure 5.15. Reconstruction is achieved by assuming slip occurs along closely spaced planar internal shears with the intervening slices moving past one another (Geo-Logic Systems, 2005). This slip likely occurs on minor extensional faults both parallel and complementary directions to the imaged shear (Solvason, 2006). In the absence of a clear indication of a predominant set of these minor faults, it is reasonable to use a starting assumption of vertical shear attributed to equal contributions from synthetic and antithetic faults.

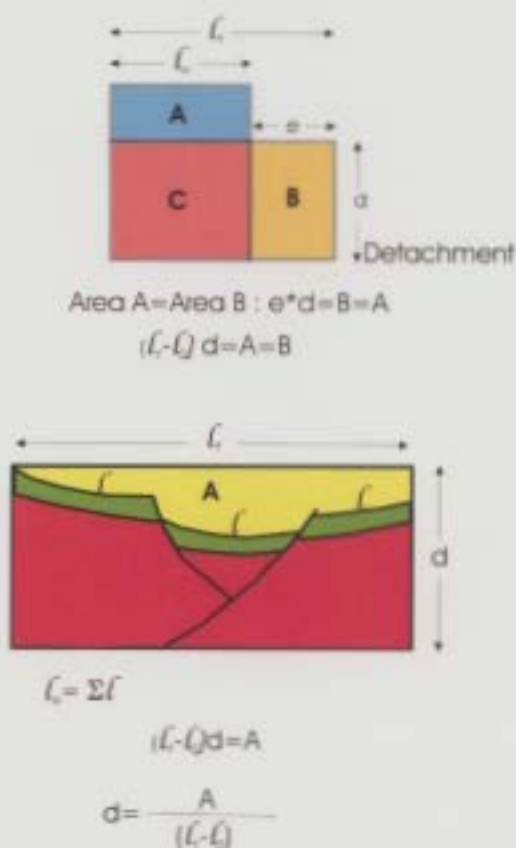


Figure 5.14. Area balance for extension. l_0 is the original length of section which is compared with the length in the deformed state and area, d is the depth to detachment (Modified from Gibbs, 1983).

5.5 Backstripping

Backstripping is the technique described in section 5.3 that is used to correct the stratigraphic record for the effects of water and sediment loading and to isolate the unknown tectonic driving forces responsible for rift basin subsidence. This process involves restoring sediment thickness at the time of deposition by taking into account the effects of sediment and water loading and making isostatic adjustments (Watts, 1997). The aim of backstripping is to analyze the subsidence history of a basin by modeling a

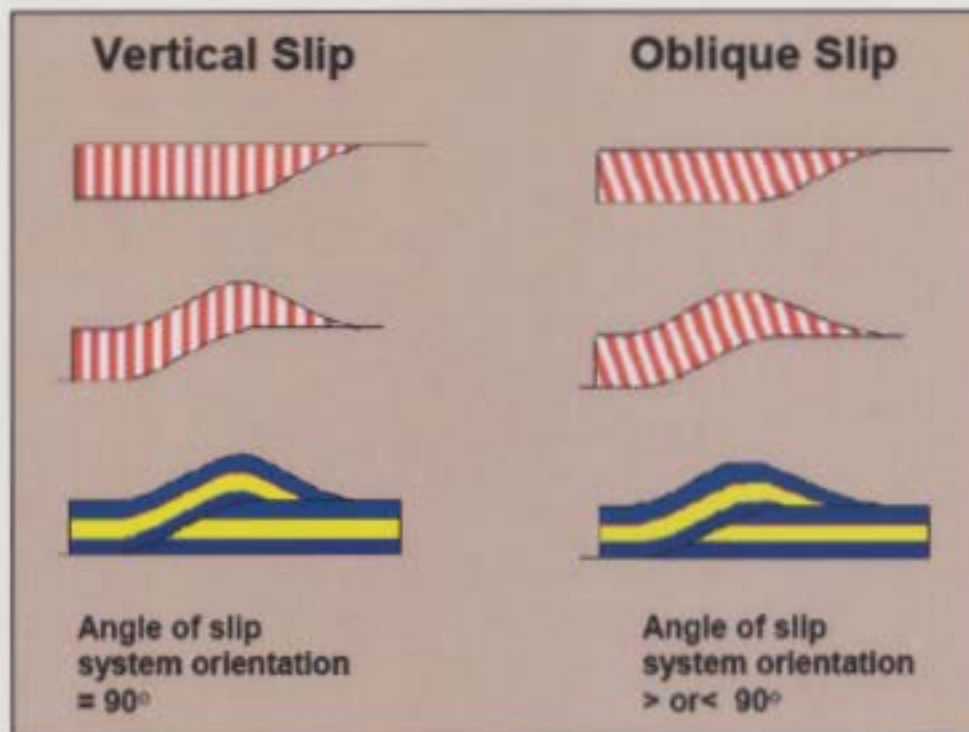


Figure 5.15. Comparison of vertical and oblique slip kinematic models. These types of models are typically applied in extensional environments, and are based on area preservation between deformed and restored states. The vertical slip model maintains horizontal bedlength distances.

progressive reversal of the depositional process. In extensional basins, backstripping is used to determine the magnitude of lithospheric stretching from the postrift subsidence. Backstripping results can also be used for hydrocarbon modeling, and in prediction of geological features such as paleobathymetry and paleotopography (Roberts et al., 1998).

There are two main types of backstripping: Airy, which is one dimensional, and flexural, which is two dimensional. The fundamental difference between these two models involves how the sediment load is treated. In an Airy model, isostatic loads are compensated locally, i.e. immediately beneath the load. In a flexural approach, however, the load is distributed regionally (Roberts et al, 1998; Watts, 2001) .The concept behind Airy backstripping is shown in Figure 5.16. This figure shows two columns of the crust and upper mantle that before and after loading are in isostatic equilibrium. Balancing the pressure at the base of the two columns gives:

$$\rho_w g W_d + \bar{\rho}_s g S_i^* g T = Y_i \rho_w g + \rho_c g T + x \rho_m g \quad (5.8)$$

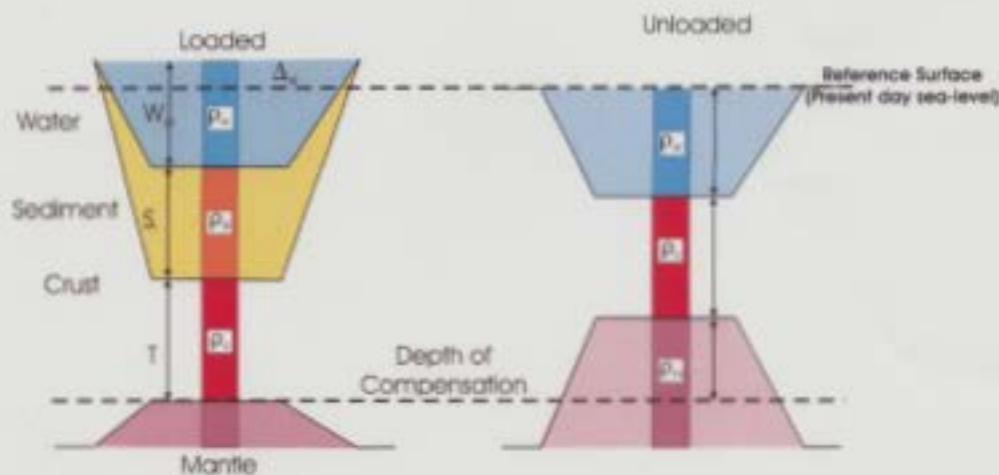


Figure 5.16. The principles of Airy backstripping. Modified from Watts, 2001.

Where W_{di} , S_i and Y_i are the water depth, decompacted sediment thickness and tectonic subsidence of the i th stratigraphic layer; T and ρ_c are the mean crustal thickness and density of the crust, and ρ_w , ρ_m and $\bar{\rho}_{si}$ are the densities of the water, mantle and decompacted sediment; respectively (Watts, 2001).

From 5.8

$$x = W_{di} + S_i^* + T - (Y_i + \Delta_{sli} + T) \quad (5.9)$$

Where Δ_{sli} is the height above mean sea-level above or below the reference surface.

Therefore:

$$Y_i = W_{di} + S_i^* \left[\frac{(\rho_m - \bar{\rho}_{si})}{(m - \rho_w)} \right] - \Delta_{sli} \frac{\rho_m}{(\rho_m - \rho_w)} \quad (5.10)$$

Equation 5.10 is known as the “backstripping” equation, which allows the tectonic subsidence to be determined from the stratigraphic data. The first term in the equation is the water-depth term, the second is a sediment loading term, and the third is a sea level loading term. The water depth term refers to the depth of deposition of a particular stratigraphic unit. Estimating water depth in the past is difficult but can be achieved if certain depth indicators (i.e. benthic microfossils, sedimentary facies, and distinctive geochemical signatures) are known. However, this term was ignored in this study as insufficient data, particularly on the outer Labrador Shelf and slope, was available to

estimate the paleobathymetry. The final term in the backstripping equation is the water loading term, which is due to global sea level changes. This term was also ignored in this study.

The sediment loading term describes the deformation of the crust and mantle due to the sediment load, and includes both a thickness and a density term (Watts, 2001). As sediments are modified by processes such as compaction, a correction must be applied to account for this modification (Watts, 2001). Additionally, compaction must be accounted for in balance calculations and subsequent palinspastic reconstruction, as it likely is synchronous with and post-dates the tectonic deformation (Gibbs, 1983). In LithoTect, the fundamental assumption for decompaction is that the amount of solid material in a unit of rock remains constant, while the pore spaces change from deformed to restored states (Geo-Logic Systems, 2005). This equality allows calculation of the decompacted thickness (GeoLogic Systems, 2005).

The procedures used in Airy 1D backstripping can be applied to a two dimensional cross section with a flexural, rather than local, response to the sediment loading (Roberts et al. 1998). In this form of backstripping, sediment thickness data are used to derive the tectonic subsidence along a profile or from an isopach map of a basin, as shown in Figure 5.17. A major limitation of the technique is the requirement of information on the spatial variations occurring in the strength of the underlying lithosphere (Watts, 2001). The procedure for flexural backstripping is similar to that followed for Airy backstripping except that sediments are flexurally unloaded (Watts, 2001).

In cases where flexural isostatic corrections cannot be applied, two dimensional backstripping of cross sections can also be accomplished using an Airy isostatic correction. In this instance, the flexural rigidity is assumed to be zero. A suite of restored sections is produced, but the isostatic calculations have operated only vertically, without consideration of laterally adjacent loads (Roberts et al., 1998). As LithoTect software

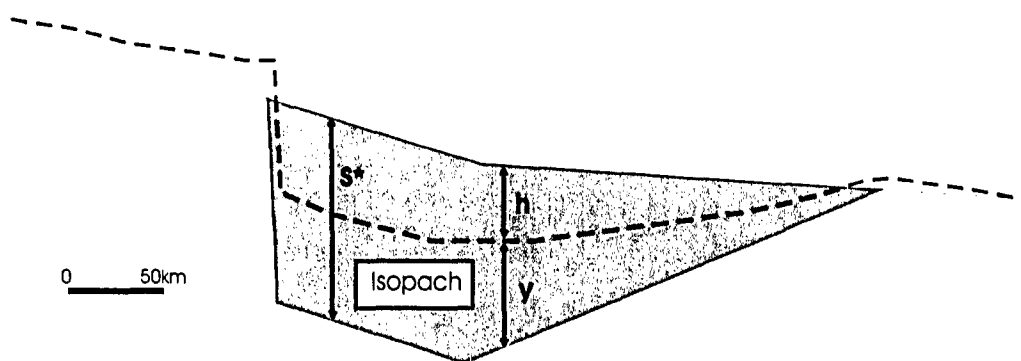


Figure 5.17. The principles of flexural backstripping. The shaded region shows a wedge of sediments. The dashed line shows where the sediment wedge would be in the absence of sediment loading. Modified from Watts, 2001.

computes Airy isostatic corrections, this procedure was utilized in this study.

Use of Airy corrections in 2D backstripping requires specific considerations when interpreting the resulting cross-sections. Because the Airy method does not acknowledge lateral differential loading, isostatic corrections can result in restoration of structural highs which are too deep and structural lows that are too shallow, as the subsidence history of these features is amplified by adjacent structures (Roberts et al., 1998).

Additionally, Airy backstripping can result in internal deformation of fault blocks by vertical simple shear during restoration. This deformation is an artifact of backstripping with Airy isostasy and does not reflect structures occurring from real geological events (Roberts et al., 1998). Although there are issues with using the Airy method in a 2D situation, the sections resulting from the technique are useful for giving an indication of the paleobathymetry/topography and also for defining major depocentres.

To gain further insight into the evolution of the margin, the backstripping technique was combined with fault restoration and section balancing. These methods permitted the unextended and extended lengths of the section to be calculated, which in turn allowed the amount of extension to be estimated (Gibbs, 1983).

5.6 Results

Each profile was systematically restored using the techniques described in the preceding sections. Figures 5.18 and 5.19 depict the Labrador and Orphan Basin profiles at each reconstruction stage. The unextended and extended lengths, as well as calculated extension values are summarized in Table 5.1. Figure 5.20 shows the areal variation of the stretching values calculated from the profiles.

Overall, the extension factors derived from the restorations are lower than expected, as higher values of extension are predicted by two-layer lithospheric stretching models (Dehler and Keen, 1993). With a two layer model, β values along the southern Labrador margin are predicted to range from 1.28 on the shelf to 1.57 (Beaumont and Issler, 1987). In the Orphan Basin the predicted β values range from 1.25 to > 2.5 (Dehler

and Keen, 1993). Table 5.1 indicates that the maximum β values predicted from the reconstructions are 1.06 on the Labrador margin and 1.14 for the Orphan Basin.

To verify the amount of extension calculated from the restored sections, the fault heaves across the top prerift horizon were measured. These measurements were taken on the initial depth converted sections with no vertical exaggeration, as depicted in Figure 5.21. Table 5.2 contains the measurements and obtained extension values: the first column indicates the profile; the second column displays the measured length of each prerift basement segment along the profile and the sum of these segments (in bold); column 3 indicates the heave measurement across each fault and the sum of these measurements (in bold); and column four indicates the extended length of the profile. The unextended length (column 5) was calculated by subtracting the fault heave sum (bottom of column 2) from the extended profile length (column 4). The sixth column is the stretching factor, β , which is calculated from the extended to unextended length ratio. This procedure was used in the analysis of the remaining profiles, which are summarized in Table 5.1.

Comparison of these values with those obtained from the balanced section restoration show similar results along the Labrador margin, with β values ranging from 1.02 to 1.06. However, the stretching values estimated from the fault heave measurements for the Orphan Basin range from $\beta=1.12$ to $\beta=1.27$, which is greater than the β range of 1.04-1.14 calculated from the balanced section restoration. To investigate if this discrepancy is a function of the decompaction and isostatic corrections applied during the backstripping process, the Orphan Basin profiles were reconstructed without

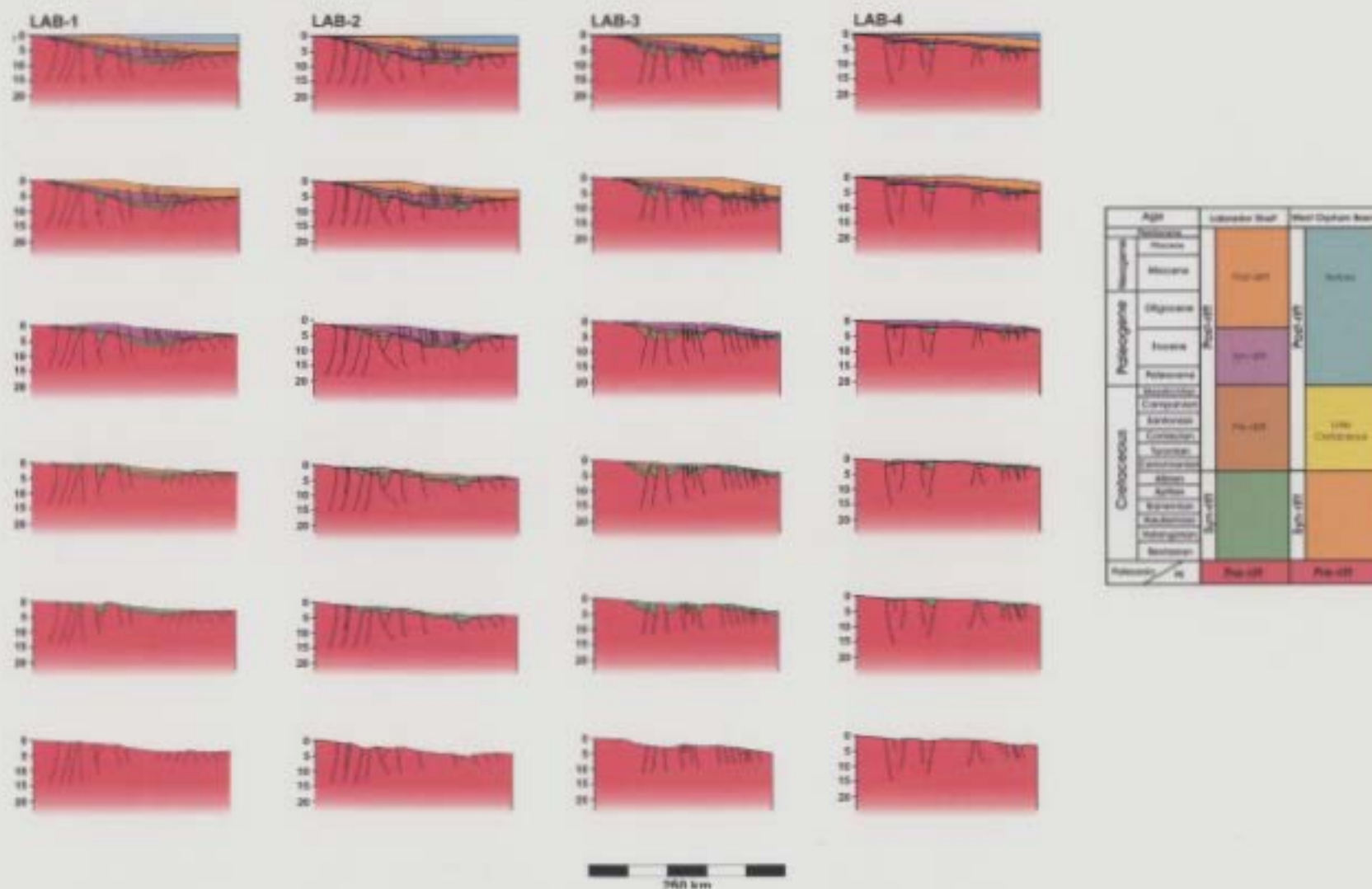


Figure 5.18. Restored and balanced Labrador Shelf profiles. Each color represents a tectonic sequence, as indicated on the timescale chart. The top profile represents the present day margin stratigraphy and structure, on the margin. Each subsequent profile is backstripped and isostatically adjusted to represent the structure and stratigraphic configuration of the margin during each tectonic stage.

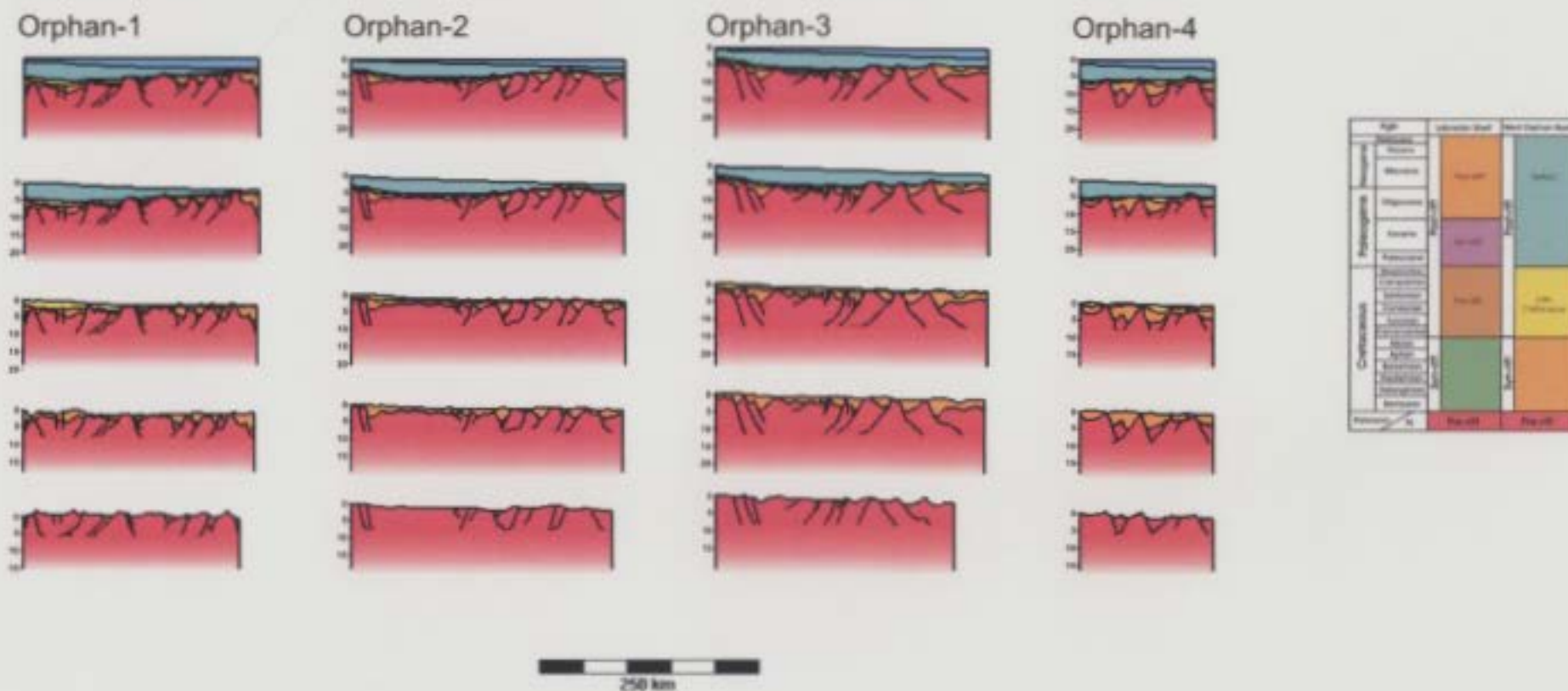


Figure 5.19. Restored and balanced West Orphan Basin profiles. Each tectonic sequence is represented by a color, as indicated on the timescale chart. The top profile represents the present day stratigraphy and structure on the margin. Each subsequent profile is backstripped and isostatically adjusted to represent the structure and stratigraphic configuration of the margin during each tectonic stage.



Figure 5.20. Areal distribution of calculated extension values in the West Orphan and South Hopedale basins. β values estimated from profile restorations are shown in red, and β values calculated from fault heave measurement are shown in black.

Table 5.1.

Backstripped Kinematic Restoration (LithoTect)					
Profile	Extended Length (km)	Unextended Length (km)	Actual Extension (km)	Percentage Stretched (km)	Extended/Unextended
LAB-1	266.45	252.37	14.08	5.284293488	1.0557911
LAB-2	258.808	248.695	10.113	3.907529906	1.040664267
LAB-2	238.194	226.041	12.153	5.102143631	1.053764583
LAB-4	242.884	238.472	4.412	1.816504998	1.018501124
Orphan 1	266.993	245.492	21.501	8.053020117	1.087583302
Orphan 2	311.875	297.08	14.795	4.743887776	1.0498014
Orphan 3	313.055	272.559	40.496	12.93574611	1.148577005
Orphan 4	152.627	151.376	1.251	0.819645279	1.00826419
Fault Heave Calculation					
Profile	Extended Length (km)	Unextended Length (km)	Actual Extension (km)	Percentage Stretched (km)	Extended/Unextended
LAB-1	268.372	255.874	12.498	4.656968685	1.048844353
LAB-2	260.633	248.132	12.501	4.796399535	1.050380443
LAB-2	241.8617	227.8397	14.022	5.797528091	1.061543269
LAB-4	243.9262	238.609	5.3172	2.17983964	1.022284155
Orphan 1	271.451	240.288	31.163	11.48015664	1.129690205
Orphan 2	316.07528	256.48328	59.592	18.85373636	1.232342631
Orphan 3	316.667	273.254	43.413	13.70935399	1.158874161
Orphan 4	154.096	120.528	33.568	21.78382307	1.278507899
Uncorrected Kinematic Restoration (LithoTect)					
Profile	Extended Length (km)	Unextended Length (km)	Actual Extension (km)	Percentage Stretched (km)	Extended/Unextended
Orphan 1	266.993	236.013	30.98	13.12639558	1.131263956
Orphan 2	311.875	246.216	65.659	26.66723527	1.266672353
Orphan 3	313.055	269.675	43.38	16.08602948	1.160860295
Orphan 4	152.627	118.151	34.476	29.17960914	1.291796091

This table indicates the extended and unextended lengths, the actual and percentage extension, as well as the extended to unextended ratio (β factor) for each profile. These values were obtained from backstripped vertical slip restorations, fault heave measurement, as well as vertical slip kinematic restorations without application of decompaction and isostatic corrections.

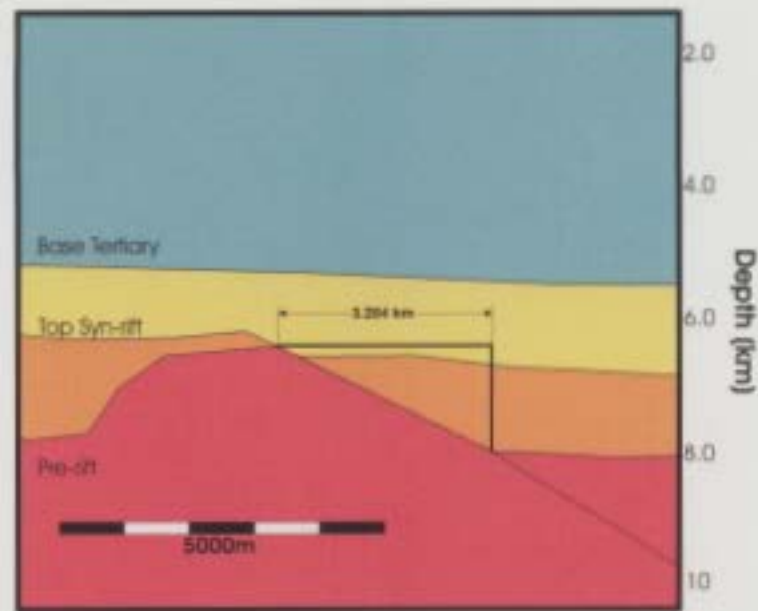


Figure 5.21. Example of a fault heave measurement.

application of these corrections. The extension values obtained from the uncorrected restorations range from $\beta = 1.13$ to $\beta = 1.29$, and are summarized in Table 5.1. These values are similar to those obtained from fault heave measurement, which suggests that the corrections applied to the profiles during backstripping affected the fault geometry and the subsequent vertical slip restoration. A comparison of an Airy isostatically corrected and decompacted reconstruction with the uncorrected reconstruction is shown in Figure 5.22. Towards the eastern West Orphan Basin, the fault geometry is complex and the variation in basement topography is significant, which suggests that a flexural correction may be more appropriate. Because of the discrepancy associated with calculating the extension from the restorations, the values obtained from fault heave measurement were used in the extension analysis. The isostatic restorations, however,

provide a meaningful indication of the general paleobathymetry and evolution of the margin during each tectonic stage.

Although the calculated extension factors are not as high as estimates from a two layer lithosphere model, which range from $\beta = 1.28$ to $\beta = 1.57$ for the Labrador Shelf and 1.25 to >2.5 for Orphan Basin (Beaumont and Issler, 1987; Dehler and Keen, 1993), they do show correlation between extension and syn- and post-rift sediment thickness variation. The Labrador Shelf has lower estimates of extension and higher postrift to synrift sediment thickness ratios. The present day synrift thickness ranges from approximately 1.5 km in the southeast to 3 km in the northwest, while the present day postrift sequence ranges from 3.6 km in the southeast to 7km in the northwest. Profile LAB-4 has the lowest calculated extension value ($\beta = 1.02$) and the lowest synrift sequence thickness (1.5 km). The remaining profiles have extension values of $\beta = 1.05$ -1.06, with the highest calculated extension associated with the profile with the thickest synrift sequence, LAB-3. In the West Orphan Basin, the extension estimates from fault heave measurement range from $\beta = 1.13$ to $\beta = 1.27$, which are higher and more varied than those of the Labrador Shelf. There are significant differences in the post and synrift sediment thickness across the profiles (Figure 5.18). The east contains thicker synrift but thinner postrift sequences, ranging from 3.0-4.6 km and 0.9 to 2.4 km, respectively. In contrast, the west contains thicker postrift but thinner synrift sequences, which range from 4.6-7.0km and 1.0-2.8 km, respectively. The profile with the largest extension, $\beta = 1.27$, contains the thickest synrift sequence of 4.6 km. The profile with the least extension has the thickest postrift sequence of approximately 7km.

The anomalously thin synrift sequences and thick postrift sequences observed in the West Orphan and South Hopedale basins may be accounted for by a non-uniform

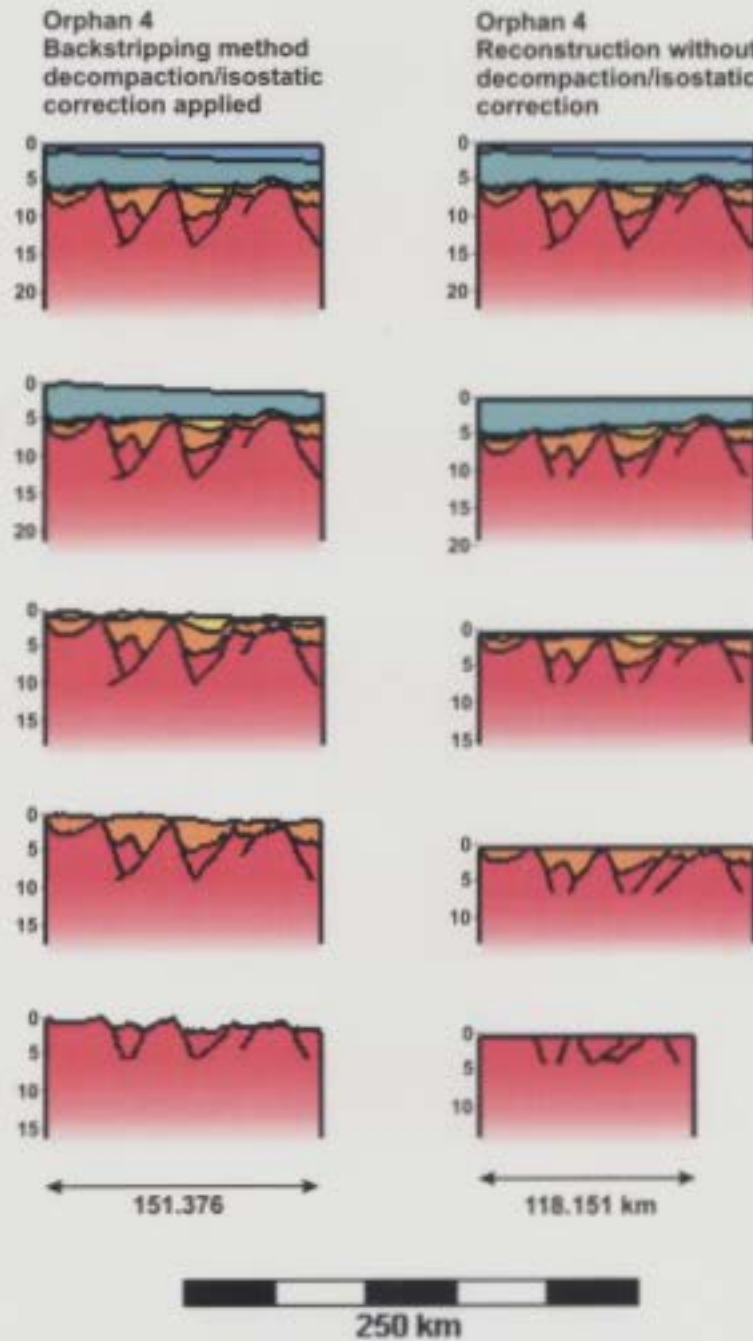


Figure 5.22. Comparisons of vertical slip reconstruction with and without isostatic and decompaction corrections applied (left and right sides, respectively). The unextended length is less on the uncorrected profile, which implies that the isostatic and decompaction corrections affect the vertical slip restorations.

Table 5.2

Line	Basement lengths (km)	Heave measurements (km)	Unextended length (km)	Extended Length (km)	Extended/Unextended
oro-114	6.819	0.392	256.48328	316.07528	1.232342631
	9.253	1.415			
	96.312	3.002			
	5.637	2.224			
	11.662	1.741			
	9.41848	14.212			
	4.517	5.606			
	9.669	2.232			
	18.595	2.864			
	14.217	14.873			
	13.278	2.151			
	13.079	7.367			
	19.022	1.513			
	25.0048				
Sum	256.48328	59.592			

This table indicates the total basement length, the measured fault heaves across the top basement, the calculated unextended profile length and the measured extended profile length. The B factor is calculated from the extended to unextended profile length ratio. A more detailed explanation of this process is contained in the text. A similar procedure was carried out for each profile, with the results summarized in Table 5.1

extension model, where the crust and subcrustal lithosphere can extend independently (Meredith and Egan, 2002). This type of model provides more flexibility in explaining basin geometry and stratigraphic evolution (Meredith and Egan, 2002). Geodynamic models that integrate crustal thinning and thickening, as well as thermal, isostatic and surface processes, suggest that the ratio and magnitude of syn and postrift subsidence may be controlled by deep lithospheric processes (Meredith and Egan, 2002). These processes include enhanced extension of the mantle-lithosphere, and action of transient thermal anomalies such as the growth and decay of hotspots or changes in thickness and temperature of the thermal lithosphere during and since the time of rifting (Meredith and Egan, 2002).

The margins of both the West Orphan and Hopedale basins also have significant postrift stratigraphic onlap, known as “steer’s head” geometry (Figure 5.23). This stratigraphic onlap extends over the prerift Paleozoic Cartwright Arch and St. Anthony Basin, which are devoid of Mesozoic synrift sediments. Several theories have been put forward to explain this geometry, which include sea level fluctuations through geologic time and increased flexural rigidity of the continental lithosphere after rifting (Vail et al., 1977; Watts, 1982; White and McKenzie, 1988). However, a two layer lithospheric stretching model with increased mantle stretching could also account for this type of geometry (White and McKenzie, 1988; Meredith and Egan, 2002).

The eastern Black Sea Basin has thin synrift and thick postrift sequences (Meredith and Egan, 2002), which are similar to those identified in the South Hopedale and West Orphan basins. Geodynamic models of the Black Sea region cannot reproduce

the subsidence when the magnitude of extension is based solely on the amount of fault controlled deformation ($\beta=1.13$). However, models that incorporate increased deformation in the lower crust and mantle lithosphere, with $\beta_m = 3.2$, give a pattern of subsidence more comparable to that evident from seismic data. These models suggest that increased extension of the mantle lithosphere leads to increased lithosphere heating at the time of rifting and subsequently greater magnitude of thermally driven subsidence in response to the re-equilibration of the highly perturbed temperature field (Meredith and Egan, 2002). However, significant space problems arise from the exaggerated stretching of the lower lithosphere (Meredith and Egan, 2002). A variation of the model where the total amount of stretching in the crust and lithospheric mantle is the same but distributed differently in each could account for these space problems (White and McKenzie, 1988).

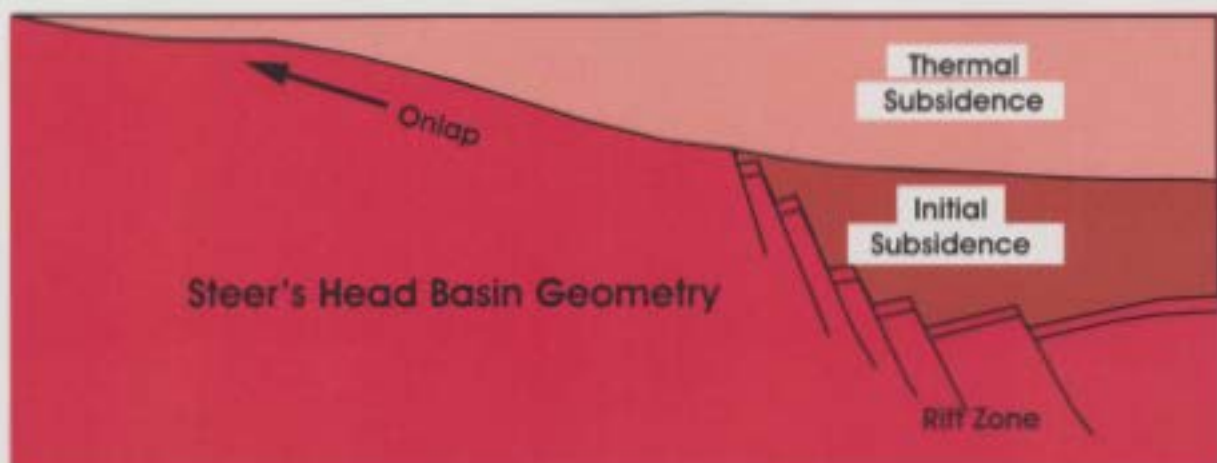


Figure 5.23. Typical "Steer's head" geometry showing onlap of postrift sediments onto prerift basement at the basin margin.

Another factor affecting the syn to postrift sediment thickness ratio is erosion occurring prior to postrift deposition. Thermal uplift due to non-uniform lithospheric stretching or by short term inversion structures can result in removal of synrift

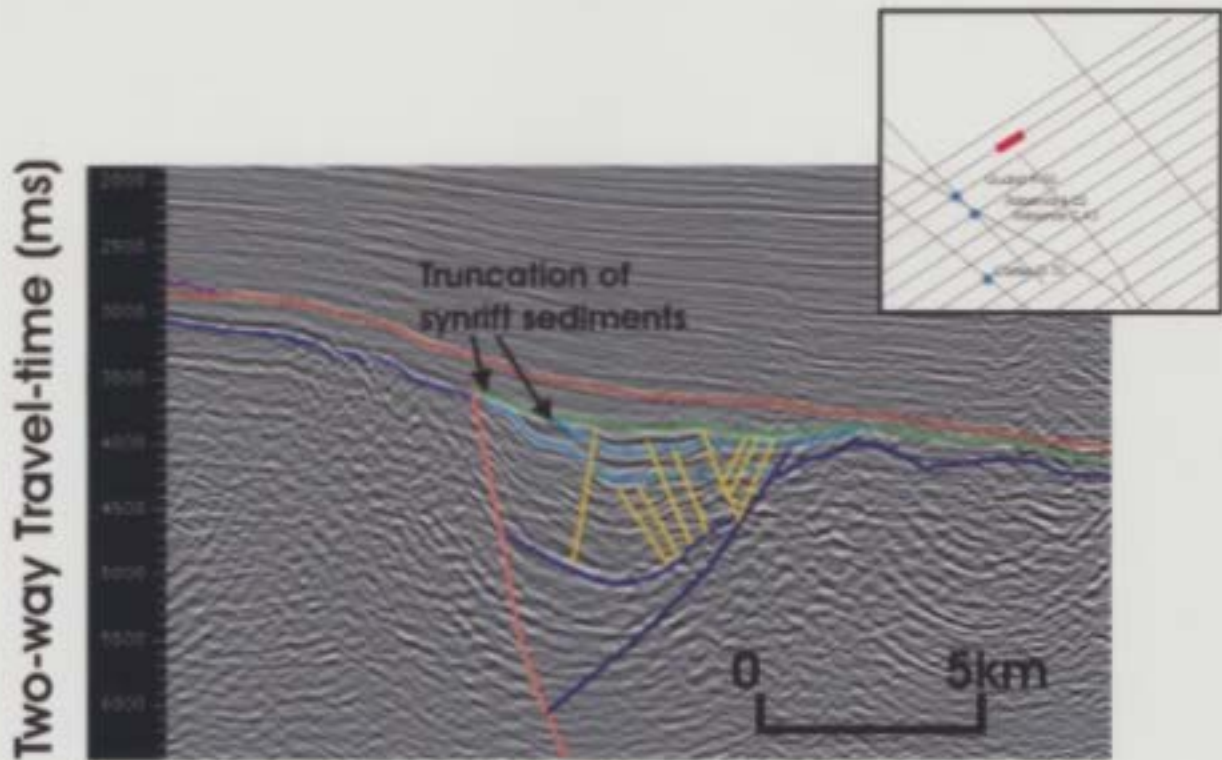


Figure 5.24. The faulted synrift sequence in the South Hopedale Basin is truncated by the Avalon unconformity (green horizon), which implies that this sequence is partially eroded.

sequences, which are effectively replaced by postrift sediments. This replacement affects the post to synrift sequence ratio, and is not accounted for in the McKenzie stretching model. Examination of seismic profiles in both the Hopedale and West Orphan basins shows truncation of the synrift sequences (Figures 5.24 and 5.25), which indicates that erosion occurred in these areas. These total erosional effects are not accounted for in the

fault heave measurement or in the restorations, which offers another explanation for the anonymously high post- to syn-rift sediment ratios.

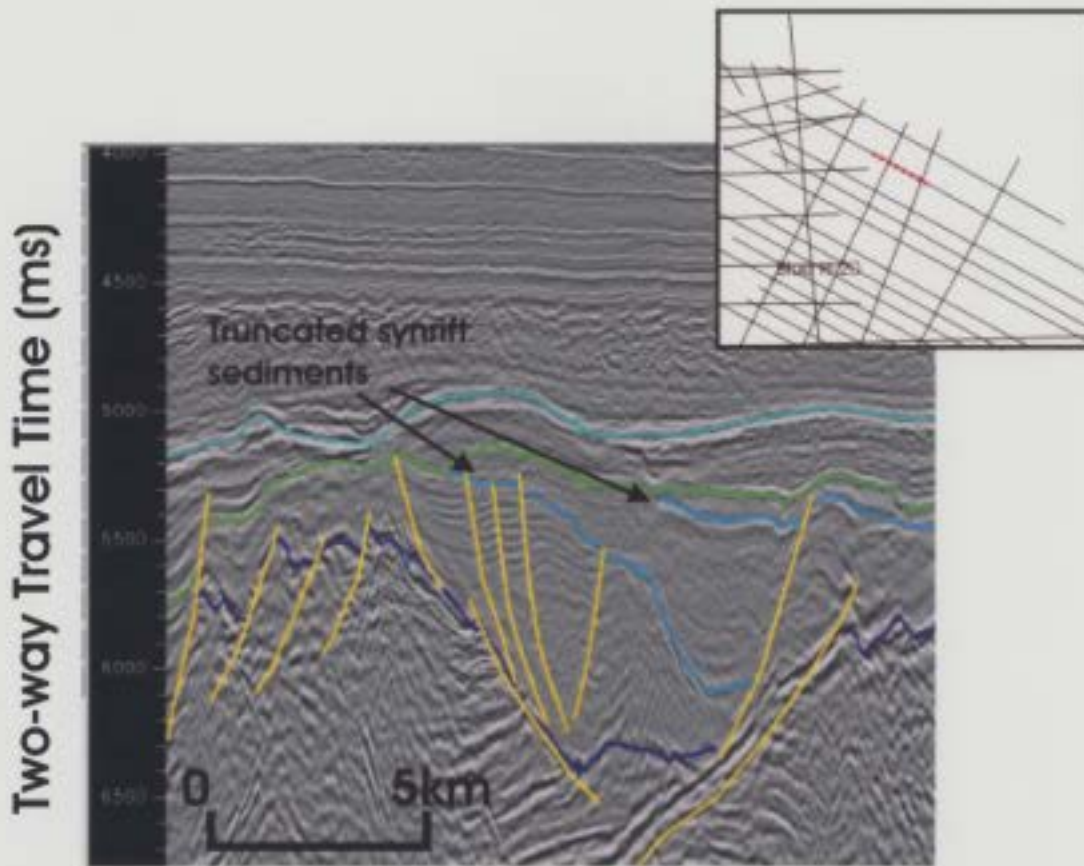


Figure 5.25. The faulted synrift sequence in the West Orphan Basin is truncated by the Avalon unconformity (green horizon), which implies that this sequence is partially eroded.

5.6.1 Hopedale Basin

Reconstructions of the Labrador profiles indicate that extension increases towards the northwest, and that the shelf break prograded eastwards during geologic time. At both the synrift and predrift reconstructions, the outer shelf appears to have been closer to sea-level, suggesting that sequences beneath the present day slope and deep water may have been deposited in shallower water, which could have implications for source and reservoir rock deposition.

Profile reconstructions at postdrift time indicate a substantial thickness variation within the postdrift sequence. The main depocentre was likely in the central part of the shelf at this time, as the postdrift sediments reach a maximum thickness of approximately 4.8 km along profile LAB-3 (Figure 4.9). The sequence thins to 3.2 km in the north and 2.9 km in the south. However, this unit is still thicker than the cumulative thickness of the synrift, predrift and syndrift sequences in the south. In contrast, the postdrift sequence is thinner than the combined thickness of the older sediments in the north. This implies that the earlier tectonic stages were dominant in the north and that the main depocentre shifted southwards during postrift time.

At the time of active seafloor spreading, the main sediment depocentre was likely farther north than in later Oligocene to Pleistocene time. This is inferred from the thickness of the syndrift sequence along profiles LAB-1 and LAB-2 (Figure 4.9). To the south, these sediments thin and have a uniform thickness of approximately 1.6 km. However, in the northwest, the thickness of this unit varies substantially along the length of the profiles. Profile LAB-3 has a much thicker, 2.4 km thick syndrift sequence landward of the slope break, while profiles LAB-1 and LAB-2 contain sequences seaward of the slope break that are approximately 4 km thick. These syndrift sequences are affected by numerous extensional faults.

In the time after rifting but prior to the onset of seafloor spreading, the sediments were thickest in the landward areas of profiles LAB-3 and LAB-2, with a range of 1.8-2.7 km. On LAB-2, the predrift sediments thicken towards the extensional faults, indicating that some faults were active at this time. Profile LAB-4 contains the thinnest predrift

sequence, ranging from 0.5-1.2km, which appears to have been deposited in much shallower conditions. As Airy 2D backstripping tends to underestimate the paleobathymetry, this area could have been above sea level and affected by erosional processes. Erosion may explain the thinner sedimentary sequences in this region in comparison to profiles further north.

Reconstruction to synrift time shows that the rift age sediments are confined to half graben structures and are thicker on the inner part of the shelf. The thinnest sequences, ranging from 0.4-2 km, are found on profile LAB-4. On all profiles, the sequence is generally 0.5-1 km thick seaward, with localized areas of thicker sedimentation (Figure 4.9). The thickest synrift sequence, approximately 3.6 km, occurs on profile LAB-3. On profiles LAB-1 and LAB-2 the maximum thickness ranges from 2.5 -2.8 km. On all profiles, the sediments thicken substantially towards the extensional faults, indicating major fault activity during this time.

5.6.2 Orphan Basin

The Orphan Basin profile reconstructions depict thick postrift sequences in the west that thin significantly to the east. The Base Tertiary to top synrift sequence has the most drastic thinning, particularly along profiles Orphan-1 and Orphan-2, where it thins from 4-5 km to approximately 1-1.5km. The sequence also thins on profiles Orphan-3 and Orphan-4, but there are localized areas of thicker postrift sedimentation. There is little change in the profile lengths from Late Cretaceous to present, which confirms that only minor extension has occurred since the cessation of rifting (Solvason, 2006).

Reconstructions to synrift time show half graben confined sequences in the east that range from 4.2 to 5.7 km in thickness. The synrift sequence is thinner and more continuous in the west, with an average thickness range of 1-1.6 km. In localized areas, the thickness range increases to 3-3.9 km. These local increases are associated with half graben structures adjacent to east-dipping extensional faults in the westernmost part of the basin. On all profiles, sediments thicken towards the extensional faults, suggesting that they were active during this time. The restorations, in particular profile Orphan-1, also indicate that the western part of the basin was at a higher elevation during this phase. This is significant as erosion of this region may have sourced reservoir sandstones in areas adjacent to the highs. Comparison of the length of the synrift reconstruction to the prerift reconstruction shows considerable difference, and points to the bulk of extension occurring at this time.

5.7 Considerations

In these restorations, a vertical slip kinematic model was used. This model assumes that all displacement occurs vertically and no displacement is accommodated in various oblique directions (Solvason, 2006). The restorations also assume that all extension occurred in the plane of the profiles. However, Orphan Basin has been affected by multiple rifting episodes where the extension vector rotated with time, so these assumptions may not be valid within this area. On the Labrador Shelf, there was only one rifting phase and a slight rotation of the extension vector, so these assumptions may be more applicable.

Another assumption made during the restoration is that the lower layer acted like “toothpaste” and accommodated the fault displacement, which permitted irregularities in the shape of the basement layer. This is particularly evident in the Orphan profiles, where there are low-angle extensional faults with numerous folds and bends. The folds and bends become more prominent and take on more unnatural geometries with each restoration stage.

Additionally, the calculated extension is limited by the profile length, which is particularly significant in the Orphan Basin. The Orphan profiles extend further into the East Orphan Basin, which is outside the area of interest for this project. However, as greater extension likely occurred further eastwards, this could account for the lower extension estimates obtained in this study.

Another factor to consider is that the amount of extension estimated from the geometry of normal faults in basement is often less than that estimated from whole crustal thinning observed on seismic sections or estimated from subsidence (Keen and Dehler, 1993). This difference suggests that the upper crust may be decoupled from the lower crust (Keen and Dehler, 1993). As well, the lower extension values may reflect the probable presence of many small, seismically unmappable extensional faults. If mapping these faults was possible, it could increase the extension calculated through normal fault geometries. This may explain the lower extension values obtained in this study.

In correcting for sediment loading, an Airy model was used for isostatic compensation. However, as the lithosphere exhibits finite strength, a flexural model for isostatic compensation might be more realistic (Keen and Dehler, 1993). The main effect

of a stronger lithosphere is to increase the postrift subsidence relative to synrift subsidence, as higher temperatures would keep the lithosphere relatively weak until the postrift thermal cooling phase (Keen and Dehler, 1993). A stronger lithosphere also distributes the subsidence over a significantly wider zone. Analysis of sediment loads in extensional basins indicate that lateral variation within synrift and early postrift sediments is controlled by extensional faulting and rotated block geometry (Keen and Dehler, 1993, Roberts et al., 1998). In general, the synrift and early postrift basin floor will be influenced by the short wavelength fault-block geometry, which means that the effects of differential loading are at a maximum. In this case a flexural model is most appropriate. However, once the rift induced topography is filled, the lateral variation in loading becomes more subdued and the results using flexural and Airy isostatic corrections will converge (Roberts et al., 1998). Consequently, in areas containing significant amounts of synrift sediments, the flexural model is likely more appropriate. However, in areas where the synrift sediments are thinner, such as the West Orphan and Hopedale basins, flexural effects may not be as important (Roberts et al., 1998; Keen and Dehler, 1993). The load distribution is another consideration, as both the Orphan Basin and Labrador Shelf are wider than the flexural wavelength. This load distribution suggests that the long wavelength response to sediment loading may be more accurately approximated by the Airy model.

Another factor in assessing the isostatic response is the variation of mantle temperature with time. This will have a major effect on uplift of the seabed during a hot

phase of rifting, but would not be included in the local isostatic correction calculated by LithoTect (Hall, 2007 pers. comm.).

The depth of the Moho should also be considered in areas of deep water. Towards the eastern end of the Orphan profiles the water depth range increases to 2.2 to 3 km. At these depths, the Moho depth is typically higher than it is towards the landward part of the basin. The depth to Moho was estimated by doing an Airy mass-balance calculation. Figure 5.26 is a simplified profile showing the water depth variation, average sediment and crustal thickness and density. Mass balance of the left and right sides gives

$$\rho_w W_{di} + \rho_{sed} S_{sedi} + S_c \rho_c = \rho_w W_d + \rho_{sed} S_{sed} + \rho_c (D_i - x) + \rho_m X \quad (5.11)$$

Where ρ_w , ρ_{sed} , ρ_c , ρ_m are the densities of the water, sediments, crust and mantle, respectively, and W_{di} , S_{sedi} , S_c are the water depth, sediment thickness and basement thickness on the west side of the profile. W_d , and S_{sed} are the water depth and sediment thickness on the east end of the profile, and D_i and X refer to the compensation depth and Moho upwarp. Solving this equation gives $X=10.53$ km, which allows depth to Moho, D , to be calculated

$$D = D_i - X = 14.47 \text{ km}$$

This calculation implies that areas assumed to be lower crust on the sections may actually be mantle, which would affect the, isostatic adjustments calculated during the restoration

process. It also suggests that the region is more significantly stretched than what the estimates from the balanced section reconstruction and fault heave calculations show.

A final consideration is that the restoration process did not take erosional effects into account. Consequently, reconstructions of the margin back to prerift conditions are rough estimates as the original size and shape of some features were likely affected by erosional forces (Solvason, 2006).

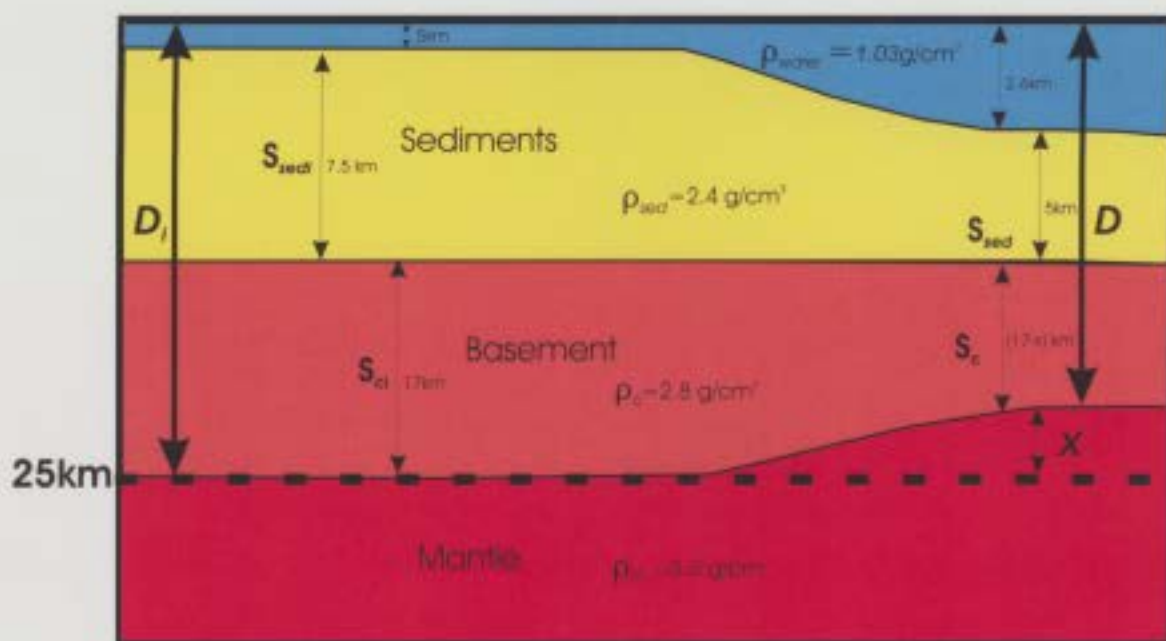


Figure 5.26. Schematic diagram showing the mass water depth, sediment and basement thickness, and mantle upwarp (X) along a typical West Orphan Basin profile. Depth of compensation used in the mass balance is 25 km.

Chapter 6: Petroleum Prospectivity

6.1 Petroleum Overview

Considerable petroleum potential exists within the region of interest, particularly on the southern Labrador Shelf. Exploration of the Labrador margin during the 1970s to mid 1980s resulted in the discovery of 4.2 tcf of natural gas and proved the existence of a rich petroleum system (Bell and Campbell, 1990; Enachescu 2006 *a*). However, as the focus was to discover oil, and gas prices were low, development was not pursued and drilling in the area ceased (Enachescu, 2006 *a*).

Less is known about the petroleum prospectivity of the West Orphan Basin due to a limited exploration history. Only seven wells were drilled during the initial exploration cycle, and all of these are located on the crests of basement highs. Consequently, the thicker Mesozoic section interpreted to exist in deeper sedimentary sections has not been encountered (Fagan and Atkinson, 2000). Exploration in the region has been limited due to extreme water depths towards the eastern part of the basin and the presence of more prospective plays in adjacent areas (Bell and Campbell, 1990). However, the East Orphan Basin was connected to the Grand Banks and West Irish conjugate margin in the Late Jurassic, and a seaway extended from the Grand Banks into the Orphan Basin, northern Europe and the Labrador area during the Late Jurassic and Cretaceous (Mason and Miles, 1986; Coffin et al, 1992; Srivastava and Verhoef, 1992; Srivastava et al., 2000; Sibuet et al., 2005, Enachescu et al., 2005). As the Grand Banks, Labrador, West Ireland and

Northern Europe offshore areas all have proven petroleum systems, the Orphan Basin should be considered as a basin with significant petroleum potential.

The Paleozoic St. Anthony Basin may also have petroleum prospectivity, as it contains similar stratigraphy to the Deer Lake and St. Georges subbasins. Gas and oil shows have been encountered in exploration and shallow boreholes in both these areas. However, the St Anthony Basin has not been extensively explored or drilled and the existing 2D seismic reflection coverage is limited. Consequently, the discussion of petroleum potential will be restricted to the Mesozoic South Hopedale and West Orphan basins.

6.2. South Hopedale Petroleum System

Five natural gas discoveries are located on the inner shelf in the Hopedale Basin (Figure 6.1). These discoveries are located at the Bjarni H-81, Gudrid H-55, Snorri J-90, Hopedale E-33 and North Bjarni F-06 wells (Figure 6.1). Additionally, approximately 0.43m^3 of unbiodegraded oil was discovered at the North Leif I-05 borehole (Bell and Campbell, 1990). The Gudrid H-55 discovery and North Leif I-05 oil show are located within the study region. At Gudrid H-55, 0.9 trillion cubic feet (tcf) of natural gas is contained within a Late Paleozoic carbonate reservoir. Computed recoverable resources for the other gas discoveries, all in sandstone reservoirs, are 2.2 tcf for North Bjarni, 0.9 tcf for Bjarni, 0.1 tcf for Hopedale, and 0.1 tcf for Snorri (Bell and Campbell, 1990). The total natural gas potential of the Labrador margin has been estimated at 22 tcf (Enachescu 2006 *b*; Drummond, 1998).



Figure 6.1. Discovered gas fields on the Labrador Shelf. Modified from Department of Mines and Energy, Government of Newfoundland and Labrador, 1993.

Figure 6.2 depicts the lithostratigraphy, as well as proven and potential source and reservoir units in the Hopedale Basin. The proven reservoirs are the Late Cretaceous Bjarni Formation sandstones, the Paleocene-Early Eocene Cartwright (Gudrid Member) sandstones and Late Paleozoic dolomites and limestones. Additionally, the Late Cretaceous Freydis Member sandstones, and the Late Eocene-Early Oligocene Leif sandstones are potential reservoir units (Enachescu, 2006 *b*; Bell and Campbell, 1990).

6.2.1 Reservoir Potential

Erosion of the rift shoulders and intrabasinal ridges during initial intracontinental extension in Cretaceous time resulted in a major pulse of coarse clastics and the

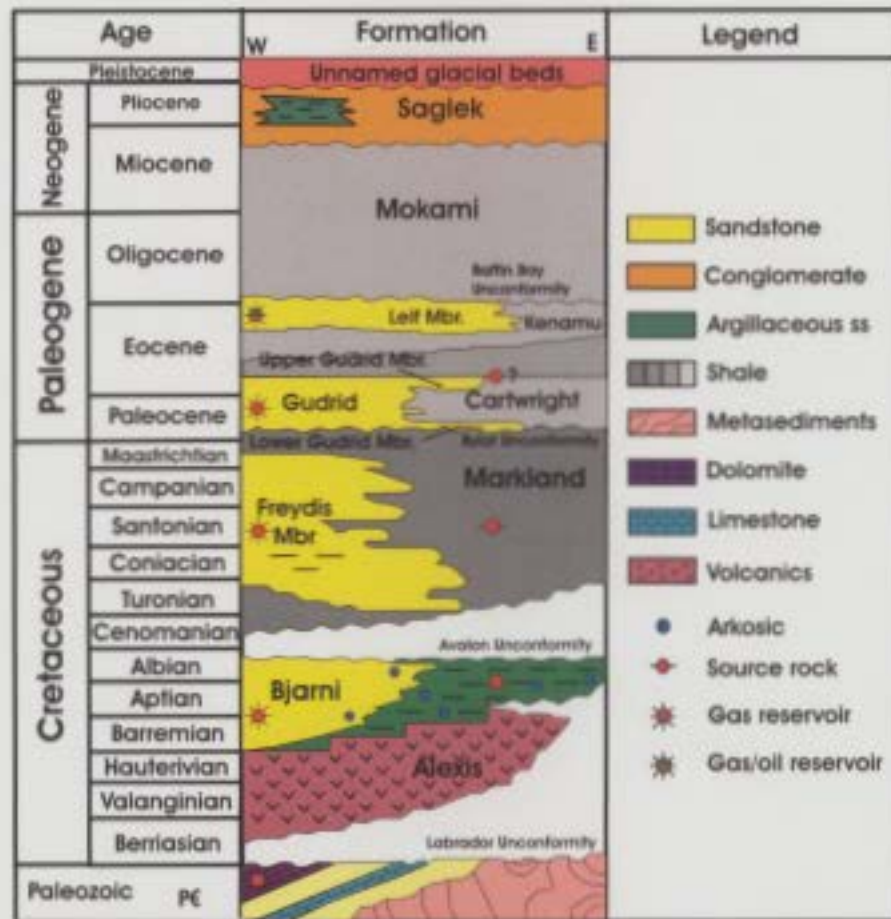


Figure 6.2. Labrador lithostratigraphy, with proven and potential reservoir and source rocks indicated on applicable formations. Modified from McWhae et al. (1980) and Enachescu (2006a).

deposition of the Bjarni sandstones (Bell and Campbell, 1990; Enachescu, 2006 b). As discussed in previous chapters, these synrift sandstones thicken towards marginal faults

of half graben structures and thin over ridges (Enachescu 2006 *b*). Figure 6.3 is an isopach map of the Bjarni Formation, which is thickest on the inner shelf. This formation contains shale intervals that are proven sources and sandstone beds that are excellent reservoirs. Thicker sequences are the most prospective hydrocarbon targets, as they likely to contain both sand and shale intervals. The Bjarni Formation is absent in the southwest and innermost shelf, and generally thins seaward. However, there are a few localized areas of thicker

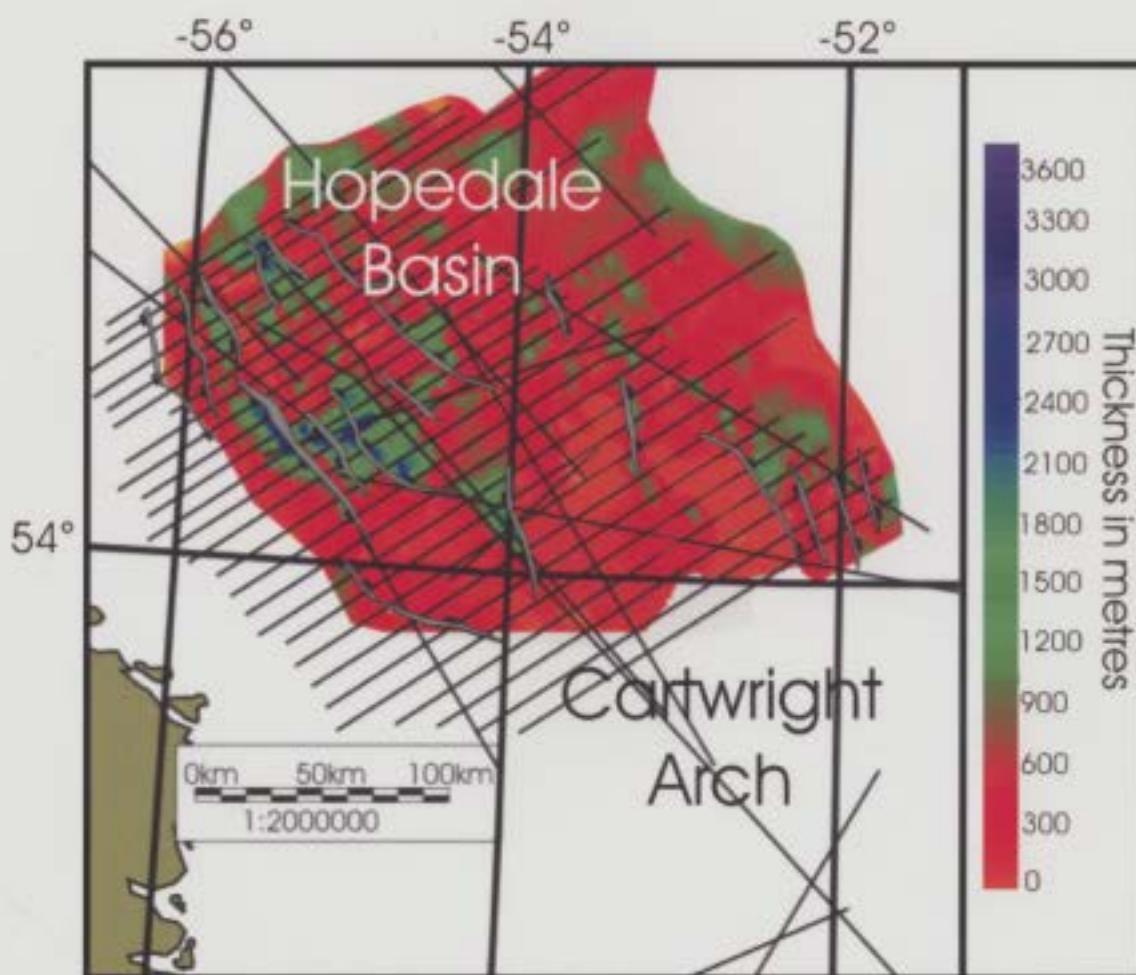


Figure 6.3. Isopach map of the synrift Bjarni Formation, which contains proven source and reservoir units.

sedimentation associated with seaward dipping faults on the outer shelf. Thicker sequences are also located adjacent to the shelf break in the southwest.

Following the initial rifting phase, a prograding wedge of latest Cretaceous and Early Tertiary marine sediments was deposited from the west. This sequence consists of predominantly marine shales, but three cycles of coarse clastic deposition formed the Freydis, Gudrid and Leif sandstones (Bell and Campbell, 1990; Enachescu

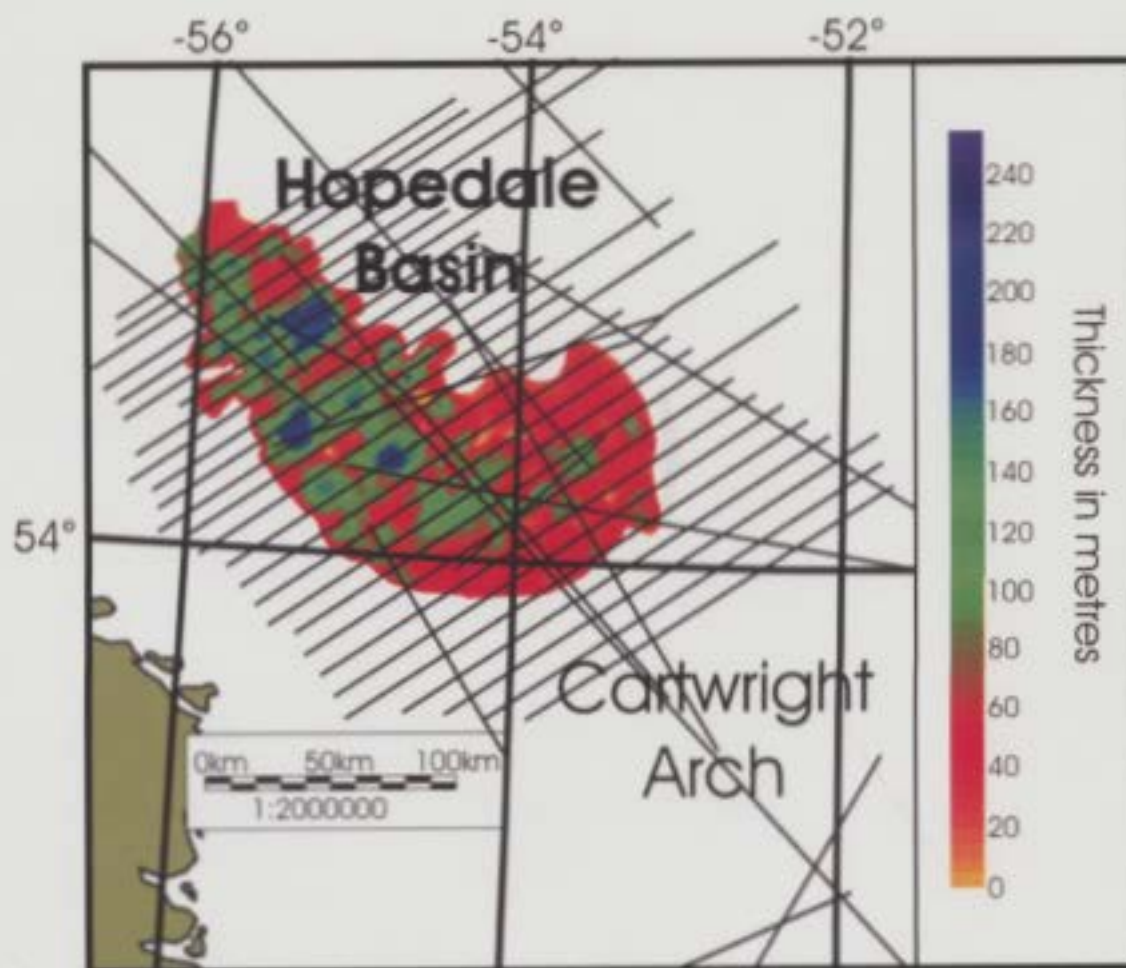


Figure 6.4. Isopach map of the postrift Cartwright Formation. The Gudrid Member sands are present along the inner shelf. In this region, however, the thickest sequences are adjacent to immature or marginally mature source intervals, so the reservoir prospectivity is limited.

2006 *b*). Figure 6.4 is an isopach map of the Cartwright Formation, which is thick on the inner shelf but thins and downlaps onto the top Markland Formation seaward. In the south, the sequence is thinner but extends further onto the shelf. This reservoir is less prospective in the study area as source intervals on the inner shelf, where this sequence is thickest, are immature to marginally mature. Consequently, long migration paths from deeper source rocks located on the outer shelf would be required for significant hydrocarbon accumulations. The Freydis Member was encountered in only one well, Freydis B-87, and was not mapped in the study area. The Leif Member was encountered in all wells in the study region, except Indian Harbour M-52, but was not mapped due to the low impedance contrast between the sandstone and surrounding fine-grained sediments.

6.2.2 Source Potential

Type III source rocks are the most prevalent on the Labrador. This type of kerogen is largely derived from land plants and generates mainly gas and condensate on maturation (Bell, 1989; Geochemistry I). There are two source rock sequences that are organically mature enough to have generated the gas and condensate accumulations present on the inner Labrador Shelf. These are the Lower Cretaceous lignite and coal bearing Bjarni Formation and the Upper Cretaceous-Paleocene Markland Formation (Enachescu, 2006 *b*; Bell and Campbell, 1990; Fowler et al., 2005). Further seaward, the marine Cartwright and Kenamu shales are potential source intervals (Enachescu 2006 *b*; Isseler and Beaumont, 1987). Additionally, analysis of hydrocarbon shows within several

wells on the Greenland margin suggest that a Mesozoic seaway may have existed on the Labrador Shelf, and that Late Jurassic and Cretaceous marine source rocks could have been deposited (Bojesen-Koefoed et al., 2004). However, no Jurassic rocks have been recovered on the Labrador side of the margin to date (Enachescu, 2006 *b*).

A limited number of intervals in Labrador Shelf wells contain source rocks that are a combination of type II and Type III kerogen. Type II kerogen usually forms from marine organic matter deposited in a reducing environment and has the potential for

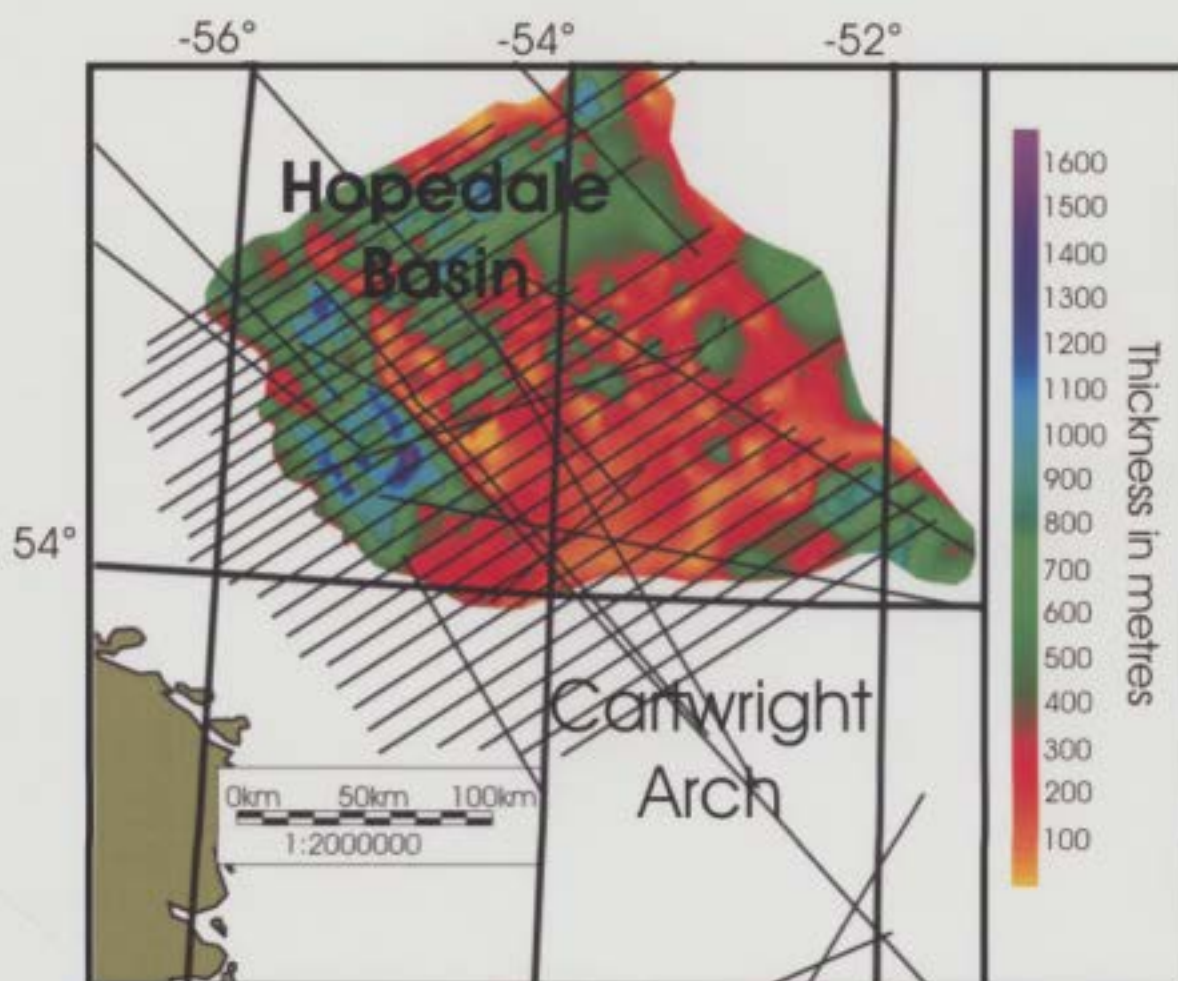


Figure 6.5. Isopach map of the postrift Markland Formation. The extension of this sequence onto the outer shelf and slope indicates significant source potential, as progressively younger sequences are predicted to become mature seawards (Beaumont and Issler, 1987).

generating oil on maturation. Source rocks that are considered type II-III have hydrogen/oxygen ratios that put them between type II and type III, and consequently may generate oil. Most of the Type III-II source rocks are Lower Cretaceous Bjarni lacustrine shales or Eocene marine shales of the Cartwright and Kenamu formations (Bell, 1989; Geochemistry I).

The Markland Formation contains terrestrially-derived organic matter, with total organic carbon ranging from 1 to 4 %. Initially, the Markland shales were considered the main source rock, but Rock-Eval analysis of cuttings, geochemical analysis of organic rich intervals and organic petrology show that the best source rocks occur in the Early Cretaceous Bjarni Formation shales (Bell and Campbell, 1990; Fowler et al., 2005). The Bjarni Formation is thickest within half graben structures, while the Markland shales are more areally extensive and thicken towards the outer shelf and slope (Figures 6.3 and 6.5) (Enachescu, 2006 *b*; Bell and Campbell, 1990). The Markland shales, along with the Kenamu and Mokami shales, also form excellent regional seals.

6.2.3 Petroleum Entrapment

There are several types of hydrocarbon traps present in the Hopedale Basin. On the inner shelf, these include drape of Bjarni sandstones over basement horsts, pinchout of Bjarni sandstones against tilted fault blocks, and drape of lower Tertiary marine sandstones above basement horsts forming anticlinal closure traps (Bell and Campbell, 1990; Fagan and Atkinson, 2000; Enachescu, 2006 *b*). On the outer shelf and slope, targeted traps are listric faults and associated roll-over structures (Enachescu, 2006 *b*).

Additionally, preserved Early Paleozoic sediments on the tops or sides of basement blocks are potential traps in the South Hopedale Basin (Bell and Campbell 1990; Fagan and Atkinson, 2000; Enachescu, 2006 *b*). Some of these trapping mechanisms are depicted in Figure 6.6.

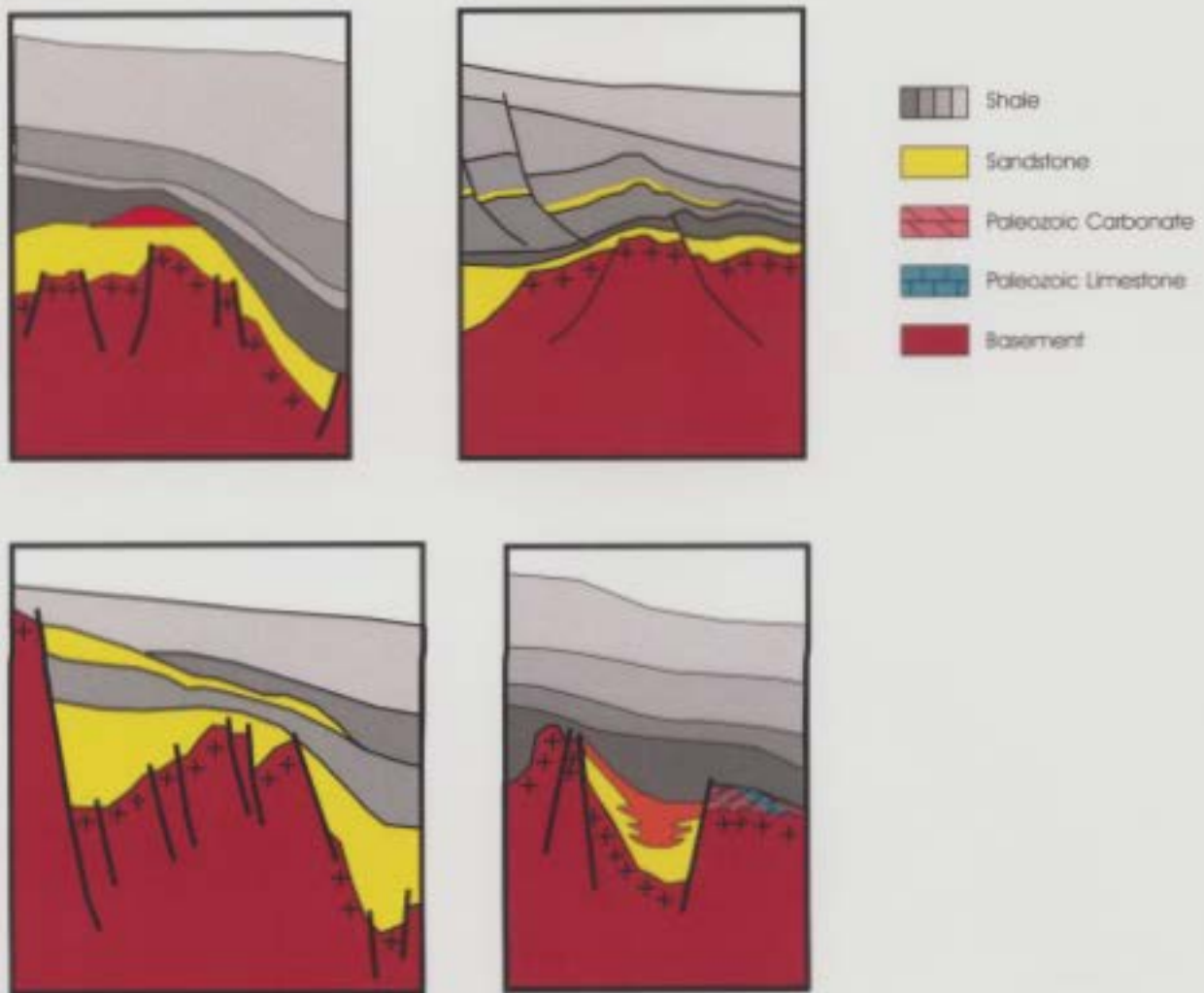


Figure 6.6. Petroleum traps targeted on the Labrador Shelf, which include: drape of Bjarni sandstones over basement horsts (top left), pinchout of Bjarni sandstones against tilted fault blocks (bottom right), drape of lower Tertiary marine sandstones above basement horsts forming anticlinal closure traps (top right and bottom left), listric faults and associated roll over-anticlines in the outer shelf (top right), and preserved Paleozoic reservoirs on rotated basement blocks (bottom right).

6.2.4 Maturation and Thermal Evolution

Limited borehole data makes mapping of maturation-depth configurations across the Labrador Shelf difficult (Bell and Campbell, 1990). However, vitrinite reflectance data from the boreholes on the Labrador Shelf suggests that R_o levels of 0.7%, the value at which significant quantities of gas and condensate are generated from Type III source rocks, occur at depths ranging from 2600 m to 3400 m (Bell and Campbell, 1990).

Maturation appears to occur less rapidly with increasing depth basinward across the Labrador Shelf, due to increased sediment rates on the outer shelf, and lower thermal gradients on the outer shelf during Tertiary time. Geothermal gradients calculated from available depth/temperature profiles from 27 wells on the Labrador Shelf indicate that the average geothermal gradient is 2.97 °C/100m, and that the thermal gradients decrease towards the outer shelf (Bell, 1989; Geochemistry I). The average thermal gradient is higher than that encountered on the Grand Banks, which has implications for the depth of generation for oil and wet gaseous hydrocarbons. On the Labrador Shelf, the oil window may occur as high as 3000 to 3500 m depth, with the threshold for wet gaseous hydrocarbons occurring at 2500m (McWhae et al., 1980).

The majority of wells on the Labrador margin are situated on basement highs that formed during the initial rift phase, and penetrate only thin synrift sequences. However, thicker sequences are present on the flanks of the highs, and may contain more mature source rocks (Bell and Campbell; Issler and Beaumont, 1987). The thermal characteristics and degree of organic maturity of areas not penetrated by boreholes have

been predicted from depth dependent extensional models calibrated with measured thermal properties from borehole samples (Issler and Beaumont, 1987).

Predictions from the extensional model are generally consistent with subsidence, organic maturity and present day temperatures on the Labrador margin determined from borehole data on the inner shelf. Thermal modeling of the Bjarni Formation predicts that oil window conditions exist ($0.58-0.65 \% R_o$) on the inner shelf and that marginal maturation occurred during the late Eocene to Oligocene (Issler and Beaumont, 1987). The zone of mature sediments is predicted to increase seaward from the Labrador coastline, with progressively younger sediments becoming mature towards the shelf edge where thick post-rift sequences exist (Issler and Beaumont, 1987). Consequently, Eocene rocks containing significant amounts of marine-derived organic matter may be within the oil window on the outer Labrador Shelf, and marginally mature Cretaceous and Paleocene rocks may be at the threshold for peak hydrocarbon generation deeper in the basin (Issler and Beaumont, 1987).

Many of the gas/condensate discovery wells are located on horst structures adjacent to thicker sedimentary sequences, and controversy exists concerning whether the hydrocarbon accumulations are products of local generation (McWhae et al., 1980) or long distance migration (Powell, 1979). All the hydrocarbon bearing reservoirs on the Labrador Shelf appear to be at maturation levels less than $0.7 \% R_o$, or are adjacent to Type III source rocks which are immature for significant gas and condensate generation. In addition, the Bjarni H-81 and Gudrid H-55 gas discoveries have high methane content. These factors suggest that vertical migration may have occurred (Powell, 1979; Bell and

Campbell, 1990). However, the hydrocarbon composition may also be a result of biogenic degradation or early thermal diagenesis of marginally mature source rocks, such as the Bjarni Formation shales (McWhae et al., 1980).

6.2.5. Prospectivity

The South Hopedale Basin has a proven hydrocarbon system, and mapping of the major reservoir and source intervals indicates several prospective areas. As mentioned, several targets on the inner shelf were drilled in the earlier exploration cycle, with a gas discovery at the Gudrid H-55 well and an oil recovery at the North Leif I-05 well. Maturation data from the boreholes indicates that the majority of wells are below the threshold for significant hydrocarbon generation (Bell and Campbell, 1990), and modeling suggests that marginally mature sediments on the inner shelf may become mature further seaward (Issler and Beaumont, 1987). In addition, the seismic reflection data used in this interpretation suggests that the reservoir and source bearing syn- and pre-drift sequences extend past the slope break into deep water. Consequently, more prospective petroleum targets may be located on the outer shelf and slope. Figure 6.7 depicts isopach maps of the Cartwright, Markland and Bjarni Formations with potential source and reservoir intervals highlighted. Areas with thicker Bjarni and Markland sequences on the outer shelf and slope were examined and potential traps are shown on reflection seismic sections.

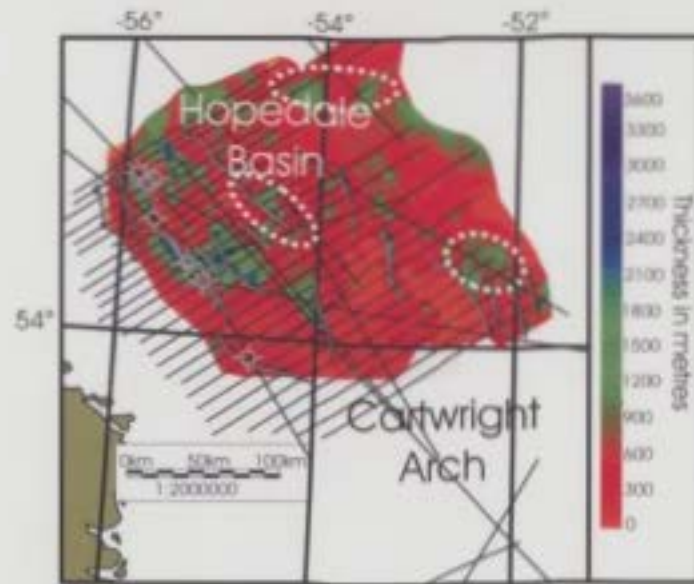
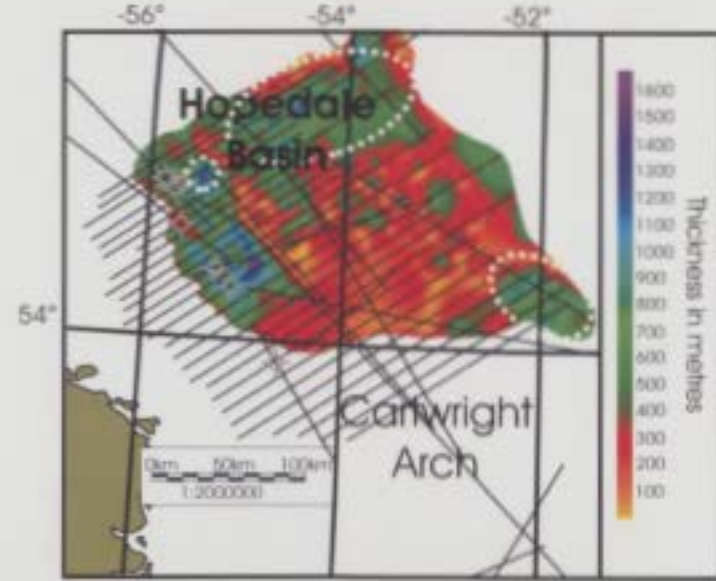
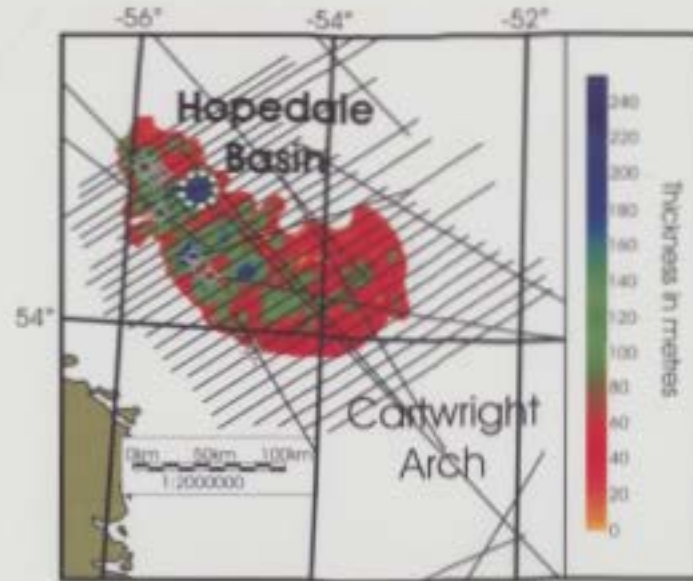


Figure 6.7. Maps showing the Cartwright (top left), Markland (top right) and Bjarni formations (bottom). Prospective areas are indicated by dashed white circles. The Gudrid member (Cartwright Formation) and the Bjarni Formation sandstones are proven reservoirs, and the Bjarni and Markland formation shales are proven sources on the Labrador Shelf. An undrilled, 2.4 km thick interval of the Cartwright Formation overlying a 1.2 km thick Markland sequence is a prospective target on the middle shelf. Half graben structures containing 1.8 km thick Bjarni intervals seaward of the North Leif 1-05 well are also prospective as Bjarni Formation shales are predicted to become increasingly mature towards the outer shelf (Beaumont and Issler, 1987). Other potential areas include the slope area in the north and south, where thicker Markland and Bjarni sequences are mapped.

Figure 6.8 indicates a deepwater prospect northwest of the Gudrid and Roberval wells, where the synrift Bjarni Formation and predrift Markland Formation are interpreted to extend onto the outer shelf and slope. Potential source rocks include Bjarni

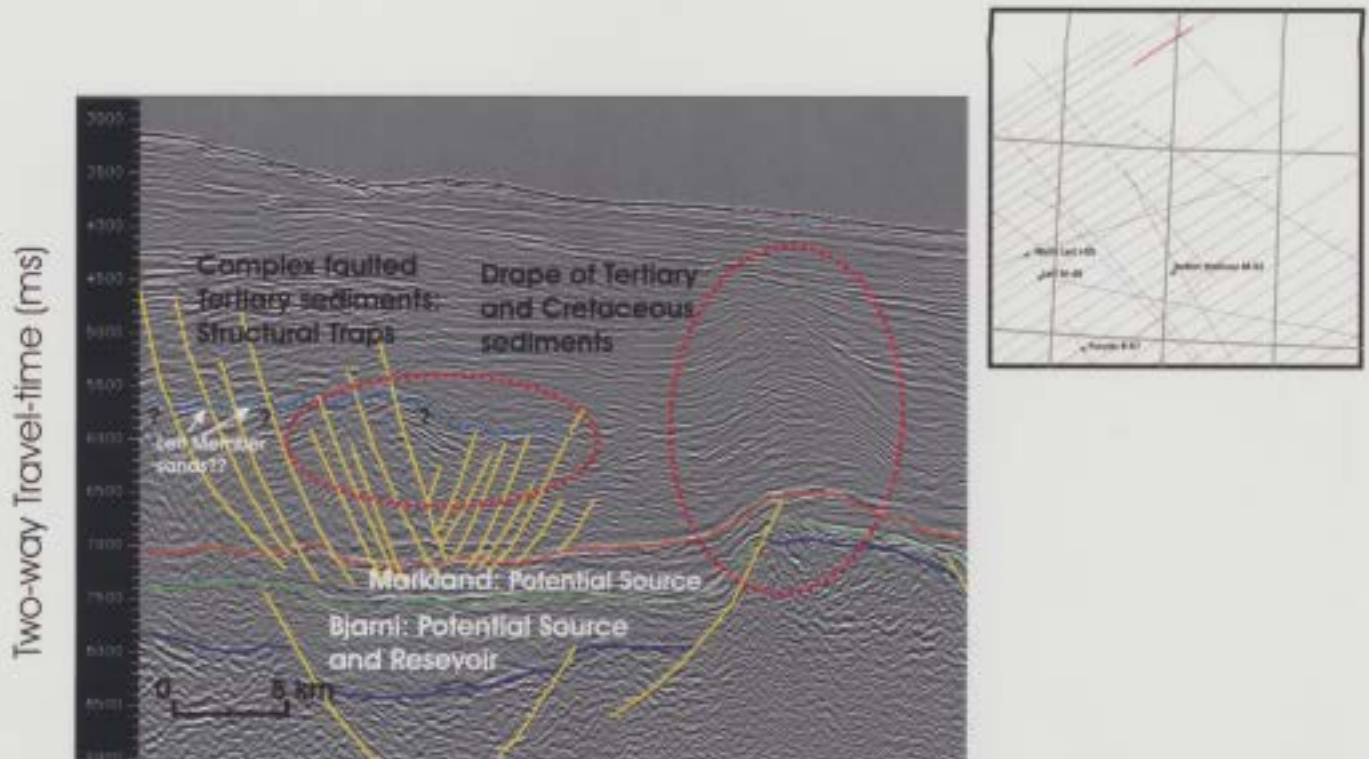


Figure 6.8. Deepwater petroleum prospect located northwest of the Gudrid and Roberval wells. Numerous extensional faults within the postrift sequence and drape of Bjarni and Markland sequences over elevated prerift basement are potential trapping mechanisms. Bjarni, Markland and Early Tertiary shales are potential source intervals, while Bjarni Formation, Leif Member, and possible turbidite sandstones are prospective reservoirs.

and Markland shales, as well as organic rich Paleocene shales, which are interpreted to become mature seaward (Beaumont and Issler, 1987). Potential reservoirs include Bjarni Formation sandstones, as well as Leif Member or turbidite sandstones. Structural traps include complex fault blocks within the postrift sequence and drape of syn- and post-rift sediments over a basement horst. The presence of adequate reservoir is a major risk

factor at this location, and the water depth increases the risks associated with drilling the structure. The Cartwright Formation, which contains Gudrid Member sandstones, is not interpreted in this area, and the Bjarni Formation is thin over the basement high. Additionally, the Leif Member sequence could not be traced to this location due to its weak seismic marker. Deepwater areas throughout the entire Hopedale Basin may contain coarse clastic sequences, such as submarine fan and ramp turbidite systems, as similar deepwater sequences occur in other Atlantic margin settings.

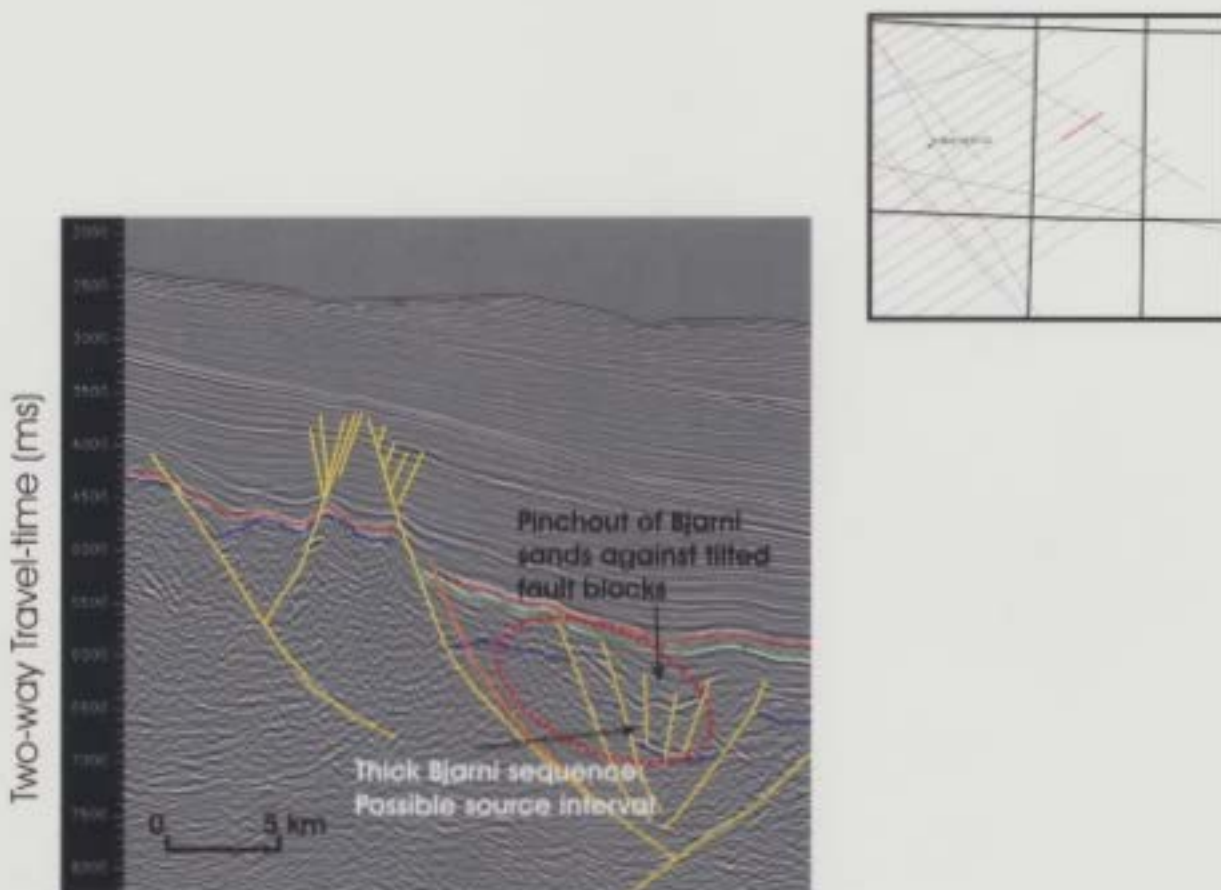


Figure 6.9. Petroleum prospect on the outer shelf southeast of the Indian Harbour well. Drape of the Bjarni Formation over a basement high forms a potential structural trap. Bjarni, Markland and Early Tertiary shales are potential source intervals, while Bjarni Formation and Leif Member sandstones are prospective reservoirs.

Figure 6.9 depicts synrift Bjarni Formation sediments overlapping the faulted prerift basement. The faulted Bjarni sequence, which contains both source and reservoir intervals, is draped over a basement high feature adjacent to the slope break. The Kenamu and Markland shales are other potential sources, and Leif Member and equivalent deepwater sandstones and prerift carbonates constitute potential secondary reservoirs at this location.

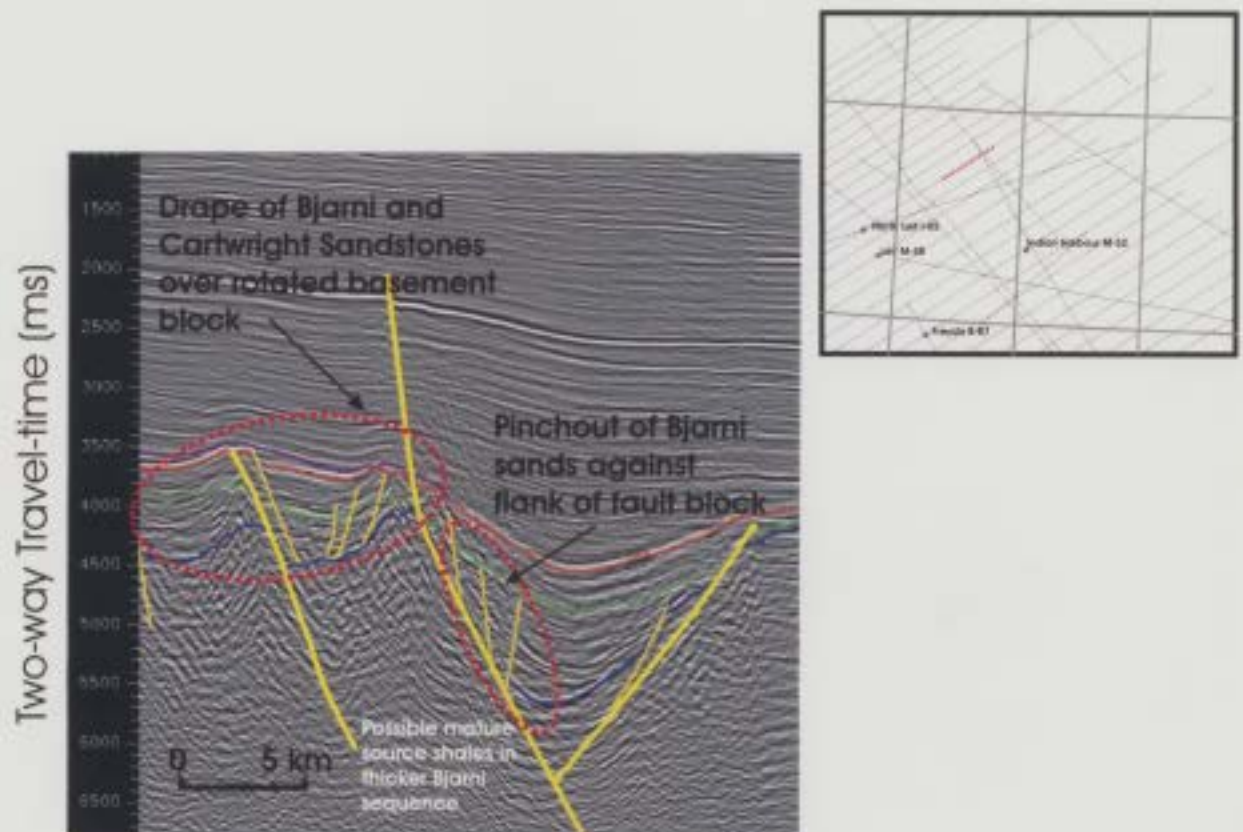


Figure 6.10. Petroleum prospect on the outer shelf northeast of the North Leif I-05 well. Drape and pinchout of the Bjarni Formation over rotated basement blocks are potential structural traps. The Bjarni, Markland and Early Tertiary shales are potential source intervals, while Bjarni Formation and Leif Member sandstones are prospective reservoirs. Paleozoic carbonate reservoirs within the prerift basement are also targets in this area. The Bjarni shales, which are marginally mature in the North Leif I-05 well, may be mature enough for significant hydrocarbon generation at this location.

Figure 6.10, located northeast of the North Leif I-05 well, shows faulted synrift Bjarni sediments over a rotated basement block and a thicker Bjarni interval abutting against an extensional fault. Potential traps include the drape of the Bjarni sands over the rotated basement block and pinch out of Bjarni sandstones against the fault or prerift basement. Additionally, drape of Leif Member equivalent sandstones or accumulations within Paleozoic carbonates are secondary targets at this location. The Bjarni shales are marginally mature in the North Leif I-05 well, and may be mature enough to generate significant hydrocarbons at this location. Other potential sources include Markland and Paleocene and Eocene shales.

6.3 West Orphan Basin Petroleum System

There were no major hydrocarbon shows or source intervals encountered during a 1974-1985 exploration cycle in the Orphan Basin. However, several boreholes encountered porous Early Cretaceous sandstones, Paleozoic limestones and sandstones and Tertiary sandstones, which are potential reservoirs in this area (Bell and Campbell, 1990; Enachescu et al., 2005).

In chapter two, both Jeanne d'Arc and Labrador stratigraphy were compared in the Orphan Basin using ties from the Hare Bay E-21 borehole. The Kenamu Formation shales were mapped throughout the northwest areas of the Orphan Basin, indicating the presence of a stratigraphy similar to that encountered on the Labrador Shelf. Towards the southeast, the Kenamu sequence thins and downlaps onto the Base Tertiary unconformity and the synrift sequence thickens and becomes more comparable to that of the Jeanne

d'Arc Basin (Enachescu et al., 2005). Consequently, the Orphan Basin is predicted to be mostly gas prone in the west and primarily oil prone towards the east (Enachescu et al., 2005).

6.3.1 Reservoir Potential

Reservoir potential in the Orphan Basin was initially thought to be limited by a primarily distal clastic environment in the postrift section, and truncation of Mesozoic

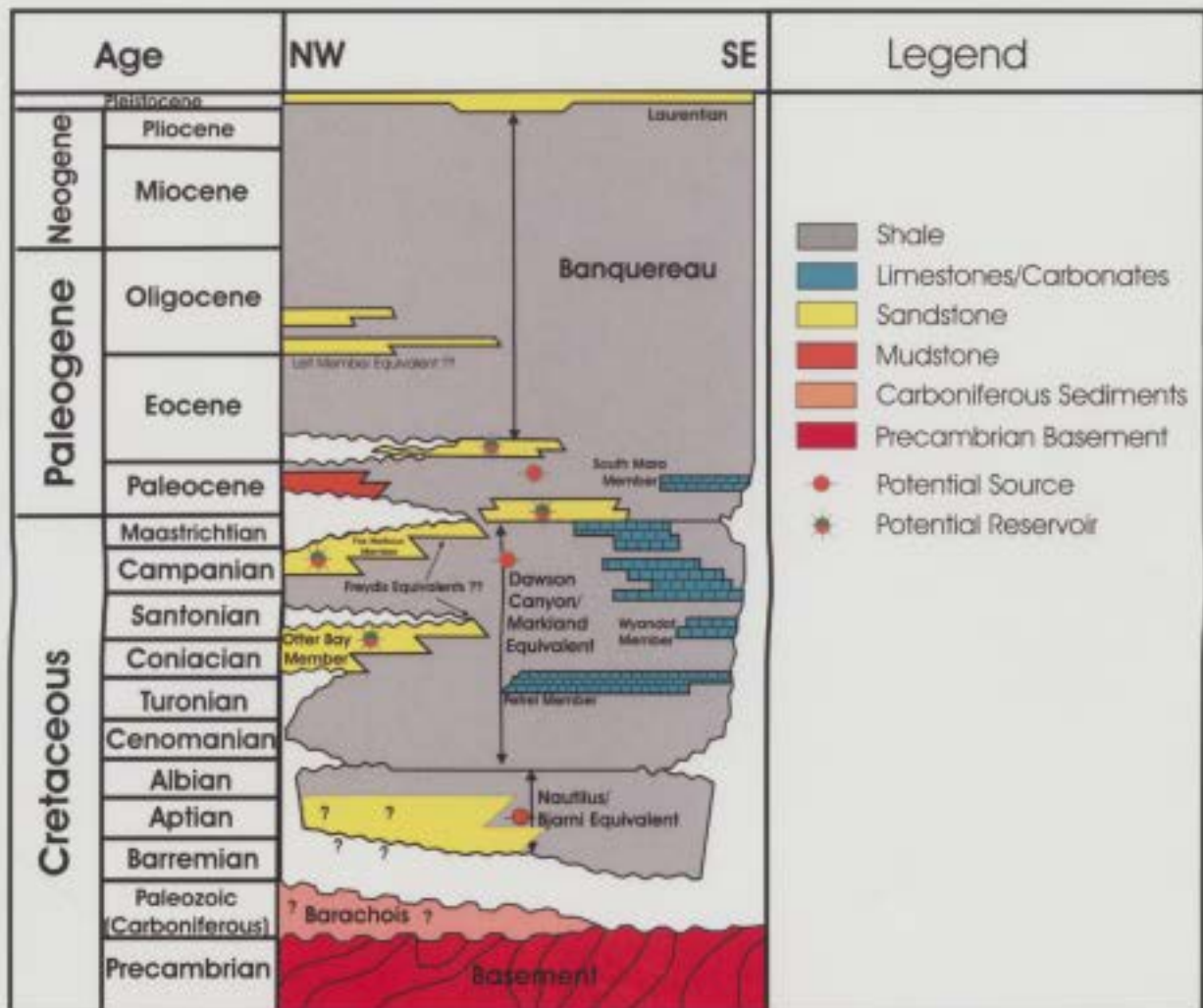


Figure 6.10. Lithostratigraphy for the West Orphan Basin, with potential source and reservoir units indicated. Modified from C-NLOPB, 2004.

and older reservoirs by erosion (Bell and Campbell, 1990). However, good to excellent sandstone reservoirs were encountered in the Blue H-28, Bonavista C-99 and Linnet E-63 wells. Seismic character and amplitude variation of more recent seismic data also suggests that coarse siliciclastic sediments are present in both the syn- and post-rift sequences in the basin. These sediments likely originated from the Bonavista platform and South Labrador area, as well as from intrabasinal ridges (Enachescu et al., 2005). Figure 6.6 shows the lithostratigraphy for the West Orphan Basin and indicates potential source and reservoir sequences. Deposition of sediments from the Bonavista platform during the postrift phase may have resulted in basin margin and basin floor siliciclastic fans of Late Cretaceous and Tertiary age (Enachescu et al., 2005). The distribution of the syn- and early post-rift sediments in the study area supports sediment sourcing from the Bonavista Platform and South Labrador areas, as well as from intrabasinal ridges. Figure 6.11 indicates the distribution of synrift sediments within the West Orphan Basin. This sequence reaches a maximum thickness of 5.5 km along the Bonavista Fault Zone and in half graben structures in the central part of the basin. Figure 6.12 is a map of the early postrift Late Cretaceous sequence, which is bounded by the top synrift and Base Tertiary unconformities. This sequence reaches a maximum thickness of 2.8 km along the southeast and northeast basin margins adjacent to the Bonavista Fault zone. Small, localized thicker intervals also occur in the central and eastern areas of the basin.

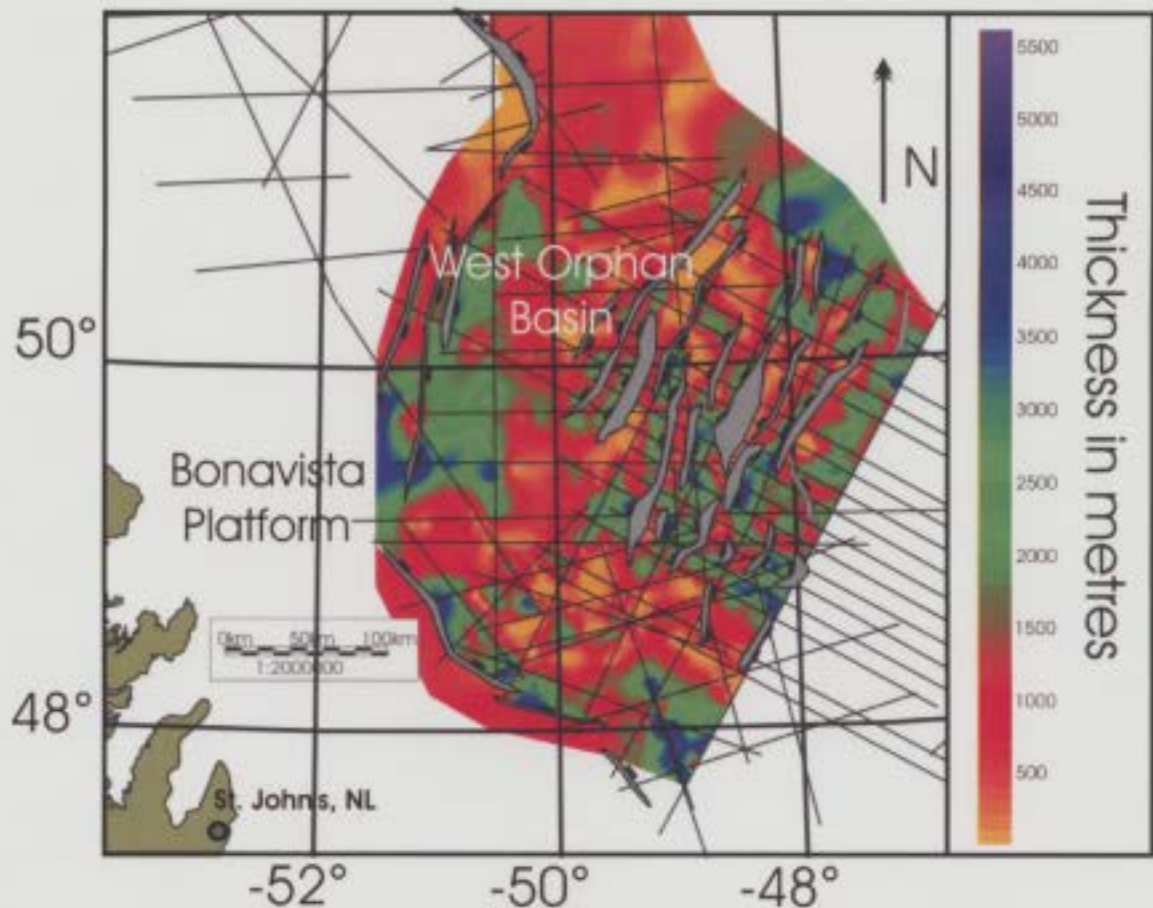


Figure 6.11. Isopach map of the West Orphan Basin synrift sequence, which likely contains reservoir and source intervals equivalent to the Bjarni Formation sandstones and shales. The thickest, and most prospective, sequences are located adjacent to the Bonavista platform and in half graben structures towards the central and eastern part of the basin.

6.3.2. Source Potential and Maturation

A hydrocarbon accumulation has yet to be identified in the Orphan Basin, but there are several prospective hydrocarbon generating intervals. These include organic rich Early Tertiary shales, which are also encountered in the Jeanne d'Arc and Hopedale basins, Early Cretaceous Bjarni equivalent shales, Late Cretaceous Markland equivalent shales, and possible Jurassic Kimmeridgian shales deposited in deep half graben

structures (Fagan and Atkinson, 2000; Bell and Campbell, 1990; Issler and Beaumont, 1987; Enachescu et al., 2005).

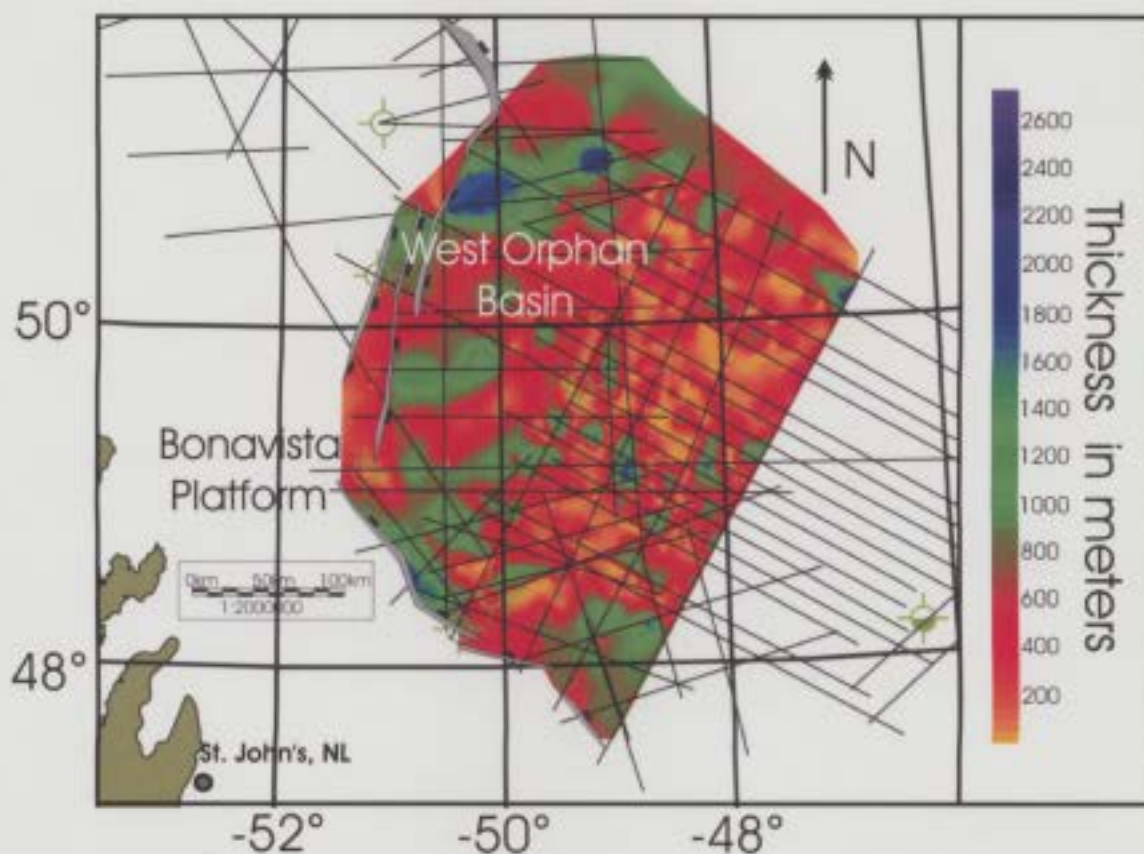


Figure 6.12. Isopach map of the West Orphan Basin Late Cretaceous postrift sequence, which likely contains sandstone intervals sourced from the Bonavista Platform or intrabasin ridges.

In the Jeanne d'Arc Basin, Early Tertiary shales are immature but are predicted to become mature in areas with a thicker postrift section, such as the West Orphan Basin (Fagan and Atkinson, 2000). Thermal modeling also predicts maturation of Early Tertiary shales towards the outer Labrador Shelf and slope, where thicker postrift

sequences exist (Issler and Beaumont, 1987). The geothermal gradient measured in the West Orphan Basin boreholes are lower than that encountered on the Labrador shelf,

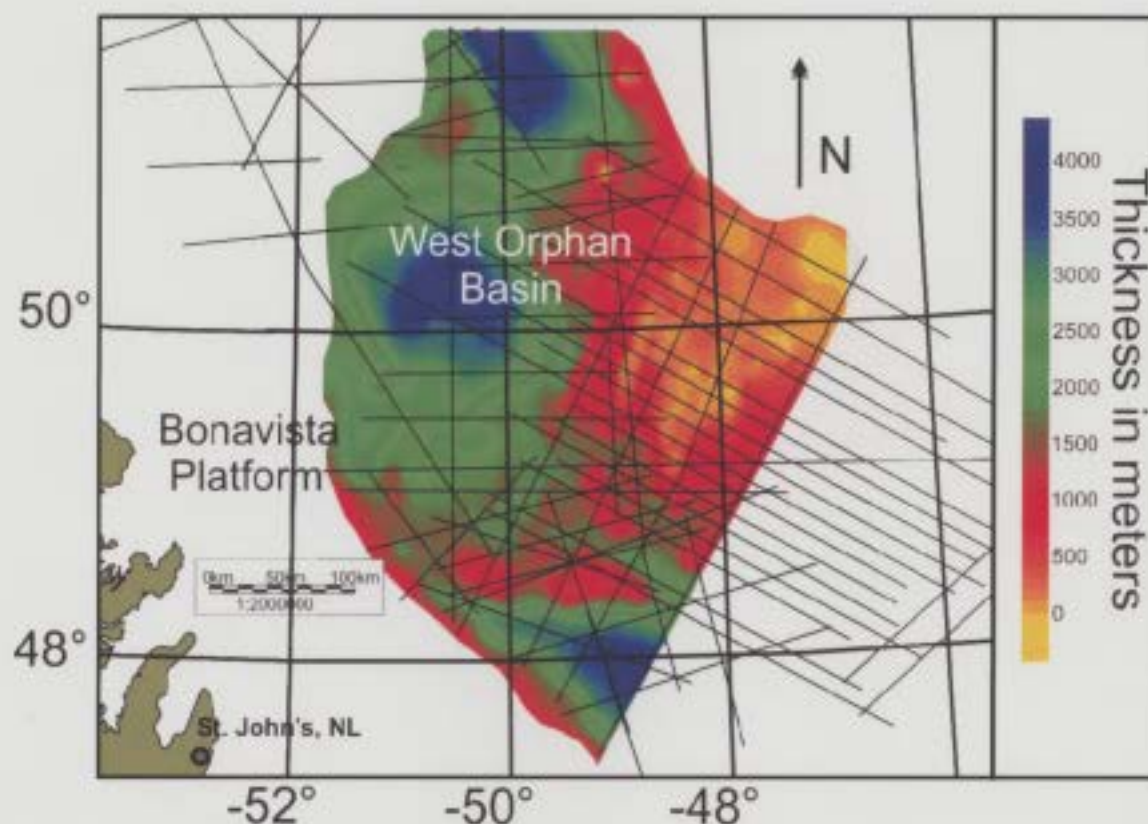


Figure 6.13. Map of the West Orphan Basin Early Tertiary postrift sequence, which contains organic rich Tertiary marine shales. These shales are thickest in the West Orphan Basin, and comparisons to Figure 6.14 indicate that the thickest sequences correspond with thick sequences of mid-to-Late Tertiary sediments, suggesting that the Early Tertiary shales are buried at sufficient depths for maturation.

ranging from 2.02 °C/100m to 2.94 °C/100m. Consequently, the oil window and threshold for wet gas generation may be deeper than that predicted for the Labrador Shelf.

The Early Tertiary sequence, bounded by the Base Tertiary and Postrift 1 unconformities, was mapped throughout the West Orphan Basin area (Figure 6.13). The map indicates the sequence reaches a maximum thickness of 4.5 km in the central West Orphan Basin and along the slope break adjacent to the Cartwright Arch. These areas

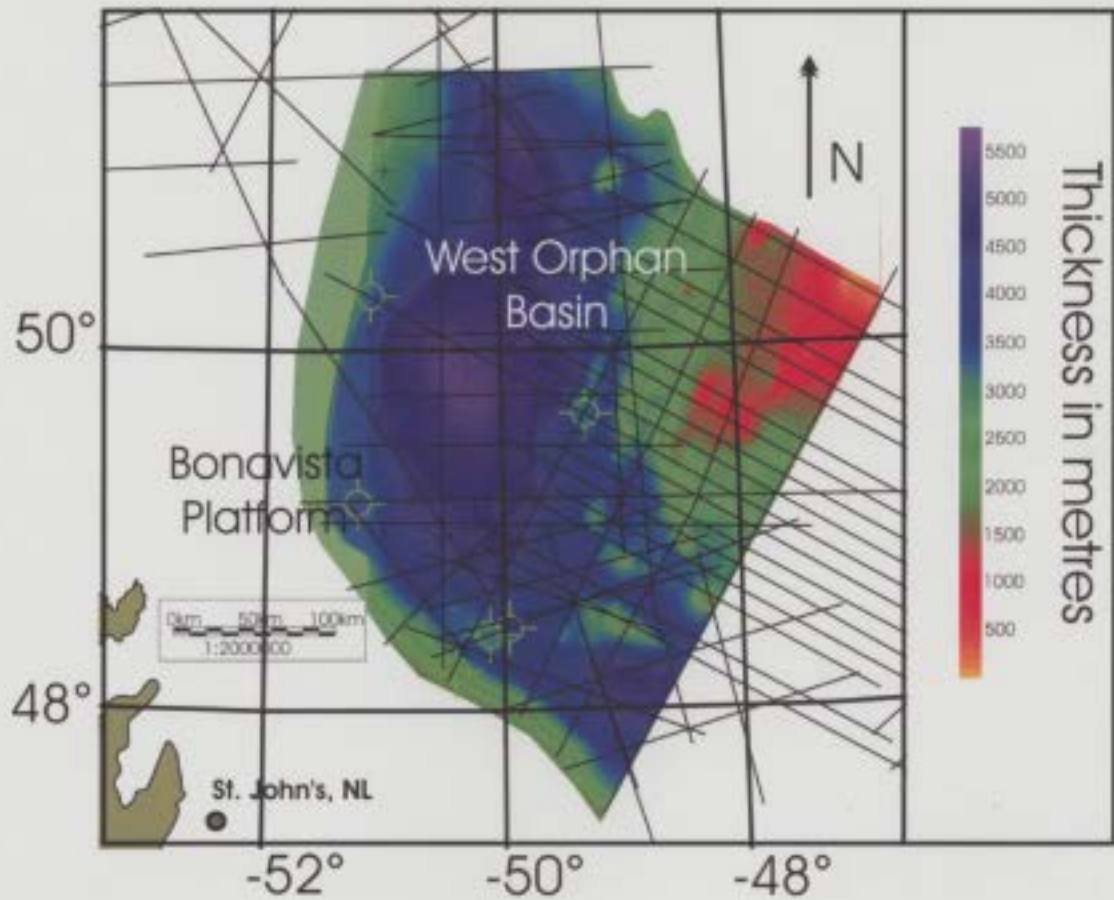


Figure 6.14. Isopach map of the mid- to Late Tertiary postrift sequence. Comparisons to Figure 6.13 indicate that the thickest intervals correspond with thick sequences of Early Tertiary sediments, suggesting that the Early Tertiary shales are buried at sufficient depths for maturation.

correspond with 5.5 km thick sequences of mid-to-Late Tertiary sediments (Figure 6.14), which suggests that the Early Tertiary shales are buried at a sufficient depth for maturation.

Two potential source intervals were encountered in the Blue H-28 borehole (Bell and Campbell, 1990; Fagan and Atkinson, 2000). These include a Cretaceous-Eocene section, with a Total Organic Carbon (TOC) exceeding 1%, and Late Cretaceous shales with a TOC greater than 2.5%. While these intervals are immature in the well, maturation levels may be greater in deeper areas of the basin, or along the flanks of basement fault blocks (Bell and Campbell). Another potential source includes the Markland shales, which are likely present within the Cretaceous section in the northwest West Orphan Basin (Fagan and Atkinson, 2000).

Towards the East Orphan Basin, where a thicker Mesozoic section containing Early Cretaceous and Jurassic sequences is more likely, the oil source Egret Member of the Rankin Formation may occur. The southern part of the Orphan Basin is in communication with the Jeanne d'Arc and Flemish Pass basins, as several troughs containing Jurassic sequences are connected across the Cumberland Fault Zone (Enachescu et al., 2005). As well, the Panther P-52, Baccalieu I-78, and Mizzen L-11 wells encountered thick Kimmeridgian source rocks, located up-dip of, and connecting with, the Orphan Basin (Enachescu et al., 2005). Analysis of oils from the Jeanne d'Arc, Flemish Pass, and Porcupine basins show geochemical similarity and confirm a geotectonic connection between the conjugate margin basins.

6.3.3. Petroleum Entrapment

Structural trapping mechanisms for the Orphan Basin include preserved prerift reservoirs located on the crests and flanks of large rotated basement blocks, drape of

Cretaceous and Tertiary sandstones over basement horsts and tilted fault blocks, roll-over anticlines and stratigraphic pinchouts of Cretaceous sandstones on the flanks of basement

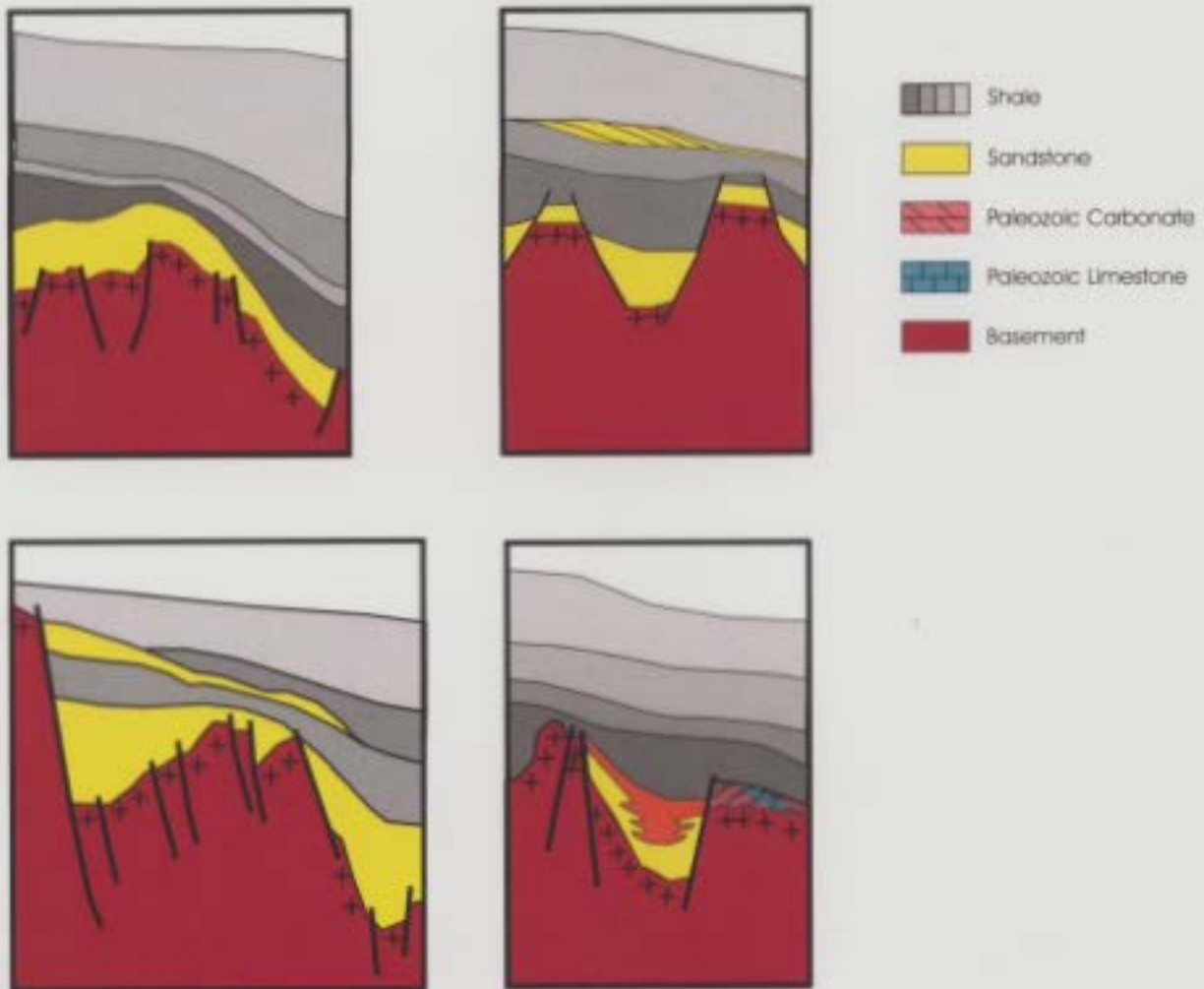


Figure 6.15. Petroleum traps targeted in the West Orphan Basin, which include: drape of synrift Cretaceous sandstones over basement horsts (top and bottom left), pinchout of synrift Cretaceous sandstones against tilted fault blocks (bottom right), drape of lower Tertiary sandstones above basement horsts and Tertiary prograding sedimentary wedges (top right and bottom left), and preserved Paleozoic reservoirs on rotated basement blocks (bottom right).

highs (Bell and Campbell, 1990; Fagan and Atkinson, 2000). As well, Late Cretaceous and Early Tertiary prograding wedges, basin margin and floor fans, and channel sandstones are identified by reflection seismic data. These features form stratigraphic traps in this area (Enachescu et al., 2005; Fagan and Atkinson; 2000).

6.3.4 Prospectivity

The prospectivity of the West Orphan Basin is less certain, as no hydrocarbons have been encountered to date. However, its juxtaposition between the gas prone Hopedale Basin and petroliferous Jeanne d'Arc Basin suggests that considerable hydrocarbon potential may exist. Maps of the prospective source and reservoir sequences were compared to identify prospective areas (Figure 6.16). Several target areas identified from these maps are shown on several seismic profiles (Figures 6.17-6.19).

Figure 6.17 is located in the central West Orphan Basin and depicts several potential hydrocarbon plays. The thicker synrift sequence is interpreted as Early Cretaceous sandstones and shales equivalent to the Bjarni Formation. A more deformed sequence, interpreted to be older Mesozoic synrift or Paleozoic sediments, is draped over a rotated basement block forming a potential structural trap. Drape of the Tertiary postrift sequence, which likely contains sandstone intervals, is also evident over the rotated basement blocks. An interpreted Late Cretaceous fan, located above the top synrift marker (highlighted in yellow), is a potential stratigraphic target. Potential sources in this area include Lower Cretaceous shales (Bjarni equivalent), Late Cretaceous shales (Markland equivalent), and Early Tertiary marine shales.

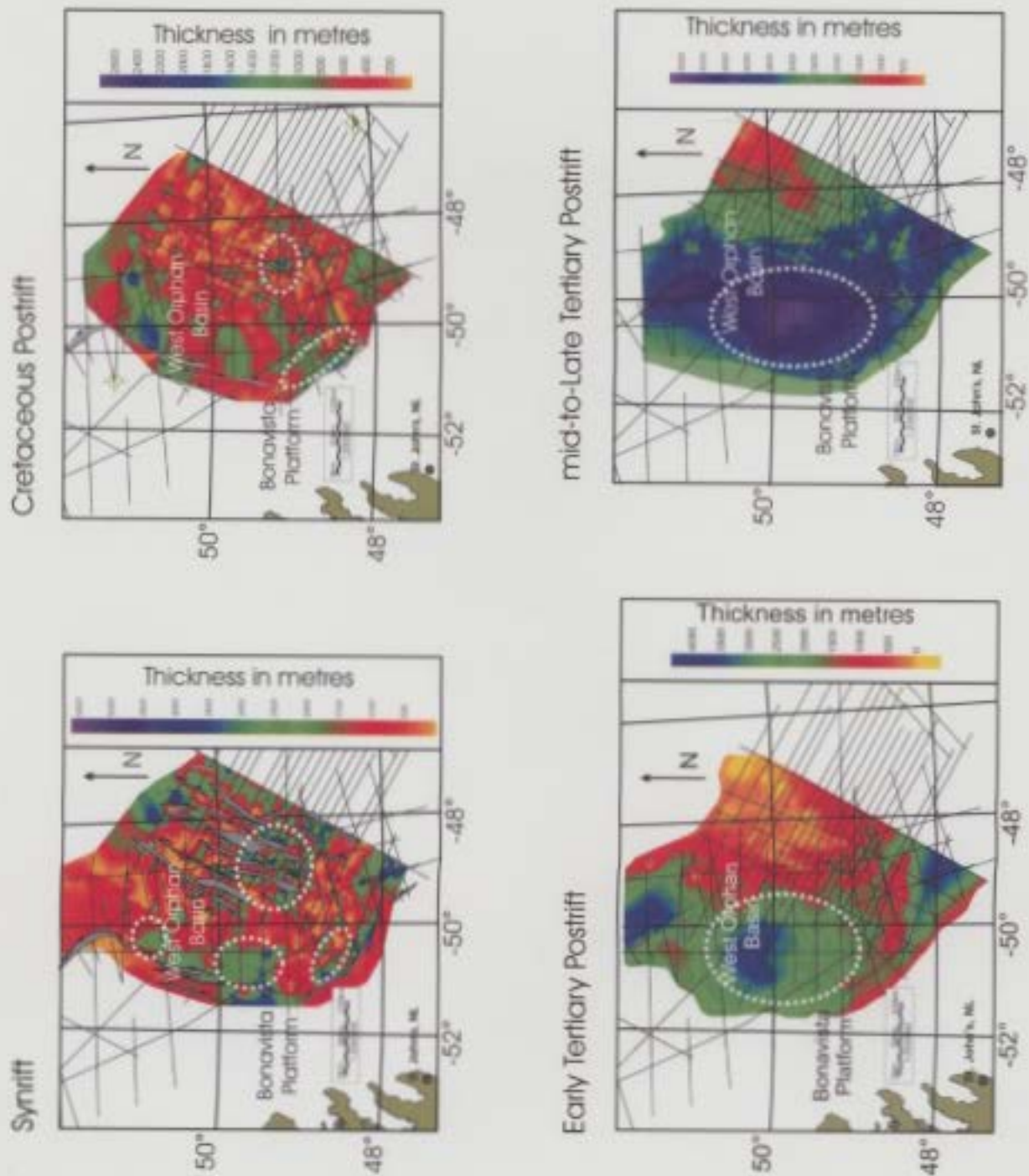


Figure 6.16. Comparison of mapped isopach intervals in the West Orphan Basin. The synrift and Early postrift sediments (bottom right and upper left, respectively) are prospective reservoir bearing intervals, with potential targets indicated by the dashed white circles. Maps of the Early Tertiary and overlying sedimentary cover (bottom right and upper right, respectively) suggest that the western area of the basin contains thick sequences of Early Tertiary marine organic rich shales that may be buried at sufficient depths for maturation.

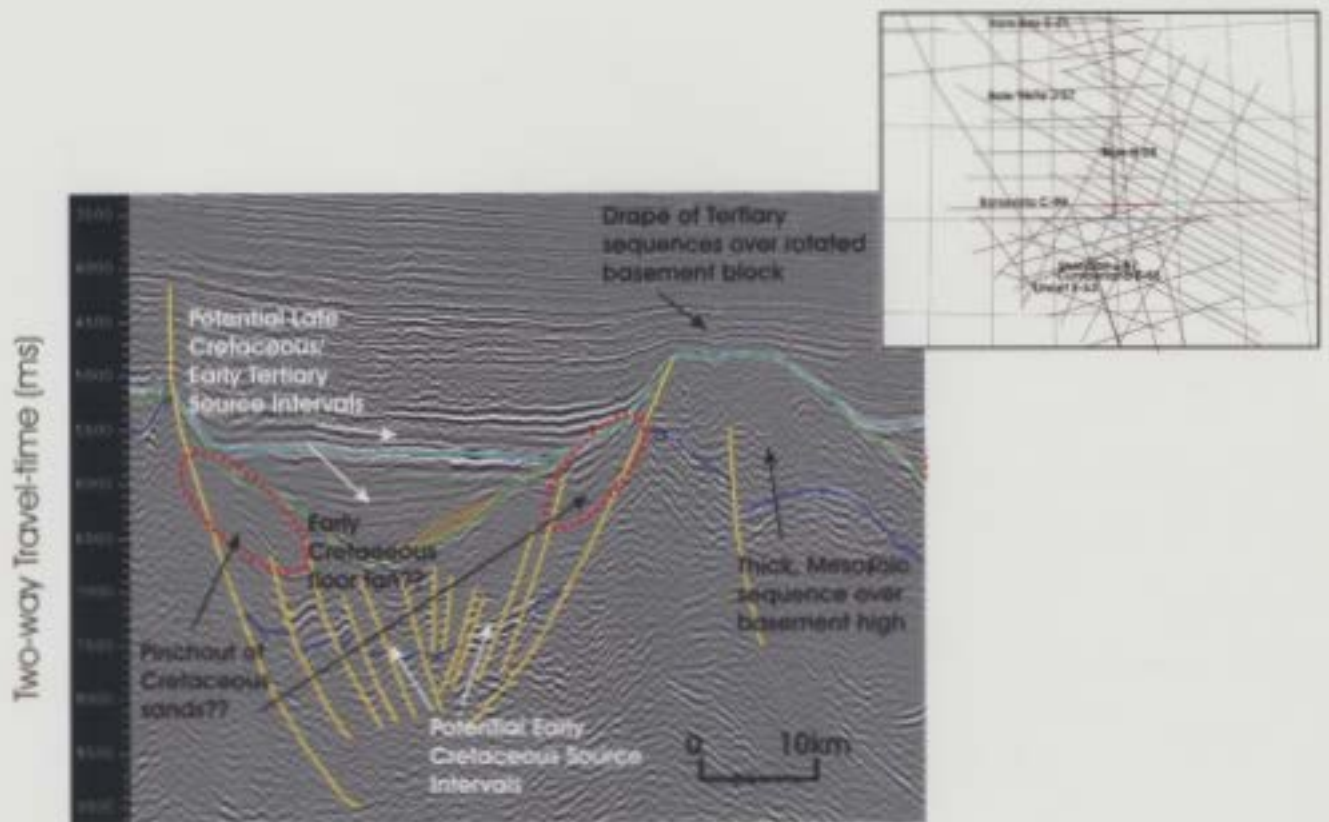


Figure 6.17. Prospective plays in the central West Orphan Basin. Major targets include synrift Early Cretaceous sandstones and older Mesozoic or prift Paleozoic sandstones or carbonates, an early postrift Late Cretaceous fan, as well as drape of Tertiary postrift sandstones over rotated basement blocks. Potential source intervals include Early Cretaceous Bjarni equivalent shales, Late Cretaceous Markland equivalent shales or early Tertiary marine shales.

Figure 6.18 depicts drape of syn- and post-rift sediments over elevated prift basement in the West Orphan Basin. Comparisons of this area to the South Hopedale Basin show stratigraphic similarity. The synrift sequence is interpreted as equivalent to the Bjarni Formation, which is a proven source and reservoir on the Labrador Shelf. Drape of the sequence over elevated pre-rift basement and pinchout of sandstone intervals against the extensional faults are potential traps. Additionally, the interval

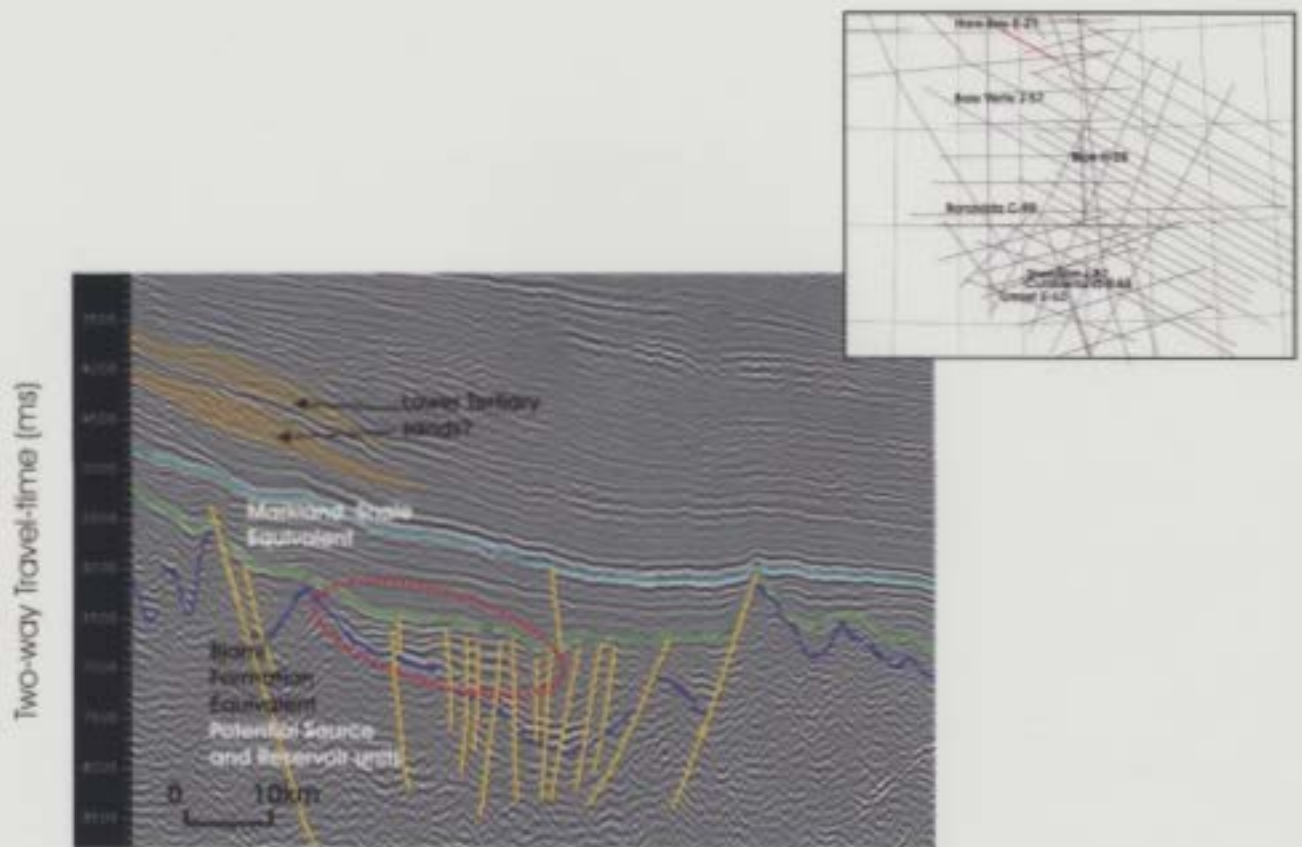


Figure 6.18. Prospective plays in the northwest West Orphan Basin. Major targets include drape of synrift Early Cretaceous sandstones over prerift basement, and Tertiary prograding wedges over a prerift basement high. Potential source intervals include Early Cretaceous Bjarni equivalent shales, Late Cretaceous Markland equivalent shales or early Tertiary marine shales.

between the top synrift and Base Tertiary markers is equivalent to the Markland shale, which is another proven source on the Labrador Shelf. To the west, a second dashed circle indicates prograding sediments within the lower postrift sequence, which is interpreted to contain sandstone reservoir and marine shale source intervals. Figure 6.19 depicts a large rollover anticline located in the central part of the West Orphan Basin. The thick synrift sequence at this location suggests that older Jurassic

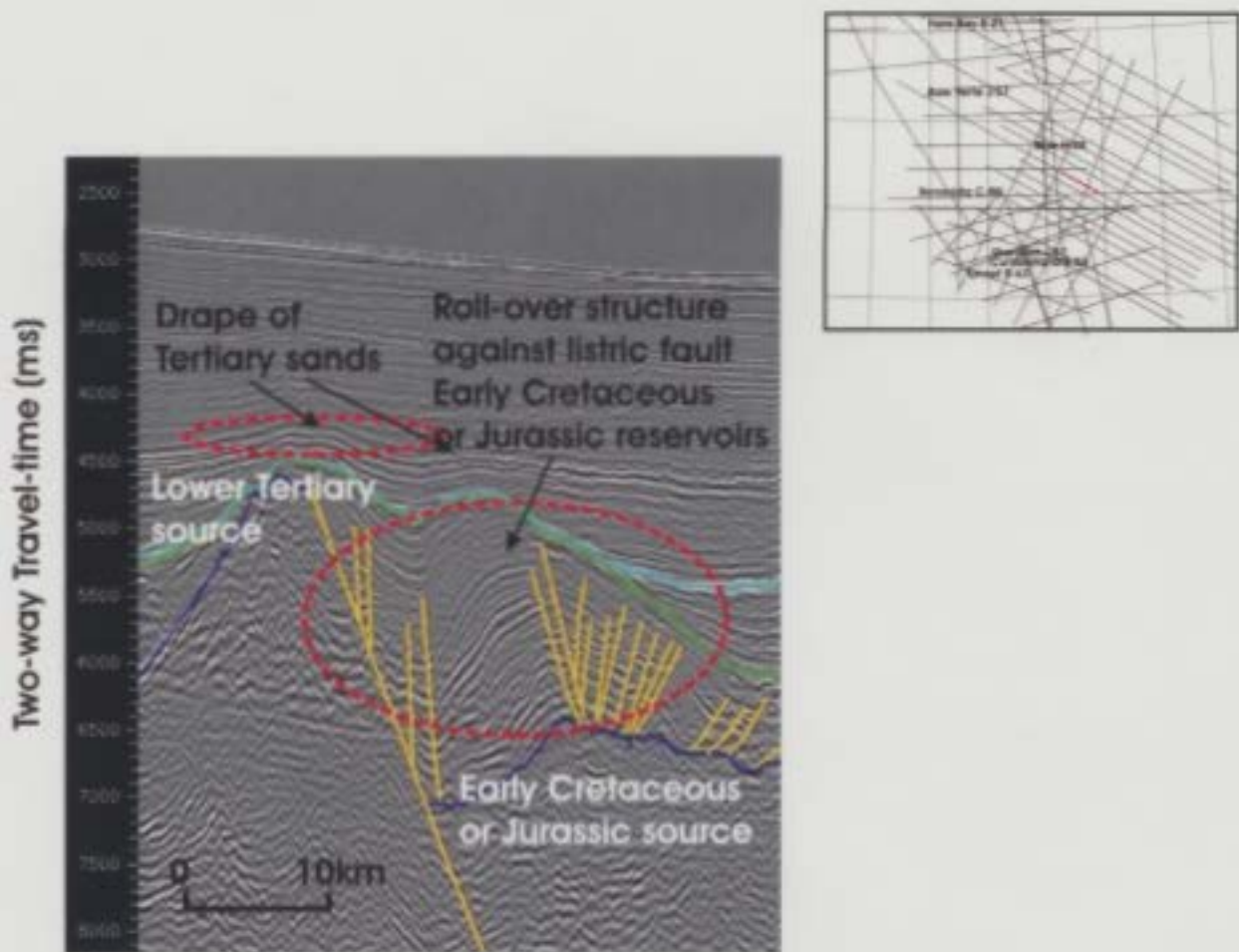


Figure 6.19. Roll-over anticline in the central West Orphan Basin. The rollover structure is interpreted to contain Early Cretaceous and possible Jurassic sandstone reservoirs sourced by Early Cretaceous Bjarni Equivalent or possible Kimmeridgian Jurassic shales. Secondary targets include drape of Tertiary sandstones over the structure, which could be sourced by Late Cretaceous Markland equivalent shales.

sediments may be present. Potential reservoirs include Early Cretaceous and Late Jurassic sandstones, as well as Early Tertiary sandstones draped over the anticline structure.

Source potential includes Kimmeridgian and Early Cretaceous Bjarni equivalent synrift shales, and postrift Late Cretaceous Markland equivalent shales.

6.4 Summary

Both the South Hopedale and West Orphan basins have considerable petroleum potential. The Hopedale Basin has a proven petroleum system, and mapping of the synrift and predrift sequences indicate that the Bjarni and Markland formation thin seawards but extend out past the shelf break and into deeper water. The areal extent of these formations suggests that petroleum potential exists on the outer shelf and slope, as marginally mature sediments on the inner shelf are predicted to become more mature seawards. Major risk factors include the deepwater location of these targets, and whether adequate thicknesses of sandstone reservoirs exist in these areas.

The West Orphan Basin does not have a proven petroleum system, but regional mapping suggests that its stratigraphy similar to that of the Labrador Shelf. This implies that significant gas potential exists in this area. Additionally, the synrift sequence thickens to the south and east, suggesting that thicker intervals of Early Cretaceous Bjarni equivalent sandstones and shales as well as Upper Jurassic sandstones and Kimmeridgian source rocks may exist.

7.0 Conclusions

The main objectives for this study were to interpret and compare the structure and stratigraphy of the South Hopedale and West Orphan basins, relate these to the evolution of the margin, and identify areas with petroleum prospectivity. These objectives were attained through 2D reflection seismic interpretation, constrained by borehole and potential fields data, and through balanced section restoration and backstripping techniques. The intervening prerift Cartwright Arch and St. Anthony Basin were also examined and interpreted to gain a better understanding of the structure and tectonic evolution of the entire Northeast Newfoundland and South Labrador shelf regions.

Numerous similarities and differences between the South Hopedale and West Orphan basins are apparent from the 2D reflection seismic interpretation. Both areas have thick postrift intervals containing similar seismic markers and sequences. The South Hopedale postrift sequence contains an extensional fault system over the slope break, which is complimented downslope by development of compressional features. Similar, thick postrift sequences were observed in the West Orphan Basin, but development of complex fault systems is not evident from the 2D seismic reflection data. In the South Hopedale Basin, the synrift sequence was mapped further onto the outer shelf and into the slope and deep water areas. The mapped synrift sequence in the West Orphan Basin is seismically comparable to that encountered in the Hopedale Basin, but thickens and becomes structurally complex towards the east and south.

While the Hopedale and West Orphan Basins appear to have similar stratigraphy, there are major differences in the orientation and areal extension of the rift systems in each area. The differences in fault trend between the Labrador Shelf and Orphan Basin regions can be attributed to the differences in original direction of rifting, and also locally to pre-existing structural fabrics. Comparisons of the South Hopedale and West Orphan basins with analogue models of orthogonal and oblique rifting indicate that the Hopedale rift system is predominantly an orthogonal rift, while the Orphan rift system is more characteristic of an oblique rift. Additionally, the South Hopedale Basin appears to contain hard-linked transfer fault systems, while more complex soft-linked accommodation zones are interpreted in the Orphan Basin.

The tectonic evolution and extension for each basin was analyzed through balanced section restoration, backstripping, and fault heave measurement. A combination of backstripping and section balancing techniques were used to estimate the paleobathymetry and extension. The extension values obtained from this technique were significantly lower than expected, particularly in the Orphan Basin. Consequently, the extension was also estimated by measuring the fault heaves across the top prerift horizon. Comparisons of these values to those obtained from the backstripped section restorations show similar results for the Labrador Shelf but higher extension estimates were obtained in the West Orphan Basin. To investigate if the discrepancy was a function of the Airy isostatic correction, the Orphan Basin profiles were restored without application of an isostatic adjustment. The obtained values from the uncorrected restorations were comparable to those obtained from fault heave measurement, which suggests that the

Airy correction is not appropriate in this region. The complex faulting and basement topography present in the east West Orphan Basin suggests that a 2D flexural isostatic correction may be more applicable. The software limitations, combined with limited access to velocity and paleobathymetry indicators, affected the results obtained from the backstripping and section balancing techniques.

Overall, the obtained extension values from the fault heave measurement were lower than those predicted from two layer lithospheric stretching models, ranging from $\beta=1.02$ to $\beta=1.06$ for the Hopedale Basin and $\beta=1.12$ to $\beta=1.29$ for the West Orphan Basin. The lower values can be explained by decoupling of the upper and lower crusts, with greater extension occurring in the lower crust, and also by the limited lengths of the profiles and the presence of seismically unmappable extensional faults. Anomalously thin synrift sequences and thick postrift sequences, along with significant postrift onlap in areas devoid of Mesozoic synrift sediments, were observed over the entire margin. These high post-to syn-rift ratios are interpreted to result from increased mantle stretching, or removal of synrift sediments through erosion.

The extension values obtained from fault heave measurement and uncorrected balanced section restoration do show correlation between the amount of extension and variations in syn- and post-rift thicknesses. The Labrador Shelf has lower estimates of extension and higher to syn-to post-rift thickness ratios. A greater range of overall higher extension values were obtained for the West Orphan Basin, which has a greater variation of post- and syn-rift thicknesses across several profiles.

Both the South Hopedale and West Orphan basins have significant petroleum potential. The Hopedale Basin has a proven petroleum system, and current mapping suggests that the reservoir and source bearing synrift sequence extends onto the outershelf and into deep water areas. A significant gas discovery is located on the inner shelf, where source intervals are immature to marginally mature. This discovery suggests that greater potential likely exists on the outer shelf and slope, where source intervals are predicted to be more mature and several prospective structural targets are identified. The Orphan Basin does not have a proven petroleum system, but mapping indicates that similar stratigraphy to the Labrador Shelf is present in the northwest part of the basin. To the east and south, the stratigraphy becomes more comparable to the oil prolific Jeanne d'Arc Basin. Consequently, the Orphan Basin has considerable petroleum potential and numerous potential structural and stratigraphic targets are identified in the area.

The outer shelf and deep water areas of the Hopedale Basin, and the deeper sections of the West Orphan Basin, contain complex structural features and thick sedimentary sequences. Exploratory drilling in these areas would further constrain the seismic interpretation and relate the seismic and stratigraphic sequences to those encountered on the inner Labrador Shelf and in the Jeanne d'Arc Basin. Additional work on the margin should also include acquisition of more recent seismic reflection data across the Cartwright Arch, and adjacent deepwater areas, to further define the stratigraphic relationships between the South Hopedale and West Orphan basins. Additionally, a more detailed structural analysis using a closer spaced 3D seismic

reflection grid would permit a more robust structural model for comparison with analogue rift models, and for analysis of extension through balanced section restorations.

References

- Balkwill, H.R., McMillan, N.J., Maclean, B., Williams, G.L., and Srivastava, S.P., 1990, Geology of the Labrador Shelf, Baffin Bay, and Davis Strait, Chapter 7 in Geology of the Continental Margins of Eastern Canada, M.J. Keen and G.L. Williams (eds.); Geological Survey of Canada, Geology of Canada, no.2., pp.293-348.
- Balkwill, H.R., 1987, Labrador Basin: Structural and stratigraphic style; in Sedimentary Basins and Basin Forming Mechanisms, C. Beaumont and A.J. Tankard (ed.); Canadian Society of Petroleum Geologists, Memoir 12, pp. 17-43.
- Bell, J.S. (coordinator), 1989, East Coast Atlas Basin Atlas Series, Labrador Sea. Geological Survey of Canada, Atlantic Geoscience Centre, Dartmouth, N.S.
- Bell, J.S., and Cambell, G.R, Petroleum Resources, Chapter 12 in Chapter 7 in Geology of the Continental Margins of Eastern Canada, M.J. Keen and G.L. Williams (eds.); Geological Survey of Canada, Geology of Canada, no.2., pp. 677-720.

- Bell, J.S., and Howie, R.D., 1990, Paleozoic geology; Chapter 4 in Geology of the Continental Margins of Eastern Canada, M.J. Keen and G.L. Williams (ed.); Geological Survey of Canada, Geology of Canada, no.2., pp.141-165.
- Boggs, Sam Jr., 2001, Principles of Sedimentology and Stratigraphy, 3rd edition, Prentice Hall Publishing, Upper Saddle River, New Jersey, 717 p.
- Bojesen-Koefoed, J.A., and Nytoft H.P. and Christiansen, F.G.,2004, Age of oils in West Greenland: was there a Mesozoic seaway between Greenland and Canada? Geological Survey of Denmark and Greenland, Bulletin 4, pp. 49-52.
- Bradley, D.C., 1982, Subsidence in Late Paleozoic basins in the Northern Appalachians, Tectonics, v. 1, pp.107-123.
- Bulnes, M., and McClay, K., 1999, Benefits and limitations of different 2D algorithms used in cross-section restoration of inverted extensional faults: application to physical experiments, Tectonophysics, vol 312, pp.175-189.
- Canada-Newfoundland and Labrador Offshore Petroleum Board (C-NLOPB), 2007, Schedule of Wells: Newfoundland and Labrador Offshore area, Jeanne d'Arc Basin lithostratigraphy, Retrieved, 2007, from <http://www.cnlopb.nl.ca>

Canadian Aeromagnetic Data Base, 2007, Geoscience Data Repository, Geological Survey of Canada, Earth Sciences Sector, Natural Resources Canada, Government of Canada.

Canadian Geodetic Information System, 2007, Geoscience Data Repository, Geodetic Survey Division, Earth Sciences Sector, Natural Resources Canada, Government of Canada.

Cawood, P. A., McCausland, P.J.A., and Dunning, G.R. 2001, Opening constraints from the Laurentian margin in Newfoundland, *GSA Bulletin*, v. 113, no.4, p.443-453.

Cawood, P.A., van Gool, J.A.M., and Dunning, G.R., 1995, Collisional tectonics along the Laurentian margin of the Newfoundland Appalachians, in *Current Perspectives in the Appalachian-Caledonian orogen*, GAC Special Paper 41, pp. 283-302.

Chalmers, J.A., 1991, New evidence on the structure of the Labrador Sea/Greenland continental margin. *Journal of the Geological Society of London*, vol. 148, pp.899-908.

Chalmers, J.A., and Laursen, K.H. 1995, Labrador Sea: extent of continental crust and the timing of the start of sea floor spreading, *Marine and Petroleum Geology*, vol.12, 205-217.

Chian, D. & Loudon, K.E. 1994. The continent-ocean crustal transition across the southwest Greenland margin. *Journal of Geophysical Research*, v. 99, pp. 9117–9135.

(a) Chian, D., and Loudon, K.E., and Reid, I., 1995, Crustal structure of the Labrador Sea conjugate margin and implications for the formation of nonvolcanic continental margins, *Journal of Geophysical Research*, vol.100, no. B12, pp.24 239-24 253.

(b) Chian, D., Keen, C., Reid, I. and Loudon K.E., 1995, Evolution of nonvolcanic rifted margins of the Labrador Sea, *Geology*, v. 23, pp.589-592.

Chian D, F. Mariller, J. Hall, and G. Quinlan, 1998, An improved velocity model for the crust and upper mantle along the central mobile belt of the Newfoundland Appalachian Orogen and its offshore extension: *Canadian Journal of Earth Sciences*, vol.35 pp.1238-1251.

Coffield, D.Q., and Schamel, S., 1989, Surface expression of an accommodation zone within the Gulf of Suez rift, Egypt, *Geology*, v.17, pp.76-79.

Coffin M.F., L.M. Gahagan, L.A. Lawver, T.-Y. Lee, and E. Rosencrantz, 1992, Atlas of Mesozoic/Cenozoic reconstructions (200 Ma to Present day): Plates progress report No 1-0192, University of Texas Institute for Geophysics, Technical Report no. 122, 49p.

Colman-Sadd, S. P., and Swinden, H.S., 1984, A tectonic window in central Newfoundland: Geological evidence that the Appalachian Dunnage Zone may be allochthonous: Canadian Journal of Earth Sciences, v.21, pp. 1349-1367.

Colman-Sadd, S.P. Dunning, G.R., Dee, T., 1992, Dunnage-Gander relationships and Ordovician orogeny in central Newfoundland, a sediment provenance U/Pb age study: American Journal of Science, v. 292, pp. 317-355.

Dehler, S.A., and Keen, C.E., 1993, Effects of rifting and subsidence on the thermal evolution of sediments in Canada's east coast basins, Canadian Journal of Earth Sciences, vol.30, pp. 1782-1798.

Dewhurst, D.N., Cartwright, J.A., and Lonergan, L., 1999, The development of polygonal fault systems by syneresis of colloidal sediments, Marine and Petroleum Geology, vol.16, no. 8, pp. 793-810.

D'Lemos, R.S., Holdsworth, R.E., 1995, Samarium-neodymium isotopic characteristics of the northeastern Gander zone, Newfoundland Appalachians, in *Current Perspectives in the Appalachian-Caledonian orogen*, GAC Special Paper 41, pp 239-252.

Drummond, K.J., 1998, East coast gas-the big picture. CERI Eastern Canadian Natural Gas Conference, Halifax, Nova Scotia.

Dunning, G.R., O' Brien, S.J., Colman-Sadd, S.P., Blackwood, R.F., Dickson, W.L., O'Neill, P.P., and Krogh, T.E., 1990, Silurian orogeny in the Newfoundland Appalachians: *Journal of Geology*, v.98, pp. 895-913.

Enachescu, M.E., 1987, Tectonic and structural framework of the Northeast Newfoundland continental margin; in *Sedimentary Basins and Basin-forming mechanisms*, C. Beaumont and A.J. Tankard (eds.), Canadian Society of Petroleum Geologists, Memoir 12, pp.117-146.

Enachescu, M.E., 2002, Enigmatic basins offshore Newfoundland, *Canadian Journal of Exploration Geophysics*, vol. 28, no.1, pp.44-61.

- (a) Enachescu, M.E., 2006, Hopedale Basin: Favorable geology, advanced technology may unlock Labrador's substantial resource, *Oil and Gas Journal*, v.104, no. 23, pp 29-34.
- (b) Enachescu, M.E. 2006, Hopedale Basin, Atlantic off Labrador poised for modern exploration round: *Oil and Gas Journal*, v.104, no. 24, pp. 36-42.
- (c) Enachescu, M.E., 2006, Call for Bids NL06-2, Parcels 1 to 3, Regional Setting and Petroleum Geology Evaluation, Government of Newfoundland and Labrador, Department of Natural Resources, pp. 1-55.

Enachescu, M.E., Einarsson, P., Feir, A., 2007, Extent of sedimentary basins and oceanic crust domain in the northern Labrador Sea, CSPG Gussow Geoscience Conference, Banff, Alberta.

Enachescu, M.E., Kearsey, S., Hardy, V., Sibuet, J., Hogg, J., Srivastava, S.A., Fagan, A., Thompson, T., and Ferguson, R., 2005, Evolution and petroleum potential of Orphan Basin, Offshore Newfoundland, and its relation to the movement and rotation of Flemish Cap based on plate kinematics of the North Atlantic, 25th Annual Bob F. Perkins Research Conference: Petroleum Systems of Divergent Continental Margin Basins.

Enachescu, M.E., and Fagan, A., 2004, Newfoundland and Labrador Call for Bids NF04-01: Government of Newfoundland and Labrador, Department of Natural Resources, 35p, 20 fig, Retrieved from http://www.gov.nl.ca/mines&en/oil/call_for_bids_nf04_01.stm.

Fagan A., and Atkinson, I., 2000, Sedimentary basins and hydrocarbon potential of Newfoundland and Labrador, Report 2000-01, Department of Mines and Energy, Energy Branch, Government of Newfoundland and Labrador, 71 p.

Fowler, M.G., Stasiuk, L.D., and Avery, M., 2005, Potential petroleum systems in the Labrador Shelf and Baffin Bay areas, offshore eastern Canada, abs. GAC/MAC/CSPG/CSSS Conference, Halifax, NS. <http://www.gac.ca/ANNMEET/2005Abstracts.html>

Funck, T., Loudon, K.E., and Reid, I., 2001, Crustal structure of the Grenville Province in southeastern Labrador from refraction seismic data: evidence for a high-velocity lower crustal wedge, Canadian Journal of Earth Sciences, vol. 38, pp. 1463-1478.

Gawthorpe, R.L., and Hurst, J.M., 1993, Transfer zones in extensional basins: their structural style and influence on drainage development and stratigraphy, Journal of the Geological Society, London, vol. 150, pp.1137-1152.

Gibbs, A.D., 1984, Structural evolution of basin margins, *Journal of the Geological Society*, London, 141, 609-620.

Gibbs, A.D., 1989, Structural styles of basin formation, *in* *Extensional Tectonics of the North Atlantic Margins*, Tankard, A.J., and Balkwill, H.R. (eds), *American Association of Petroleum Geologists Memoir 46*, pp.81-93.

Government of Newfoundland and Labrador, Department of Mines and Energy, Offshore Petroleum maps, Significant discoveries offshore Labrador. Retrieved in 2007 from: <http://www.nr.gov.nl.ca/mines&en/maps/offshore/SDOL.pdf>

Grant, A.C., and McAlpine K. D., 1990, The continental margin around Newfoundland; Chapter 6 in *Geology of the continental margin or Eastern Canada*. M.J. Keen and G.L. Williams (ed.); Geological Survey of Canada, *Geology of Canada*, no.2., pp.239-292.

Hall, J., 2008, Pers. Comm.

Hall, J., Langdon, G., Roberts, B., Hawkins, D., Fagan, A., Knight, I. and Kilfoil, G.1992, Reflection seismic imaging of the Carboniferous St. George coalfield, western Newfoundland: a reappraisal of Paleozoic stratigraphic thickness: *Bulletin of Canadian Petroleum Geology*, v.40, no.4, pp.321-334.

Hall J., Mariller F., and Dehler, S., 1998, Geophysical studies of the structure of the Appalachian orogen in the Atlantic borderlands of Canada, *Canadian Journal of Earth Sciences*, v.35, pp.1205-1221.

Hansen, D.M., Shimeld, J.W., Williamson, M.A., and Lykke-Anderson, H., 2004, Development of a major polygonal fault system in Upper Cretaceous chalk and Cenozoic mudrocks of the Sable Subbasin, Canadian Atlantic margin, *Marine and Petroleum Geology*, vol. 21, no.9, pp.1205-1219.

(a) Haworth, R.T., Grant, A.C. and Folinsbee, R.A., 1976, Geology of the continental shelf of southeastern Labrador; in Report of Activities, Part C, Geological Survey of Canada, Paper 76-1C, pp. 61-70.

(b) Haworth R.D., Poole, W.H., Grant, A.C., and Sandford B.V., 1976b, Marine geoscience survey northeast of Newfoundland; in Report of Activities, Part A, geological Survey of Canada, paper 76-1A, pp. 7-15.

Issler, D. R., and C. Beaumont, 1987, Thermal and subsidence history of the Labrador and West Greenland continental margins, *in* C. Beaumont and A. J. Tankard (eds.), *Sedimentary basins and basin-forming mechanisms: Canadian Society of Petroleum Geologists Memoir 12*, pp. 45-69.

Keen, C.E., Dehler, S.A., 1993, Stretching and subsidence: rifting of conjugate margins in the North Atlantic region, *Tectonics*, vol.12, no.5, pp. 1209-1229.

Keen C.E., Potter, P., and Srivastava S.P., 1994, Deep seismic reflection data across the conjugate margins of the Labrador Sea, *Canadian Journal of Earth Sciences*, vol.31, pp. 192-205.

Keen, C.E., Loncaravic, B.D., Reid, I., Woodside, J., Haworth, R.T., Williams, H., 1990, Tectonic and Geophysical overview; Chapter 2 in *Geology of the Continental Margins of Eastern Canada*, M.J. Keen and G.L. Williams (ed.); Geological Survey of Canada, *Geology of Canada*, no.2., pp.31-85.

Keen C.E., Keen, M.J., Nichols, B., Reid, I., Stockmal, G.S., Colman-Sadd, S.P., O'Brien, S.J., Miller, H., Quinlan, G., Williams, H., Wright., J., 1986, Deep seismic reflection profile across the northern Appalachians, *Geology*, vol. 14, no.2, pp.141-145.

Keep M., and McClay, K.R., 1997, Analogue modeling of multiphase rift systems, *Tectonophysics*, vol. 273, pp. 239-270.

Kennedy, M.J. and McGonigal, M.H., 1972, The Gander Lake and Davidsville Groups of northeastern Newfoundland: New data and geotectonic implications, *Canadian Journal of Earth Sciences*, v.9, pp.452-459.

Keppie, J.D., 1992, Structure of the Canadian Appalachians, Department of Natural Resources, Halifax, Nova Scotia, pp.1-91.

Langdon G. and Hall J., 1994, Devonian-Carboniferous tectonics and basin deformation in the Cabot Strait area, Eastern Canada: AAPG Bulletin, v.78, no.11, pp.1748-1774.

LithoTect Reference Guide, 2005, LithTect Help Documentation v.1.25, Geo-Logic Systems, LLC.

Louden, K.E., 2002, Tectonic evolution of the East Coast of Canada, CSEG Recorder, vol.27, no.2, pp. 37-48.

Mason, D.G., and P.R. Miles, 1986, Development and hydrocarbon potential of Mesozoic sedimentary basins around margins of North Atlantic, AAPG Bull., v. 70, pp. 721-729.

McClay, K.R., and White, M.J., 1995, Analogue modeling of orthogonal and oblique rifting, Marine and Petroleum Geology, vol. 12, pp. 137-151.

McClay, K.R., Dooley, T., Whitehouse, P., Mills, M., 2002, 4-D evolution of rift systems: Insights from scaled physical models, AAPG Bulletin, v.86, no.6, pp. 935-959.

McKenzie, D.P., 1978, Some remarks on the development of sedimentary basins, Earth and Planetary Science Letters, 1978, vol. 40, pp.25-32.

McNicoll, V.J., van Stall, C.R., Waldron, J.W.F., 2001, Accretionary history of the northern Appalachians; SHRIMP study of Ordovician-Silurian syn-tectonic sediments in the Canadian Appalachians, Geological Association of Canada, Mineralogical Association of Canada meeting, St John's, Newfoundland, v.26, Abstract, p.100-101

McWhae, J.R.H., Elie, R., Laughton, K.C. and Gunther, P.R., 1980, Stratigraphy and petroleum prospects of the Labrador Shelf, Bulletin of Canadian Petroleum Geology, v.28., p. 460-488.

Meredith, D.J., Egan, S.S., 2002, The geological and geodynamic evolution of the eastern Black Sea basin: insights from 2D and 3D tectonic modeling, Tectophysics, vol.350, pp. 157-179.

Nance R.D., and Murphy, J.B., 1994, Contrasting basement isotopic signatures and the

palinspastic restoration of peripheral orogens, Example from the Neoproterozoic Avalonian-Cadomian belt, *Geology*, v.22, pp.617-620.

Nance R.D., and Murphy, J.B., 1996, Basement isotopic signatures and Neoproterozoic paleogeography of Avalonian-Cadomian and related terranes in the circum-North Atlantic, *Geological Society of America Special Paper 304*, pp.333-346.

O'Brien, S.J., Wardle, R.J., King, A.F., 1983, The Avalon Zone: A Pan African terrane in the Appalachian orogen in Canada, *Geological Journal*, v.18, pp.185-222.

O'Brien S.J., Dickson, L.W, Blackwood, R.F., *Geology of the central portion of the Hermitage Flexure area, Newfoundland, in Current Research, Rep. 86-1*, Newfoundland Department of Mines and Energy, pp.189-202.

O'Neill, P.P., 1991, *Geology of the Weir's pond area, Newfoundland (NTS 2E/1)*: Newfoundland Department of Mines and Energy, Geological Survey Branch Report, v.91-3, pp.144.

Piasecki, M.A.J., 1995, Dunnage zone boundaries and some aspects of terrane development in Newfoundland, in *Current Perspectives in the Appalachian-Caledonian orogen*, GAC Special Paper 41, pp.323-348.

Powell, T.G., 1979, Geochemistry of Snorri and Gudrid condensates, Labrador Shelf: implications for further exploration, in Current Research, Part C, Geological Survey of Canada, Paper 79-1C, pp.91-95.

Rebesco, M., and Stow D.A., 2001, Seismic expression of contourites and related deposits: a preface, Marine geophysical Researches, vol.22, pp. 303-308.

Roberts, A. M., Kusznir, N.J., Yielding, G., Styles, P., 1998, 2D flexural backstripping of extensional basins: the need for a sideways glance, Petroleum Geoscience, vol.4, pp.327-338.

Rodgers, J., 1968, The eastern edge of the North American continent during the Cambrian and Early Ordovician, in Studies in Appalachian geology, northern and maritime, Zen, E., et al. (eds.), New York, Wiley Interscience, pp. 141–149.

Roest, W.R., and Srivastava, S.P., 1989, Seafloor spreading in the Labrador Sea: A new reconstruction, Geology, vol. 17, pp.1000-1003.

Robertson, A.H.F., 2007. Geochemical evidence for the sedimentary and diagenetic development of the Mesozoic–early Cenozoic Newfoundland rifted margin, northwest Atlantic (Ocean Drilling Program Leg 210, Site 1276). In Tucholke, B.E., Sibuet, J.-C., and Klaus, A. (Eds.), *Proc. ODP, Sci. Results*, 210: College

Station, TX (Ocean Drilling Program), 1–63.

doi:10.2973/odp.proc.sr.210.105.2007

Ryan, R.J., and Zentilli, M., 1993, Allocyclic and thermochronological constraints on the evolution of the Maritimes Basin of eastern Canada, Atlantic GeoScience Society, Annual Colloquium and Symposia, Halifax, Nova Scotia, Program with Abstracts.

Schaltegger, U., Desmurs, L., Gianreto, M., Müntener, O., Meier, M, Frank, M., Bernoulli, D., 2002, The transition from rifting to sea-floor spreading within a magma-poor rifted margin: field and isotopic constraints, *Terra Nova*, vol. 14, pp.156-162.

Sibuet, J.-C., S.P. Srivastava, M.E. Enachescu, and G. Karner, 2005, Lower Cretaceous motion of the Flemish Cap in respect with North America: Implication for the formation of Orphan Basin and Flemish Cap/Galicia Bank conjugate margins: 6th Petroleum Geology Conference: North West Europe & Global Perspectives, NSF Intermargins workshop, Pontresina Conference.

Sinclair, I. K., K .D. McAlpine, D. F. Sherwin, N. J. McMillan, G. C. Taylor, M. E. Bast, G. R. Campbell, J. P. Hea, D. Hanao, and R. M. Procter, 1992, *Petroleum*

resources of the Jeanne d'Arc Basin and Environs, Grand Banks, Newfoundland:
Geological Survey of Canada, Paper 92-8, 48 p.

Skelton, A.D.L, Valley, J.W., 2000, The relative timing of serpentinisation and mantle
exhumation at the ocean-continent transition, Iberia; constraints from oxygen
isotopes, *Earth and Planetary Science Letters*, v.178, pp.327-338.

Solvason K.L.M., 2006, Crustal Structure and Formation of the Southeast Newfoundland
Continental Margin. Phd Thesis, Memorial University, St. John's, Newfoundland
and Labrador.

Srivastava S.P., and Rouest, W.R., 1995, Nature of the thin crust across the southwest
Greenland margin and its bearing on the location of the ocean-continent
boundary, in *Rifted ocean-continent boundaries*, Banda E., Torni, M. Talwani, M.
(eds), NATO Advanced Science Institutes Series, Series C: Mathematical and
Physical Sciences, vol. 463, 1995, pp. 95-120.

Srivastava S. P. and Keen, C. E., 1995, A deep seismic reflection profile across the
extinct Mid-Labrador Sea spreading centre, *Tectonics*, vol.14, no.2. pp. 372-389.

Srivastava, S.P., and J. Verhof, 1992, Evolution of Mesozoic sedimentary basins around
the North Central Atlantic: a preliminary plate kinematic solution, *in*, J. Parnell,

ed., Basins on the Atlantic Seaboard: Petroleum Geology, Sedimentology and Basin Evolution: Geological Society Special Publication, no. 62, pp. 397-420.

Srivastava, S., J.-C. Sibuet, S. Cande, W.R. Roest, and I.R. Reid, 2000, Magnetic evidence for slow seafloor spreading during the formation of the Newfoundland and Iberian margins: *Earth and Planetary Science Letters*, v.182, pp. 61-76.

Stockmal G.S., Colmann-Sadd, S.P., Keen, C.E., Mariller, F., O'Brien, S.J., and Quinlan, Garry M., 1990, Deep seismic structure and plate tectonic evolution of the Canadian Appalachians, *Tectonics*, vol.9, pp. 45-62.

Stow, D.A., Faugères, J.C., Howe, J.A., Pudsley, C.J., Viana, A.R., 2002, Bottom currents, contourites and deep-sea sediment drifts: current state-of-the-art, in *Deep-Water Contourite Systems: Modern Drifts and Ancient Series, Seismic and Sedimentary Characteristics*, Stow, D.A., Faugères, J.C., Howe, J.A., Pudsley, C.J., Viana, A.R, (eds) Geological Society, London, Memoir 22, pp. 7-20.

Srivastava, S. P., and Roest, W.R., 1999, Extent of oceanic crust in the Labrador Sea, *Marine and Petroleum Geology*, vol. 16, pp. 65-84.

Tucholke, B.E., J.-C. Sibuet, A.Klaus, and the scientific party, 2004, *Proceedings ODP*,

Initial Reports, Leg 210.http://www-odp.tamu.edu/publications/210_IR/210ir.htm

Tucholke, B.E., Sibuet, J.-C., and Klaus, A. (Eds.), 2007. *Proc. ODP, Sci. Results*, 210: College Station, TX (Ocean Drilling Program). doi:10.2973/odp.proc.sr.210.2007

Tucholke, B.E., and Sibuet, J.-C., 2007. Leg 210 synthesis: tectonic, magmatic, and sedimentary evolution of the Newfoundland-Iberia rift. *In* Tucholke, B.E., Sibuet, J.-C., and Klaus, A. (Eds.), *Proc. ODP, Sci. Results*, 210: College Station, TX (Ocean Drilling Program), 1–56. doi:10.2973/odp.proc.sr.210.101.2007

Umpleby, D.C., 1979, *Geology of the Labrador Shelf*; Geological Survey of Canada, Paper 79-13, 34 p.

Vail, P.R., Mitchum, R.M., Todd, R.G., Widmier, J.M., Thompson, S., III, Sangree, J.B., Bubb, J.N. and Hatlelid, W.G., 1977, Seismic stratigraphy and global changes of sea level, *in* *Seismic Stratigraphy—Applications to hydrocarbon exploration*, Payton C.E. (ed.), American Association of Petroleum Geologists Memoir 26, pp.49-212.

- Valverde-Vaquero, P., and van Staal., C., Relationships between the Dunnage-Gander Zones in the Victoria Lake-Peter Strides pond area, 2001, Report 2001-1 Current Research, Newfoundland Department of Mines and Energy, pp.1-9.
- van der Velden, A.J., van Staal, C.R., and Cook, F.A. Crustal structure, fossil subduction, and the tectonic evolution of the Newfoundland Appalachians: Evidence from a reprocessed seismic reflection survey, GSA Bulletin, v.116, no.11/12, pp.1485-1498.
- Van der Voo, R., 1988, Paleozoic paleogeography of North America, Gondwana, and intervening displaced terranes, Comparisons of paleomagnetism with paleoclimatological and biogeographical patterns, Geological Society of America Bulletin, v.100.,p.311-324.
- van Staal, C.R., Dewey, J.F., Mac Niocoill, C. and McKerrow, W.S., 1998, the Cambrian-Silurian tectonic evolution of the northern Appalachians and British Caledonides, History of a complex, west and south-west Pacific-type segment of Iapetus, *In* The past is key to the present, Blundell D.J. and Scott, A.C. (eds.), Geological Society (London) Special Publication 143, pp.199-242.
- Waldron, J.W.F, Anderson, S.D., Cawood, P.A., Goodwin, L.B., Hall, J., Jamieson, R.A.,

Palmer, S.E., Stockmal, G.S., and Williams, P.F., 1998, Evolution of the Appalachian Laurentian margin, Lithoprobe results in western Newfoundland, Canadian Journal of Earth Sciences, v.35, pp.1271-1287.

Wardle, R.J. and Hall., J, 2002, Proterozoic evolution of the northeastern Canadian Shield: Lithoprobe Eastern Canadian Shield Onshore–Offshore Transect (ECSOOT), introduction and summary, vol.39, no.5, p. 563-567.

Watts, A.B., Karner G.D., and Steckler, M.S., 1982, Lithospheric flexure and the evolution of sedimentary basins: Royal Society of London Philosophical Transactions, ser.A., v.305, pp. 249-281.

Watts, A.B., 2001, Isostasy and Flexure of the Lithosphere, Cambridge University Press, Cambridge, United Kingdom.

Wernicke, B., 1985, Uniform-sense normal simple shear of the continental lithosphere, Canadian Journal of Earth Sciences, vol. 22, pp.108-125.

White, N., McKenzie, D., 1988, Formation of the “steer’s head” geometry of sedimentary basins by differential stretching of the crust and mantle, Geology, vol.16, pp.250-253.

- Williams, E.P., 1974, Geology and petroleum possibilities in and around the Gulf of St. Lawrence, American Association of Petroleum Geologists Bulletin, v.58, pp.1136-1155.
- Williams H., 1964., The Appalachians in northeastern Newfoundland—A two-sided symmetrical system: American Journal of Earth Sciences, v.262, p.1137-1158.
- Williams, H., 1979, The Appalachian orogen in Canada: Canadian Journal of Earth Sciences, v.16, p.792-807.
- Williams, H.(ed.), 1995, Geology of the Appalachian-Caledonian orogen in Canada and Greenland, Geological Survey of Canada, Geology of Canada, Ottawa, no.6.
- Williams, H. and Hatcher, R.D., 1982, Suspect terranes and accretionary history of the Appalachian Orogen, Geology, vol. 10, pp.530-536.
- Williams, H., Hatcher, R. D. Jr. 1983. Appalachian suspect terranes. *In* Contributions to the Tectonics and Geophysics of Mountain Chains, Geological Society of America Memoir 158, R. D. Hatcher Jr., H. Williams, I. Zietz (eds.), Boulder, Colorado pp. 33-53.
- Williams, H. and Piasecki, M.A.J., 1990, The Cold Spring mélangé and a possible model



